AWESOM

Airborne Wind Energy System on Mars

Final Report

DSE Group 23

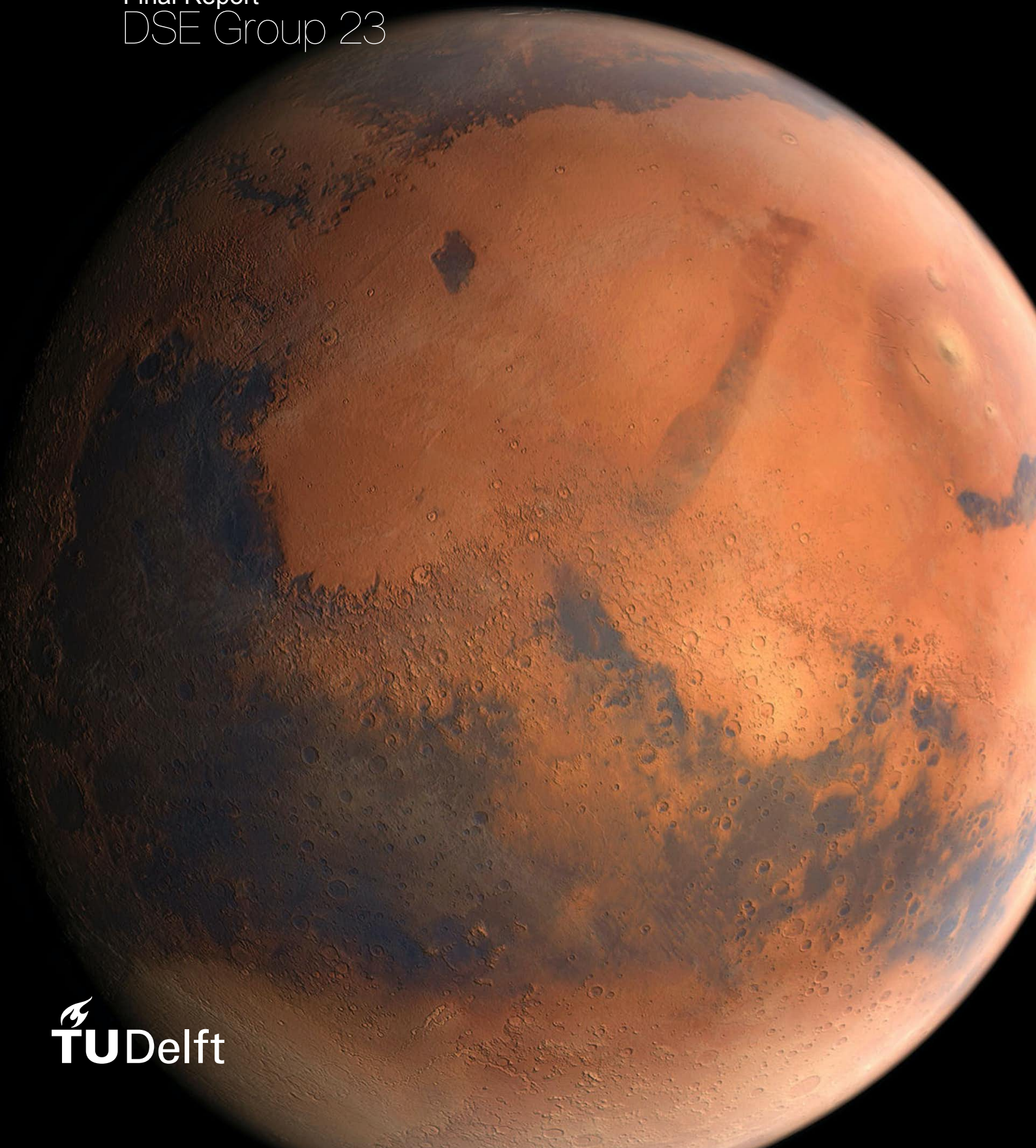

TU Delft

AWESOM

Airborne Wind Energy System on Mars
Final Report

by

Name	Surame	Student Number
Matéo	Caruso	4796268
Dilge	Gül	4821165
Varvara	Isidorova	4819136
Walter	van der Klugt	4532236
Matthijs	de Lange	4785487
Thomas	Meyer Ranneft	4597753
Alberto Cornel	Popescu Cabo	4839927
Kriharen	Tiagoo	4810147
Badhrinarayanan	Sambath	4665295
Loek	Sanders	4805232

Institution:	Delft University of Technology	
Place:	Faculty of Aerospace Engineering	
Date:	June 29, 2021	
Supervisors:	Dr.-Ing. Roland Schmehl	Principal tutor
	Dr. Ir. Yinglu Tang	Coach
	Dr. Ir. Stefano Speretta	Coach
Teaching Assistant:	Fernando Corte Vargas	

Cover image retrieved on April 22, 2021 from https://wibnet.nl/heelal/zonnestelsel/mars/mars-de-rode-planeet

TU Delft

Summary

Creating extraterrestrial habitats has been a goal for many years. Mars is a prime location due to its relative habitability compared to other planets in the solar system. Yet it still poses many challenges for human habitation. The Rhizome project, being funded by the European Energy Agency, is to use a renewable energy system as its form of power production. Airborne Wind Energy System on Mars (AWESOM) will address this challenging problem presented the Rhizome project.

This report describes 10 weeks of work towards the conceptual design of a Martian based airborne wind energy system coined AWESOM. AWESOM is capable of providing 10 kilowatts of nominal power to a Martian habitat for 5 Martian years. This means that the system has to account for seasonal fluctuations and will make use of a compressed carbon dioxide long term energy storage solution, that is capable of storing enough energy during the months where power generation is plenty and transferring this energy to the habitat during the low power production periods. This period has been identified to be somewhere in the months of Martian summer. The basic idea of the system is that a wing is connected to a tether that is spooled onto a drum connected to a generator. To produce power, this wing is flown up to 300 m in altitude and as a result the drum is rotated when the tether reels out. This pulling force of the drum induces a torque on the motor and hence power is generated. To reel in back the wing, the aerodynamics of the kite is altered to reduce the pulling force which in turn results in a net surplus of power generated as less energy is needed to reel in the kite than the reeling out. This process is known as the pumping cycle and multiple of them take place over the period of a day to generate the required power for the habitat.

An extensive weather model was used, namely: the Mars Climate General Circulation Model. This allowed for the wind profile within the location of the site to be studied and as a result a new location was selected for improved wind conditions compared to the location chosen by last year's DSE group. This climate model was also incorporated into the performance model of the entire kite system, providing valuable insights into the iterative process of selecting and sizing the system characteristics. The aerodynamics characteristics of the system primarily consists of selecting the airfoil of the wing subsystem and optimizing the relevant parameters. The Wortmann FX63137 was deemed to be the most aerodynamically suitable for this application and the wing was sized with a 60 m^2 surface area and a span of 20 m. Control of the wing is important to both the power generation capability as well as the survivablility of the kite. The wing is to fly in a figure of eight trajectory. This allows for the wing to exploit higher cross wind speeds and subsequently generate more power. The figure of eight path also prevents the main tether from tangling with the control tethers.

Another critical component of the system as a whole are the structural characteristics of the wing as it heavily influences the weight of the kite and this has a knock-on effect on the sizing of every other subsystem. A structural model was developed to determine the size of the wingbox, canopy, ribs and truss members. For each element, the failure modes were investigated and taken into account during the normal and worst case scenario operations of the wing. As a result, the mass of the wing was determined to be 79.7 kg. The ground station consists of the main power generating components which convert mechanical to electrical energy. It was determined that a high torque, low speed, direct drive motor is ideal to avoid the use of a gearbox which substantially increases the efficiency of the system as a whole. To fulfill the seasonal needs, a 70 kW motor was chosen after considering all necessary efficiency loses. The main drum being were the main power generation tether is spooled on has as size of 0.6 m diameter.

To ensure that the entire operation of the system is as autonomous as possible, various take-off and landing methods were considered. After performing a trade-off, a vertical mast and horizontal boom configuration was chosen where the main tether and control tethers are fed through respectively. This entire system sits on rotating platform which allows for the kite operation to be independent of wind direction as it can swivel in all directions. Launching is assisted by rovers which have been decommissioned from the RHIZOME project and modified to fit the launch tasks.

A comprehensive risk assessment was done to ascertain the risks that the system might face during its entire life cycle. Various risk mitigation strategies were identified to reduce the impact and likelihood of the most critical ones.A RAMS analysis was also carried out and it was concluded that the system is able to comply with most the requirements that were set forth. Through the financial analysis, it is determined that the total production cost of the system is 22.8 % of the allocated cost budget. The return on investment is deduced to be from educational means. This includes the education of the public on the importance of space exploration as well as scientific breakthroughs that can both be incorporated into Earth based and space based energy generating technologies.

Nomenclature

List of Abbreviations

Abbreviation	Definition
AC	Alternating current
AR	Aspect Ratio
AWE	Airborne Wind Energy
AWESOM	Airborne Wind Energy System on Mars
BJ	Binder Jetting
DC	Direct current
ESA	European Space Agency
FBD	Free Body Diagram
FBS	Functional Breakdown Structure
FFD	Functional Flow Diagram
FMECA	Failure Modes Effects and Cause Analysis
GCM	General Circulation Model
HiL	Hardware-in-the-Loop
ITS	Interplanetary Transportation System
MAC	Mean aerodynamic chord
MCD	Mars Climate Database
MGC	Mean geometric chord
SLM	Selective Laser Melting
SSLS	Selective Solar Light Sintering
SWOT	Strength Weakness Opportunity & Threat

List of Symbols

Latin Symbol	Definition	Unit
C_D	Wing drag coefficient	-
C_{D_0}	Zero lift drag coefficient	-
C_L	Wing lift coefficient	-
C_M	Wing moment coefficient	-
D	Drag force	N
d	Diameter	m
E	Young's Modulus	N/m^2
e	Oswald efficiency factor	-
F	Force	N
F_t	Tension force	N
f	Reeling factor	-
I_{xx}	Moment of inertia about x-axis	m^4
L	Lift force	N
l	Length	m
l_s	Solar longitude	°
P_{out}	Reel-out power	kW
P_{in}	Reel-in power	kW
S	Wing area	m^2
t_{out}	Reel-out time	s
t_{in}	Reel-in time	s
T	Temperature	K
t	Thickness	m
V	Volume	m^3
v_{k_τ}	Wing's tangential velocity	m/s
v_w	Wind velocity	m/s
W	Weight force	N

Greek Symbol	Definition	Unit
α	Angle of attack	°
δ	deformation	-
$\eta_{tqmotor}$	Torque motor efficiency	-
$\eta_{conroller}$	Motor controller/inverter efficiency	-
η_{buffer}	Buffer storage efficiency	-
$\eta_{friction}$	Frictional loses	-
$\eta_{reelout}$	Reel-out efficiency	-
η_{reelin}	Reel-in efficiency	-
$\eta_{pumping}$	Pumping efficiency	-
$\eta_{electrical}$	Electrical efficiency	-
θ	Elevation angle	°
Λ_{LE}	Leading edge sweep angle	°
μ	Banking angle	°
ρ	Atmospheric density	kg/m^3
σ	Normal stress	N/m^2
τ	Time	s
ϕ	Azimuth angle	°

Contents

1 Introduction

Life on other planets has been a dream for humanity for a long time. As a result of today's level of technology, it is possible not only to visit outer space or send unmanned vehicles to other celestial bodies, but also to start planning a way of creating habitable areas beyond Earth, coming a step closer to the once impossible dream. Mars is one of the most promising locations for this, being a terrestrial planet with sufficiently hospitable conditions. The Rhizome project [1], funded by the European Space Agency, is about designing a habitat on Mars. Their plan for doing this is through 3D printing walls and structures within already present natural cavities with the use of small robots. Rhizome needs not only to provide a habitat, including the supply of energy for the mission. To account for fluctuations in availability of natural energy sources, the habitat must be powered by renewable energy in several complementary ways, including a wind energy system as suggested by NASA [1] and this report covers its design, however looks at an airborne wind energy system which was previously recommended by the ARIES DSE project from last year [2].

AWESOM was launched with the objective of designing a system capable of covering the 10 kW energy demand of the habitat. It will assisted by a solar array to cover for the time periods with insufficient wind.

The objective of this report is to present the final design of AWESOM while explaining all the reasoning behind the design choices made and to plan for the future of the project.

The report will be presented in the following structure, chapter 2 starts the report off with a detailed analysis of the Martian environment as well as an update of the location for the AWESOM. The Martian Climate Database was used to get more accurate predictions of the weather. A detailed understanding of the Martian environment was created first as it is the most important contributor to defining the design space. Before diving deep into the detailed design of AWESOM, chapter 3 presents a summary of the previous design steps taken in addition to the requirements and a feasibility study to further define the design space and present the history of why the detailed design is heading in the presented direction. chapter 4 elaborates upon a system layout as a follow up from the preliminary design decisions presented in chapter 3. chapter 4 also presents a functional analysis to define the work packages and sequence of the project. The following chapter, chapter 5, further defines the design space by looking at the market involved in the AWESOM project. Subsequently, the resources of the project are allocated in chapter 6 for technical and non-technical aspects of the project. Once the design space has been properly identified, a more detailed design is presented and reasoned for per sub-system in chapter 7. Having defined the detailed design, the next step involved checking if the design satisfied the requirements through an analysis of the performance of the system which was done in chapter 8. It is vital to explain how various subsystems will communicate with one another which was done in chapter 9. chapter 10 is a logical follow up once the system configuration and functional structure has been defined as now a detailed risk analysis can be performed. chapter 11 verifies and validates the calculation performed previously alongside software used in order to make sure the design was not obtained using faulty methods. Having checked that the design was calculated correctly, a important aspect of the project is analysed in chapter 12; here the sustainability of AWESOM is evaluated and methods in order to improve it are discussed. chapter 13 defines how AWESOM will be produced which is the next step in the design process in order to ensure a efficient and fault free construction. chapter 14 analyses the Reliability, Availability, Maintainability, and Safety in a RAMS analysis. A top level requirement of the project were the overarching costs of AWESOM, therefore, chapter 15 evaluates the cost of the system. Lastly a timeline was created via a Gantt chart describing the future steps of the project beyond DSE in chapter 16 and the report is wrapped up with a conclusion in chapter 17.

[1] http://www.roboticbuilding.eu/2020/03/11/11th-march-our-idea-rhizome-development-of-an-autarkic-design-to-robotic-production-and-operation-systen on 21st June 2021]

2

Analysis of Martian Environment

In order to enable a successful design for an AWE system, it is necessary to have good knowledge of the environment that it has to operate in. This chapter describes the Mars Climate Database (MCD) that is used to determine the environment of Mars throughout the year. Then, the location of the habitat is reevaluated and the results are presented. Finally, the implications on the system and sensitivity are discussed.

2.1. Mars Climate Database

The Martian environment will be analysed by using the Mars Climate Database (MCD)[3, 4]. This database includes data from a general circulation model (GCM) of Mars. The GCM uses a grid with steps of 5.625°in longitude and 3.75°in latitude, resulting in a spatial resolution of 332.7 by 221.8 km. To create a more detailed spatial resolution, the MCD uses post-processing tools, such as a gravity model and data sets produced by Mars Orbiter Laser Altimeter (MOLA) Team. The MOLA data was used at a resolution of 32 pixels per degree, resulting in a higher resolution of 1850 meter resolution at the equator where the grid is the largest. To determine high resolution variables, the pressure is predicted by the GCM at the high resolution grid, this pressure is then used to determine the other variables such as density and wind speeds.

The database allows to model various conditions: the solar maximum, average and minimum can be modeled in combination with the climatology average conditions and the planetary-wide dust storm conditions. Furthermore, the model allows to simulate the dusty conditions with solar maximum (warm) and low dust conditions (cold). An option to simulate specific conditions of certain years is also present.

It is possible to know in advance what solar conditions will be present on a certain day since the solar activity has a periodicity to it: the Sun rotates around its axis in 27 days, the magnetic cycle of the Sun takes 11 years. This information will be useful during the operation of the kite to be able to predict the conditions and, therefore, the power output. During the design phase, it is important to consider both maximum and minimum conditions to be able to produce sufficient power on average [1].

2.2. Mars Climate Database Use Cases & Limitations

Although the MCD is a very useful tool, it does have its limitations. The vertical grid for instance, has 49 data points with the closest to the ground being at approximately 5 m altitude and the highest at around 250 km altitude. The distances between vertical stations increases as altitude increases. Still, only five grid points are present within the first 400 m of the atmosphere. In between these grid points data points are interpolated.

The interpolation used is valid within the grid lines of the model, this means that to get values that lie outside of the vertical grid, i.e. below and above the boundary layer, a different method needs to be used. Since the kite will be relatively low to the ground, only the lower boundary of the grid is of importance. This method however is less accurate than the interpolation, thus all wind data used will be taken from an altitude of 5 m or higher.

[1] http://www-mars.lmd.jussieu.fr/mars/info_web/MCD5.3_ddd.pdf [Accessed on June 1, 2021]

2.3. Comparison with the Various Lander Data

Table 2.1: Comparison between the wind speeds obtained by the Phoenix mission and the wind speeds obtained from the model.

Ls	local hour	wind speed	model average conditions	model year 29
83	09:00	3	3.25	1.5
	11:00	4	3	0.5
	17:00	4	4	2.6
97	06:00	3	2.2	2.1
	08:00	4	2.45	2.2
	12:00	4	1	0.6
	22:00	6	1.6	1.6
111	04:00	4	1.5	1.7
	09:00	5.5	1.2	0.9
	12:00	4	0.6	1.4
	20:00	5	2	1.6
125	04:00	2	1.8	2.2
	07:00	3.5	2.1	2.6
	11:00	6	2	2
	14:00	5	4	4.3
	18:00	5	3.5	3
	22:00	3.5	1.6	1.6
140	03:00	3	2.6	2.6
	05:00	3	4	3
	10:00	3	4.2	4.5
	11:00	5	5.2	5.4
	15:00	8	7.3	7
	17:00	6	4.4	5.2
	19:00	4	2.1	1.9

There are a few ways to estimate how much the actual conditions might differ from the ones predicted by the model. One of the easiest checks that can be run is the check on the data obtained from various landers over the years. Comparisons of the wind speeds data has been done for the Viking 1, InSight and Phoenix landers. The predicted wind does not show a good fit, and the daily pattern of wind fluctuation is also off for both the InSight and Phoenix.

However, the order of magnitude of the wind speeds is correct. In the case with the Phoenix data, the model more often underestimated rather than overestimated the speeds. This is good for the design since in the context of the project, the model represents the more negative scenario. In this particular case, the model included an option for the conditions of the year that the Phoenix mission has been gathering the information. However, the modified model has provided an even worse match than the ”climatology average conditions”.

However, with regards to the InSight mission, the model has vastly overestimated the values. The closest scenario turned out to be the ”cold scenario”: low dust and minimum solar activity. However, even this model has overestimated the wind speeds three times over in the worst matched data point.

The Spirit and Opportunity rovers did not have a wind measurement device on board. The Pathfinder mission had a windsock, but the data that was found did not show what time of the day the measurements were taken since the concern of the experiment was simply the surface roughness. Therefore, it is impossible to use this data to check the model.

The most extensive data was found for the Phoenix lander, which had the averaged velocities over a significant time period (22-23 days) that can be seen in Figure 2.1. The Table 2.1 shows the information about the average speeds extracted from Figure 2.1 and the information given by the model. The first column gives an average solar longitude of the measurement time (the data in the Figure 2.1 gives the average of these wind speeds.), the second column gives the average wind speed registered by Phoenix. The third and fourth columns give the wind speeds for the same location, time and the Solar longitude presented on the left. The third column presents the average scenario, and the right one presents the scenario for the 29th year on Mars, which is the year the data was collected.

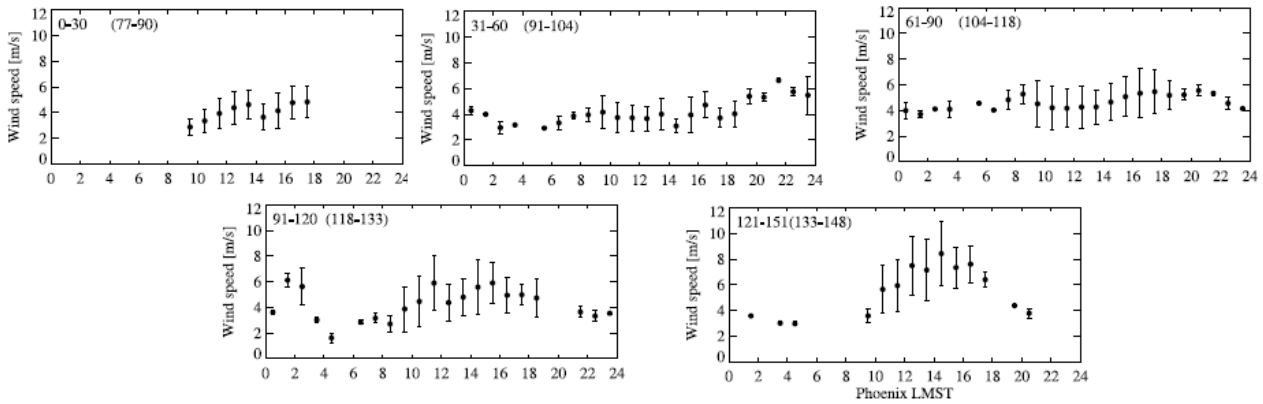

Figure 2.1: Averaged wind speeds from Phoenix lander

Figure 2.2: Viking 1 wind data comparison from a particular day with the wind speeds predicted by the model.

Ls	time	registered wind speed	model wind speeds
108	02:40	3.41	3.1
108	16:30	2.64	3.7
113	05:00	2.66	3.5
113	23:30	0.63	2.6

Figure 2.3: Table displaying the average wind speeds registered by the InSight lander from sol 143 to sol 145 alongside the wind speed values given by the model for the corresponding time of the year.

time	average over 3 sols	model average conditions	cold scenario
0:00	3.9	13.5	7.3
6:00	4.8	8.5	5.3
12:00	5.3	17.7	8.4
18:00	3.1	18.8	9

The model does not predict the real situation for InSight well with any settings. However, it is possible to see that the ”cold scenario” provides the best approximation of all. Indeed, the temperatures registered by the InSight are even lower than the ones predicted by the cold scenario.

2.4. Updated Habitat Location

The next step is to reevaluate the decision on the location of the habitat made by the previous design team [5]. Their chosen location was Deuteronilus Mensae and was chosen because of its relatively easy access to water, flat terrain and access to metal/silicon on the surface. However, their method shows that although wind speeds is highly rated, so are other factors that might be of lesser importance to our system. Additionally, their chosen location did not score the highest in terms of wind speed out of all candidates. Furthermore, wind data from [3] shows that wind speeds in this area are not sufficient for providing power at many points during the day. Thus a new location is proposed, Protonilus Mensae, located at a longitude and latitude of roughly 50.141° and 42.109° respectively. This location was found in a NASA presentation on potential habitation sites in the Protonilus Mensae area [2]. The location shows potential as it conforms to a list of threshold factors that support life and science on Mars:

- NASA concluded it has potentially been habitable in the past.
- It has potential for present habitability.
- It has potential for water ice/ice regolith mixture.
- It might have potential for water ice to be closer than 3 meters to the surface.
- It has at least a 50 km^2 region of flat and stable terrain with sparse rock distribution

These factors however, are also present in the Deuteronilus Mensae. The deciding factor that made this location much better is the larger availability of wind. A seasonal comparison was done in Figure 2.4, 2.5, 2.6 and 2.7, where the wind velocity was plotted compared to the altitude and the local time of day. This was done at four different solar longitudes, 0, 90, 180 and 270° which are the equinox of martian spring, summer, autumn and winter in the northern hemisphere. The solar longitude is an indication of where Mars is in its orbit around the sun.

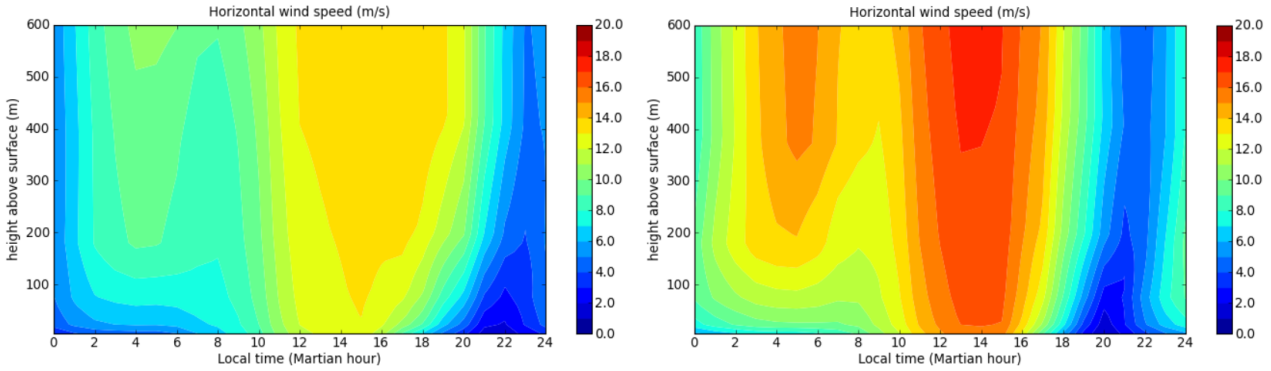

Figure 2.4: Wind velocity profile of Deuteronilus (left) and Protonilus (right) in spring.

[2]https://www.nasa.gov/sites/default/files/atoms/files/protonilus_mensae_presentation_tagged.pdf [Accessed on June 22, 2021]

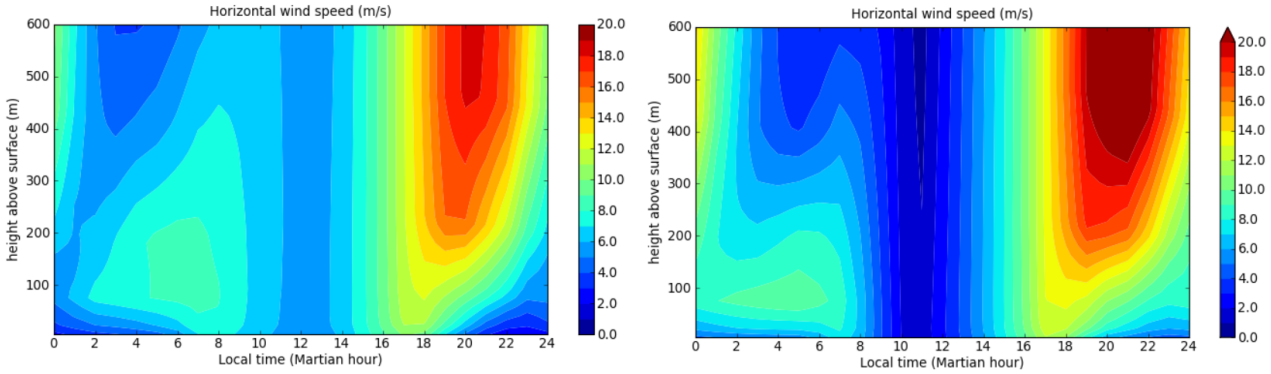

Figure 2.5: Wind velocity profile of Deuteronilus (left) and Protonilus (right) in summer.

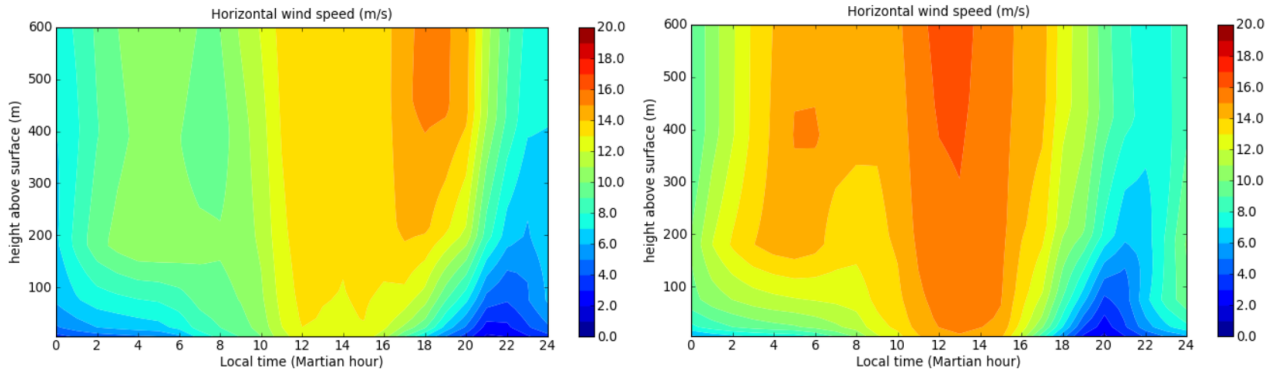

Figure 2.6: Wind velocity profile of Deuteronilus (left) and Protonilus (right) in autumn.

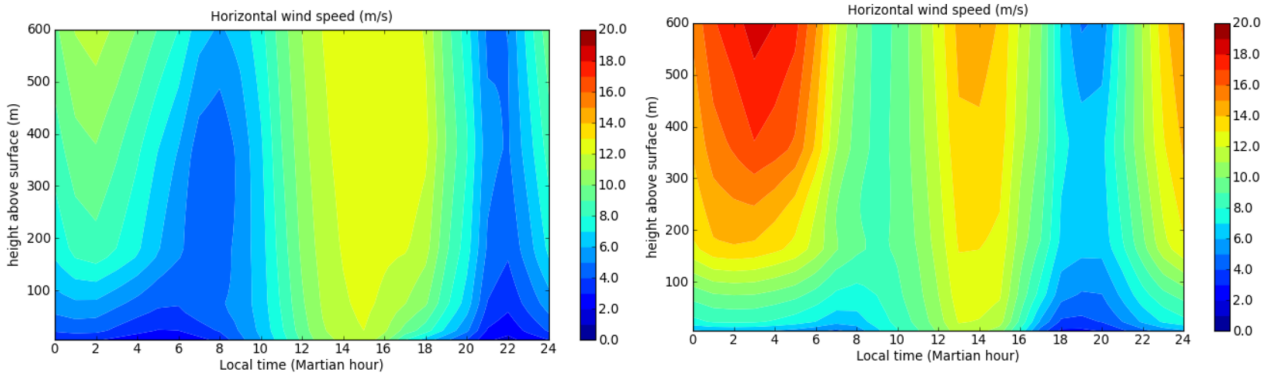

Figure 2.7: Wind velocity profile of Deuteronilus (left) and Protonilus (right) in winter.

It has to be noted that the comparison only incorporates four days of the year, meaning reality might tell a different story. Nevertheless, it can be seen from the comparison that for each season the Protonilus Mensae area has higher wind speeds and therefore offers more potential for an AWE system.

2.5. Results for the Operation Site from the Mars Climate Database

This section provides the results for the chosen location for various seasons and weather scenarios. In subsection 2.5.1 the wind profile of a few days in every season is shown, in subsection 2.5.2 average wind speeds per season are shown and in subsection 2.5.3 a probability distribution of every season is shown.

2.5.1. Daily Wind Velocity Profile

The MCD was used to plot a detailed wind velocity profile for the chosen location at 42.109 North latitude and 50.141 East longitude. Furthermore it was plotted 13 times, for solar longitudes of 0 to 360 for every 30 degrees, to get a feeling of how the wind speeds change over the Martian year, these plots can be seen in Figure 2.8, 2.9, 2.10, 2.11, 2.12 and 2.13. However, the plot for 360 degrees was omitted since it is very similar to the plot for 0 degrees, as it is the same time of year.

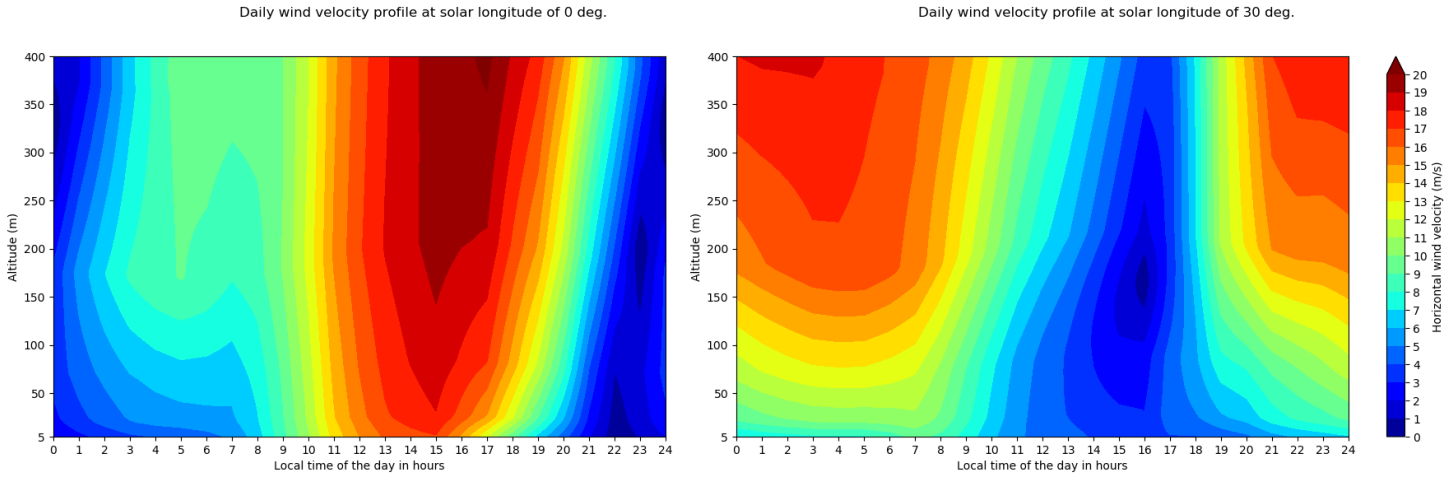

Figure 2.8: Wind velocity profiles of spring equinox and late spring.

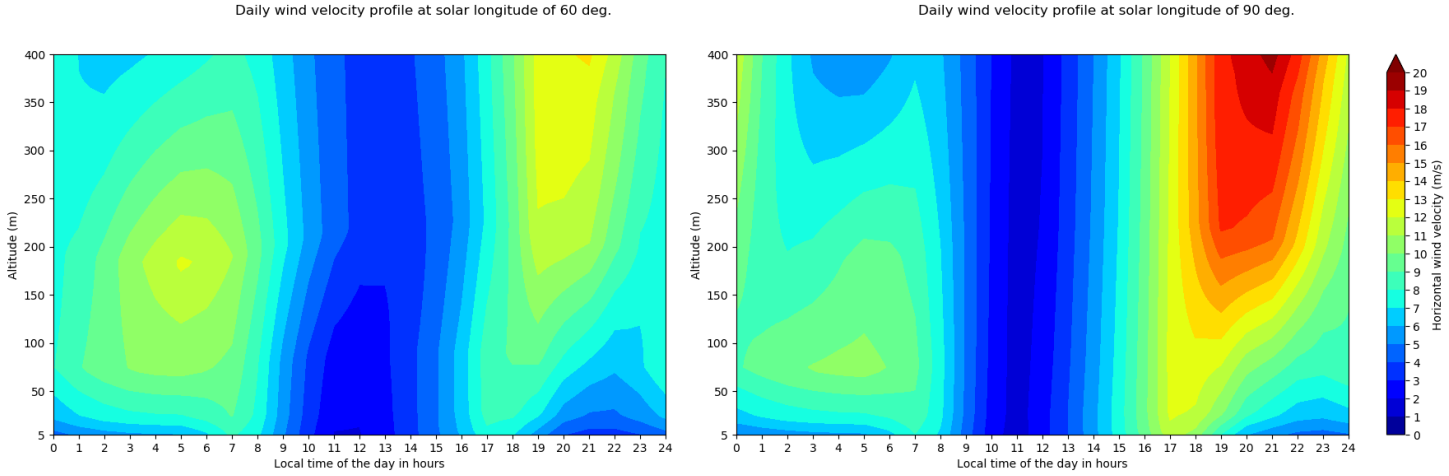

Figure 2.9: Wind velocity profiles of early summer and summer equinox.

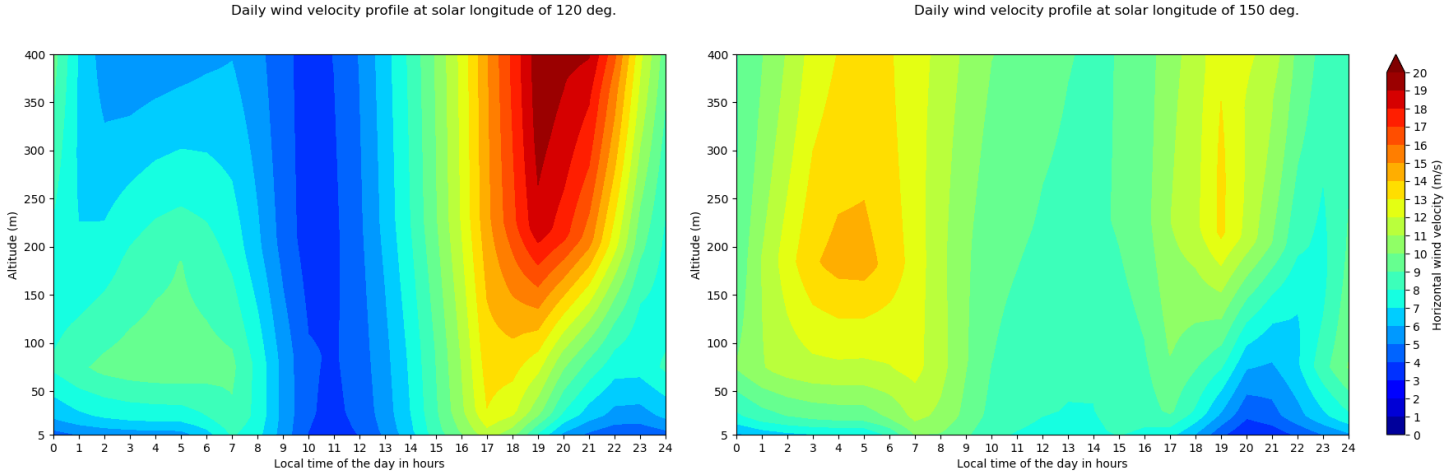

Figure 2.10: Wind velocity profiles of late summer and early autumn.

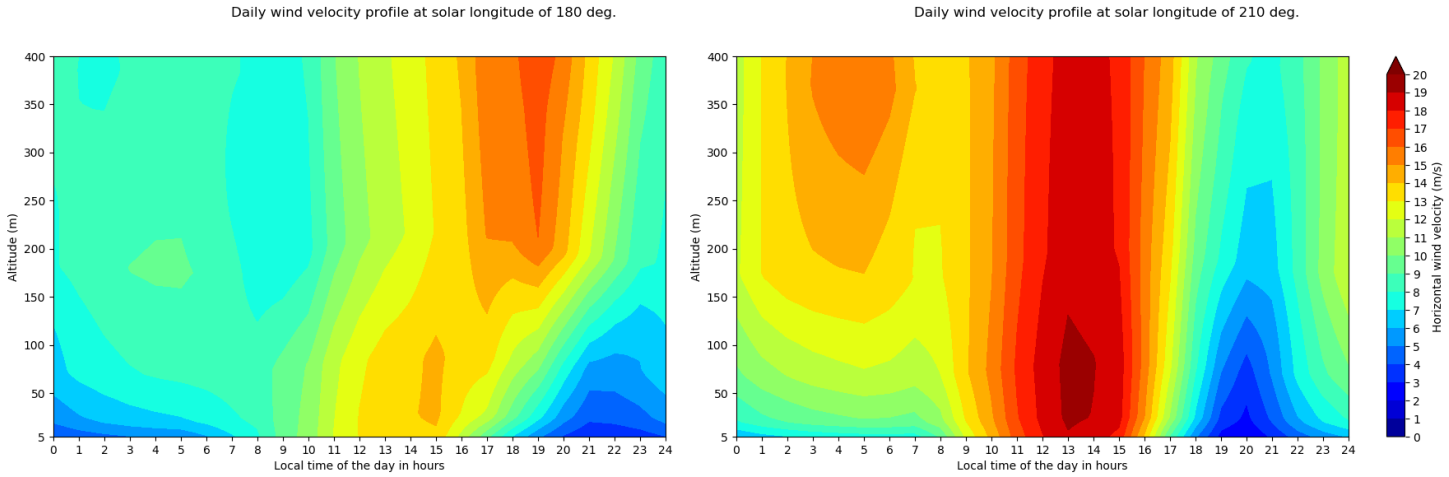

Figure 2.11: Wind velocity profiles of autumn equinox and late autumn.

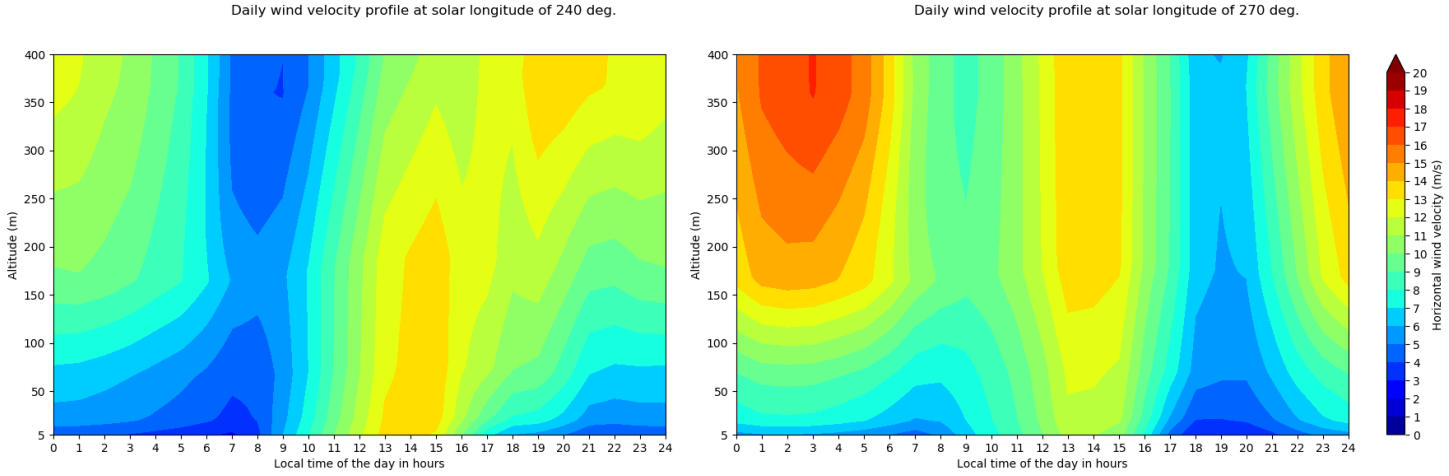

Figure 2.12: Wind velocity profiles of early winter and winter equinox.

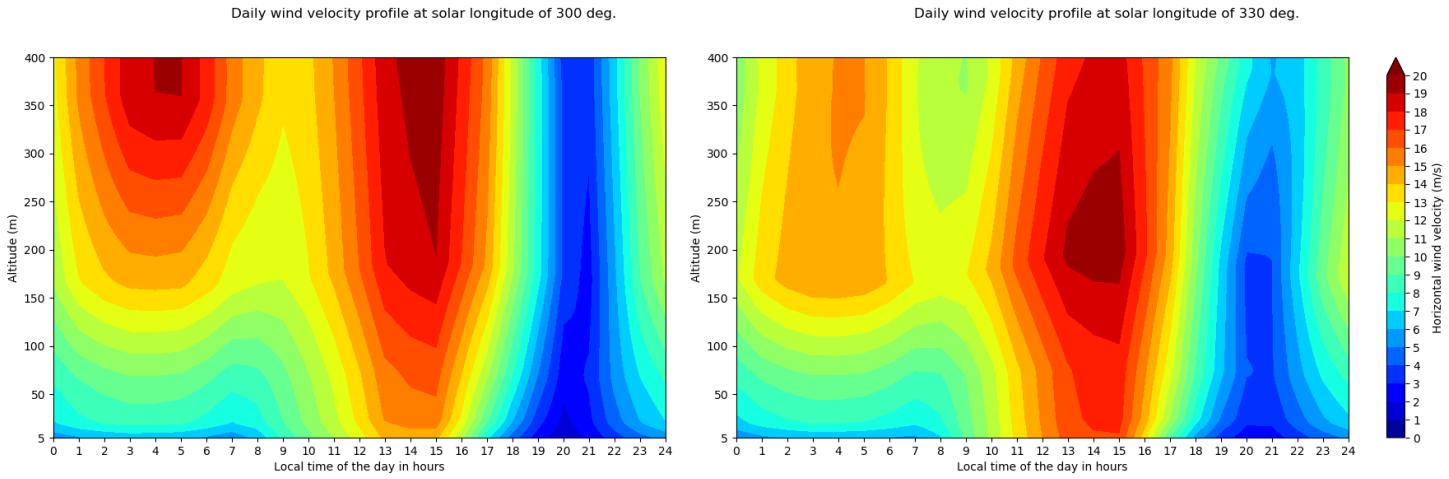

Figure 2.13: Wind velocity profiles of late winter and early spring.

The profiles plotted here have a data point in altitude for every 5 meters and a data point in time for every hour, for a total of 2000 data points per graph. From the graphs it can be seen that during spring, summer and winter there are periods in the day where the wind speed is significantly lower for all altitudes than the rest of the day. Furthermore, it can be noted that this does not happen at the same time for all days. In spring for instance, it can be seen that this period of low wind speed happens late in the evening and night at 0 ° solar longitude, but early in the afternoon for 30 degrees longitude.

Especially in summer it is noticeable that the wind speeds are significantly worse than during the rest of the year with large portions of really low wind speeds and shorter high wind speeds time periods. In autumn however, it can be seen that the wind speeds are relatively high, at some altitudes never dropping below 7 m/s. Finally,

in winter and spring there are some smaller time periods where the wind speeds are very low, however this is largely made up for by large portions of the day with extremely high wind speeds.

To get a better idea of how the wind speed changes with altitude, vertical wind velocity profiles are made. These are shown to indicate some interesting points in time that might not be completely clear when looking at the daily wind velocity profiles shown before. In the graphs below it can be seen that in general wind velocity increases with increasing altitude. However, in Figure 2.14 and 2.15 it can be seen that while altitude increases, wind velocity actually stays fairly constant. Furthermore, in Figure 2.21 and 2.20 it becomes apparent that wind velocity can actually go down with increasing altitude. However, these examples are the minority. In the cases where wind speed does increase with altitude the largest increase is usually made within the first 200 m, after that the increase is only marginal.

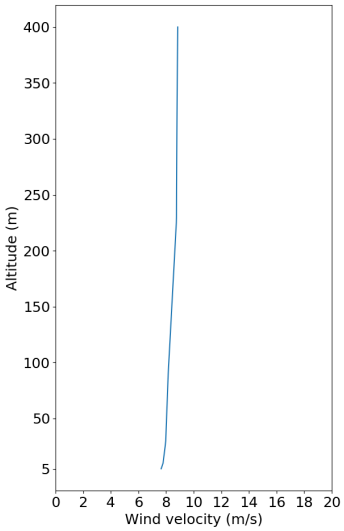

Figure 2.14: Vertical wind profile at solar longitude of 150 degrees and at a local time of 14 hours

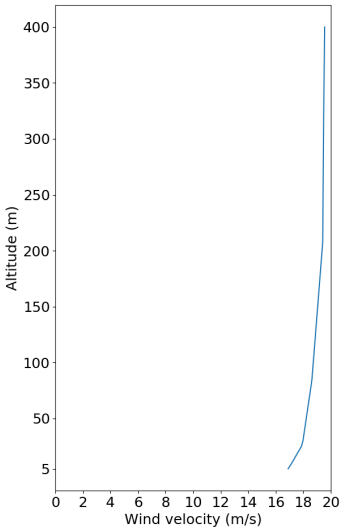

Figure 2.15: Vertical wind profile at solar longitude of 0 degrees and at a local time of 15 hours

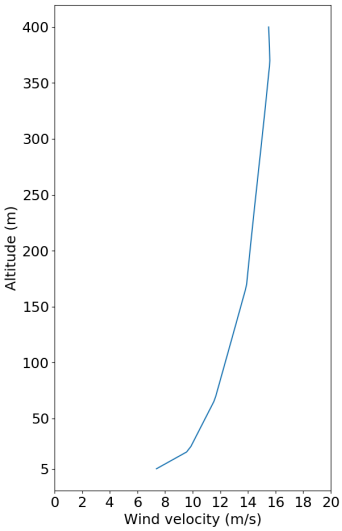

Figure 2.16: Vertical wind profile at solar longitude of 210 degrees and at a local time of 4 hours

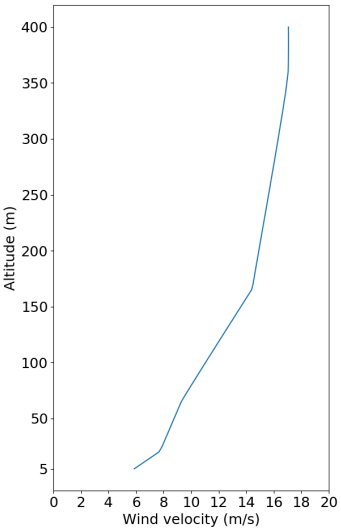

Figure 2.17: Vertical wind profile at solar longitude of 270 degrees and at a local time of 3 hours

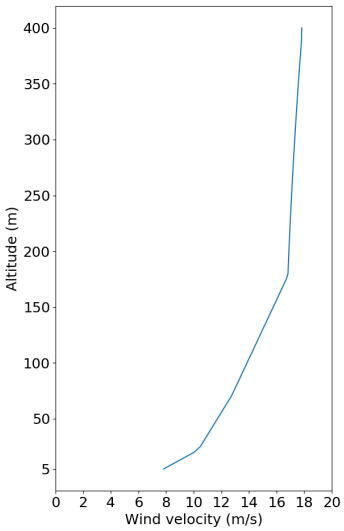

Figure 2.18: Vertical wind profile at solar longitude of 30 degrees and at a local time of 4 hours

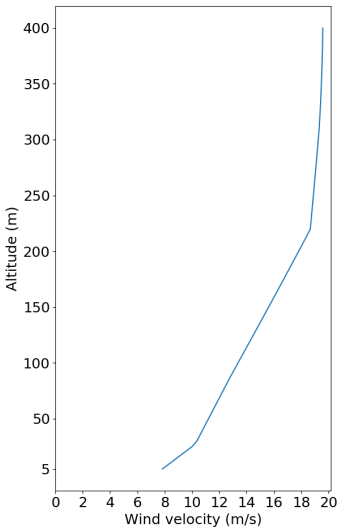

Figure 2.19: Vertical wind profile at solar longitude of 120 degrees and at a local time of 19 hours

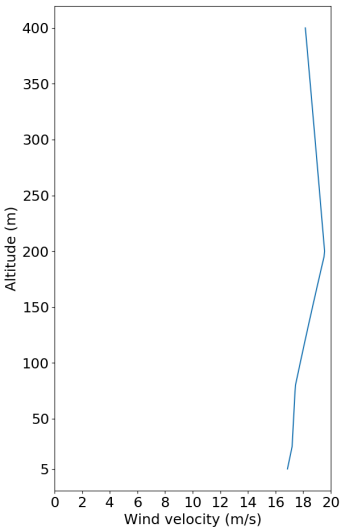

Figure 2.20: Vertical wind profile at solar longitude of 330 degrees and at a local time of 14 hours

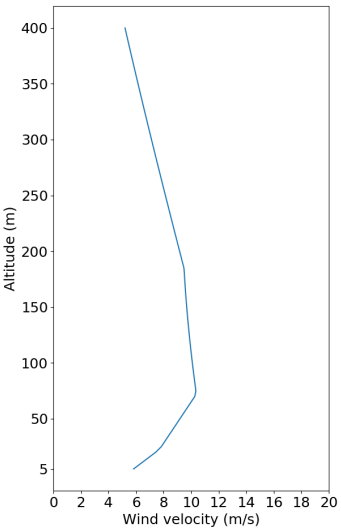

Figure 2.21: Vertical wind profile at solar longitude of 90 degrees and at a local time of 5 hours

2.5.2. Average Wind Speeds

For comparison the average wind speeds are plotted for 8 periods, late spring(0-45), early summer(45-90), late summer (90-135), early autumn (135-180),late autumn(180-215), early winter(215-270),late winter(270-315) and early spring(315-360). The data for these periods are plotted for 4 different altitudes above the surface, 5, 105, 205 and 405 meters and the results can be seen in Figure 2.22 and 2.23. To calculate the average, for 45 days in the season the wind speed is taken at every hour and the desired altitude, then this was averaged. The result of this is a sketch of what the average day in these days would look like.

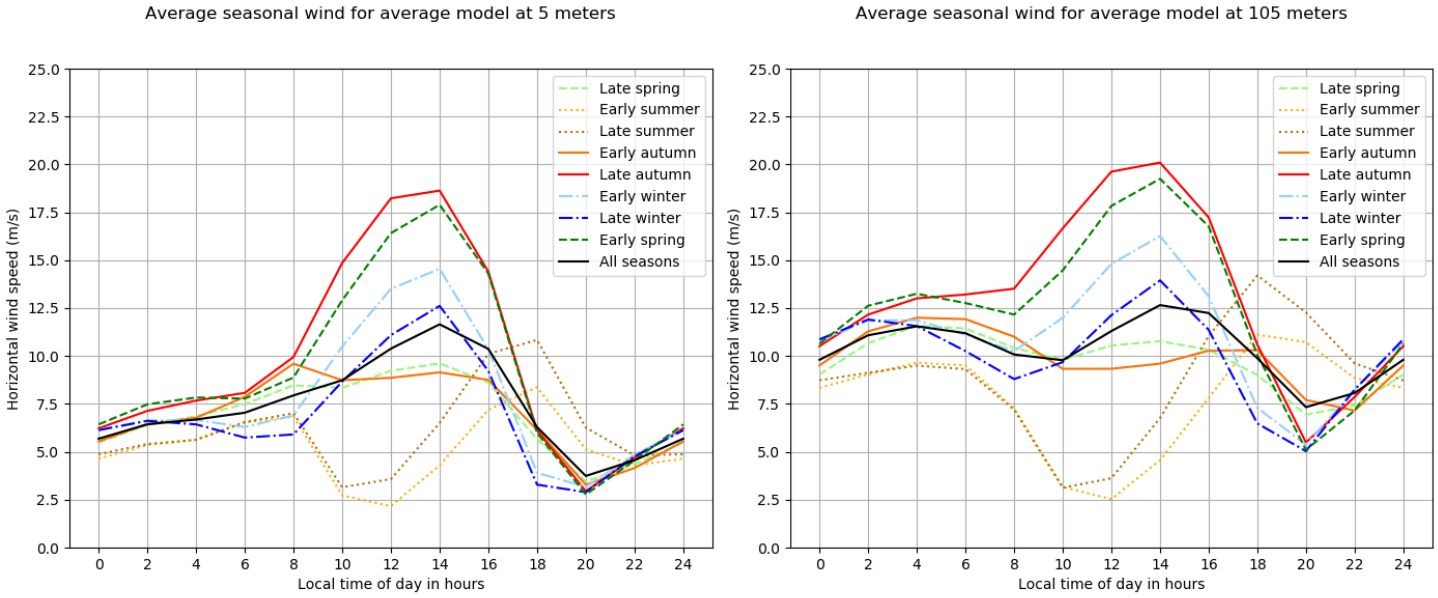

Figure 2.22: Average daily wind speeds at 5 and 105m altitude.

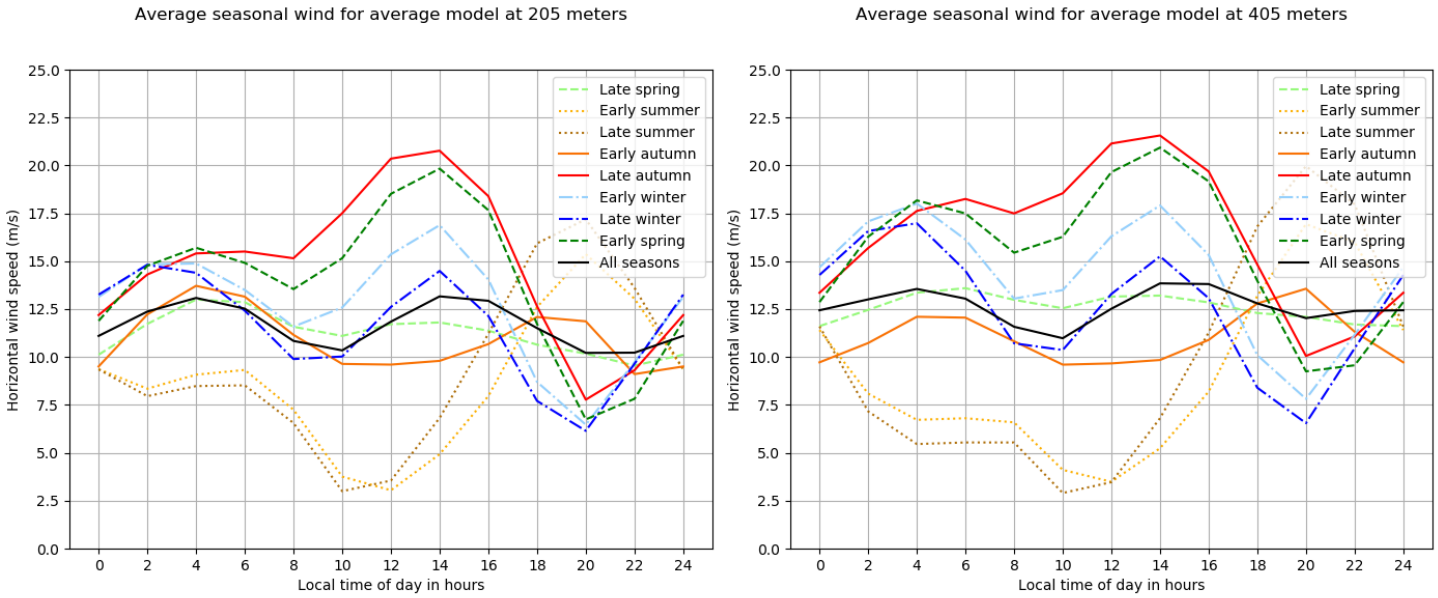

Figure 2.23: Average daily wind speeds at 205 and 405m altitude.

The data used for these graphs is slightly more rough than for the previous analysis, this was done since now 361 days are evaluated, while before only 13 days were evaluated. For the calculations of the average however, the level of detail in the previous analysis was deemed unnecessary.

However, it should be noted that this data should be used carefully, as the minimal wind speeds during periods of the day are averaged out due to the shift in time of the low wind speed periods. This can also be seen in the line of the average velocity of all seasons, which does not see the great deviations that some of the seasons have.

2.5.3. Wind Speed Probability Density

In Figure 2.24 the probability density of the wind speeds can be seen for multiple seasons. The data for these graphs is the same data used to create the averages in subsection 2.5.2, so every season consists of 45 days, each consisting of 21 data points in altitude and 13 data points in time, this gives every density graph a total of 12285 data points. All wind speeds were categorised in terms of magnitude and the fraction of each category was calculated. Finally the result was interpolated to create a smoother graph.

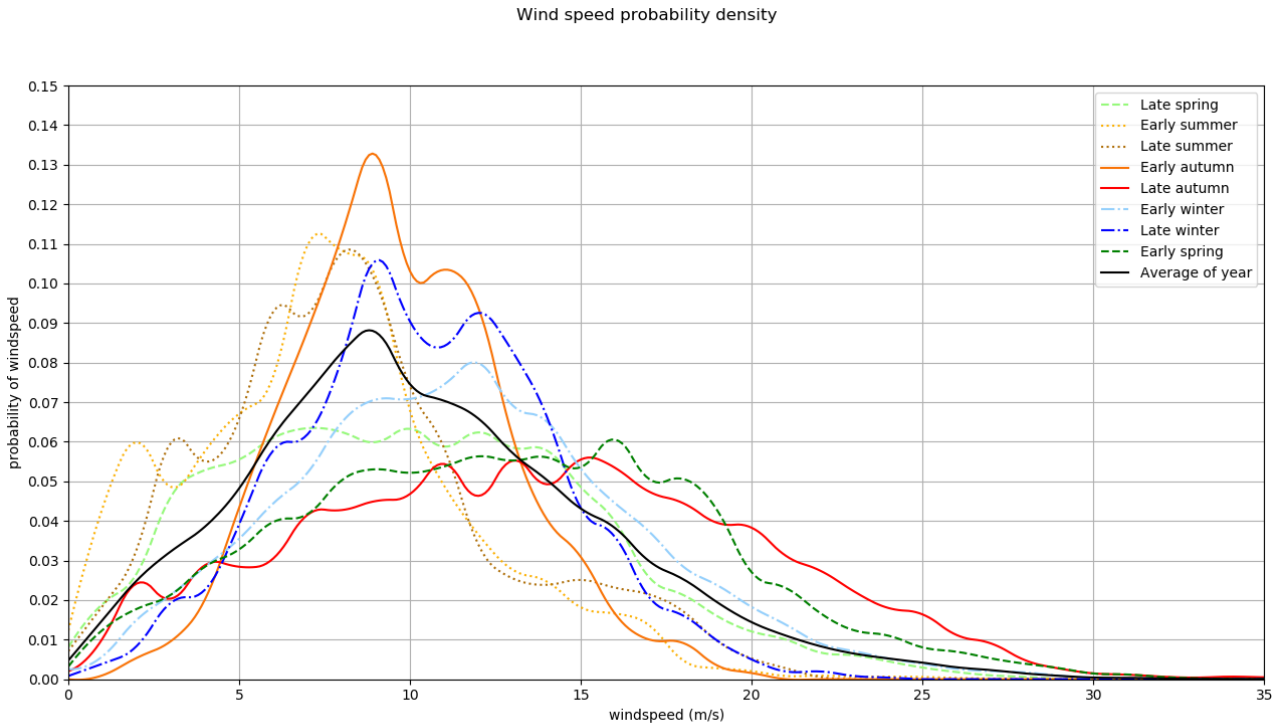

Figure 2.24: Probability density of wind speeds for different seasons

From the plot it can be seen that especially in summer and late spring the wind speed fraction of really low wind speeds (sub 5 m/s) is a lot higher than in the rest of the year, this again indicates that in these seasons there are large portions of time where it will not be possible to fly because the required wind speed to stay in the air is not reached. Late spring however, does not peak at the low wind speeds that summer does, late spring will consistently reach high wind speeds which produce the most power.

Furthermore it can be seen that in early autumn the fraction of really low wind speeds is really small. However, the graph peaks really early which means that the fraction of really high wind speeds is also fairly low and this is actually the part that generates the most power since power production scales with v_w^3.

Another important thing to note is the maximum wind speeds reached. It can be seen that wind speeds of over 25 m/s are reached in almost every season, especially in spring winter and autumn. These extremely high wind speeds can result in a too high force on the tether and the structure, which can lead to catastrophic events.

2.6. Influence on the Subsystems and Operations

These results lead to a few considerations for subsystem design; the most important parameters for operation are, wind speed to be able to fly, cut-out speed and maximum wind speed. From the data presented in this chapter a number of important parameters can be seen. First of is the portion of time that the wing cannot produce power due to too little wind or too high wind. At very low wind speeds, the wing will not produce enough lift to produce a meaningful resultant force while at too high speeds, the aerodynamic force will be exceeding the maximum force that can be sustained by the structure and tether. Additionally, in subsection 2.5.1 it became apparent that especially during summer the wind speeds are relatively low, which means that during the other seasons this deficit needs to be accounted for. This results in the need for high power generation during the seasons when wind is abundant thus resulting in a high peak power generation.

Furthermore, in subsection 2.5.1 it became clear that during almost every season there are periods of time where the wing most likely won't be able to fly due to too little wind speeds. Thus at these times the kite needs

to land. With this many landing and launching operations, a robust landing and launching system must be created. Furthermore, the most power will be generated during periods of very high wind speeds, to make optimal use of these high wind speeds, the system must be able to withstand high aerodynamic loads which leads to a robust structure made of materials with a high strength to weight ratio.

2.7. Verification of Data Acquisition

The data in the MCD is acquired from Fortran subroutines, these subroutines are called in a separate file which creates a text file with the desired outputs. The desired outputs in this case are: solar longitude, local time of day, altitude, horizontal wind speeds (Meridonal and zonal), temperature and density. Two different text files are made, 1 containing 13 different days, once every 30 degrees, with 2000 data points in the day, 80 in altitude and 25 in time. The second text file contains data for 361 solar longitudes (0-360), where every day has 273 data points, 21 in altitude and 13 in time. The first text file contains more data points per day and gives a nice overview of the seasons. The second data file can be used for the performance model where the data for an entire year can be used to determine the yearly power generation.

Thus to check whether the database got the right output, the only thing that needs to be checked is whether or not the text file has the right amount of lines. For the first data file, this needs to consist of 13·80·25 lines, or a total of 26000 lines. The second file needs to consist of 361·21·13 for a total of 98553 lines, both of these are correct.

2.8. Sensitivity Analysis

The data produced by the MCD is generated using a seed to determine the random numbers necessary for the creation of large and small scale variabilities. For this analysis only one seed was used to generate the data. This can have several implications. The fact that random numbers are generated might lead to a result that lies either on the low end or the high end of the possible outcomes. It is also possible that these small scale variabilities only have a marginal impact when looking at large amounts of data such as on a yearly scale, but this has not been investigated. Even so, these small impacts in terms of wind speed, density and temperature could impact the performance of the system. As a recommendation for future endeavors, it is recommended to extend the amount of data gathered from the MCD by taking data for multiple years by changing the seed used for the random number generation.

3

Evaluation of Conceptual Design

In this chapter, the previous design steps taken will be summarized to give some background information on the chosen configuration. First, the current list of requirements will be listed in section 3.1. The requirements are partially provided by the stakeholders and partially determined by the design team, and they will serve as the basis of the design decision which will be presented in detail within this report. Then, in section 3.2, the results of the previously carried out trade-off will be summarized. Finally, in section 3.3, the feasibility study of the conceptual design from the last design phase will be performed.

3.1. Requirements

It is crucial to determine the list of requirements before the design process in order to know the required characteristics and also the constraints imposed on the design space. Below in Table 3.1, the requirements that were derived from the constraints provided to the design team can be found together with some justification to why each requirement was derived.

Table 3.1: Requirements born from constraints and their justifications.

Requirement Index	**Requirement**	**Justification**
CON-LE-01	The AWE system shall adhere to guidelines established by the resolution 2222 (XXI) of 19 December 1966 of the United General Assembly.	This requirement originates from stakeholder requirements as the space organizations are bounded by this law and are key stakeholders in the mission.
CON-LE-02	The mission shall not interfere with other missions that are to be in operation or already in operation.	This requirement originates from stakeholder requirements as conflicts could arise if this were to happen.
CON-CT-01	The production of each one of the AWE systems on Earth shall be less than 500,000 €.	This requirement originates from the risk analysis and stakeholder requirements considering ESA is a stakeholder.
CON-TM-02	A preliminary design of the AWE system shall be provided by 10 students.	This requirement originates from the project specifications, namely the team in charge of this project is composed of 10 students.
CON-SF-02	The AWE system shall not damage the Mars habitat while in operation.	This requirement originates from the risk analysis and stakeholder requirements considering ESA is a stakeholder.
CON-SF-03	The AWE system shall not damage the Mars habitat in case of failure.	This requirement originates from the risk analysis and stakeholder requirements considering ESA is a stakeholder.
CON-SF-04	The AWE system shall not hurt anyone while in operation.	This requirement originates from the risk analysis and stakeholder requirements considering ESA is a stakeholder.
CON-DG-01	The mass of the AWE system shall be less than 200 kg	This requirement originates from the stakeholder needs and is to be complied with.
CON-DG-03	The AWE system shall be designed for a lifetime of 5 Martian years.	This requirement originates from the stakeholder needs and is to be complied with.
CON-DG-04	The AWE system shall fit in a volume of 3 m^3	This requirement originates from the stakeholder needs and is to be complied with.

The requirements can also be born from other sources, such as the environment where the system will be functioning or the required interface between different subsystems and so on. Therefore, it is very important to determine technical requirements with care as well. Below in Table 3.2, the list of technical requirements can be found with their corresponding justifications.

Table 3.2: Technical requirements and justifications

Requirement Index	Requirement	Justification
TEC-AIR-01	The airborne system shall be able to withstand 25 m/s wind gusts.	This requirement originates from a conducted risk assessment on AIR system failure (failure mode 1.1.1a).
TEC-AIR-07	The tether shall withstand 12000 N of tensile force.	This requirement originates from a conducted risk assessment on AIR system failure (failure mode 1.2.1 & 1.2.2).
TEC-AIR-08	The airborne system shall have a cut out speed of 20 m/s during nominal operation.	This requirement originates from a conducted risk assessment on AIR system failure (failure mode 1).
TEC-AIR-09	The tether shall be able to withstand 25 m/s wind gusts.	This requirement originates from a conducted risk assessment on AIR system failure (1.2.1 & 1.2.2).
TEC-AIR-11	The airborne system shall be able to stay airborne at 5 m/s wind speed.	It is desirable to avoid landing and launching procedures as much as possible. Lower wind speed to stay airborne aids this.
TEC-AIR-12	The airborne system shall withstand 3340 cycles of temperature fluctuation from -190°C to 20°C.	The system shall survive the 5 Martian years of operation time without (physical or performance-wise) damage due to temperature fluctuations.
TEC-AIR-13	The airborne system shall withstand $1.7 \cdot 10^7$ cyclic loadings caused by the varying loads during the figure of 8.	The system shall survive the 5 Martian years of operation time without (physical or performance-wise) damage due to temperature fluctuations.
TEC-AIR-14	The canopy of the wing shall deflect less than 0.01 m under aerodynamic loads.	In order to avoid the loss of aerodynamic properties, the deflection of the canopy shall be limited to 0.01 m [6].
TEC-AIR-15	The wing shall twist at most 3.23 degrees throughout the span of the wing.	This requirement follows from an attempt to avoid the loss of aerodynamic properties while simultaneously creating a reasonable distribution of twist. This is further explained in the structural characteristics section (c.f. subsection 7.3.5).
TEC-AIR-16	The wing shall deflect at most 0.5 meter in total throughout the span of the wing.	This requirement follows from an attempt to avoid the loss of aerodynamic properties. This is further explained in the structural characteristics section (c.f. subsection 7.3.5).
TEC-CL-05	The control system shall withstand 3340 Martian temperature fluctuation cycles from -190°C to 20°C.	This requirement originates from a conducted risk assessment on CL system failure.
TEC-GE-01	The generator shall have a 90% average efficiency.	This requirement originates from system operation prerequisites.
TEC-GE-02	The generator shall be able to provide a torque 1000 Nm.	This requirement originates from system operation prerequisites.
TEC-GE-07	The connecting wires shall be able to withstand 3340 Martian temperature fluctuation cycles from -190°C to 20°C.	This requirement originates from a conducted risk assessment on GE system failure (failure mode 4.2.1).
TEC-GE-08	All electric connecting points shall be protected against cyclic loading.	This requirement originates from a conducted risk assessment on GE system failure (failure mode 4.2.1 & 4.2.2).
TEC-PS-01	The power storage system shall have a capacity of 50 MWh.	This requirement originates from system operation prerequisites.
TEC-PS-02	The power storage system shall provide an output of 10 kW.	This requirement originates from stakeholder needs and is to be complied with.

TEC-PS-09	All electric connecting points within the power storage system shall be protected against cyclic loading.	This requirement originates from a conducted risk assessment on power storage system failure (failure mode 4.1).
TEC-PS-10	The voltage of the generator shall be matched to the voltage of the power storage system	This requirement originates from a conducted risk assessment on PS system failure (failure mode 4.1).

3.2. Summary of Trade-off Study

In the previous design phase, several trade-off steps have been taken in order to come up with the conceptual configuration of the system. Table 3.3 below summarizes the results of the trade-off processes that were carried out for each main element in the table.

Table 3.3: Trade-off summary table

System Element	Chosen design option
Wing	Swept flying wing
Control unit	On-ground
Tether	Dyneema
Buffer Storage	Supercapacitor

For the wing, the chosen concept is a semi-rigid swept wing. The choice of a semi-rigid wing was made due to the high power performance it can provide while still staying acceptable in terms of volume and mass budgets. It was also deemed as the most durable choice compared to fully rigid or flexible wing options. Then, to perform a one level deeper trade-off, swept wing and C-kite concepts were compared. The swept wing option was the outcome of this trade-off due to its high power performance compared to the semi-rigid C-kite.

The summary of the trade-off performed for the wing can be seen in Table 3.4. The following trade-off performed to choose the type of semi-rigid wing is also presented in Table 3.5.

Table 3.4: Trade-off table for wing subsystem.

	Power Performance (C_L^3/C_D^2)	Mass (kg/m^2)	Volume	Durability	Cost (€/kWh)
Rigid	297.55	2.5	stiff structure	not very durable	0.07-0.12
Semi-rigid	76.8	0.5	partially foldable	relatively more durable	0.05-0.06
Flexible	78	0.5-0.6	easily foldable	not very durable	0.15

Table 3.5: Trade-off table for semi-rigid wing options

	Power Performance (C_L^3/C_D^2)	Mass	Volume	Complexity
Swept wing	261,04	lightweight structure and materials	partially foldable	new technology
C-kite	76.8	lightweight structure and materials	partially foldable	long history of use

After the wing concept was chosen, a trade-off was done for the control unit. Firstly, the type of control system was traded off between on-ground and off-ground options. The result was the use of on-ground control due to its lower complexity and cost. With this choice, the need of a separate trade-off for the powering of the control unit was eliminated since the actuators will be on ground and can be powered directly from the ground station.

A summary of the control unit trade-off can be found below in Table 3.6.

Table 3.6: Trade-off table for control unit mechanism.

	Drag Contribution	Mass	Design Complexity	Cost
On-ground	low enough	within constraints	simple configuration	cheaper
On-tether	lower than required	within constraints	many additional elements	cheap enough

The third step was to choose the tether for the power generation and also for the controls. After comparing several materials, Dyneema came out as the best option. The final configuration was determined to consist of one main tether for power generation and two control tethers connected to the tips of the wing. The summary of the tether trade-off can be seen below in Table 3.7.

Table 3.7: Trade-off table for tether choice [7] [8]

	Specific Strength [GPa/(g/cm^3)]	Fatigue strength	Yield stress [GPa]	Critical Temperature ° C	Cost (€/kg)
Dyneema (UHMWPE fiber)	2.99 - 3.87	Creep:good, Abrasion: excellent	2.9 - 3.75	-150	38.9 - 54.3
Zylon (PBO fiber)	3.69 - 3.74	Creep: excellent, Abrasion: bad	5.68 -5.8	-60	118 - 189
Vectran (Polyarylate fiber)	2.07 - 2.28	Creep: excellent, Abrasion: excellent	2.9 - 3.2	-80	30.7 - 38.9
Titanium Beta-C alloy	0.17	Creep: good, Abrasion: good	0.825	890	-

Lastly, the short term buffer storage for the continuous functioning of the AWE system was traded-off. Among a flow battery, supercapacitor and flywheel concepts, the supercapacitors were evaluated as the best option due to their high power density and efficiency along with being safe and having a wide operational temperature range. The summary of the buffer storage trade-off can be seen below in Table 3.8.

Table 3.8: Trade-off table for the buffer storage subsystem.

	Reliability (4)	Durability (5)	Mass (4)	Volume (3)	Performance (5)
Vanadium Redox Flow Battery	Meets requirements	Meets requirements	Somewhat heavy	Meets requirements	Low performance
Supercapacitor	Meets requirements	Meets requirements	Meets requirements	Takes up more volume than preferred	Good performance, meets requirements
Flywheel	Somewhat unreliable	Very reliable, exceeds requirements	Meets requirements	Takes up more volume than preferred	Underperforms

The configuration that consists of these chosen concepts will be presented in chapter 4 after the feasibility study in section 3.3 in case changes are required if some design choices turn out to be non-feasible.

3.3. Feasibility Analysis

Before moving onto the next design phase where more detailed design decisions will be made, the current design should be checked for feasibility. In order to do this, the configuration resulting from the trade-off process will be evaluated. In the previous design step [9], the performance of the system's conceptual sizing was evaluated using the following parameters.

Table 3.9: Constant parameters for performance analysis.

Parameter	Value	Unit
Wing mass	30	kg
Wing area	50	m^2
Tether drag coefficient	1	-
Tether length	400	m
Tether diameter	3	mm
Tangential wing speed	120	m/s
Atmospheric density	0.0146	kg/m^3

In order to deem the system feasible, these numbers should be checked. First of all, the wing mass over area ratio should be considered. The parameters above suggest a wing with 0.6 kg per square meter. Looking at existing systems with similar configurations such as Enerkite [1], it is seen that this ratio is about 2.5 kg per meter square. It is expected that a lower value than 2.5 is going to be achieved considering the low atmospheric density and low gravitational acceleration. Moreover, more effective design and production methods are expected to be available considering it is a space application which will be built in about 10 years from today. However, a decrease of 76% is a significant assumption, and therefore it is likely that the wing will weigh heavier than

[1] https://www.enerkite.de/en/ [Accessed on May 7, 2021.]

30 kg. Yet, this is not a risk that would make the configuration unfeasible. The system is expected to produce enough power even with a heavier wing. On the other hand, this is likely to cause the mass budget not to be met. At this point, the design team decided to prioritise the power performance of the system, and the mass budget issue will be evaluated again later when the design is finalised.

The second element to be checked after the wing is the tether. Two main reasons that would make the chosen configuration unfeasible are the wing or tether breaking due to the forces acting on them. Considering the 3 mm thickness, the tether can carry a force of 6.6 kN. With some back of the envelope calculations, a maximum lift force of 6 kN is expected using a lift coefficient of 1.2 for the wing. These values show that the tether will be able to carry the load exerted on it due to lift generation. Another point in operation where the force on tether gets to a significant point is the turns during the wing's trajectory. An estimated force of 6 kN on the tether is enough to sustain a turn with a radius of 100 m and a banking angle of 45 degrees. It is possible to decrease the force by either increasing the banking angle or the turn radius. The turn radius of 100 m is above the average found for existing Earth-base systems, but again due to the low atmospheric density and low gravitational acceleration, it is feasible to have a bigger turn radius. This is due to the fact that the increase in tether length will not affect the system as adversely as it does on Earth. It is also expected that the structure of the wing can be made strong enough to survive the inertial loads experienced by it during the turns. Especially the points of connection for the main tether and control tethers will be designed with special attention to make sure of sufficient strength.

All in all, with the current fund of knowledge of the design team, these preliminary numbers are not found unfeasible, and therefore the next design phase will be continued with the chosen configuration.

4

System Configuration

In this chapter the configuration of the system will be presented to set a foundation to the design process, along with the market analysis and resource allocation. In section 4.1, the layout of the system that resulted from the trade-off study as explained in section 3.2 will be visualised. Then, the functional analysis will be carried out section 4.2. This analysis is also aimed at creating a meaningful basis for the design process.

4.1. System Layout

Now that the conceptual design is evaluated and the feasibility of the configuration is verified, the system layout can be described in this section. Below in Figure 4.1, the visualised layout of the system can be seen.

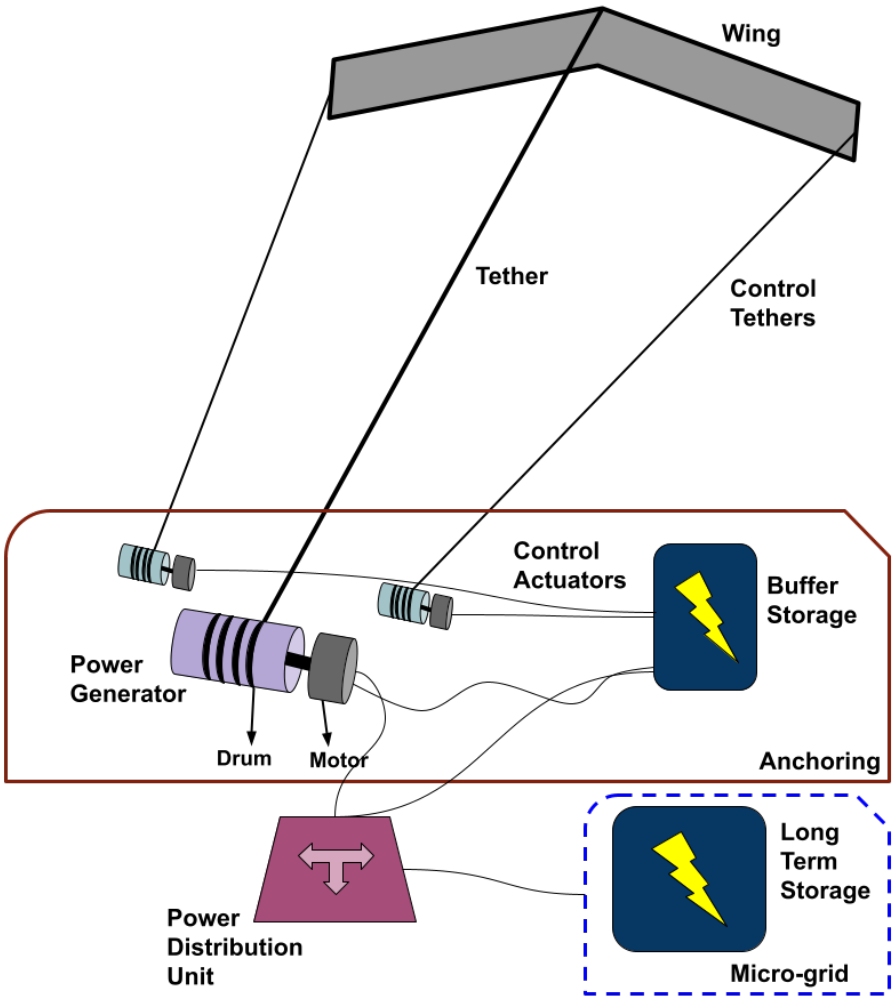

Figure 4.1: System layout of AWESOM.

As expressed in the figure, the system generates power via the lift force generated by the swept wing and the tether that is connected to the generator. The wing is controlled with two control tethers, connected to one actuator each.

4.2. Functional Analysis

This section will present the functional breakdown structure in subsection 4.2.1 and the functional flow diagram in subsection 4.2.2 of the airborne wind energy system which encompass the various work packages and in what order they will be executed.

4.2.1. Functional Breakdown

The Functional Breakdown Structure (FBS) explores the six stages of the life cycle of the AWE system and lists the important processes and operations that are part of its mission. The Functional Breakdown can be found in Figure 4.2. The mission phases identified in the FBS are discussed here-after:

- **Production on Earth:** During the production on Earth it is necessary to make all the parts of the system that cannot be produced on Mars. This includes all the electronics, light weight structures and the motor. In fact, only the low-performance parts such as the anchoring system and shielding for electric components can be produced on Mars, since the tensile strength of martian regolith is not very high. In the production process, it is necessary to source the materials, transport them to the correct facilities, manufacture parts. Besides, it is necessary to test and inspect all the parts in order to identify deficiencies and manufacture new ones if such are discovered. After that, the parts are transported to the assembly facility and assembled. Lastly, they are packaged for transportation to the launcher.
- **Transportation** covers all the stages of the parts that are manufactured on Earth from being transported from the assembly and packaging station to the installation site on Mars. First of all, they are shipped to the launcher which delivers them to an orbit around Mars. After that, a special lander transports them to the martian surface. The transportation from Earth to Mars will partially be designed by the Design Synthesis Exercise Group 7, tasked to work on the project entitled *Space Transportation Segment for project MARCH (Martian Autarkic Research and Colonization Habitat)*. Lastly, the robots or the astronauts put them in a vehicle that transports them to the installation site.
- **Production on Mars** involves making all the parts that can be created from martian regolith, most likely, by the method of 3D printing, as this technology can be assumed to be available with the Rhizome project. These parts are then shipped to the installation site. Lastly, the parts must be inspected for damage in case the transportation caused any issues, if so, repairs/replacements must be carried out.
- **Installation** on Mars starts with the astronauts examining all the parts for damage. If everything is in order, they can go on to assembling the subsystems and then systems. Afterwards, the airborne system shall be tested to assess its integrity. If it does, the AWE system can be connected to the grid and start providing electricity to the Martian habitat.
- **Operation on site** consists of several processes. The system has to convert the wind energy to electrical energy, supply it to the long-term storage and short-term storage and transfer energy to the grid. The system will feature monitors to share its health status and receive information about the weather conditions to go into a safe mode if a storm is approaching. As detailed in the FBS, it is also necessary to do some maintenance procedures in order to replace broken details or patch the damaged parts.
- **Performing end-of-life procedure** is the final phase of the mission. First extension of the mission should be evaluated as this relates to the sustainability requirement of this project. If the power system is in acceptable condition, it might be decided to keep using it for a longer time than initially expected with repairs or replacements where necessary. If life extension is not done, or after the extended period of life extension, the system shall be decommissioned. For each part of the system, it will be decided if they can be reused, recycled, up-cycled or disposed of.

4.2.2. Functional Flow Diagram

Next to the functional breakdown diagram, a Functional Flow Diagram (FFD) is provided in Figure 4.3. The FFD shows the chronological sequence of the different tasks that are to be completed from production to end-of-life of the AWE system. The mission states are further split over different levels: The top level shows the main mission phases of the system. Going further down the levels, each task is split into various sub-tasks. Conditional statements such as IF, AND and OR are used to indicate the flow of the mission sequence. In the FFD, IF statements are used to identify different scenarios, providing the condition to be fulfilled on the arrow connecting elements. AND statements indicate that all tasks are to be completed simultaneously. Finally, OR statements are used to identify distinct scenario the AWE system shall encounter.

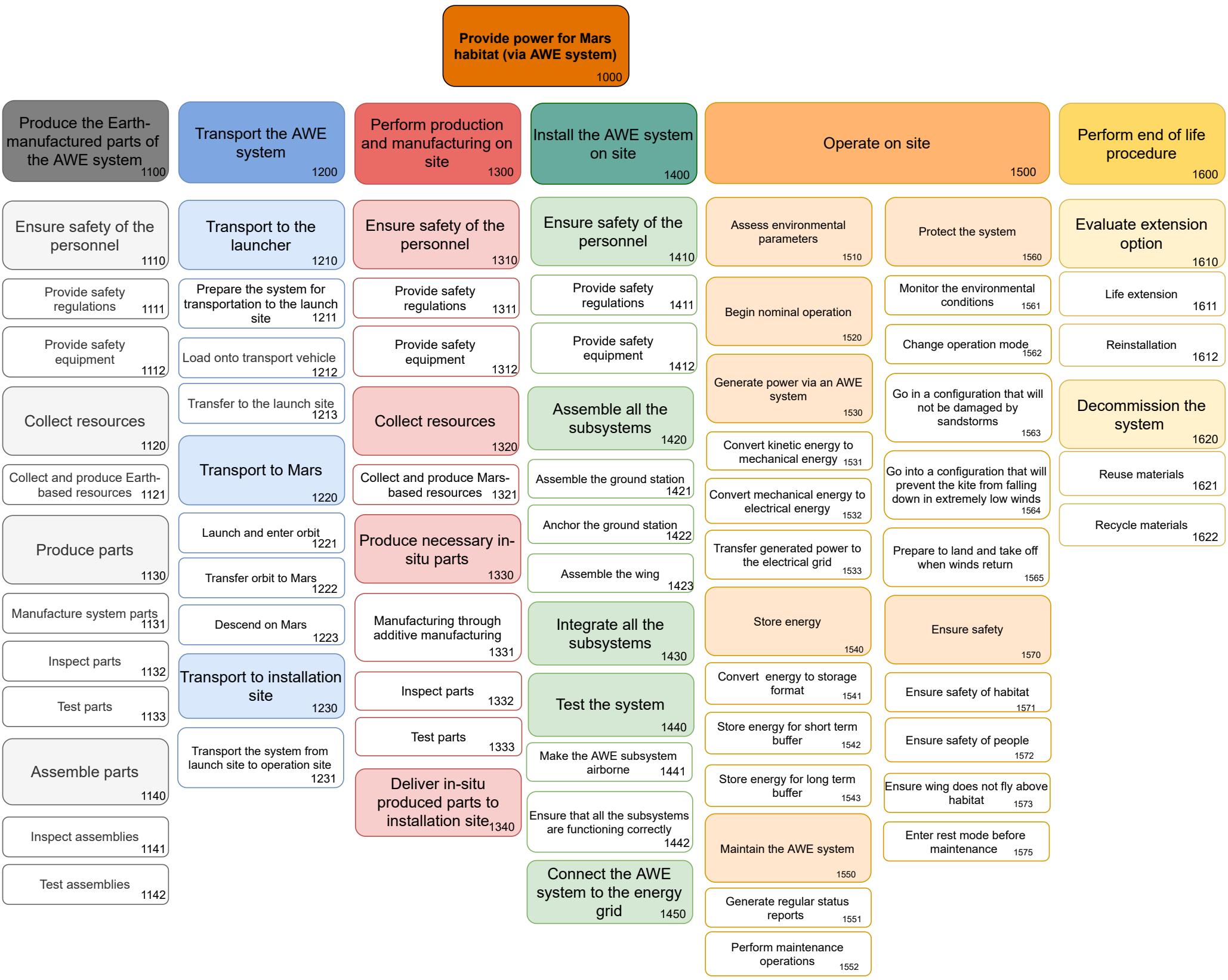

Figure 4.2: Functional Breakdown Structure

Produce the Earth-manufactured parts of the AWE system
1100
Transport the AWE system
1200
Perform production and manufacturing on site
1300
Install the AWE system on site
1400
Perform end of life procedure
1600
Operate on site
1500
Ensure safety of the personnel
1110
AND
Provide safety regulations
1111
Provide safety equipment
1112
Collect resources
1120
Collect and produce Earth-based resources
1121
Produce parts
1130
Manufacture system parts
1131
Inspect parts
1132
IF
Test parts
1133
IF
Assemble parts
1140
IF
Inspect assemblies
1141
IF
Test assemblies
1142
Transport the AWE system
1210
Prepare the system for transportation to the launch site
1211
Load onto transport vehicle
1212
Transfer to the launch site
1213
Transport to Mars
1220
Launch and enter orbit
1221
Transfer orbit to Mars
1222
Descend on Mars
1223
Transport to installation site
1230
Transport the system from launch site to operation site
1231
Perform production and manufacturing on site
1300
Ensure safety of the personnel
1310
AND
Provide safety regulations
1311
Provide safety equipment
1312
Collect resources
1320
Collect and produce Mars-based resources
1321
Produce necessary in-situ parts
1330
Manufacturing through additive manufacturing
1331
Inspect parts
1332
IF
Test parts
1333
IF
Deliver in-situ produced parts to installation site
1340
Install the AWE system on site
1400
Install the AWE system on site
1400
Ensure safety of the personnel
1410
AND
Provide safety regulations
1411
Provide safety equipment
1412
Assemble all the subsystems
1420
Assemble the ground station
1421
Anchor the ground station
1422
Assemble the wing
1423
Integrate all the subsystems
1430
Test the system
1440
Make the AWE subsystem airborne
1441
IF
Ensure that all the subsystems are functioning correctly
1442
IF
Connect the AWE system to the energy grid
1450
Operate on site
1500
Operate on site
1500
Assess environmental parameters
1510
IF
Safe to operate the AWE system
Begin nominal operation
1520
Generate power via an AWE system
1530
Convert kinetic energy to mechanical energy
1531
Convert mechanical energy to electrical energy
1532
Transfer generated power to the electrical grid
1533
Store energy
1540
Convert energy to storage format
1541
AND
Store energy for long term buffer
1543
Store energy for short term buffer
1542
Maintain the AWE system
1550
Generate regular status reports
1551
OR
Perform maintenance operations
1552
OR
Protect the system
1560
Monitor the environmental conditions
1561
Change operation mode
1562
Go in a configuration that will not be damaged by sandstorms
1563
OR
Go into a configuration that will prevent the kite from falling down in extremely low winds
1564
Prepare to land and take off when winds return
1565
Ensure safety
1570
AND
Ensure safety of habitat
1571
Ensure wing does not fly above habitat
1573
No flying in uncontrolable conditions
1574
AND
Ensure safety of people
1572
Enter rest mode before maintenance
1575
No flying in uncontrolable conditions
1576
AND
Perform end of life procedure
1600
Safe to enter nominal operation
IF
OR
Perform predictive maintenance on the system
1582
Wait for bad flying conditions to pass
1584
Land the wing
1581
Put wing into parking orbit
1583
Place the AWE system into safe-mode
1580
L.life extension
1611
Relinstallation
1612
OR
Evaluate extension options
1610
Perform end of life procedure
1600
Decommission the system
1620
AND
Reuse materials
1621
Recycle materials
1622

Figure 4.3: Functional Flow Diagram

5
Market Analysis

This chapter identifies and analyses the analysis of the markets involved in the AWESOM project. Firstly, the key stakeholders are listed in section 5.1. Then, the target market together with its growth opportunities will be described in section 5.2. The level of competition will also be touched upon, in section 5.3. Consequently, the SWOT analysis will be presented in section 5.4. The market analysis also serves the the design process by giving a deeper understanding on how certain requirements are driven by the market, which will be elaborated upon in section 5.5.

5.1. Key Stakeholders

The key stakeholders are individuals or organisations that are not only impacted by the project but also has some authority over it. In order to design a system to meet all the desired requirements, it is essential to identify all the key stakeholders involved in the mission so that the proposed design can consider the benefit of these involved parties. For AWESOM, the following key stakeholders have been identified:

- **ESA:** As the project aims at providing an airborne wind energy system capable of covering the energy usage of the Martian habitat part of the Rhizome project, ESA is an important stakeholder for the design of the AWE system.
- **TU Delft:** This project is part of the AE3200 Design Synthesis Exercise course, provided at TU Delft during the third year of the BSc Aerospace Engineering. Therefore, TU Delft is a key stakeholder in this project. In fact, high level requirements were provided by the supervisor, Dr.-Ing. Roland Schmehl, at the start of this project and shall be complied with by the proposed designed.
- **Political Stakeholders:** A Political Stakeholder is a person or group who has an interest or a stake in the government or public affairs of a countryn[1]. In the AWESOM project, the various governments part of ESA as well as their respective space agencies are all considered to be the Political Stakeholders.
- **Other Stakeholders:** This includes various individuals who are directly or indirectly involved during the course of the mission. This includes: astronauts and engineers. It is essential to maintain their safety and health during the design phase of the mission.

5.2. Target Markets and Growth Opportunities

The markets catering to the AWESOM projects are the space exploration and renewable energy sectors. In the past few decades, there has been a growing number of people and organizations ushering in the era of renewable energy to prevent further damage to the Earth and the environment. Recently, the applications of these technologies are starting to be implemented in the space sector as well.

As the need for decarbonization in energy production is becoming more and more urgent, the renewable energy sector is steadily growing. In 2017 the worldwide renewable energy market value was valued at 928 billion US dollars and is expected to grow to 1.5 trillion US dollars by 2025[2]. Furthermore, it is projected that in 2021 the total share of energy produced by renewables will be 30%, their highest share since the industrial revolution[3]. One of the fastest growing renewable energy sectors is the wind energy. This is mostly due to the steady decline of its costs, and it is now being considered more cost competitive than even the new fossil fuel power plants[4]. Although this report will focus on energy generation on Mars, new innovations on Earth-based wind energy sector will still be greatly beneficial to the development of an AWE system on a different planet.

The space exploration industry is a small subset of the global space economy. This is due to the fact that it is a new industry and only a handful of companies are able to meet the desired requirements to compete with each other. In order to make the space exploration industry grow faster and in a sustainable fashion,

[1] https://www.stakeholdermap.com/political-stakeholders.html[AccessedonJune5,2021]
[2] https://www.alliedmarketresearch.com/renewable-energy-market [Accessed on May 27, 2021]
[3] https://www.iea.org/reports/global-energy-review-2021 [Accessed on May 27, 2021]
[4] https://www.grandviewresearch.com/industry-analysis/wind-power-industry [Accessed on June 3, 2021]

implementing existing technology on Mars to support a future habitat would be the cornerstone of the process. This is where the AWESOM project catalyse the process by making use of the wind energy present on Mars to supply electrical power to a future colony. A key factor to ensure the project is economically feasible is by minimizing the total cost of designing, constructing and transporting the system while using sustainable development strategies in the process. If successful, it would attract more individuals and organisations into space explorations as well as provide a partial solution to space colonization. By becoming a multi-planetary species, the chances of the human race surviving future calamities are increased. However, if the project is unsuccessful, it would provide valuable insights in preventing future missions from suffering the same.

5.3. Competition

Rhizome project is not alone in planning a human habitat on Mars. Therefore, AWESOM is not going to be the on project working on how to power a potential human planet on Mars, leading to some competition in the market. Some competitors include but are not limited to:

- **NASA:** NASA has been sending scientific instruments to study other celestial bodies for decades. The Mariner 9 was launched successfully on May 30, 1971[5]. and became the first artificial satellite of Mars when it arrived and went into orbit. Ever since then, NASA have made gradual progress over time in understand Mars and the strategies to colonise it. Even though they do not have an active project on airborne wind energy on Mars, they are a potential competitor in this field due to their objectives and experience.
- **Tekniker:** The Tekniker technology centre will lead the HORACE project whose ultimate goal is to develop the first-ever wind turbine generator to be used in the future on Mars as a secondary power source. Therefore, they qualify as a competitor to AWESOM in terms of harnessing the wind energy on Mars.
- **SpaceX:** SpaceX Mars program is a development program initiated by Elon Musk and SpaceX in order to facilitate the eventual colonization of Mars. SpaceX's aspirational goal has been to land the first humans on Mars by 2024, but in October 2020 Elon Musk named 2024 as goal for an uncrewed mission[6]. In order to power the future colonies, renewable sources of energy will most likely be utilized in the form of AWE systems.
- **Skysails:** SkySails is a Hamburg-based company that sells kite rigs to propel cargo ships, large yachts and fishing vessels by wind energy. Ships are pulled by an automatically-controlled foil kite[7]. Although SkySails is an Earth-based company, it uses a very similar power generation technique used in the AWESOM project.
- **Other ground-based AWE projects:** Several universities and small organisations involved in utilizing AWE system are still in their infancy and are yet to become fully commercial. Some of these include: University of Freiburg, TU Hamburg, and the UpWind Project by The University of Porto.

5.4. SWOT Analysis

The SWOT Analysis in Figure 5.1 is used for planning the design phase of the mission to help the group identify their strengths, weaknesses, opportunities and threats. This gives the group an overview of factors involved when taking decisions or performing an action.

The strengths and opportunities are internal and external elements respectively that contribution to the achievement of the mission goal. On the other hand, the weaknesses and threats are harmful for the achievement of the mission goal, internally and externally. Internal elements are related to the organization where the external elements relate to the environment.

[5]https://mars.nasa.gov/mars-exploration/missions/mariner-8-9[Accessed on June 5, 2021]
[6]https://en.wikipedia.org/wiki/SpaceX_Mars_program [Accessed on June 5, 2021]
[7]https://en.wikipedia.org/wiki/SkySails [Accessed on June 5, 2021]

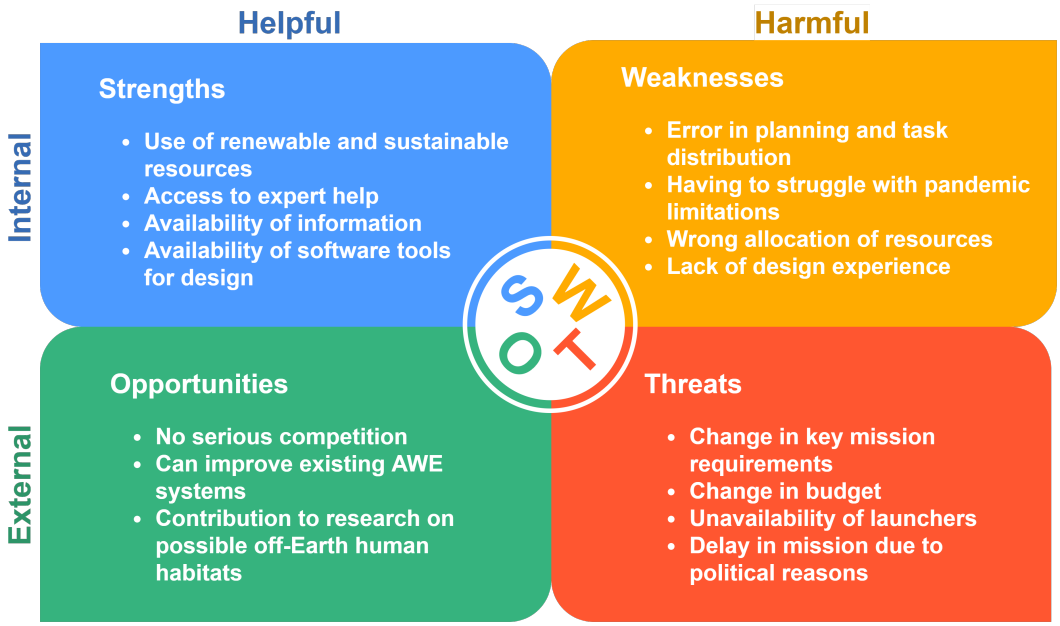

Figure 5.1: SWOT analysis for AWESOM.

5.5. Requirements Driven by Market Analysis

Once the stakeholders and markets are identified, the requirements imposed by the external sources have to be considered. These requirements are listed as follows:

- **CON-LE-01:** The AWE system shall adhere to guidelines established by the resolution 2222 (XXI) of19 December 1966 of the United General Assembly.
- **CON-CT-01:** The production of each one of the AWE systems on Earth shall be less than 500,000€.
- **CON-DG-02:** The mass of the AWE system shall be less than 200 kg.
- **CON-DG-03:** The AWE system shall be designed for a life-time of 5 Martian years.
- **CON-DG-04:** The AWE system shall fit in a volume of 3 m^3.

The justifications used to formulate the requirements stated above have been mentioned in Table 3.1.

6

Resource Allocation

In this chapter the resources used for the Airborne Wind Energy System are allocated. First, in section 6.1, the technical resources are allocated. Then, in section 6.2, the non-technical resources are defined and allocated.

6.1. Technical Resource Allocation

To start the resource allocation, first the subsystems and the resources have to be defined. In the baseline report ([10]) a preliminary resource allocation was already made. This was updated, by specifying more subsystems for a more accurate resource allocation. Please note that the resource allocation provided in this section serves as a guideline for the preliminary characterisation of the system. This resource allocation is thus subject to change as a more refined design is developed. The updated resource allocation can be seen in Table 6.1:

Table 6.1: Resource allocation

Subsystem	**Mass, kg**	**Volume, m^3**	**Cost, €**
Wing	30	0.6	50,000
Tether, control tethers and drum	20	0.06	50,000
Control unit	20	0.15	62,500
Power generator	30	0.3	75,000
Ground station structure and housing	10	0.6	37,500
Buffer storage	24	0.06	37,500
Launch system	6	0.15	37,500
Spare parts	60	1.08	150,000
Total	200	3	500,000

6.1.1. Wing

As found in the midterm report [9], the area of the wing is to be 50 m^2, to be able to generate enough lift and enough power. Using the density of nylon, and adding some weight for the wing box and the ribs, a preliminary weight estimate of 30 kg was made. Thus, this value was used for the resource allocation as well. It should be noted, however, that this estimate is very optimistic and further research should be conducted on the feasibility of such a light wing. Further, although the wing is has a very large volume at 50 m^2, it would for the most part encompass a lot of gas. Thus, it would be able to be folded up very tightly, allowing it to fit in a much smaller volume. This volume was estimated to be 0.6 m^3.

6.1.2. Tether, Control Tethers and Drum

The specifications of the tether and the control tethers were already found in the midterm report [9]. The volume can be calculated using the strength of Dyneema, the material chosen for the tether and the control tethers. Assuming that five spare tethers will be used, the diameter was found to be 3.32 mm. Assuming that the maximum length of the tether that could be chosen is 1000 m, the volume can be calculated to be 0.009 m^3. The same can be done for the control tethers: assuming ten spare control tethers, the diameter was found to be 1.37 mm. Thus the control tether volume would be 2 x 0.0015 m^3. Consequently, the total volume used by the tether and control tethers was found to be 0.012 m^3. Furthermore, using the density of Dyneema, the mass was found to be 10.9 kg for the main tether and 2.3 kg per control tether, totalling a total mass of 15.5 kg.

To size the drum, the D/d ratio was used. Again, looking at the midterm report [9], a D/d ratio of 100 was to be used. Thus, the diameter of the main drum would be 100 times larger than the main tether diameter, which results in a drum diameter of 0.228 m.

The final volume allocation for the tether, control tethers and drum is 0.06 m^3. This is enough to store everything including a safety factor. The mass allocated equals 20 kg, which is enough to include both the tether and the control tethers, leaving 4.5 kg for the drum.

6.1.3. Control Unit

The mass of the control unit was assumed to be similar to current Earth based kite control units, such as the one used in the Kitepower Falcon 100 kW[1]. Even though this system is able to provide about ten times more power than required for this project, keeping its components in mind, it is expected to have a similar mass. This control unit consists of motors for steering and an on-board wind turbine to power the electronics on it, and has a mass of 23 kg. As the control unit was traded-off to be placed on-ground, as summarised in chapter 3, it is safe to assume that a mass budget of 20 kg for the control unit shall be achievable. In fact, as the control unit will be placed on-ground, there is no need for power generation system on the control unit (e.g. wind turbine generator), leading to a lighter design. Regarding the control unit volume, 0.25 m^3 was assumed in the baseline report [10]. However, this estimate was considered larger than necessary based on the conceptual design of the AWE system. The control unit volume allocated was therefore lowered to 0.15 m^3. Namely as the control unit will not be airborne anymore, it shall not require any padding or protective shielding against drop-damage, thus reducing its volume.

6.1.4. Power Generator

Looking at existing generators that are currently being used in for example electric cars or professional multi-copter, references can be found for the generator of the Airborne Wind Energy system. Sizing for a power output of around 30 kW, generators with a mass of around 20 to 30 kg were found. This was then reflected in the mass allocation. The allocated volume for the generator is 0.3 m^3. Although generators widely vary in size, 0.3 m^3 was expected to fit the generator.

6.1.5. Ground Station

The ground station subsystem includes the housing of the ground-based subsystems along with the load bearing structure and the anchoring. This would have to weigh quite a lot, and take much of the volume in the rocket. Thus, it was decided that most of the ground station parts will be manufactured on Mars, and thus would not need to be taken into account in the mass budget. These parts include much of the general structure and shielding. The only part that would need to be transported from Earth, and thus would be included in the resource allocation, is the load-bearing structure of the ground station. As this structure would have to be strong enough to carry the majority of the loads induced by the kite and tether, it cannot be manufactured on Mars.

6.1.6. Buffer Storage

From the midterm report ([9]) the required capacity for the buffer storage was found to be 347.2 Wh. This was found assuming a reel-in time of 75 seconds and a reel-out time of 120 seconds. Using the power needed during these phases, and considering the efficiencies, the total needed capacity could be found. To find the required mass and volume of the supercapacitor, its specific energy (Wh/kg) and its energy density (Wh/L) could be used. These were found to be 9 Wh/kg and 8 Wh/L respectively. This then leads to a buffer storage volume of 0.0434 m^3 and a mass of 38.6 kg. In the allocation table it can be seen that the allocated volume for the buffer storage equals 0.06 m^3. This is slightly more than required as a safety factor is applied. The allocated mass, however, is less than what we found in the midterm report. Due to the limited amount of mass available to allocated, more mass could not be allocated to the buffer storage subsystem. Thus, it will be crucial to reevaluate the specific energy of the supercapacitor, and the power generation efficiencies to allow for a lower required capacity.

6.1.7. Launching and Landing System

The launch system structure has not yet been evaluated in detail, however the use of in-situ resources to produce its primary structure was envisioned during the baseline and midterm phase. The anchoring system and other complex parts of the launching and landing system would be produced and transported from Earth. The structural components, however, can and should be manufactured on Mars. The mass and volume budgets allocated for this system is lower than the ground-station one as less equipment shall be produced on Earth.

6.1.8. Spare Parts

The spare parts subsystem is allocated the most mass and volume out of all the subsystems. This is due to the fact that it is assumed that at least one extra kite, along with multiple extra tethers, and other more general spare parts will be required to be transported from Earth. Thus, the total mass and volume needed should show this.

[1] https://kitepower.nl/resources/product/New%20Powerful%20Ways%20-%20The%20Kitepower%20Falcon%20100kW.pdf [Accessed on May 27, 2021]

6.1.9. Cost

To allocate the production costs of the previously mentioned subsystems, due to limited knowledge on this aspect, it was assumed that the most expensive part sent to Mars would be the spare parts. In fact, as those were assumed to comprise an extra wing, multiple back-up tether and other extra parts, it is safe to assume that the cost of spare parts would be higher than the two subsystems combined.

From the remaining budget available, it was assumed that the power generator subsystem would be the second most expensive as it is an heavy, complex and essential system that cannot be manufactured on Mars. For the same reason, the control unit is ranked third in the production cost allocation, it would require complex and precise electronics and is expected to be smaller than the power generator. Besides, the wing and tether-control tether subsystems were allocated 50,000 € each as they are primary subsystems, yet assumed less complicated to produce, hence less expensive.

Finally, the three remaining subsystems, namely the ground station structure, the buffer storage and the launch system were allocated the remaining part of the budget. This decision was taken as those subsystems are either less complex or smaller than the previously stated subsystems.

6.2. Non-Technical Resource Allocation

The non-technical resource allocation is related to the identification and distribution of organisational aspect over the life-time of the AWE system. For this project, the main non-technical resources are defined as follows:

- **People:** People relates to the human resources required for the project to be completed. Namely, this category includes the personnel required to oversee, design, build, maintain and operate the AWE system. The human resources expected can be further detailed as follows:

  – **Management (MNG):** Managers are required to oversee the whole mission, as well as managing the different departments.

  – **Engineering (ENG):** Specialist in various fields of engineering are required for several stages of the mission, namely to develop, design, test and validate the AWE system.

  – **Manufacturing (MAN):** Specialist in product design and manufacturing would also be required in order to produce the system based on the specifications from the engineers.

  – **Installation (INS):** Installation refers to the personnel required to install the system on its operation site.

  – **Operation (OPE):** Operation relates to the personnel required to operate the system. Their main task would be to perform maintenance.

- **Time:** Time is another important non-technical resource. In fact, one of the three dimension system engineering is time, as delay in the schedule of a project induces risk in the system.

- **Tools:** Tools refers to the technological resources necessary to complete the project. Four tools were identified as follows:

  – **Software (SOFT)**

  – **Machinery (MACH)**

  – **Testing facilities (TEST)**

  – **Building tools of Mars habitat (TOOL)**

- **Waste:** Waste represents the amount of waste created by each phase of the project, and it is desired for it to be as minimal as possible in order to meet the sustainability goals

Please note that the tags written in parentheses will be used during allocation.

The project is divided into eight phases: Design, Production on Earth, Production on Mars, Testing, Installation, Operations, Maintenance and End-of-Life. The non-technical resource allocation among these phases is presented in Table 6.2.

Table 6.2: Non-technical resource allocation.

	People	Time [days]	Tools	Waste [%]
Design	MNG, ENG	600	SOFT	5
Prod on Earth	MNG, MAN	100	MACH	35
Prod on Mars	MNG, INS	100	MACH, TOOL	5
Testing	MNG, ENG	250	TEST	10
Inst	MNG, INS	15	TOOL	5
Operations	MNG, OPE	1765	SOFT	7
Maintenance	MNG, INS	60	TOOL	13
End of life	MNG, OPE, INS	20	TOOL	20

7

System Characteristics

After the initial analysis presented in the previous chapters, the preliminary design phase is initiated. This chapter presents the design considerations and sizing that have been done for each of the subsystems of the AWE system. Since all the departments often needed to use each other's outputs as their inputs, all the design steps were actually taken simultaneously. Therefore, it is not possible to present them in a the "correct" order as there is none. The ordering of this chapter is therefore not significant, and it should be noted that the whole process was iterative and all departments worked together with systems engineers leading them. In section 7.1 a selection of airfoils is analysed in 3D for assumed wing parameters. The airfoil with optimal performance within the range of to be expected wind velocities and for typical wind speeds throughout the year is then selected. After that, the wing parameters are updated to better fit the weight requirement. section 7.2 dives into the different aspects of the control system, the optimal flight path is determined, the minimal turning radius, the sensors and actuators used to track and control the kite position and velocity and the control software. In section 7.3 the structure and material composition of the wing is designed by analysis of the operational loads and possible failure modes after which compliance with the requirements is verified. Next, section 7.5 analyses the power generation characteristics by outlining the required ground station configuration, sizing the required motor, drum and buffer storage. section 7.6 describes the operations and logistics required for safe transportation, production on Mars and installation of the system. For take-off and landing a trade-off is done to find the most safe and efficient option. After that the maintenance plan and the End-of-Life plan are discussed.

7.1. Aerodynamics Characteristics

In order to generate sufficient power throughout the various seasons of the Martian year, the wing design is crucial and therefore this chapter looks at explaining the steps taken to reach the the final configuration of the wing. The first phase in the wing design is evaluating how the wing design performs with various possible airfoils and picking the best option which was done in subsection 7.1.2. In order to pick the most adequate airfoil a trade-off will be performed in the mentioned subsection. Lastly, wing parameters such as the sweep or aspect ratio were tweaked to check what the optimum wing design is, which is done in subsection 7.1.4.

7.1.1. Requirements

In Table 7.1 the relevant requirements used to guide the aerodynamics design are included. CON-DG-01 was important as the size of the wing would have a significant contribution to the mass of the system and since wing size is a characteristic determined in this section, the requirement is relevant. CON-DG-04 is again directly linked to the size of the wing and hence is important to take into account. TEC-AIR-11

Table 7.1: Relevant requirements of aerodynamics characteristics

Requirement Index	Requirement	Justification
CON-DG-01	The mass of the AWE system shall be lessthan 200 kg	This requirement originates from the stakeholder needs and is to be complied with.
CON-DG-04	The AWE system shall fit in a volume of 3 m^3	This requirement originates from the stakeholder needs and is to be complied with.
TEC-AIR-11	The airborne system shall be able to stay airborne at 5 m/s wind speed.	Why do we have this requirement, how was it determined, etc.
TEC-PS-02	The power storage system shall provide an output of 10 kW.	This requirement originates from stakeholder needs and is to be complied with.

7.1.2. Airfoil Choice Trade-off

In this sub-section, four airfoils will be traded-off using XFLR5 information and by simulating their performance using a Python code. In order to create a trade-off table, comparison criteria will be defined as a first step.

Subsequently, the weights of these criteria will be defined, and the column width in the tables will represent the weight chosen for each criteria. All chosen concepts will be evaluated for each of these criteria and their performance will be presented in the table using colour coding. The chosen colour coding is as follows: green is defined as exceeding requirements, blue is linked to the option meeting requirements, yellow correlates to the option having deficiencies and lastly, red indicates that the option is unacceptable for the corresponding criteria. The criteria weights are given on a scale of 5 in order to give the more important criteria a bigger influence in the trade-off. The chosen trade-off evaluation characteristics are:

- **Maximum electrical power at various wind velocities (5)** The maximum power generated at various wind velocities is a critical parameter as it shows how much energy can be stored at different wind speeds. This is of course vital for the AWES to achieve its main requirement; providing the habitat with a constant 10 KW of power as mentioned in Table 7.1 by the TEC-PS-02. Therefore, this gets the highest possible weight factor: 5.
- **Maximum electrical power production at average wind velocities (5)**: The power production at average wind velocities is also important as it indicates how well the system will perform in the common martian conditions and combines well with the first criteria which takes has more emphasis on what the power production in the more uncommon extreme wind velocities. Hence, since this criteria directly affects how well the top level power requirement will be met, it is weighted as a 5.
- **Minimum operational wind velocity (4)** The minimum operational wind velocity is important as it determines how often the wing will have to land due to low wind speeds which is obviously desired to be as low as possible as each landing is a complex operation and is more risky than staying in flight. Additionally, the lower the minimum flight speed, the larger the amount of time the wing can generate electricity. Hence, an airfoil which enables a low minimum flying velocity is desired and this criteria is rated a 4 as it is slightly less critical than the previous 2 criteria. Additionally, this criteria relates to the TEC-AIR-11 requirement as shown in Table 7.1
- **Moment of inertia (3)** The moment of inertia of the wing is also critical for the design as the structure will have to withstand high loads, and an airfoil with a higher moment of inertia will be more beneficial in this aspect and will save structural weight. However, this criteria does not directly affect top level requirements and hence is rated as a 3; criteria affecting power production are deemed more critical. This criteria relates to the mass requirement CON-DG-01 in Table 7.1.

The aforementioned criteria will be used for the trade-off of the various airfoil options and will be weighted as described.

In order to evaluate minimum flight speed and the power production at various flight speeds or power production at the average flight speeds, the data from XFLR5 was analysed in Excel and with the use of a Python code. For this analysis, wing design parameters were used from the results of calculations done in [9] and were slightly updated as a result of a preliminary power production model becoming available. This lead to: a surface area of 58.3 m^2, a wing span of 22 m, a sweep of 17.86° and a root and tip chord of 3 m and 2.3 m, respectively. The moment of inertia was found by evaluating the wing box height for each of the airfoils for a chord length of 1 m using their thickness/chord ratios. The formula for a thin walled circular wingbox: $Ixx = \pi \cdot (\frac{d}{2})^3 \cdot t$ was then used to find the influence the different airfoils have on the moment of inertia.

The following airfoils were chosen for the trade-off mainly due to their high lift and high L/D characteristics for the Reynolds numbers to be experienced on Mars:

- AH 79-100 A
- E591
- Wortmann FX 63-137
- SG6042

The corresponding profiles of the chosen airfoils can be seen in Figure 7.1, Figure 7.2, Figure 7.3 and Figure 7.2.

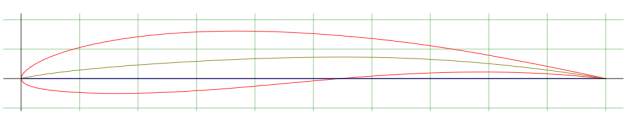

Figure 7.1: AH 79-100 A airfoil

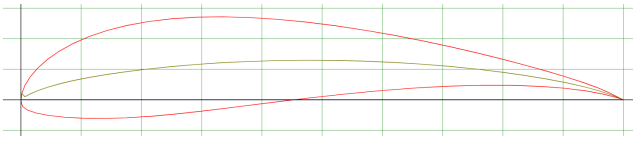

Figure 7.2: E591 airfoil

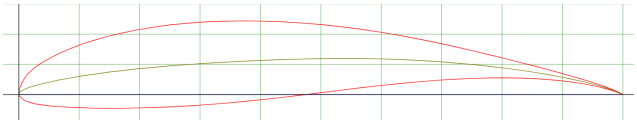

Figure 7.3: Wortmann FX 63-137

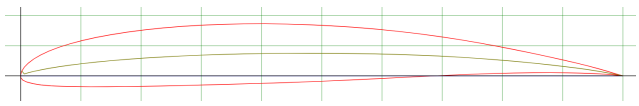

Figure 7.4: SG6042

In Figure 7.5 the graph of the power production against the wind velocity can be seen. The cut out wind speed was dictated by the maximum tangential wing speed, due to the fact that L/D determines the tangential speed (v_{k_τ}) the wing reaches. At wind speeds lower than the cut out wind speed, the wing could adjust its angle of attack in order to lower L/D and thereby v_{k_τ}, however there is a limit to this as it will reach its stall angle.

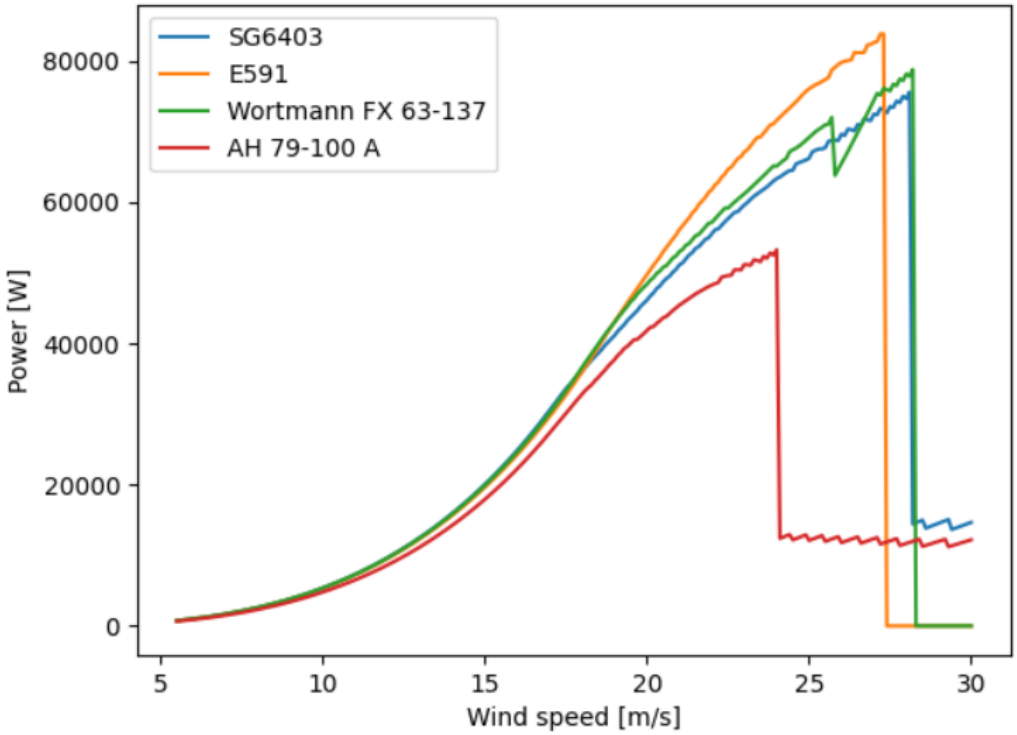

Figure 7.5: Power production from cut in to cut out wind velocity

Figure 7.5 indicates that at low wind velocities all airfoils perform relatively equally. However, at higher wind velocities the performances start to diverge. Namely, the E591 airfoil performs slightly worse than the SG6403 or the Wortmann FX 63-137 at intermediate wind velocities (10 m/s to 17.5 m/s) however, at higher velocities (after 20 m/s) the performance increases a lot and shows better power output than the rest of the airfoil options. On the other hand, the Wortmann and the SG6042 perform better than the E591 at wind velocities around 10 m/s to 17.5 m/s but then their performance does not increase as rapidly with the Wortmann airfoil yielding slightly better results than the SG6043. The worst performer is by far the AH 79-100 A, which falls below all other curves at roughly 7.5 m/s.

The graph describing the power production at average wind speeds throughout the year can be seen in Figure 7.6. This was generated by taking the average of the cubic speeds for 8 points throughout the year. Based on these velocity averages the power production was calculated for the various wing designs with the different airfoils.

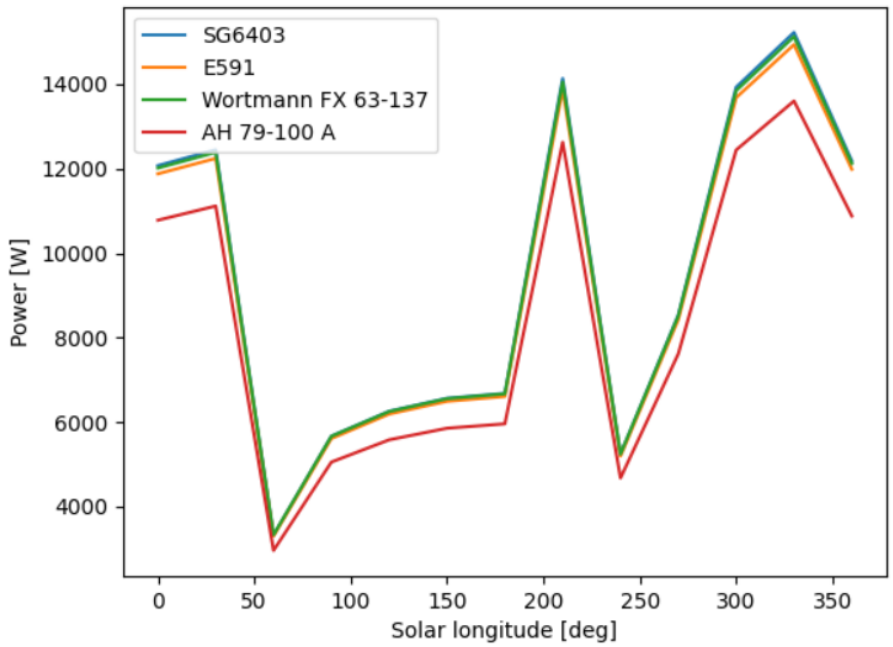

Figure 7.6: Power production during the year for average wind speeds

Figure 7.6 shows how the Wortmann and SG6403 airfoils performed the best and were closely matched throughout the whole yearly cycle. On the other hand, the E591 performed worse and the AH 79-100 A was the worst. The reason for this may be due to their lower performance at wind speeds close to the average wind speed values.

Subsequently, the next step was to asses the second criteria of the trade-off; the minimum operational wind velocity. The following minimum flight velocities were found by finding the velocity point where nonzero power production started:

- AH 79-100 A: 2.6 m/s
- E591: 2.4 m/s
- Wortmann FX 63137: 2.4 m/s
- SG6042: 2.4 m/s

As can be seen above, there are three best performers in this category. The E591, Wortmann FX 63-137 and SG6403 all have an excellent minimum operational wind speed of 2.4 m/s, whereas the AH 79-100 A is slightly worse at 2.6 m/s.

Lastly, the moment of inertia of the airfoil options were evaluated. The wing box inserted will have a circular cross section and it will be placed with its center at the position of the maximum thickness. Therefore, the height of the wingbox will be roughly equal to the maximum thickness of the airfoil and it will be assumed that this is the case. In order to have a fair comparison, the radius of the wing box will be evaluated for the 4 airfoils all with the same chord length. Since moment of inertia of a thin walled circle is proportional to the radius cubed, the structural rigidity that the airfoil shape allows can be evaluated.

Table 7.2: Airfoil trade-off

	Maximum power production at various wind velocities	**Maximum electrical power production at average wind velocities**	**Minimum operational wind velocity (m/s)**	**Moment of inertia contribution (m^3)**	**Points**
AH 79-100 A	Underperforms at all velocities	Worst performer	2.6	0.000125	**21**
E591	Performs well only at higher velocities	Intermediate performer	2.4	0.0004837	**41**
Wortmann FX 63-137	Good perfomance at common velocities	Best performer	2.4	0.0003215	**48**
SG6043	Good performance at common velocities	Best performer	2.4	0.000125	**45**

Table 7.2 shows the final results of the trade-off for the airfoil. In order to quantify the outcomes of the trade-off in a less subjective manner, each colour will be coupled to a weight. Green will be linked to a value of 3, blue to 2, yellow to 1 and red to 0. Despite not being the best performer in some cases, the Wortmann FX 63137 was chosen as the final option as in terms of power production criteria it performs the best yet still has a relatively good minimum flight speed and has a higher moment of inertia than the SG6042 airfoil which is its close competitor. Subsequently, the Wortmann helps also satisfy the requirements in Table 7.1. The points accumulated by the Wortmann airfoil also indicates its better overall performance

7.1.3. Airfoil Trade-off Sensitivity Analysis

In order to check if the trade-off was done correctly, it is important to do a sensitivity check on the weights and criteria that were used.

The first thing that is slightly curious when inspecting the table is the minimum operational wind velocity since each airfoil has the same value except for the AH 79-100 A, which scores lower but with still a very good value. It has to be inspected if this difference in scores results in a different outcome since it might not be fair to exclude this airfoil for having only a slightly worse performance in a criteria where the requirement for each of the options is already met. Therefore the trade-off was done without considering this criteria, which resulted in the scores shown in Table 7.3. There it can be seen that this trade-off criteria yields the same ranking as before, which means that it was not problematic to give the AH 79-100 A a worse score. However it can also be concluded that this criteria is redundant as there is a very underwhelming difference between the four airfoils.

Table 7.3: Sensitivity analysis: removing minimum operational wind velocity

Airfoil	**Points**
AH 79 100-A	13
E591	29
Wortmann FX 63-137	36
SG6043	33

The weights of the 2 power criterion could also be altered in order to check the effect on the outcome of the trade-off. Since they have initially a weight of 5, the only option is to reduce the weight factor. A reasonable change is to 4 as both criteria are still very important for the design choice. The outcome of the aforementioned change can be seen in Table 7.4. Despite the altering of the weights of the criteria the Wortmann airfoil still remained the best performing.

Table 7.4: Sensitivity analysis: changing weights of power characteristics

Airfoil	**Points**
AH 79 100-A	17
E591	34
Wortmann FX 63-137	39
SG6043	36

7.1.4. Parameter Optimization

Parameters such as wing area, aspect ratio or sweep were optimised in this section in order to produce a final design for the wing. The design parameters used in subsection 7.1.2 yielded a structural weight that was too high due to the high loads and the slender shape of the wing. Hence, further modifications were made and analysed in order to check what sort of design changes would enable a more feasible design. However, incorporating the design alterations also affected the the power output of the system and therefore new configurations were again analysed in XFLR5.

Initially the parameters chosen for the wing were based on equations for the optimal (C_L^3/C_D^2) ratio as Equation 7.1 shows that this produces the best power per unit of area [11]. Although the equations are very idealised it was a good enough for a preliminary sizing estimate. The equations relating the C_L and C_D to $C_{D,0}$ at optimum power efficiency could be used as the $C_{D,0}$ was known from the airfoil choice from an XFOIL analysis provided [1]. The chosen airfoil can be seen in Figure 7.7. The MH 81 airfoil was chosen due to its maximum thickness 12.9% at 25.4% chord as well as its maximum camber of 3.3%. C_R was substituted for $\sqrt{C_L^2 + C_D^2}$ in Equation 7.1.

[1] http://airfoiltools.com/airfoil/details?airfoil=mh81-il[Accessed on June 1, 2021]

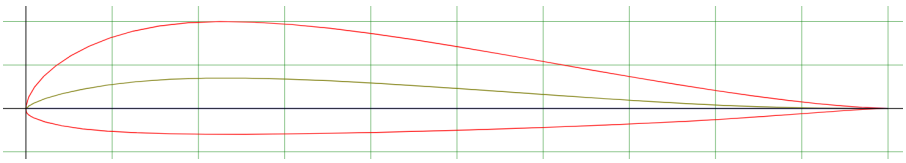

Figure 7.7: MH 81 airfoil [2]

$$\frac{P_{opt}}{P_w S} = C_R \left[1 + \left(\frac{L}{D}\right)^2\right] \left(\frac{4}{27} sin^3(\theta) \cos^3(\phi)\right) \tag{7.1}$$

At the optimum power efficiency [11]:

$$C_L = \sqrt{3 C_{D,0} \pi A R e} \tag{7.2}$$

$$C_D = 4 C_{D,0} \tag{7.3}$$

Additionally [11]:

$$e = 4.61 \left(1 - 0.045 AR^{0.68}\right) (\cos \Lambda_{LE})^{0.15} - 3.1 \tag{7.4}$$

Subsequently, by plugging equation Equation 7.2, Equation 7.3 and Equation 7.4 into equation Equation 7.1, as well as using common values of $\theta = 60\,\mathrm{deg}$ and $\phi = 0\,\mathrm{deg}$. A desired power output of 18 kW was chosen as this was thought at the time to be the needed traction power for a 10kW electrical power output. Consequently, Equation 7.1 was simply in terms of aspect ratio, leading edge sweep and surface area which could be chosen for optimum power performance. Using an iterative process through an excel sheet, the characteristics of the wing could be altered to find an optimum power output. This lead to an aspect ratio of 8.3, a surface area of 50 m^2 and therefore a C_L of 0.97, a C_D of 0.08 (at optimum power output) and a wingspan of 20.37 m. However, after developing a preliminary model which was less idealised for the power production, it turned out that slightly different wing characteristics were needed, namely: a surface area of 58.3 m^2, a wing span of 22 m, a sweep of 17.86 deg and a root and tip chord of 3 m and 2.3 m.

It was deemed that the optimum values for aspect ratio, sweep and taper ratio should be maintained if possible as aerodynamically it was ideal according to the optimum (C_L^3/C_D^2). However, the structural mass yielded relatively high values (70 kg) and should be reduced if possible. Moreover, the yearly surplus energy production was 1,995,719 Wh which accounts for 35% of the total energy production. Therefore, a code was produced in order to evaluate if changing the characteristics of the wing would be beneficial for its mass and would not overshoot the yearly energy production too much. The new wing design lead to a surplus energy production of 111385 Wh which is equivalent to 2% of the yearly energy production. This was deemed acceptable, however the structural weight benefit was yet to be analysed before a decision was to be made to go with the updated wing design. Below in Table 7.5 the dimensions of the original wing and the updated design can be seen.

7.1.5. Airfoil Analysis Code Verification

The functions that read the XFLR5 files were verified by inspection. Their outputs were visually compared by comparing it to their corresponding cell in the data file.

Table 7.5: Parameter comparison of optimal aspect ratio wing vs low aspect ratio wing

Characteristic	Original Design	Low AR Design
Wing Span (m)	22.00	20.00
Area (m^2)	58.30	60.00
Mean Geom. Chord (m)	2.65	3.00
Aspect Ratio	8.30	6.67
Taper Ratio	1.30	1.40
Root to Tip Sweep (deg)	17.86	16.96

The updated design lead to a mass reduction of roughly 15 kg and, as stated before, the new design still reached the necessary power production throughout the year. Since the surplus energy production was only 2% of the total energy production in a year it was deemed that a surface area of 60 m^2 was sufficient. Subsequently, the corresponding requirements for the wing design shown in Table 7.1 were helped to become satisfied by the design of the wing presented.

7.1.6. Recommendations

The wing design presented above is far from optimal and would still benefit from the use of more alterations made to the design. However, due to time constraints some ideas were not possible to implement. This subsection goes over the possible improvements that could be made to the wing design.

Wing twist is one feature not Incorporated but that could be beneficial. Wing twist allows the wing tip effective angle of attack to be lower. Since the section of the wing used to steer is towards the end of the wing, the twist allows for controllability at higher angles of attack since stall is delayed.

Winglets are another addition that would greatly benefit the wing. Winglets allow for a reduction in lift induced drag as the wing tip vortices of the wing are reduced. This improves the L/D performance as well which is beneficial for power production.

Additionally, dihedral could be Incorporated for better stability of the wing, however this would cause maneuverability losses. This may not be desirable but is worth evaluating.

Lastly, it has to be noted that the considerations in this section did not incorporate the effect of possibility that dust accumulates on the wing, which would move the flow transition forward and thereby decreases the performance. The choice of neglecting this was based on two assumptions. It was discovered through a conversation with Jorge Vago, the ESA project scientist on the Exomars program, that dust storms in the southern hemisphere do not raise the dust higher than 0.5 m, meaning that during airborne operation the wing would never accumulate dust. Secondly, it was assumed that even if the wing would accumulate dust during landing or take-off, it would be shaken off by the vibrations induced in the canopy from flying as well as the varying ballooning effect. If further research were to be carried out, this assumption should be verified in case the dust particles are actually not shaken off completely and what sort of effects this would have on the aerodynamic performance of the wing.

7.2. Control Characteristics

In this section, the control characteristics are identified and elaborated upon. First, in subsection 7.2.1, the requirements associated with the control system are mentioned. In subsection 7.2.2, the flight path of the wing is explained. In subsection 7.2.3, the algorithm used by the system is discussed. Then, in subsection 7.2.4, the turning radius of the flight path is calculated, followed by a description of the different sensors and actuators used in subsection 7.2.5. Finally, the software used to control the wing is defined in subsection 7.2.6.

7.2.1. Requirements

Table 7.6: Relevant requirements of control characteristics

Requirement Index	Requirement	Justification
TEC-CL-05	The control system shall withstand 3340 Martian temperature fluctuation cycles from -190°C to 20°C	This requirement originates from the stakeholder needs and is to be complied with.

7.2.2. Flight Path

For the flight path of the wing, a figure of eight trajectory has been chosen. This decision is based on two main reasons. Firstly, unlike circular trajectories, the figure of eight does not cause the tether and control control tethers to get tangled. Then, it is also deemed as the most efficient flight path in terms of making use of the cross-wind flight. Now that this trajectory is chosen, it has to be designed and sized. This is also crucial to the structural and power characteristics since the turn radius of the figure of eight affects the inertial loads experienced by the wing, setting a limit to the tangential wing speed which directly influences the power generation performance of the system. The power generation cycle with the figure of eight motion can be seen in Figure 7.8.

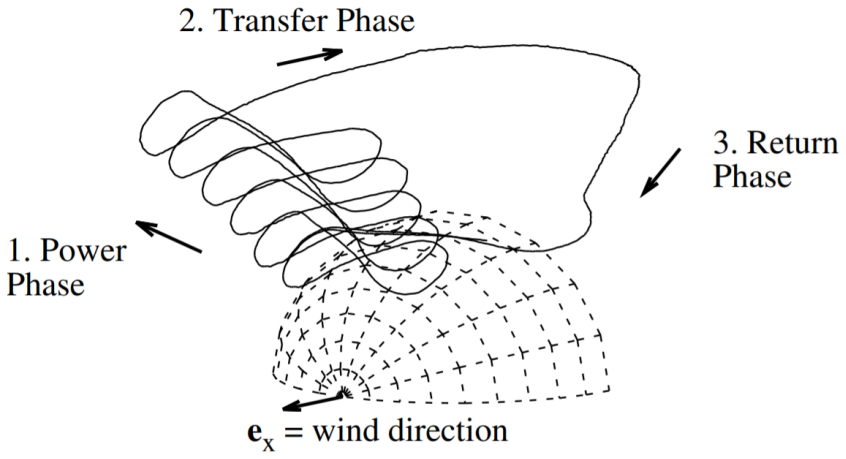

Figure 7.8: Power generation cycle using a figure of eight flight path[12].

According to [13], there are two conditions to define a figure of eight trajectory, namely following a way-point and having a set turn rate. It is also possible to recognise two types of trajectories: an up-loop where the kite performs the turn by going upwards and down-loop where the turn happens via a downwards motion. The first one needs to compensate for gravitational forces while the upwards turn leading to lower forces during turns and higher forces during the rest of the trajectory. On the other hand, for the down-loop trajectory, the compensation happens during the center region, leading to smaller forces but also less force variation throughout the flight path. Next to smaller variation in tether force, the down-loop trajectory is also more beneficial in terms of lower required wind speeds[12]. Considering the system configuration and the environmental constraints, the down-loop figure of eight trajectory is preferred for AWESOM.

The prediction of the current position of the kite is a challenging task because of the nonlinear kite movements. The optimal solution requires a probability density function, which requires an infinite number of parameters. In order to estimate the state of the wing, a Double Exponential Smoothing-Based Prediction (DESP) will be used. DESP is a smoothing algorithm presented by LaViola (2003) that runs faster than Kalman and extended Kalman filter-based predictions. Since it runs faster, it does not need to predict as far in the future as a slower one. LaViola concluded that DESP is accurate, fast, robust and simple. [14]

7.2.3. Flight Path Control Algorithm:

The algorithm[14] determines the actual measurement data prediction and its derivations recursively at a time step t. The measured data at a time t is x_t, its prediction is p_t and its derivation b_t. In economical papers refer to b_t as the trend, but the mathematical representation is the derivation of x_t over time. Furthermore α represents the weight on the current measurement x_t and is the weight on the current derivation b_t.

For t = 0:

$$p_0 = \alpha x_1 \tag{7.5}$$

For t = 1:

$$p_1 = \alpha x_1 + (1-\alpha)p_0 \tag{7.6}$$

$$b_1 = p_1 - p_0 \tag{7.7}$$

For t > 1:

$$p_t = \alpha x_t + (1-\alpha)(p_{t-1} + b_{t-1}) \tag{7.8}$$

$$b_t = \beta(p_t - p_{t-1}) + (1-\beta)b_{t-1} \tag{7.9}$$

If Equation 7.5 is used during sensor fusion, x_t transforms to a vector from a scalar. This is given by the equation:

$$\vec{x}^t = (x_{t1}, x_{t2}, \ldots, x_{tn}) \tag{7.10}$$

The weights that are put on the sensors is also represented by a vectors $\vec{\alpha}^t$ and the weight on the derivative is β_t still scalar. The weights at time t is:

$$\vec{\alpha}^t = (\alpha_{t1}, \alpha_{t2}, \ldots, \alpha_{tn}) \tag{7.11}$$

where

$$\forall_i \in [1,\dots,n] \cdot (\alpha_{t_i}, \beta_{t_1}) = \begin{cases} \alpha_i, \beta_i & \text{, if } x_i \text{ is valid} \\ 0, 0 & \text{, otherwise} \end{cases} \tag{7.12}$$

For $t = 0$, if $\sum_{i=1}^{n} \alpha_{0_i} > 0$:

$$p_0 = \frac{1}{\sum_{i=1}^{n} \alpha_{0_i}} \sum_{i=1}^{n} (a_{0_i} \cdot x_{0_i}) \tag{7.13}$$

The estimation combining the data of n sensors at a time τ is p_t and the derivation is b_t. For $t = 1$, if $\sum_{i=1}^{n} \alpha_{1_i} > 0$, otherwise start over:

$$p_1 = \sum_{i=1}^{n} \alpha_{1_i} x_{1_i} + \left(1 - \sum_{i=1}^{n} \alpha_{1_i}\right) p_0 \tag{7.14}$$

$$b_1 = p_1 - p_0 \tag{7.15}$$

For $t > 1$:

$$p_t = \sum_{i=1}^{n} \alpha_{t_i} x_{t_i} + \left(1 - \sum_{i=1}^{n} \alpha_{t_i}\right) (p_{t-1} + b_{t-1}) \tag{7.16}$$

$$b_t = \beta_{t_i} (p_t - p_{t-1}) + (1 - \beta_t)(b_{t-1}) \tag{7.17}$$

7.2.4. Turning Radius

To accurately estimate the turning radius during the figure of eight maneuvers of the wing, all the forces acting on the kite must first be identified. This is followed by a construction of a free body diagram:

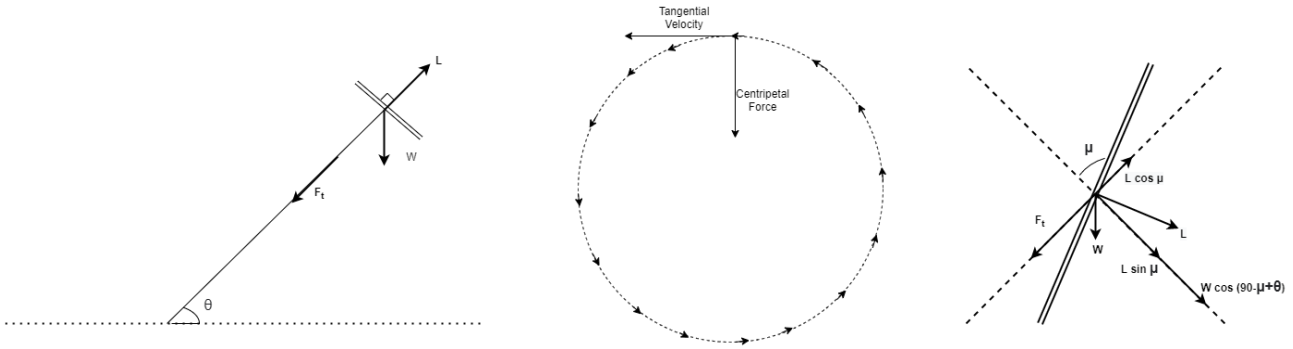

Figure 7.9: Free body diagram for turning flight.

In Figure 7.9 three different FBD's are shown. First the FBD of the wing with no bank angle can be seen. Here, L indicates the lift force which acts perpendicular to the wing surface, W is the weight, F_T is the tension in the tether, and θ is the tether inclination angle. The second diagram shows a top down view of a turn during the figure eight motion. Here, the centripetal force and the tangential velocity are shown. Finally, the third FBD shows the wing when banked. Here, the angle μ is the bank angle of the wing, where the dotted line (from top left to bottom right) indicates the wing position when unbanked. As the tether tension will still act in the same direction as in the first figure (also indicated by the dotted line from bottom left to top right), the components of the lift and weight parallel to the tension should also be shown. Furthermore, the centripetal force acts perpendicular to the tether tension, i.e. along the unbanked wing line. Thus, the components of the lift and weight parallel to this force should be shown as well.

Once identified, the sum of the resultant forces in the radial direction must be equal to the net centripetal force. Several assumptions were made to simplify the equations of motion. The first assumption was that the tether inclination angle with respect to the horizontal(ground) axis remains constant throughout the figure of eight. In reality, the inclination angle changes slightly during flight, however, a significant amount of computing power would be required to make detailed predictions throughout the flight path. The second assumption made was that the plane of the figure of eight motion is always orthogonal to the tether. The centripetal force is given by the equation:

$$Lsin\mu + W\cos(90° - \mu + \theta) = \frac{mV^2}{R} \tag{7.18}$$

This only considers the point right before the wing starts to turn. Although the lift force always coincides with the centripetal force, the weight vector does not. As the weight always points perpendicular to the ground, and thus does not change direction throughout the turn, the equation would differ at each point. However, as the weight force is very small compared to the lift force, it was assumed that this could be neglected. Furthermore it was also assumed that the wing speed remains constant throughout the maneuver. Using these estimations, the equation holds for each point during the turn. Consequently all assumptions used to calculate the turn radius are as follows:

1. The tether inclination with respect to the ground will remain constant throughout the turn.
2. The plane of the figure of eight motion is always orthogonal to the tether.
3. The influence of the weight can be neglected.
4. The wing speed throughout the turn will remain constant.

And the formula used to calculate the radius of the turn becomes:

$$R = \frac{mV^2}{Lsin\mu} \tag{7.19}$$

The values used to calculate the radius were found to be: a kite mass of 79.7 kg, a wing speed of 120 m/s, a lift force of 8000 N, and a banking angle of 45°. This resulted in a radius of 202.9 m. It should be noted that this wing mass was found by the structures department, and the calculation is explained later in section 7.3.

The banking angle was chosen to be 45°to allow the actuators to be able to achieve this level of banking in a very short amount of time. If this angle would be much higher, for example 80°, the actuators would not be able to reel out fast enough to bank the wing before the turn. As, 45 °was set to be the maximum allowable banking angle, it was chosen to achieve the lowest possible turn radius.

Furthermore, the loads experienced by the wing should be considered, to check if the structure will be strong enough. Due to the assumptions stated previously, we find that the the force acting on the wing would be the resultant force of the tether tension force and the centripetal force. This results in:

$$F_R = \sqrt{(L\cos\mu)^2 + (Lsin\mu)^2} = L \tag{7.20}$$

Here, $L\cos\mu$ is the component of the lift force parallel to the tether during the turn as can be seen in Figure 7.9. Thus, this equals the tension. Further, $Lsin\mu$ is the centripetal force as found in Equation 7.18, assuming that the weight can be neglected. Consequently, the resultant force acting on the wing is just the total lift force generated by the wing (Equation 7.20).

7.2.5. Sensors and Actuators

Since the AWESOM project uses a ground-based control system, there is no external energy source that can supply power to sensor placed on the wing subsystem. A battery that can be placed on the wing was initially considered, however this would increase the mass and complexity of the system. The aerodynamic and structural properties calculated would also need to be recalculated. In order to minimise interference with the rest of the system, a camera mounted on the ground station was chosen. The camera chosen would need to calculate multiple parameters required to control the wing. The parameters of interest here are: altitude, acceleration and velocity in all axes, attitude and positioning, wind speeds and ground speeds, temperature and air pressure. However, the camera system might fail due to a system error or environmental effects like sand storms. Thus, secondary systems should also be considered. In addition to the camera, a line angle sensor and torque transducer will also be installed on the ground station. These are able to indicate the deflection, tension and reel in/out speed of the main tether. These in turn can be used to calculate the different parameters of interest. In addition to this, a wind speed sensor is also installed to measure the wind speed and direction during take-off and landing. The main advantage of having redundant sensors is that with four different sensor systems in place, the control unit will still be able to function if one of them fails.

The sensors chosen for the mission are summarized in the list below:

- Wind speed sensor

- Torque transducers
- Camera
- Tether angle sensor

The actuators used for the system comprise of two geared DC servomotors as stated in the previous report [9]. The motors are connected to the wing via a tether. By reeling the tether in/out, the motors can control the angle of attack, pitch and yaw of the kite. Position feedback and speed estimation are provided by incremental encoders fitted to each motor shaft. Bidirectional current is measured on each motor input to enable closed-loop torque control and analysis of the loads and power consumption during various flight maneuvers.

7.2.6. Control Software

Developing the control system software for high altitude wind energy generation is a complex task, especially if a kite controlled by a ground-based control system is utilised. Most of the research papers published on tethered AWE systems generally utilise airborne control units. The main purpose behind using a ground-based control system for this project is to reduce the weight of the wing subsystem during operation. However, using a ground-based control unit would lead to delay in the response of the wing subsystem during actuation. To automate the piloting of the kite, several sensors, actuators and flight computers are present. The sensors record the data at a certain instance in time. This is followed by the flight computers performing certain computations in accordance to the flight path. The desired input is then fed into the actuators to perform the action. In order to begin designing the software architecture, several existing designs from previous AWE systems are used. It is decided to design a dedicated software architecture, because a complex set of design goals has to be met to form a contiguous software system that controls hardware components optimised against different criteria. [15]

System Architecture

Software architecture refers to the fundamental structures of a software system and the discipline of creating such structures and systems. Each structure comprises software elements, relations among them, and properties of both elements and relations [3]. The system architecture is further classified into several categories based on their functions and purpose. These include[15]:

- **Signal Acquisition and Routing:** During this process, data acquired at different locations from sensors and users is processed and distributed to the actuators. Figure 7.10 below depicts an overview on the component distribution and the signal flows of the SkySails towing kite system. The key difference between control systems used in SkySails and this project is that the former uses an airborne control system and the latter uses a ground-based control system. However, the architecture is not affected by this difference since only the medium of transmission differs. The control unit comprises controllers, sensors and the kite control actuators. The controllers consist of several computers performing calculations and proving visual data to the user.

[3] https://en.wikipedia.org/wiki/Software_architecture [Accessed on June 8, 2021]

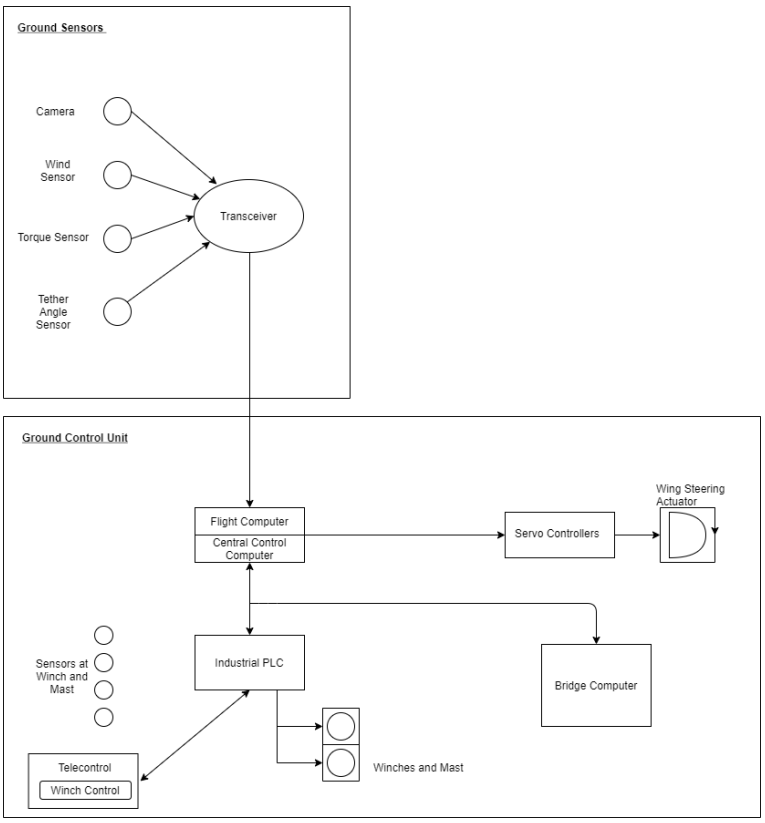

Figure 7.10: Components and signal flows of the AWESOME kite control system. The distributed system comprises the ground-based control pod with sensors placed on the ground station.

- **Failure Handling:** During this process, several measures are taken to ensure that the control system is still reliably functioning when 1 or more components fail due to increased complexity of the system. The most important feature with respect to safety is, that the controllers on the ground can fly the wing subsystem autonomously for a certain time using local sensors only. In addition to an emergency battery power supply and control strategies based on local sensor information only, an adaption of the flight control algorithms is inevitable. Following the simple acquisition-processing-distribution-principle, one would prefer to locate the complete control algorithm in the central processing computer with its abundant computation power and located next to the operator in providing graphical user interfaces. However, in order to meet the demand for autonomous flight, one has to put up with the additional complexity of locating certain parts of the flight control algorithm in the embedded control computer of the control pod. This involves the implementation of the control as a distributed system.

Software Design Solutions

The software design techniques allowing for a robust, yet configurable, control system software are described in this section. As outlined in the previous section, the hardware forms a heterogeneous system with high requirements on the maintainability and stability of the software. Different optimization criteria lead to different software designs for the particular system components. These designs are presented for the control pod, the launch and recovery system as well as for the central data processing computer[15].

- **Control Unit:** The control unit, which has been produced in small series, embeds two dedicated optimised controller boards: the flight control computer board and the motion controller board for the kite actuator. It is beneficial in terms of cost and weight to integrate the power management and the data modem circuits into the sensor data acquisition and control computer platform. Embedded controller solutions are recursively developed by balancing the demands on robustness of hardware and software. In order to increase stability of the electronic circuitry, all signal processing is limited to the required bandwidth. As a result, only those algorithms, that are required to autonomously fly the kite, are processed in the control pod. These are the navigation, data fusion and motion control algorithms. To reduce costs in the production and to ease the qualification of service technicians, the flight computer board is separated from the motion control board to follow a platform strategy for different kite sizes. As a result, only the power components have to be altered for kite size adaption.
- **Launch and Recovery System:** For launching and landing, several existing methods as well as newer ideas were shortlisted. Since these maneuvers need to be precise and safe to prevent damage to the kite

and its surroundings, the ground-based camera as well as the tether angle sensors will work in tandem to achieve a greater precision. The main parameter to focus on during landing is the ground speed of the kite and its stability. It is preferred to have low landing speed during landing, and this is achieved when the wing is made to stall. During take-off, the wind gusts should provide sufficient thrust to the stationary wing to produce a large lift force. Since the wing has no control surfaces to adjust the angle of attack, the take-off and landing system has to be chosen in such a way that the angle of attack can be changed. This allows the wing to produce the maximum possible lift force for take-off.

- **Central Data Acquisition and Processing:** The central computer makes use of an industrial PC to receive, record, process and forward data from every system component. A PC-based hardware has been chosen as it allows for easy recording of all sensor data tracks, output values of the control algorithms and auxiliary data such as algorithm parameters and user inputs. The logging produces about three gigabytes of uncompressed data per day, which is stored compressed on a hard disk. Since the data acquisition and processing main loop has to synchronise to the control cycle of the flight computer, a real-time extension has been installed to the Linux operation system. The benefits consist of the Linux high resolution timers and fast response times at the cost of an insignificantly decreased processing speed. Since the towing rope communication modems are constrained to a limited bandwidth, the communication packets exchanged with the flight computer are divided into two segments: One segment features the variable data, called isochronous data. Variables, which are updated less frequently are transmitted in multiplexed slots. The other segment consists of channel-oriented transfer of queued messages. A high priority and a standard priority queue are implemented. The high priority queue is provided for user command routing and safety-critical messages, whereas the standard queue is used to update configuration data and to transmit debug messages from the flight computer.

7.2.7. Verification of Control System

A major challenge occurs when debugging a complex overall system and establishing an accurate interplay of all involved components. In order to combat this problem, Hardware-in-the-Loop Testing is performed to ensure an efficient pre-testing of components. The major property of the setup is to rebuild the final operational computer hardware and software setup with modifications as little as possible to enhance testing coverage. Additionally, setting up the appropriate apparatus and performing tests was a major challenge since it was essential to mimic the Martian climate. Since traditional wind tunnels are based on Earth-like conditions, performing tests would require specialised equipment and modifications. Fortunately, students from the California Institute of Technology helped construct a custom wind tunnel inside a vacuum chamber at the Jet Propulsion Laboratory, which Caltech manages for NASA. The air pressure in the chamber was pumped down to approximate the Martian atmosphere[4]. Using similar technologies, the wing can be tested along with the control unit in a Martian-like environment.

Hardware-in-the-Loop(HiL) Testing:
As has been elaborated in the previous section, software design concepts have been established with special focus on component testing. However dealing with heterogeneous but closely interacting subsystems, a major challenge arises from debugging the complex overall system and establishing an accurate interplay of all involved components. While small prototype systems, which are more a kind of laboratory type setups, may still be debugged “online in the field” by a small developer team quite efficiently, this development approach is unsuitable for industrial scale systems. The operation of these large scale systems is quite costly, failures may quickly result in substantial damages and especially the airborne system is not accessible to efficient debugging methods as e.g. connecting a CAN bus sniffer or writing high-bandwidth logs.

A major challenge occurs when debugging a complex overall system and establishing an accurate interplay of all involved components. In order to combat this problem, Hardware-in-the-Loop Testing is performed to ensure an efficient pre-testing of components. The major property of the setup is to rebuild the final operational computer hardware and software setup with modifications as little as possible to enhance testing coverage. In Figure 7.11, the HiL setup established by Jochen Maab and Michael Ernhard is shown[15].

[4] https://www.caltech.edu/about/news/how-do-you-test-a-helicopter-bound-for-mars

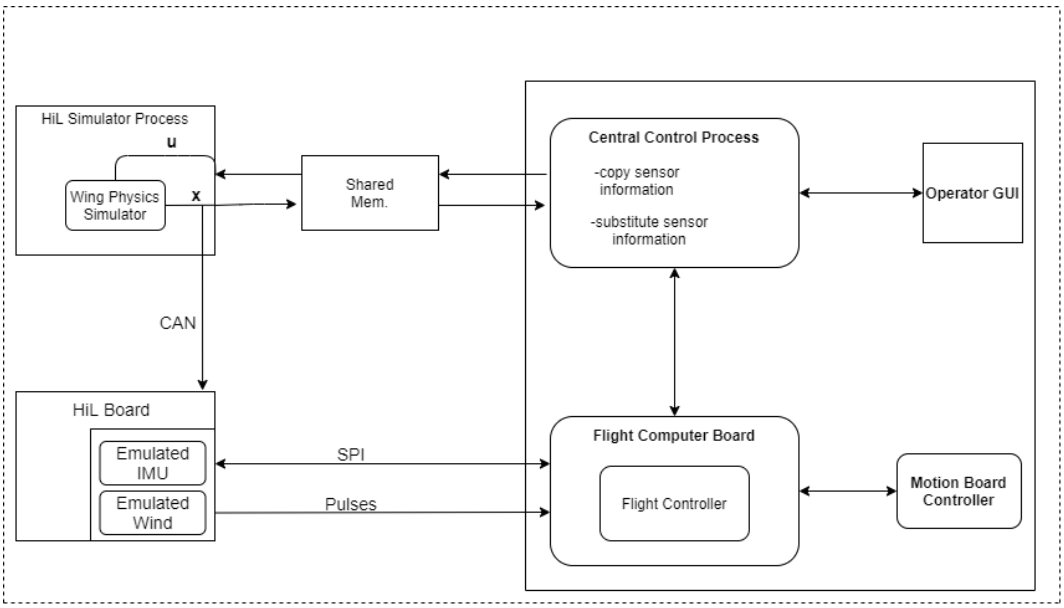

Figure 7.11: Schematic and simplified view of a hardware-in-the-loop (HiL) testing scenario.

Advantages offered by distributed processing present a temptation to select one of the distributed system architectures and to assume that experience with centralised systems can be transferred to the analysis, design, and early development stages of the new control system. However, the most serious consequences of greater use of distributed processing may not show up until late in the development cycle. Items that could introduce unexpected surprises are identified in this section, because they all affect V&V planning.

Two items stand out as being the most important: system response time and system configuration management. Of these two issues, time is by far the most important. Time is not only important for completing critical tasks by required deadlines, but also to record and store event sequences in the correct order by use of synchronization.

Event synchronization is a very important factor in data validation. It can be critically important during rapid excursions in monitoring any kind of physical flow (heat, material) because control actions are predicated on application of conservation laws. Lack of synchronization can produce the opposite control action to what is intended. Control algorithms to be used on distributed processors will have to be examined for sensitivity to synchronization latency, that is, the degree of accuracy in synchronization that can be maintained, so that problems do not develop as result of unexpected excursions.

Scheduling involves timing, task prioritization, resource management, and possibly communications management. A scheduling analysis must look for possible race conditions that can produce artificial states that may cause program execution to halt or to lose synchronization, and lead to system failure. Analysis tools for system design will have to incorporate graph theory used in understanding aspects of network behavior, queuing theory and other topics used widely in operations research.

Use of simulation for re-evaluation needs to be included as part of the maintenance support environment for distributed control systems. This is particularly important for any part of the system where timing and scheduling strategies are critical to reliable control. Performance matching is another timing-related consideration.

Communication protocols become significant design issues as the level of use of distributed processors increases. Choice or design of protocols must consider performance (timing), fault-tolerance, reliability, security, and data integrity.

7.3. Wing Structural and Material Characteristics

Given the aerodynamic configuration as characterised in section 7.1, an essential part of the system characterisation requires the sizing of the wing structure. The design of the load bearing elements of the wing will be provided in this section, starting with a summary of the main requirements specific to the structure of the wing in subsection 7.3.1, followed by a description of the loads that would apply on it and a presentation of the structural model selected in subsection 7.3.2. The various materials considered for the wing will also be presented prior to designing its structural components in subsection 7.3.3. Finally, the different structural elements of the wing, namely the wingbox, the ribs and canopy will be characterised in subsection 7.3.5, 7.3.6 and 7.3.7, and followed by some recommendations for further improvements of the structural model in subsection 7.3.9.

7.3.1. Requirements

In Table 7.7 the relevant requirements used to guide the structural design are presented. These requirements were retrieved from section 3.1, and shall be complied with by the structural model designed in this section. In Table 11.1, the compliance of the structure-specific requirements listed in Table 7.7 will be summarised.

Table 7.7: Relevant requirements of structural characteristics

Requirement Index	Requirement	Justification
CON-DG-01	The mass of the AWE system shall be less than 200 kg	This requirement originates from the stakeholder needs and is to be complied with.
CON-DG-03	The AWE system shall be designed for a lifetime of 5 Martian years.	This requirement originates from the stakeholder needs and is to be complied with.
CON-DG-04	The AWE system shall fit in a volume of 3 m^3	This requirement originates from the stakeholder needs and is to be complied with.
TEC-AIR-12	The airborne system shall withstand 3340 cycles of temperature fluctuation from -190°C to 20°C.	The system shall survive the 5 Martian years of operation time without (physical or performance-wise) damage due to temperature fluctuations.
TEC-AIR-13	The airborne system shall withstand $1.7 \cdot 10^7$ cyclic loadings caused by the varying loads during the figure of 8.	The system shall survive the 5 Martian years of operation time without (physical or performance-wise) damage due to temperature fluctuations.
TEC-AIR-14	The canopy of the wing shall deflect less than 0.01 m under aerodynamic loads.	In order to avoid the loss of aerodynamic properties, the deflection of the canopy shall be limited to 0.01 m.
TEC-AIR-15	The wing shall twist at most $3.23°$ throughout the span of the wing.	This requirement follows from an attempt to avoid the loss of aerodynamic properties while simultaneously creating a reasonable distribution of twist. This is further explained in the structural characteristics section (c.f. subsection 7.3.5).
TEC-AIR-16	The wing shall deflect at most 0.5 m in total throughout the span of the wing.	This requirement follows from an attempt to avoid the loss of aerodynamic properties. This is further explained in the structural characteristics section (c.f. subsection 7.3.5).

7.3.2. Load Analysis and Structural Design

As summarised in section 3.2, the previous stage of the design process was decisive in selecting a wing configuration. A trade-offs between several configurations led to the selection of a semi-rigid swept wing. This semi-rigid swept wing concept relies on a rigid load-bearing structure covered by a flexible canopy, also referred to as the skin of the wing, that would provide the aerodynamic shape to the structure.

For the preliminary estimation of the mass of the wing, it can be assumed that the load bearing structure would be composed of a circular shaft, extending over the full span of the wing, and placed at the maximum thickness of the airfoil. This shaft, being the wingbox of the wing, will have a variable thickness along the span, thus allowing for a lighter structure. The circular section of the wingbox has been chosen as it enables to fit the largest section inside the wing (thus increasing the moment of inertia of the section, in turn improving the resistance of the wingbox against bending), and avoids sharp edges and corners (where stress concentrations might arise). Attached to this wingbox would be the ribs. Those ribs, placed at specific intervals, shall give the aerodynamic shape to the canopy wrapping the wing, as well as transferring the load generated over the skin of the wing to the wingbox.

A schematic illustration of the structural design proposed is shown in Figure 7.12. This figure shows the placement of the wing box within the wing section (i.e at a distance $x_{airfoil,max}$ from the leading edge of the airfoil; 'airfoil, max' refers to the location on the airfoil where the thickness is maximum), as well as the placement of two ribs over the wingbox.

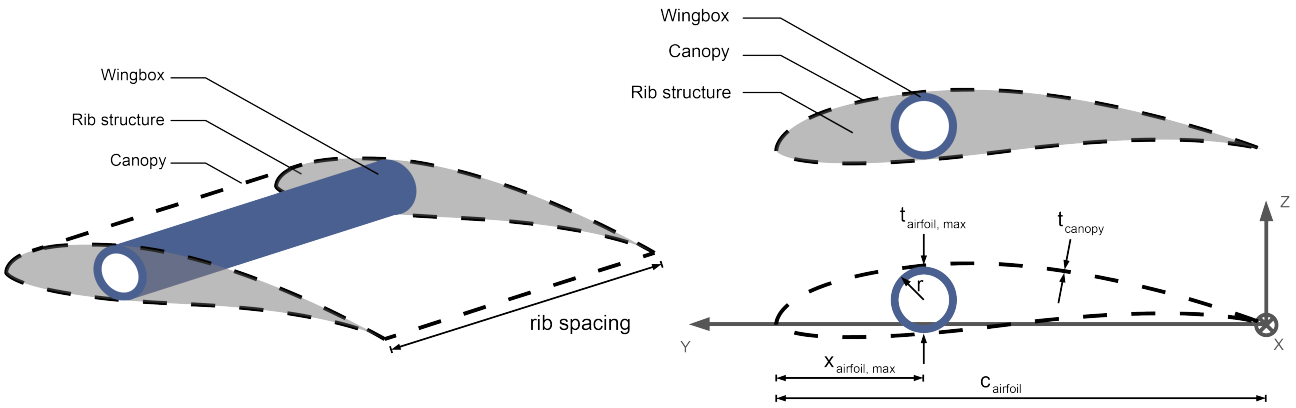

Figure 7.12: Wing structural design configuration

From this wing configuration, and prior to sizing the wingbox, the rib spacing and the ribs themselves, it is essential to consider the loads applied on the structure. In Figure 7.13, three views of the wing are shown, each showing the loads that are considered to apply on the wing. Please note the direction of the x-axis, which is shown to follow the trailing edge of the wing. This has been done to facilitate the calculation of the wingbox dimensions in the wingbox model introduced here below. The wing structure is therefore analysed from tip to root in this project.

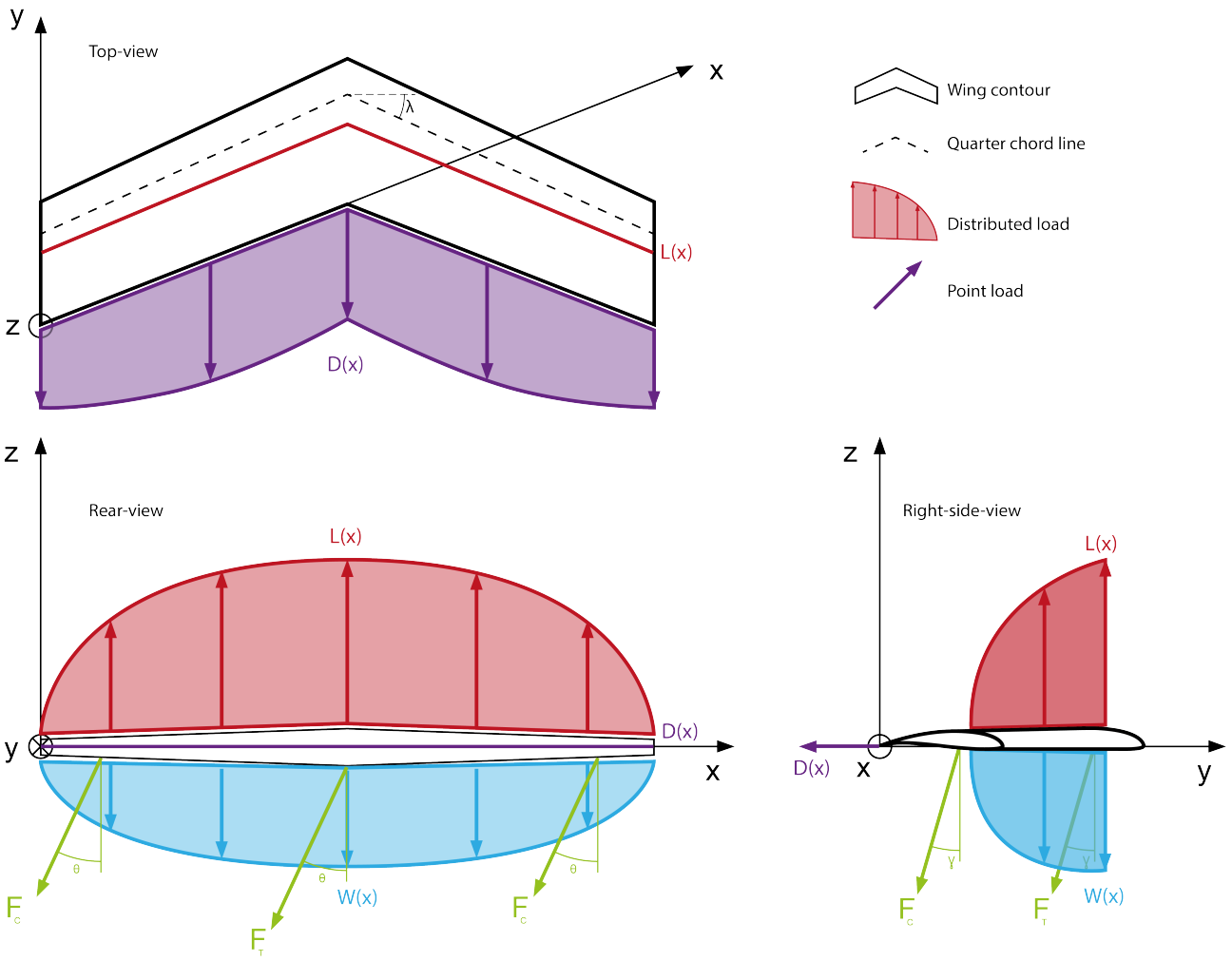

Figure 7.13: Free Body Diagram (FBD) of the wing with the assumed sign convention and their position with respect to the wing

7.3.3. Material Selection

Before designing the structure of the wing, namely the wingbox and its ribs, as well as its canopy, it is essential to identify the materials that could be used and catalogue their mechanical properties. Two sets of three materials

were identified: one with three materials that could be used for the wingbox and ribs, summarised in Table 7.8; the other set of three materials, presented in Table 7.9, will be considered when sizing the canopy of the wing. The materials selected for the canopy of the wing were retrieved from [16] and [17] as the materials used for inflatable kite were assumed to be applicable for the wing design considered for this project.

Table 7.8: Mechanical properties of materials considered for the wingbox and ribs design

Materials	**Density, kg/m^3**	**Specific Stiffness, MNm/kg**	**Shear modulus, GPa**	**Specific strength (tension), kNm/kg**	**Specific strength (compression), kNm/kg**	**Specific strength (shear), kNm/kg**
Aluminium 2014-T6 (*)	2780	28.20	27	148.92	148.92	61.87
Titanium Ti-6Al-4V (*)	4430	24.83	44	205.87	189.39	137.92
QI Carbon Fibre Epoxy	1500	32.13	18	445.33	433.33	66.66

Table 7.9: Mechanical properties of materials considered for the canopy of the wing

Materials	**Density, kg/m^3**	**Specific stiffness, MNm/kg**	**Specific strength (tension), kNm/kg**	**Service temperature range, °C**
Nylon-6	1130	4.42	730.09	-60; 255
Vectran	1400	39.29	2071.43	-100; 150
Dacron	1380	3.26	415.22	-60; 120

All materials listed here above were retrieved from the material database Granta EduPack [5]. This database provides properties for a wide range of materials and parameters such as temperature. When available, the mechanical properties of the materials listed in Table 7.8 (identified with an asterisk; (*)) were taken at a temperature of -50 °C as this approaches the service temperature that will be experienced by the wing while operating on Mars. This was indeed necessary in order to comply with requirement TEC-AIR-12. When not available for low temperature, the material properties were taken at room temperature (i.e. 23 °C).

The canopy materials considered in Table 7.9 are limited to a minimum service temperature estimated at -60 °C for Nylon-6 and Dacron and to -100 °C for Vectran. As presented in subsection 7.3.1, requirement TEC-AIR-12 cannot be complied with for such materials, as the polymers considered cannot be used up until -190 °C. As this consideration has been uncovered in a late stage of the design process, the structural characteristics of the canopy of the wing will not consider this requirement due to time constraints. However, it is essential to reconsider the material selected for the canopy in the subsequent design phase, or perform testing on the mechanical properties of the three materials listed in Table 7.9 at low temperatures (i.e. around -190 °C). Possible replacement for the polymers considered were identified by plotting the specific stiffness against the specific strength of various materials, namely fibers, plastics and elastomers, shown in Figure 7.14. As will be explained in subsection 7.3.6, the strength and stiffness are of prime importance for the canopy design. Using Granta EduPack 2020 material database, this diagram provided that polyethylene fibres (i.e. Spectra 1000 and 900), silicon carbide fibres or Kevlar fibres would perform best in terms of stiffness and strength, as well as having a minimum service temperature of -200 °C.

[5] https://www.ansys.com/products/materials/granta-edupack [Accessed on June 20, 2021]

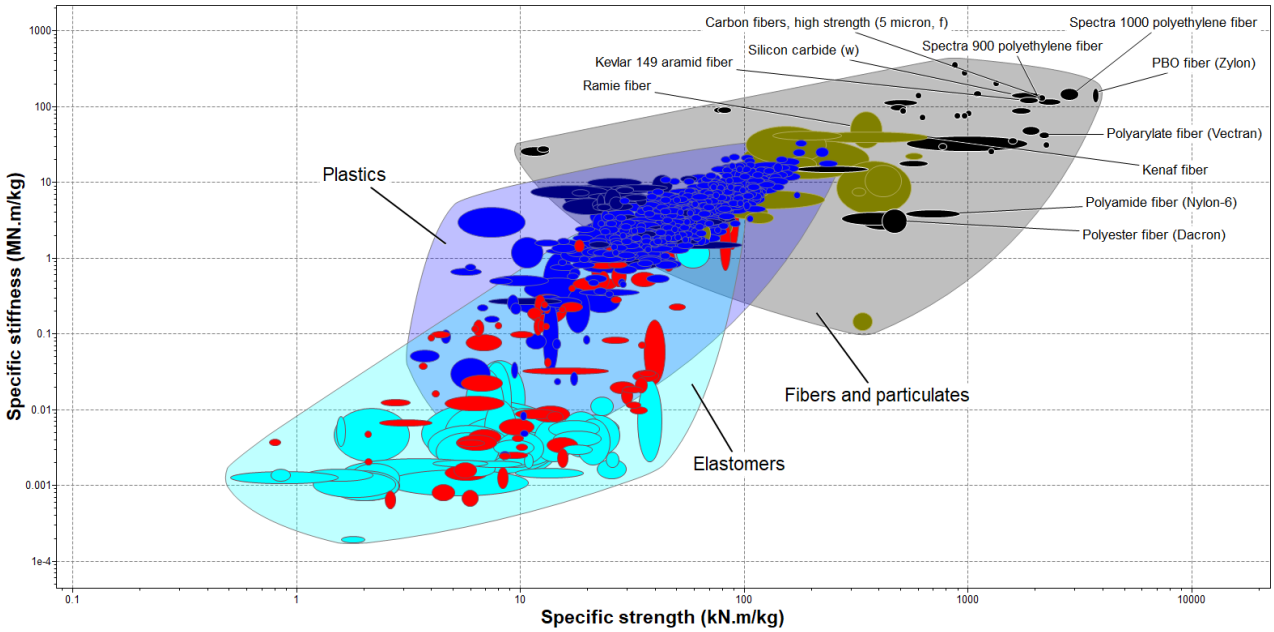

Figure 7.14: Recommended materials for future canopy design

7.3.4. Model Description

The computational model developed to characterise the structure of the wing consists of three main parts: the wingbox model, that combines all the loads, transfers the bending loads and hosts attachments to the tethers, and sizes the thickness of the wingbox along its span; the rib spacing model, that provides the rib distribution as well as the mass of the canopy; and the rib design model, that aims at sizing the ribs, which shall transfer the loads from the canopy to the wingbox by attaching the canopy in one place and giving the aerodynamic shape to the wing.

The codes for the wingbox and ribs are independent of each other and the weight of the wingbox depends on the loading and the wing configuration. The locations of the ribs depends on the canopy material, since the limiting requirement in the ribs spacing is the deflection of the canopy material. Finally, the rib design model depends mainly on the rib distributions and the wing configuration.

The primary goal of the structural model is to calculate the mass of the structure for various materials, for both wingbox, ribs and canopy. In order to accommodate for the carbon fiber epoxy, the thicknesses are increased in steps of 0.88 mm, since the single layer would be 0.22 mm [6], the sum of layers in $0°, 90°, 45°$ and $-45°$, directions would be 0.88 mm. The model was used to calculate masses for different sizes of the wing in order to ensure that the requirements for power generation are satisfied. The 60 m^2 area was chosen, since lower areas in combination with their weight do not produce sufficient power.

7.3.5. Wingbox Design

The wingbox design was done by analysing all loads present on the wing during flight, all shear forces, moments were summed up after which the normal and shear stresses were calculated. Lastly the deflection and twist of the wing were assessed. This was done by moving from the tip towards the root of the wing along the wingboxes and only taking the forces on the analysed part of the wing into account. To check the feasibility of the design each loading case had a requirement to abide. This was done by use of a python program which shall be explained in the next section. In the following paragraph the manner in which this was done will be described in more detail. First the assumptions shall be added.

- Thin walled assumption are used in calculating the shear flow, this is allowed as the thickness shall always be below 10 times the radius of the wingbox.
- Skin of the wing is assumed to not be a structural element of the wing, as it is a soft membrane.
- The effects of temperature fluctuation loading are neglected.
- Considering twist and deflection the assumption was made that it could be analyzed from the tip towards the root. This shall be further explained in the particular sections.

[6] https://www.easycomposites.co.uk/250g-unidirectional-carbon-fibre-cloth [Accessed on June 22, 2021]

The wingbox to be designed needed the biggest possible area moment of inertia, this lead to the use of a circular wingbox fitted at the highest thickness of the wing. This thickness was expressed as a function of the chord which lead to a relation of the diameter of the tube to the chord, in our case the radius was 6.85% of the chord length. All the wing characteristics determined by the aerodynamic characteristics were inputted into the model as parameters. As a sweep angle (η) is present, the formula describing the chord length perpendicular to the central axis through the wingbox is given in 7.21.

$$C(x) = \cos(\eta)(\frac{C_{root} - C_{tip}}{b/2} x \cdot \cos(\eta) + C_{tip}) \tag{7.21}$$

In this formula b describes the total wingspan and x is a variable along the wingbox axis.

Force Characterization

In the model only 4 forces were analysed, these are the lift, drag, weight and the control tether force on one side. The lift was analysed by use of points describing Cl along the span of the wing determined in the aerodynamic characteristics. As the chord varies along the wingspan as well this leads to 7.22.

$$L(x) = Cl(x)C(x)dx \cdot q \tag{7.22}$$

Here q describes the dynamic pressure and Cl(x) the liftcoefficient along the wingbox axis found in the aerodynamic analysis of the wing, note that a correction factor of $\cos(\eta)$ had to be applied to create the liftcoefficient along the wingbox axis from the liftcoefficient along the wingspan axis. This same approach has been used to quantify both the drag and the moment at the aerodynamic center. L(x) describes the amount of lift at a infinitesimal area along the wingbox central axis. The same method was used to describe the drag of the wing. The weight of the analysed part of the wing is continuously updated by calculating the cross-sectional area of the wingbox and multiplying it with the density, only the weight of the wingbox is taken into consideration. The point of application of the lift along the x-axis are described by use of the following formula 7.23.

$$x_{app} = \frac{\int_0^x L(x)x}{\int_0^x L(x)} \tag{7.23}$$

This formula is used by to determine the points of application of the weight and the drag as well. The points of application on the y- and z-axis are determined for the lift and drag to be at an assumed aerodynamic center of 0.25 of the chord. C of the The direction of the forces relative to the axis system is determined by the angle of attack and the flight path angle, banking angles are not taken into account. Both lift and drag are to be decomposed in forces in the axis system by use of the angle of attack whereas the weight is to be decomposed by use of a total angle calculated by adding the flight path angle and the angle of attack. The direction of the force of the control tether is defined by use of the angles γ and θ as depicted in 7.13.

Failure Modes

In order to asses failure of the wing, multiple constraints have been set inspired by different parameters, in this subsection these shall be explained one by one. The constraints accounted for are the following:

- Exceeding of the yield stress
- Deflection of the wing
- Twist of the wing
- Buckling

First of all the yield stress should not be exceeded. Since only elastic deformation is allowed, no forces shall create stresses above the yield stress of the material. When using carbon fiber the yield stress is different for compression and tension. The limits are found using the database of Granta Edupack [7].

Secondly the deflection of the wing has been given a constraint. A deflection causes a reduction in aerodynamic properties and should therefore, to a certain extent, be prevented. A value of 0.5 m has been set arbitrarily and is to be complied with as described in TEC-AIR-15.

Thirdly the twist of the wing has been given a limit. Again, the twist would affect the aerodynamic properties of the wing and should therefore be prevented. As a high rate of twist at the root would cause the entire wing to be twisted, a twist distribution has been determined with a relatively smaller rate of twist at the root. A distribution has been chosen arbitrarily and is defined by $Twist[°] = \sqrt{x}$. Note that x is chosen to be zero at the tip. Using this equation as a constraint leads to a low rate of twist at the root as the derivative of the given

[7] https://www.ansys.com/products/materials/granta edupack[Accessed on June 20, 2021]

function decreases with increasing x. A total angle of twist of at most 3.3 degrees is allowed. This complies with requirement TEC-AIR-16.

Lastly the buckling is to be assessed, this is by definition a mode of failure and should be prevented. Buckling, in our case, could be created by two types of loading, torsion and bending. For the two different types of loading, the expressions approximating the maximum stresses, retrieved from [18], are described in Equation 7.24 and 7.26 [18].

$$\sigma_{max} = \frac{\gamma E}{\sqrt{3(1-\mu^2)}} t/R \tag{7.24}$$

In which E describes the young's modulus, μ describes the poisson ratio, t describes the thickness and R describes the radius of the tube. γ is computed by 7.25.

$$\gamma = 1 - 0.731(1 - e^{(-\frac{1}{16}\sqrt{R/t})} \tag{7.25}$$

The equation below describes the maximum amount of shear stress before buckling in a thin-walled cylinder.

$$\tau_{max} = \frac{0.747 * \gamma^(3/4) * E}{(R/t)^(5/4) * (l/R)^(1/2)} \tag{7.26}$$

In the equation for maximum shear stress γ is defined differently to be equal to 0.586.

Methodology

In order to check for all constraints, shear force and moment diagrams are created from the tip towards the root. The sign convention used is depicted in 7.15.

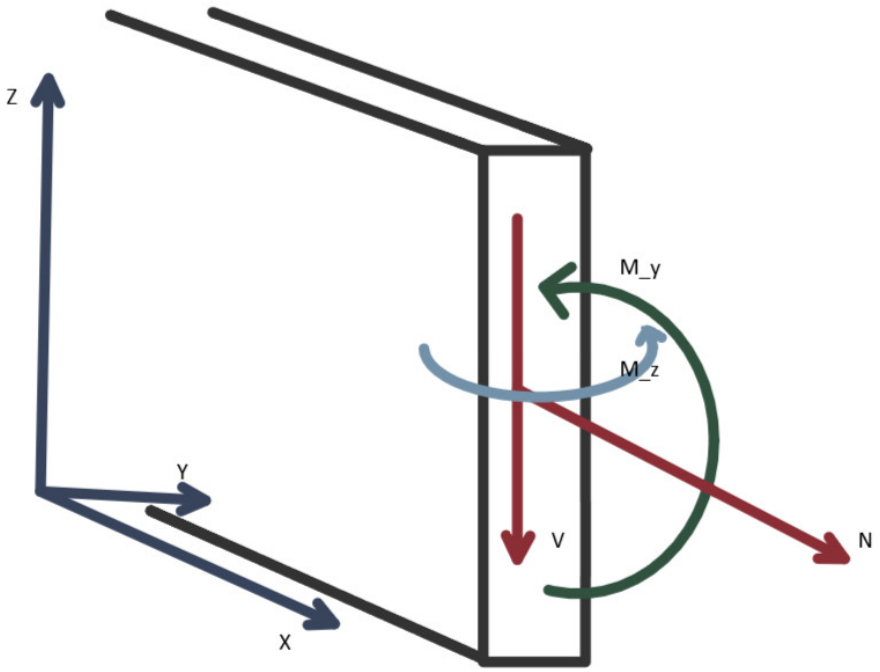

Figure 7.15: Sign convention of shear force [8]

From these diagrams the shear force and the moments at all positions are determined. All constraints shall be evaluated from these diagrams. As could be seen in the verification the moments conventions slightly differ, all moments are positive by following the right hand conventions. This has been accounted for in the formulas used. First of all the stresses are to be computed, these are computed using 7.27 [19].

$$\sigma_x = -\frac{I_{zz}M_y - I_{zy}M_z}{I_{zz}I_{yy} - I_{zy}^2} z + \frac{I_{yy}M_z - I_{zy}M_y}{I_{zz}I_{yy} - I_{zy}^2} y \tag{7.27}$$

It should be noted that equation 7.27 has already been modified to our coordinate system. As the cross-section has an axis of symmetry I_{zy} is zero and the formula is to be deduced to 7.28.

$$\sigma_x = -\frac{M_y}{I_{yy}} z + \frac{M_z}{I_{zz}} y) \tag{7.28}$$

The python program will follow the circular cross-section along its outer circumference after which both the biggest and smallest normal stresses are compared to both the compression and tension yield stress.

The deflection is to be calculated by use of 7.29 [].

$$\frac{d^2v}{dx^2} = \frac{M_y}{EI_{yy}} \tag{7.29}$$

By use of the python program the deflection is integrated and a total deflection is computed. This is done in two directions,both a deflection out of the yx-plane coinciding with an upward or downward movement of the wing and a deflection out of the xy-plane coinciding with a forward or backward movement of the wing.

Thirdly the twist is to be computed, this is done in the same manner as described for the deflection. However, the twist is given by 7.30 [19].

$$\frac{d\theta}{dx} = \frac{M_x}{GJ} \tag{7.30}$$

In this formula θ symbolises the twist in radians whereas G described the shear modulus of the material. J is the polar moment of inertia and is calculated by adding the moments of inertia around the y- and the z-axis. This equation is integrated by use of the python script.

Lastly the buckling constraints are to be complied with. Buckling due to moments perpendicular on the cross-section is determined by the normal stresses accompanying these moments. Therefore the stresses present due to the bending moments are compared with the critical normal stresses calculated by 7.24. The critical shear stress shall be compared to the actual shear stresses in the cross-section which are determined in the following manner. The shear stresses in a thin-walled structure are computed by 7.31.

$$\tau = q_s/t \tag{7.31}$$

Here q_s describes the shear flow, in a general cross-section it is calculated by use of 7.32 [19].

$$q_s = -\frac{S_x I_{xx} - S_y I_{xy}}{I_{xx} I_{yy} - I_{xy}^2} \int_0^s txds - \frac{S_y I_{yy} - S_x I_{xy}}{I_{xx} I_{yy} - I_{xy}^2} \int_0^s tyds + q_0 \tag{7.32}$$

The evaluation of this formula could be done by the use of the following insights. The axis of symmetry causes the function to decrease since I_{xy} is zero and $ds = r * d\theta$ in which θ describes the angle positive counter-clockwise while going through the circumference of the circle. Furthermore the position of the maximum shear stress could already be determined. There will be no shear stress at the axis through which the shear force is applied, the maximum shear stress shall be at an angle perpendicular to the shear force as depicted in 7.16.

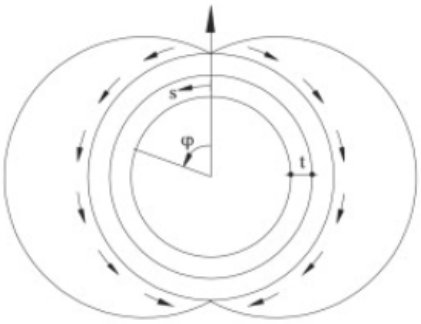

Figure 7.16: Shearflow distribution throughout circular cross-section [9]

This phenomenon is used in the derivation of the equation describing the maximum shear stress. The shear stress shall be evaluated from the axis parallel to the total shear force over a quarter of the circumference towards the point of maximum shear stress. The angle of the shear force with the x-axis has been chosen to be ϕ This leads to the derivation of 7.33.

$$q_s = \frac{-S_y t \cdot r^2}{I_{xx}} \int_{\phi}^{\phi+0.5\pi} \sin(\theta) d\theta - \frac{S_x t \cdot r^2}{I_{yy}} \int_{\phi}^{\phi+0.5\pi} \cos(\theta) d\theta + q_0 \tag{7.33}$$

This general formula is used to describe the shear force induced maximum shear stresses within the cross-section. Note that this formula has to be modified into the yz-plane used in which the positive y-axis points

towards the left. q_0 is the amount of shear flow at the point from which the shear flow has been calculated, in this case at angle ϕ. Furthermore the twist created by the forces induces a shear flow, as ϕ is defined to be at the point where the shear forces do not create a shear flow, the twist is the only shear flow at point ϕ and is thus equal to q_0. It will be computed using 7.34.

$$q_0 = \frac{M}{2A_{enclosed}} \tag{7.34}$$

The maximum shear stress found by use of 7.33 is to be compared with the maximum allowable shear stress found by the buckling equations.

Model Implementation

In order to implement all these different failure modes into a model the schematic in figure 7.17 was used.

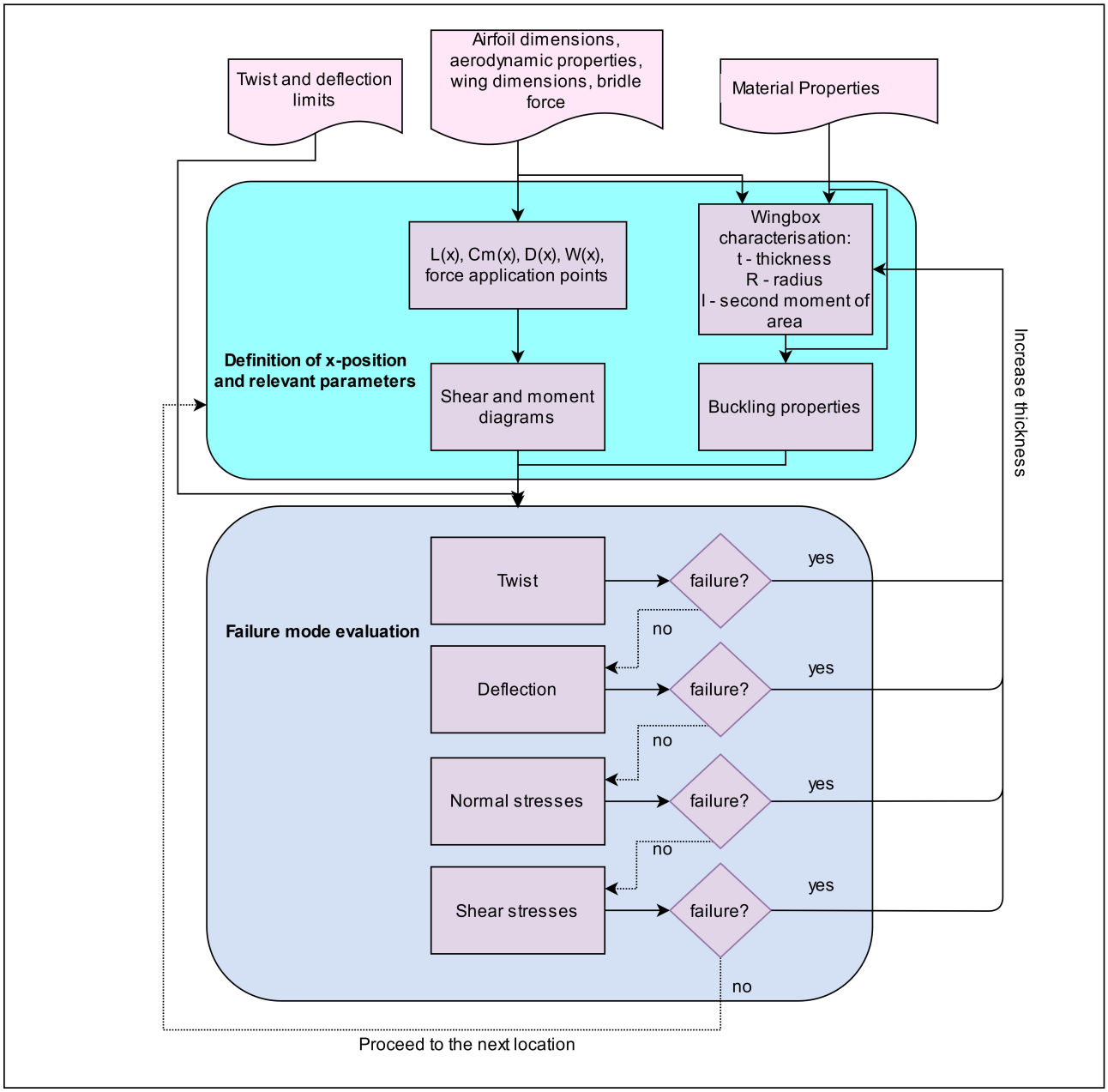

Figure 7.17: Structural analysis flow diagram

As depicted in the flow diagram the inputs of the model are the different wing characteristics, the material properties, the assumed bridle force and the chosen twist and deflection limits. After defining these parameters the position of x along the wingspan shifted each step from the tip towards the root of the wing, at each step the shear force and the internal moment were determined and the modes of failure were evaluated. If the wing failed at a certain point, the thickness was increased until the wingbox was able to withstand the present forces

and moments. The evaluation of the different failure modes was done in the sequence as depicted, this was done to decrease computation time.

Verification and Validation of the Model

In order to verify the model all aspects and all calculations need to be checked, this has been done by a combination of hand calculations and inspection of the graphs produced.

First of all the approximations describing the lift, the drag and the aerodynamic moment are to be verified, this is done by inspecting the graphs shown in figures 7.18 and 7.19.

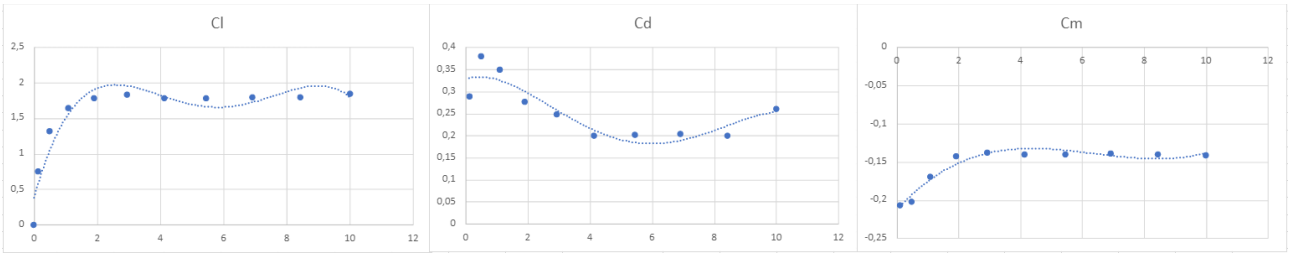

Figure 7.18: Cl, Cd and Cm graphed over the wingspan, values retrieved from XFLR 5

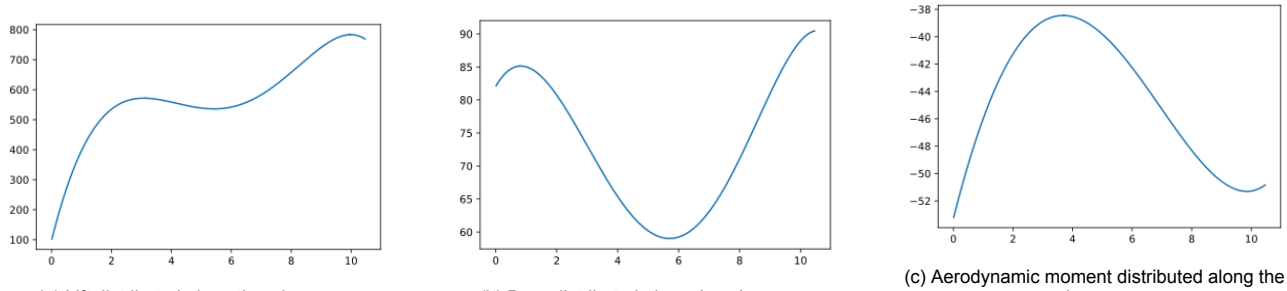

(a) Lift distributed along the wingspan.

(b) Drag distributed along the wingspan.

(c) Aerodynamic moment distributed along the wingspan.

Figure 7.19: Model output of aerodynamic forces

The upper figure shows the computed datapoints of the coefficients, a curve has been drawn in order to create a continuous function. As can be seen all distributions follow the curves of their coefficient, however as the chord length increases towards the root the total lift, drag or C_m shall be increased. These graphs have been checked in two different manners, first of all the root values are normalised by dividing the root value by 1.4, the taper ratio, and the resulting ratio between the tip and the root is checked with the coefficients. It should noted that the dynamic pressure used in this case was assumed to be at maximum load and thus a chosen velocity of 120 m/s is used. The values of total lift and total drag are found to be 10898 N and a drag of 1464 N were found to be correct. The total aerodynamic moment is found to be -892 Nm which seems reasonable if the C_m coefficients compared to the Cd values given. Note that the moment is a pitch down moment, this is because only the aerodynamic properties of the wing at an angle of attack of 20 degrees are assessed, this was initially done to analyse the loads for maximum lift.

As the shear forces acted upon the wingbox are the base on which the entire script rests, it is vital to model the shear forces correctly using the equations described the previous sections of this section. Therefore the graphs below shall show the shear force diagrams without any form of safety factor, zero angle of attack and a bridle force of 2000 N pointing downwards perpendicular on the wing. This bridle force or control tether force is assumed to be applied at the tip of the wing. The minimal thickness of the carbon fiber plate was assumed to be 0.89 mm during verification.

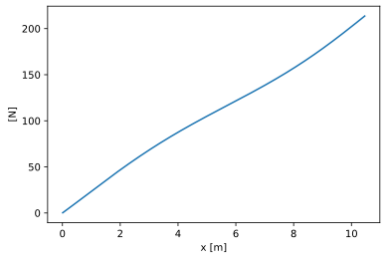

(a) Shear force diagram V_x along wingbox

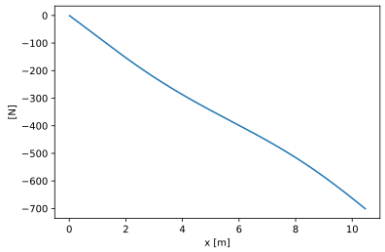

(b) Shear force diagram V_y along wingbox

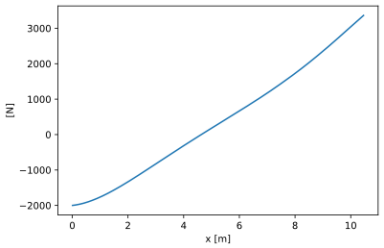

(c) Shear force diagram V_z along wingbox

Figure 7.20: Model output displayed in shear force diagrams

Considering figure 7.20, verification is easily done. The shear force in y direction shall be mainly affected by the drag of the wing, however the drag shall have to be decomposed to the chosen y-axis by multiplying with the cosine of the sweep angle. As stated in the previous section the total drag is computed to be 1464 N resulting in a drag of 732 N per wing. This coincides with the negative value of 700 at the root in figure 7.20b. Multiplying the sine of the sweep angle with the total drag results in the diagram of 7.20a. As tension is chosen to be positive in this section this shall yield a positive V_x. Lastly the shear force diagram in Z-direction is verified by inspection as well. At first the bridle creates a negative shear force at point x=0.1 after which the lift slowly increases the shear force to a root shear force of approximately 3.4 kN. This coincides with a lift per wing of 5449 N and a bridle force of 2000 N acting in opposite direction. The weight of the wingbox is negligible compared to the lift.

The moment diagrams created by the python program are shown in the Figure 7.21, These are

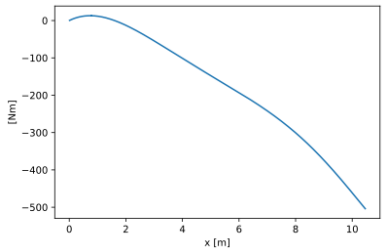

(a) Moment diagram M_x along wingbox

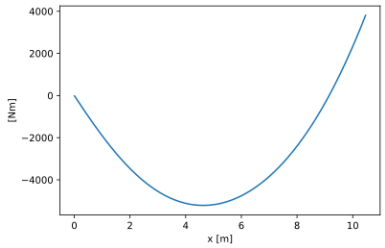

(b) Moment diagram M_y along wingbox

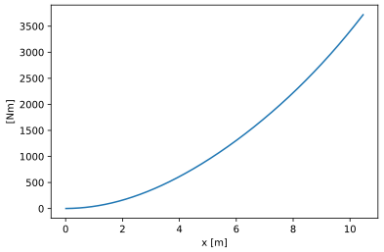

(c) Moment diagram M_z along wingbox

Figure 7.21: Model output displayed in shear force diagrams

In the figure above M_x represents the twist. As the bridle point of application is below the center of gravity of the wingbox, in this case no moment shall be created by the bridle force. Due to the angle of attack to be zero the drag is alligned with the center of gravity as well, the weight is by definition not creating any moment around the center of gravity. This leaves only the lift and the aerodynamic moment to create twist. The lift induced moment can be roughly calculated by taking the difference between the aerodynamic center and the center of gravity in chord percentage and multiplying it with the total lift and the chordlength. This yields, taking the average chord of 3 m and the difference to be 0.05, a pitch up moment of 955 Nm. As the computed aerodynamic moment of one side of the wing was found to be 446 Nm pitch down moment, this would result in a pitch up moment of approximately 510 Nm. This coincides with the diagram.

Considering the moment diagrams of M_y and M_z, these are both verified by hand computations as well. A quick glance at the drag diagram would indeed result in the diagram shown in figure 7.26c for a right-handed positive moment. The same sort of back of the envelope calculation could be done to verify the diagram describing M_y.

The formulas used to compute the twist and the deflection throughout the wingbox are to be verified as well. This shall be done by means of hand calculations. As the twist is taken from the tip towards the root the constants of integration needed while integrating from equation 7.30 towards the actual twist are unknown, and taken to be zero. This leads to the following graph 7.22.

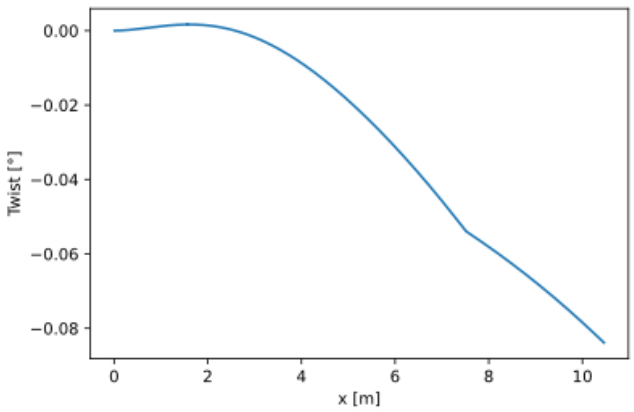

Figure 7.22: Twist diagram along the wingbox

It should be noted that the twist at the root of the wing should be zero. The graph should thus be twisted until both the rate of twist and the total twist are equal to zero at the end of the wingspan. During the running of the script however this rotation can not be done and the twist as shown in the graph is compared to the set limits. This approximation is believed to be valid for very small angles of twist and small rods.

As described in equation 7.30, the twist is dependent on the diagram of M_x, the youngs' modulus and the moment of inertia. Comparing the diagram with the diagram in figure 7.26a, the shapes seem very similar. Furthermore the point where the rate of twist equals zero has been computed by the script to be at 1.6 coinciding with M_x. At a point between 6 and 8 a kink is present, this is due to an increasing thickness at this point, increasing the moment of inertia which could be seen in figure 7.27.

The deflection has been computed in the same manner, by integrating while letting the computer take small steps. The following figure displays the upwards positive deflection of the wing.

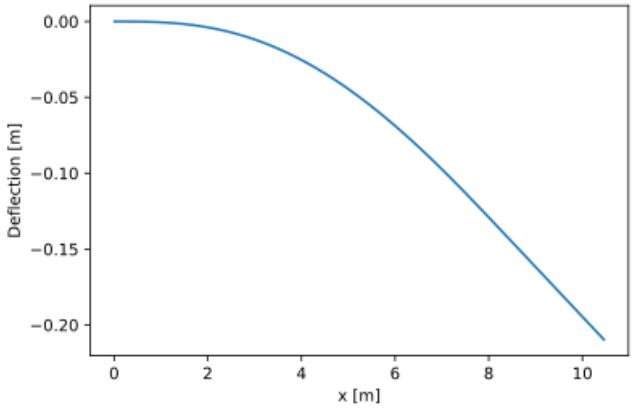

Figure 7.23: Deflection diagram along the wingbox

Again the diagram should be twisted until both the derivative of the deflection and the deflection itself is zero at the root. This approximation is believed to be valid for small angles of deflection as present in our case. When comparing this with the diagram of M_y this graph shows its similarity's.

It has been found however that the assumption taken is invalid, therefore the total deflection was calculated afterwards to check if requirements have been met. A new derivation calculating the total deflection of the wing was found. To implement this, the model computes the total deflection and compares it with the requirements. In this paragraph the derivation of the formula shall be shown after which the results shall be updated accordingly.

In figure 7.24 a graphical depiction of the derivation has been depicted.

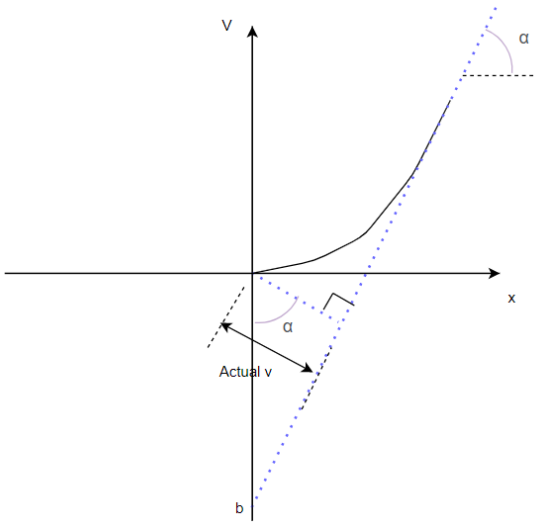

Figure 7.24: Derivation of actual deflection formula

In order to correctly calculate the deflection as seen from the root, the entire graph should be twisted. The deflection is defined as the distance Def. depicted in the figure. This distance could be found by finding the intersection point between the blue and the red line. The red line is mathematically defined by 7.35.

$$\begin{aligned} v_{red} &= \frac{dv}{dx}_{end} * x + b \\ b &= v_{end} - \frac{dv}{dx}_{end} * x_{end} \end{aligned} \tag{7.35}$$

The blue line is defined by equation 7.36.

$$v_{blue} = -\frac{1}{\frac{dv}{dx}_{end}} * x \tag{7.36}$$

When the intersection is found, Pythagoras' theorem can be used to calculate the total deflection. This same derivation is to be used to describe the total twist relative to the root.

Considering the normal stresses computed throughout the wingbox these have been verified by hand calculations to be correct. Furthermore the outputted diagrams have been shown in figure 7.25.

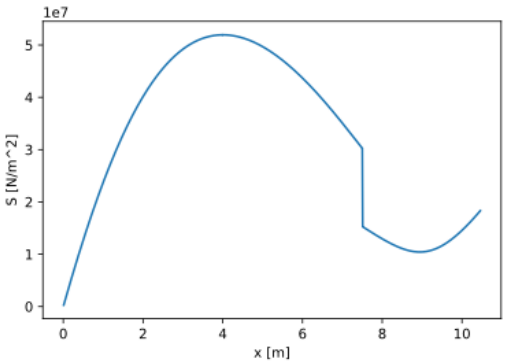

(a) Compression normal stress along the wingbox, a positive stress is chosen to depict compression stresses

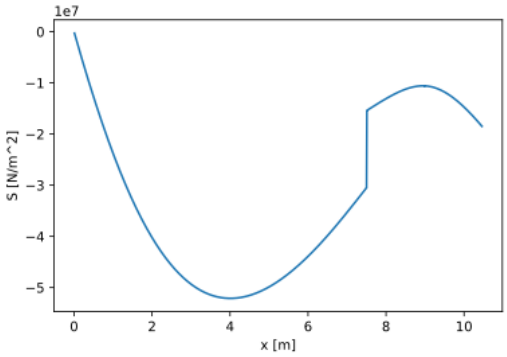

(b) Tension normal stress along the wingbox, a negative stress is chosen to depict tension stresses

Figure 7.25: Normal stress diagrams

As can be seen the normal stresses coincide, as expected, with the diagram of M_y mainly, the kink in the cable is caused by the increase in thickness as shown in 7.27. Note that compression has been chosen to be a positive normal stress.

The formulas used for the shear stresses have been verified by hand, this was done by comparing answers of the model to textbook examples. Furthermore the independence of the maximum shear force induced shear

flow to the angle of the shear force has been verified. This leads to a certain confidence in the maximum shear flow calculations. Furthermore as the twist induced shear flow is just a simple formula given by equation 7.34 this was easily verified by hand calculations as well. The sign convention used could have caused trouble since the maximum shear force induced shear flow was calculated in one direction only, which could be the opposite of the twist induced shear flow. This obstacle has been avoided by the use of taking the absolute of both calculated shear flows which, since the shear force induced shear flow is symmetric, shall always be correct. In the figure below the shear force induced shear flow diagram has been given over the span of x, compared to the shear forces and the thickness change of the wingbox, the shearflow throughout the wingbox is believed to be reasonable.

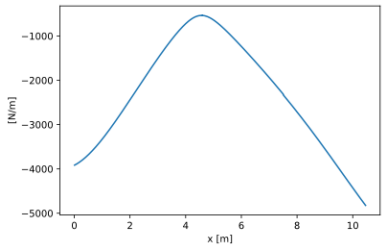

(a) Shear force induced shear flow along the wingspan

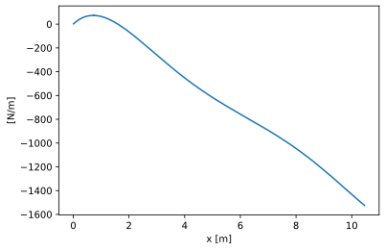

(b) Moment induced shear flow along the wingspan

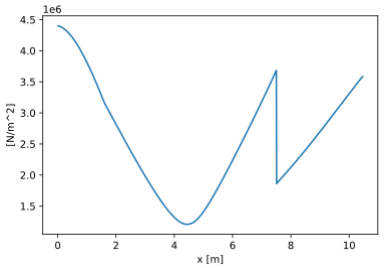

(c) Maximum shear flow along the wingspan

Figure 7.26: Shear flow diagrams

As can be seen when comparing the diagram of V_z with the shear force induced shear flow diagram, both coincide. As V_y does not have a great magnitude compared to V_z it does not have as big of an influence. The great kink is caused by the change of thickness at that point along the axis as shown in figure 7.27.

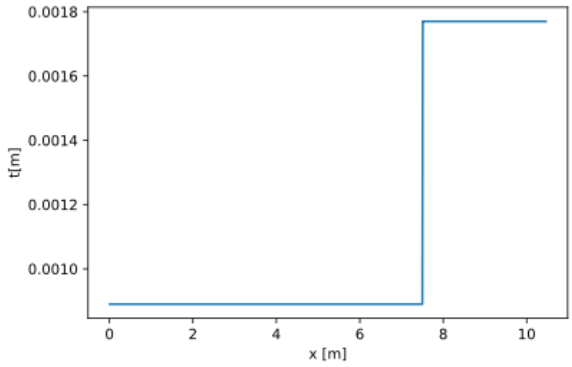

Figure 7.27: Thickness t along the wingbox

Results

To analyze the results of the wingbox a safety factor of 1.25 has been added to all forces, an angle of attack of 20 degrees has been used to characterize the maximum lift and drag, lastly the velocity is taken to be 120 m/s, the maximum speed. The minimum thickness of the carbon fiber plate is 0.88 mm and this shall be the minimum thickness and the stepsize of the carbon fiber. As the most important input shall be the force of the control tether, in figure 7.28 the weight for half the wingbox is examined for different values of control tether force.

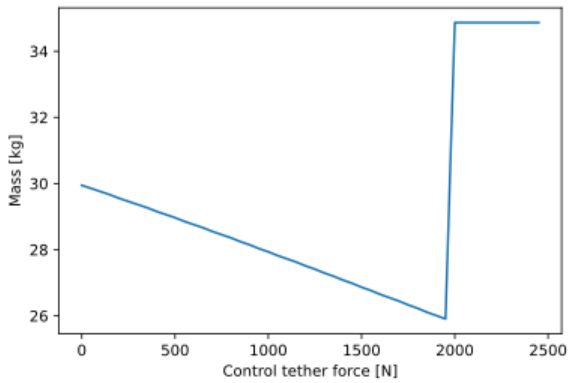

Figure 7.28: Weight dependence on maximum force of the control tether

As could be seen in the graph the weight is determined by determining a range of allowable control tether forces. Assuming the 10 percent load on the control tether, this would lead to a tether force of around 550 assuming 11 kN of lift. This leads to a total weight of 57.9 kg of the wingbox. As is shown the structure will be able to withstand higher tether forces if necessary, lower tether forces however is not accommodated for, thus a minimal tension shall have to be kept on the control tether. The reason the weight increases so suddenly at around 2000 is because the structure is unable to withstand the amount of shear at the tip caused by the bridle force. The deflection and the twist stay within their limits throughout all different cases.

Figure 7.29 displays the thickness throughout the wingbox.

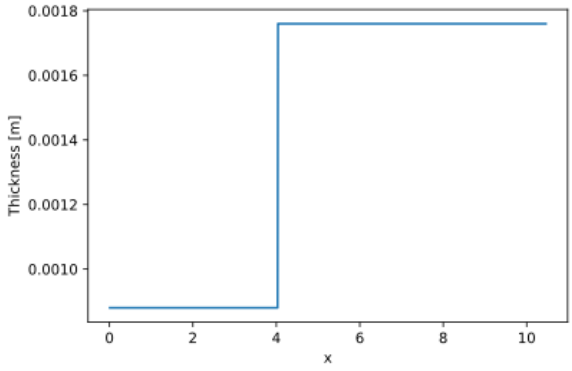

Figure 7.29: Thickness t along the wingbox

This leads to a total weight of the wingbox of 57.9 kg. The twist was found to be -0.08 degrees throughout the wingbox, read pitchdown 0.08 degrees, and the total deflection was found to be 21.8 cm upwards.

Sensitivity analysis

In this section the sensitivity of the program for mistaken inputs shall be displayed, this is done by changing the following inputs slightly, by 5 percent. Forces such as lift shall not be changed as these follow from performance requirements and are thus not variable.

1. Young's Modulus
2. Shear modulus
3. Compression yield stress
4. Thickness of the wing

Only the case which lead to the result above has been examined, the results of this sensitivity analysis are summarized in table 7.10.

Total mass [kg]	-5 %	+5%
Young's modulus	58.16	57.30
Shear modulus	57.71	57.71
Compression yield strength	57.71	57.71
Thickness of the wing	55.03	60.41

Table 7.10: Sensitivity analysis

The shear modulus and the compression yield strength do not change the outcome much, this is because the buckling limits are the limiting factors. These do not depend on the shear modulus or the compression yield strength. The thickness of the wing only increases the weight, this is caused by the theoretically redundant thickness induced by the layering of the carbon fiber. A bigger radius results in more material while the thickness can not decrease due to the minimal thickness of the carbon fiber layer. The young's modulus changed the weight significantly as well, this is due to its importance in buckling requirements.

7.3.6. Rib Spacing

The main functions of the ribs in the structural design proposed for the wing are to transfer the load generated over the skin to the wingbox, as well as giving the aerodynamic shape to the wing. As the skin of the wing is made of a flexible membrane, also called canopy in this report, it is expected to deform as it needs to transfer the aerodynamic loads generated over its surface to the ribs. This deformation behaviour due to the distributed load applied over its surface can be referred to as a ballooning effect. This ballooning effect can be visualised in Figure 7.30. This deformation of the skin of the wing shall be limited as this is expected to alter the aerodynamic properties of the whole wing, as this changes the aerodynamic profile of the wing. In order to limit this ballooning behaviour, the rib distribution along the wingspan shall be tuned to accommodate an acceptable skin deflection, as specified in the requirement TEC-AIR-14. This section will present the rib spacing methods applied to determine the rib distribution, followed by a verification and validation of those approaches. This section will then be concluded by a summary of the optimal rib distribution.

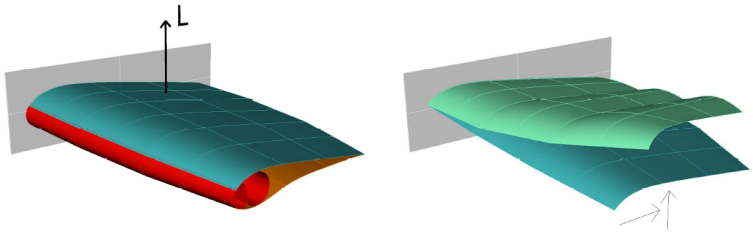

Figure 7.30: Typical canopy deflection of inflatable kite, with ballooning effect shown on the right (Illustration retrieved from [16])

Rib Spacing Methods

The methods to evaluate the deflection of the canopy differ in their working principle, however the rib spacing iteration relies on the same process: a canopy spanning half the wing is evaluated for deflection. If this deflection is too large, the rib pitch is decreased by a small increment and the deflection is evaluated again. Iterating this process until the rib spacing achieved leads to a canopy deflection lower or equal to the allowable skin deflection decided upon provides a rib distribution over the half-wing span. This iterative process is illustrated in Figure 7.31, where one observes the rib pitch is decreased until an acceptable canopy deflection is achieved. In fact, one could suspect that a shorter rib spacing shall lead to a smaller deflection of the skin; this fact will be verified here after. Two methods have been used in this project to provide a preliminary estimate of the canopy deflection due to a given distributed loading. Those are discussed here after.

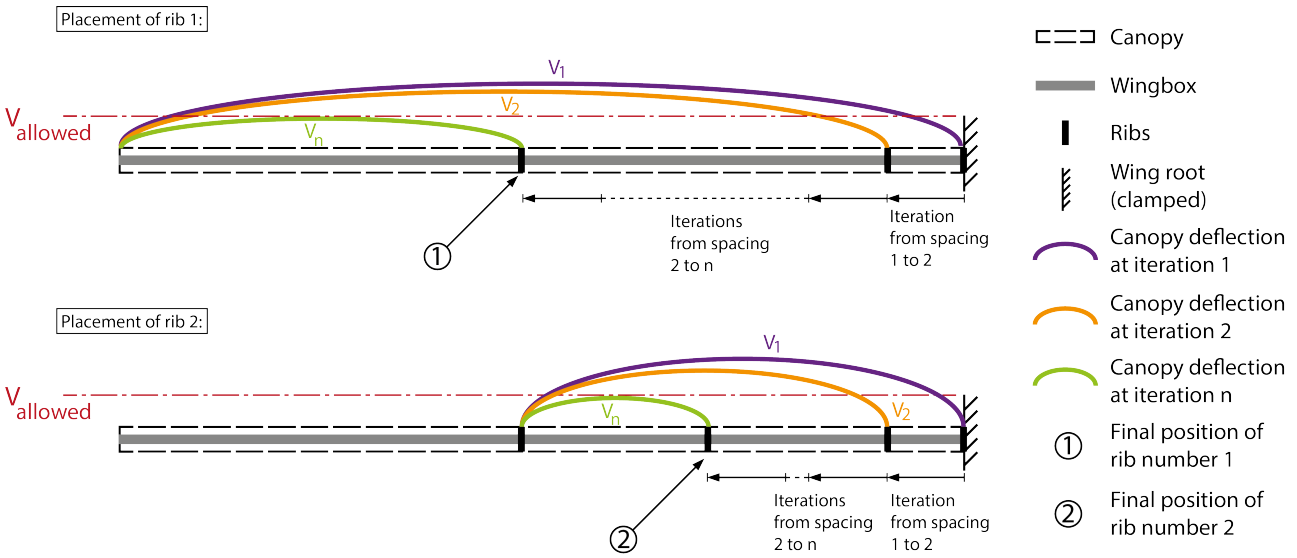

Figure 7.31: Illustration of the rib spacing iterative process

The first approach considered can be referred to as the elastic deflection method. Assuming a generic loading situation over half a wing as shown in Figure 7.32, where a distribution load $L(x)$ is applied on this half wing, the elastic deflection method computes the deflection of the skin between two ribs (shown by thick vertical line in the diagram) and check whether the deflection induced over this rib spacing is acceptable.

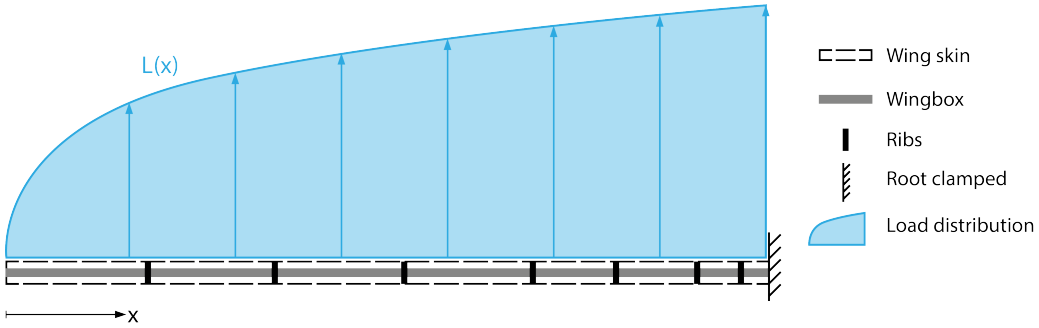

Figure 7.32: Distributed load over the half wing considered for the rib spacing calculation

To determine the ribs positioning that would limit the membrane deflection, this method assumes that the skin between two ribs can be modelled as a thin plate, as illustrated in Figure 7.33. By integrating the distributed load distribution acting over the thin plate considered, a resultant force P of the distributed load can be applied at a distance a from the left-rib, as expressed in Equation 7.37. From this resultant force, one can compute the elastic deflection curve of the plate using the integral method as introduced in [19]. In fact, assuming the flexural rigidity (i.e. EI, where E is the Young's modulus of the beam; I its moment of inertia) is constant along the length of the beam (which will be verified later on), one can compute the deflection of the beam, defined as $v(x)$, by double integration of the internal moment $M(x)$ in the beam, as expressed in Equation 7.38. From this expression, for a point load P applied at a distance a from the left-rib, the deflection $v(x)$ of the canopy spanned over the two ribs is derived to be expressed as Equation 7.39 and 7.40. Please refer to Figure 7.33 for a visualisation of the deflection of the skin, and the situation considered.

$$P = \int_{i_{start}}^{i_{end}} L(x)\,dx \qquad and \qquad a = \frac{\int_{i_{start}}^{i_{end}} L(x)x\,dx}{\int_{i_{start}}^{i_{end}} L(x)\,dx} \tag{7.37}$$

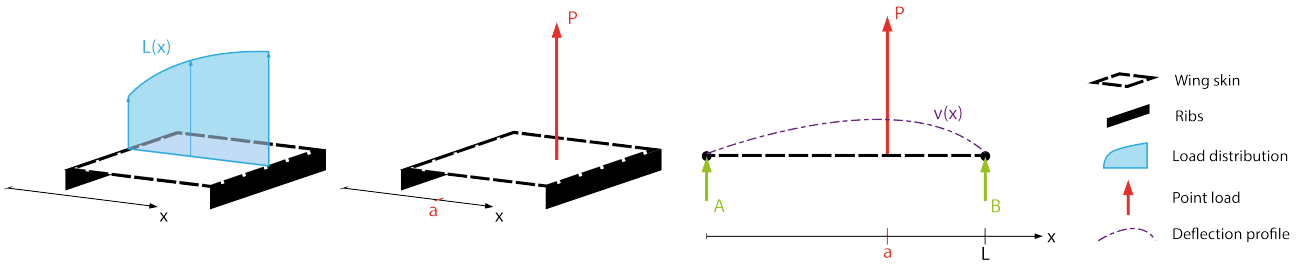

Figure 7.33: Rib spacing configuration considered for the elastic deflection method

$$EI\frac{d^2v}{dx^2} = M(x) \tag{7.38}$$

$$v(x) = \frac{1}{EI}\left(\frac{A}{6}x^3 + C_1x + C_2\right) \qquad \forall x \in [0, a] \tag{7.39}$$

$$v(x) = \frac{1}{EI}\left(\frac{A+P}{6}x^3 - \frac{Pa}{2}x^2 + C_3x + C_4\right) \qquad \forall x \in [a, L] \tag{7.40}$$

In Equation 7.39 and 7.40 the integration constants C_1, C_2, C_3 and C_3 are obtained from boundary conditions and continuity equations, and the reaction force A is evaluated by performing the equilibrium equations. Those are expressed such that:

$$C_1 = \frac{-1}{L}\left(\frac{L^3}{6}(A+P) - \frac{1}{2}PaL^2 + \frac{1}{2}Pa^2L - \frac{1}{6}a^3P\right)$$

$$C_2 = 0$$

$$C_3 = C_1 + \frac{1}{2}Pa^2$$

$$C_4 = C_1a + \frac{1}{3}Pa^3 - C_3a$$

$$A = P\left(\frac{a}{L} - 1\right)$$

The second method considered relies on the elongation of the canopy in axial loading and is therefore referred to as the elongation method in this report. As mentioned previously, the rib spacing iterating process remains unchanged: a given spacing between two ribs is assumed, the canopy spanning these two is evaluated for deflection, if the deflection is above the allowed threshold, the spacing is reduced and re-evaluated, otherwise the next section is evaluated. However, compared to the elastic deformation method, the elongation method does not assume the canopy to be a beam under bending, rather it is considered as a beam under axial loading. The distributed loading acting on the canopy between the two ribs considered is integrated and replaced by a resultant load P using Equation 7.37. This point load is then assumed to act in the plane of the canopy, thus loading it axially. From this axial load P, and assuming the canopy deforms elastically until it yields, the skin will elongate by an amount δ expressed in Equation 7.41, given that its Young's modulus is defined as E, the length of the canopy between the ribs is L, and the cross-sectional area of the skin is defined as A [19]. For a visual representation of the elongation method, please refer to Figure 7.34.

$$\delta = \frac{PL}{EA} \tag{7.41}$$

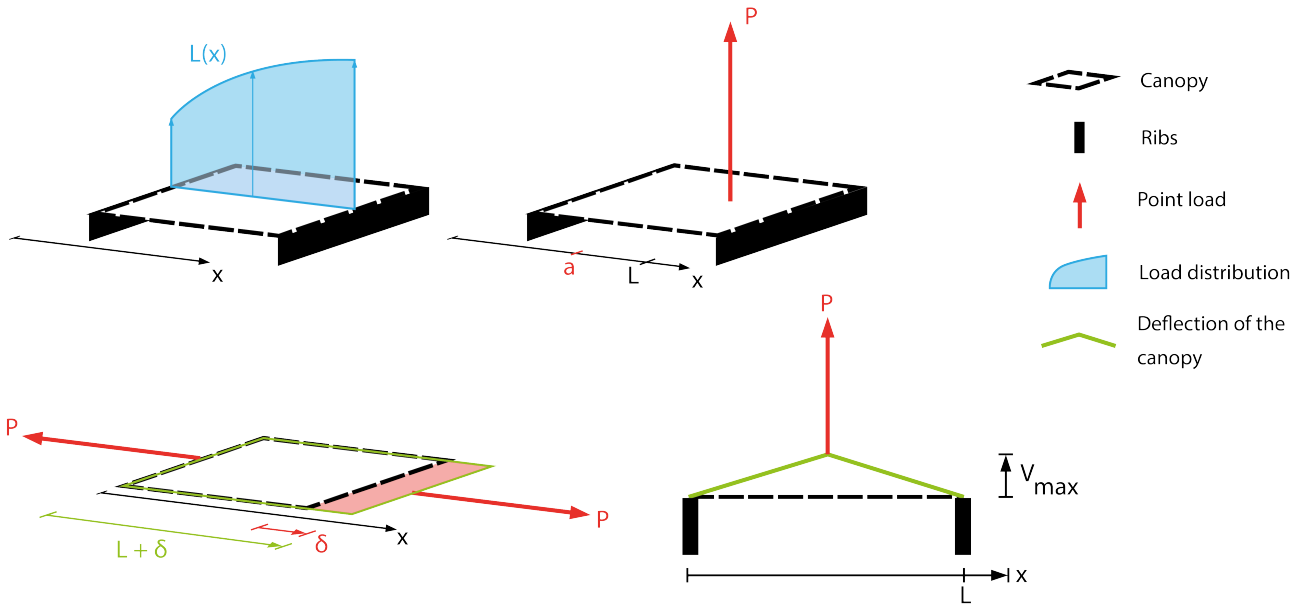

Figure 7.34: Rib spacing configuration considered for the elongation method

As the rib are assumed to remain fix during this elongation, one can compute the maximum out-of-plane deflection v_{max} of the canopy based on the elongation δ and the initial length of the skin L. In fact, as shown in Figure 7.34, a preliminary estimate of the deflection v_{max} can be obtained using the pythagorean theorem. The expression for the maximum deflection of the canopy spanned between two ribs a distance L apart is given by Equation 7.42. Please note that while computing the elongation of the canopy due to axial loads, the normal stress is evaluated and verified against the tensile yield stress of the material, thus avoiding the material to fail. If the yield stress is exceeded, the rib spacing is reduced as this would lower the distributed load applied on the section of canopy, thus reducing the axial load elongating the skin.

$$v_{max} = \sqrt{\left(\frac{L+\delta}{2}\right)^2 - \left(\frac{L}{2}\right)^2} \tag{7.42}$$

The rib spacing computational model developed in Python as presented here above can also be represented in a flow chart as shown in Figure 7.35. In this illustration, the inputs, both in the code and imported from a separate file, are presented on the top, followed by a short description of the five main functions of the model. Finally, the output of the model are shown on the lower part of the diagram, namely being the rib distribution obtained from the elastic deflection method and from the elongation method, as well as the mass of the canopy.

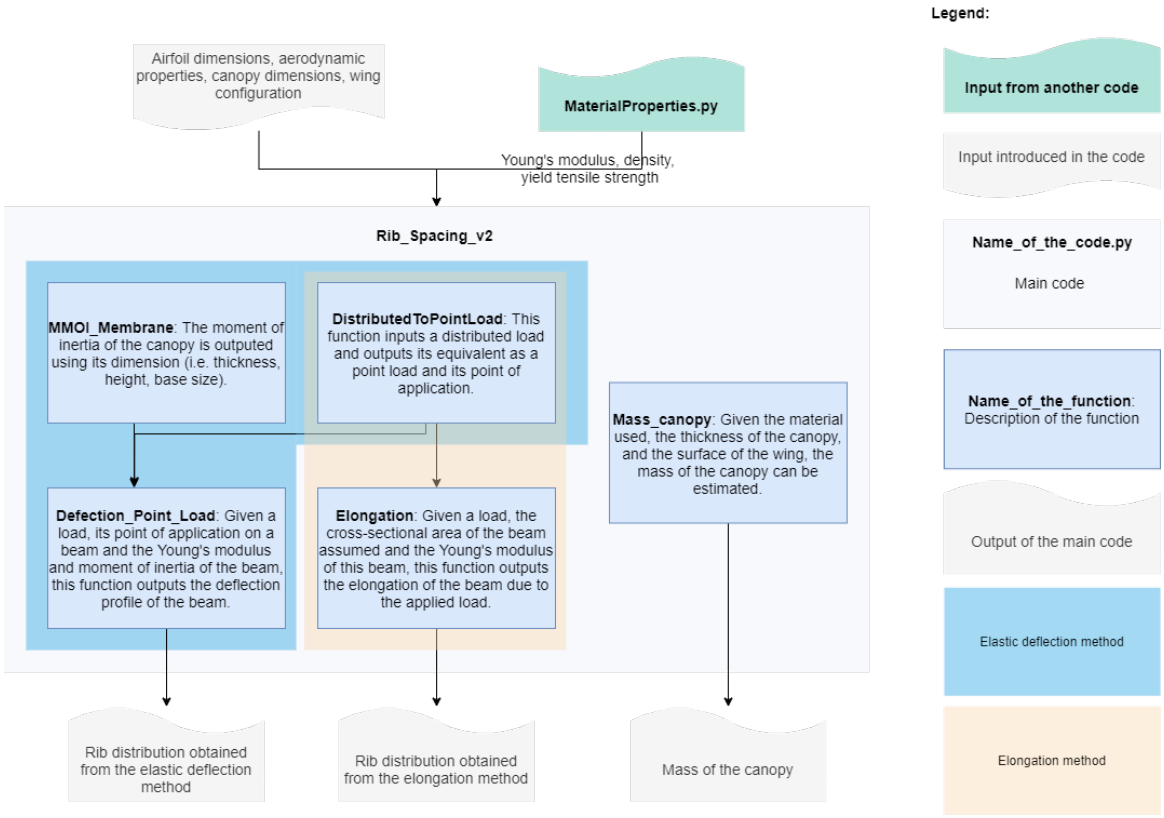

Figure 7.35: Schematic representation of the rib spacing model in a flow chart

Verification of the Rib Spacing Model

Verification is an essential step while developing any computational model, this step aims at confirming that the model has been developed correctly. To verify the rib spacing model, its diverse modules will independently be tested through unit tests, and the larger whole of the code will be verified through system tests. The unit tests will first be introduced and discussed, followed by system tests.

One of the most important part of the rib spacing model is the canopy deflection calculation. For the elastic deformation method, the deflection of the skin was derived from Equation 7.38, providing the expression $v(x)$ as stated in Equation 7.39 and 7.40. One unit test that could verify this module would be to compare the deflection provided by the model to hand calculations for simple situations. Namely, one could test to apply a point load in the middle of the beam, which shall provide a symmetric deflection around the point of application of the load. This is indeed verified as shown in Figure 7.36, showing the deflection of a beam of length 6 m, Young's modulus and moment of inertia both set to one, with a point load of 1 N applied at several instance (i.e. from 1 to 5 m along the beam). This figure indeed shows that a symmetric deflection is obtained by applying the point load in the middle of the beam (i.e. at 3 m). This in turn proves that the constants of integration of Equation 7.39 and 7.40 have been correctly assessed as they lead to a continuous deflection profile over the full span of the beam. One can also observe that for symmetric placement of the point load with respect to the middle of the beam (e.g. with loads at 2 and 4 m), the deflections have a similar profile, simply mirrored around the middle line of the beam. Please note that hand calculations were also performed, and the elastic deflection module was verified against text-book examples.

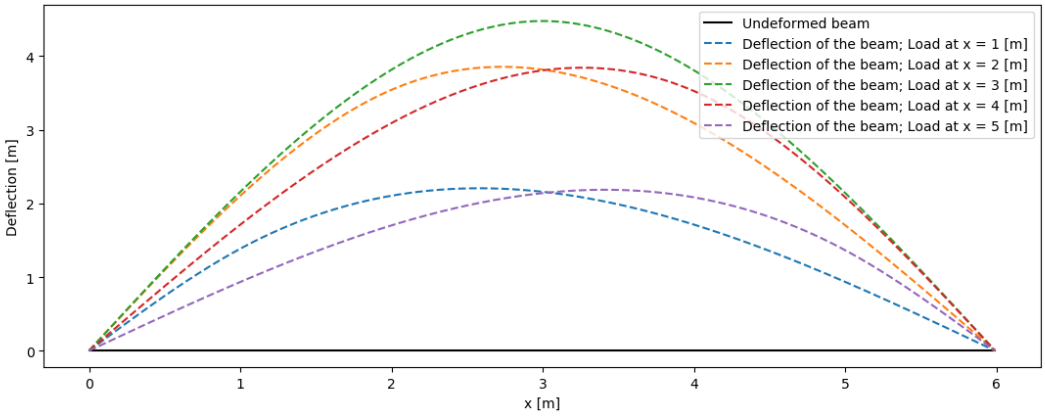

Figure 7.36: Verification of the elastic deflection calculation module.

Besides the elastic deflection method, the elongation method shall also be verified. This approach relies on verifying that Equation 7.41 is implemented correctly and that the elongation δ calculated is accurately passed on to determine the deflection of the canopy. This is indeed correctly implemented in the code as assuming a load $P = 300$ N, a length $L = 1$ m, a Young's modulus $E = 510^6$ Pa and an area $A = 0.0003$ m^2 returns an elongation of $\delta = 0.2$ m as provided by the program. Furthermore, from this elongation, the maximum skin deflection can be estimated using Equation 7.42. Analytically, this expression estimates the maximum canopy deflection to be of $v_{max} = 0.3317$ m as estimated by the model.

Besides, both methods relies on a module transforming a given distributed load $L(x)$ to a resultant point load and distance of application, P and a, respectively, as defined in Equation 7.37. Such a module can be verified by inputting simple load distributions (e.g. uniform, or ramp) and confirm that the provided resultant load and distance match the expected one. For a uniform load distribution defined as $L(x) = C$, where C is a constant real number (e.g. set to $C = 3$ N/m), over a span of 3 m, the resultant load expected shall be $P = 3 \cdot 3 = 9$ N, and shall be placed at a distance $a = 1.5$ m. Similarly, for $L(x) = x$, and over the same span, one shall expect a resultant load of $P = 9$, placed at a distance $a = 2$ m from the left-most point of the span. This is indeed what is computed while running the program for the specified load distributions and spans.

As system tests, the model will be evaluated for a simple loading, namely an uniform loading of 100 N/m in this case, and a constant chord length distribution (i.e. meaning that the taper ratio of the wing shall be set to one, thus a wing with the same chord length at the root and at its tips). For such a situation, the rib distribution along the span of the wing shall be evenly spaced, in fact a constant rib spacing shall be observed. This is indeed observed in Figure 7.37, where the rib spacing is evaluated to be constant, with every rib spaced by 3.46 m.

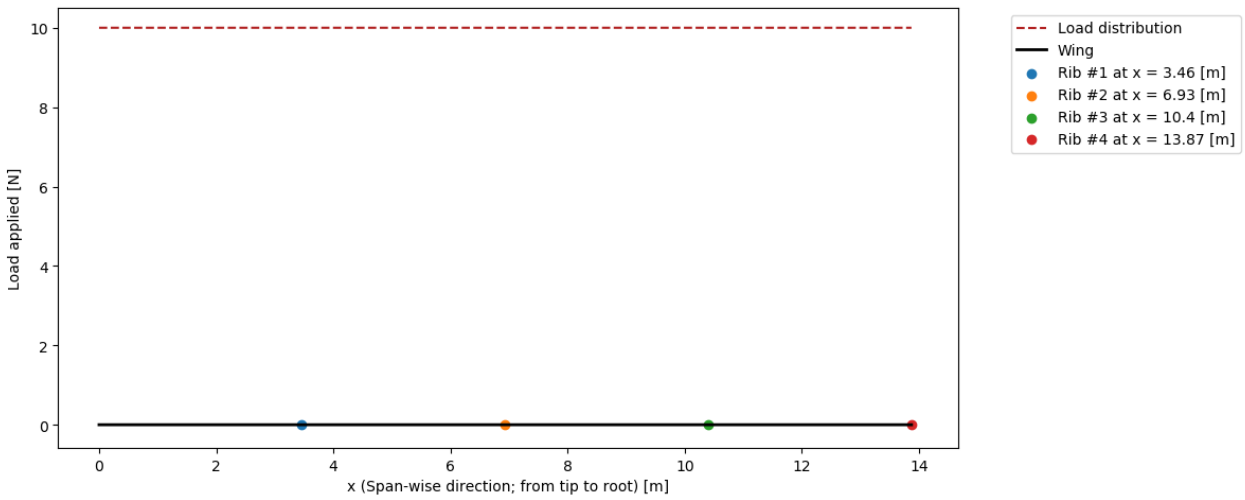

Figure 7.37: System test verifying that the rib spacing methods properly combines every module

Validation of the Rib Spacing Model

Besides verification, validation of a computational model the rib spacing method is the following important step.

As the rib spacing model was shown to be implemented correctly in Python through verification, validation shall be performed in order to confirm that the model chosen appropriately represents the system considered. Validation can be performed by comparing computational predictions to experimental observations. Due to project constraints, access to experimental results was not achievable. Nevertheless, to validate the rib spacing model, the assumptions made to derive the elastic deflection method as well as the elongation method will be evaluated. Indeed, assessing the validity of the assumption made shall highlight the predictive capabilities of the model.

Regarding the elastic deflection method, a major assumption made was that the canopy can be assumed to be a beam able to resist bending. However, due to its thickness (i.e. in the order of the millimeter) substantially lower compared to its width or length (i.e. in the range of few meters), the skin would not be able to resist pure bending as its moment of inertia, calculated from Equation 7.43, would be considerably low. The bending stiffness of the canopy is indeed negligible as mentioned in [17]. In fact, while running the elastic deflection model for some given lift distribution over a twenty meter span wing, the model estimates that 141 ribs shall be placed on one half wing as shown in Figure 7.38.

$$I_{yy} = \frac{1}{12} b t^3 \tag{7.43}$$

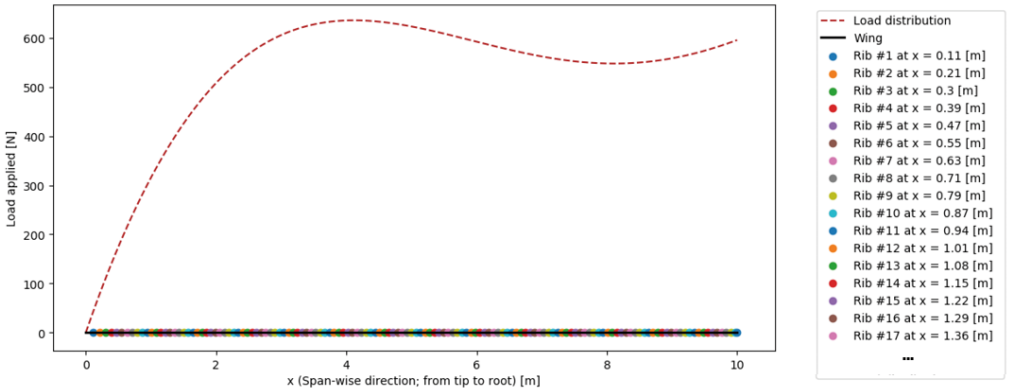

Figure 7.38: Rib distribution over half a wing using the elastic deflection method

The rib distribution provided in Figure 7.38 can be explained by the fact that the moment of inertia of a thin plate, calculated using Equation 7.43, is substantially low since the membrane is a thin structure (in this equation, b represents the base length of the canopy, approximately the chord length in this case and t represents the thickness of the canopy). This fact can be proven as increasing the moment of inertia to a more refined assumption, as expressed in Equation 7.44, provides a more reasonable rib distribution as shown in Figure 7.39, where it is estimated that only five ribs would be required. In Equation 7.44, a new variable h is introduced and represents the semi-height of the wing at the location of interest. Please refer to Figure 7.40 for an illustration of the cross-sections used to calculate the moments of inertia, please refer to Figure 7.40.

$$I_{yy,refined} = \frac{1}{12} b t^3 + b t h^2 + 2\left(\frac{1}{12} t h^3 + \frac{t}{2} h^2\right) \tag{7.44}$$

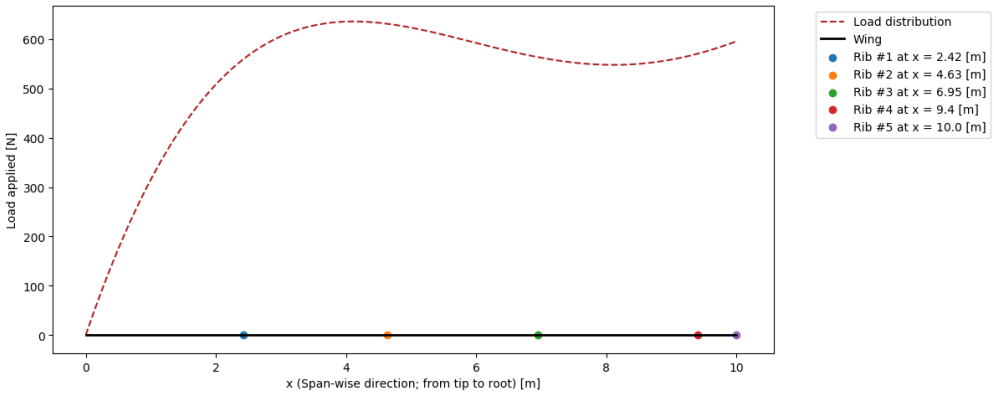

Figure 7.39: Rib distribution over half a wing using the elastic deflection method with a refined moment of inertia

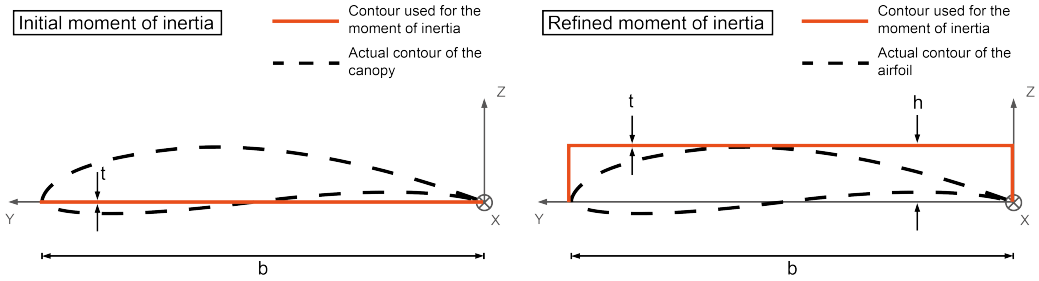

Figure 7.40: Illustration of the sections considered for both initial moment of inertia (left, used in Equation 7.43) and refined moment of inertia (left, used in Equation 7.44)

Regarding the second method, namely the elongation method, the major assumption made to apply it to estimate the deflection of the canopy is to model the skin as a beam under axial loading. It is safe to make such a statement as flexible membrane can withstand axial loading, on the contrary to being able to resist bending loads as assumed in the first method. Another major assumption made in the elongation method is that the elongation that the canopy would experience if loaded axially by the same load as the one applied over its surface is comparable to the actual deflection of the skin if it were to be measured. However, to properly validate the elongation method, thus the rib spacing model, experimental results shall be obtained in order to compare the prediction of the model to legitimate measurements. A recommendation for later stages of this project would be to perform testing on the three canopy materials proposed, namely by clamping two ends of some length of membrane, applying some point load at a distance over the span of the membrane, measure the deflection observed and compare it to the prediction made by the model for the same loading and configuration conditions. In such a manner, the model could be validated to some extend.

Hence, the elastic deflection method cannot be validated for the purpose of rib spacing of a flexible canopy wing. As the elongation method was validated for this purpose, as its assumptions were found to apply for flexible materials, this method shall be preferred for the remaining of this project and will be used in the next section to provide the rib distribution results for the considered wing design.

To refine the validation of the rib spacing model, next to validating the assumptions made in the model, one should perform a sensitivity analysis. The sensitivity analysis performed for the rib spacing model consists in varying the input given to the program by a small amount and evaluate whether the results change in a predictable fashion or not. Such a sensitivity analysis is performed by varying the Young's modulus of the materials, which should directly influence the rib distribution as a stiffer canopy would deflect less. This is performed for the three materials listed in Table 7.9, varying the Young's modulus from 4.5 GPa for Dacron, to Nylon at 5 GPa, to 55 GPa to Vectran. The results are shown in Figure 7.43, 7.41 and 7.42, respectively. As expected, the rib distribution for Dacron and Nylon slightly varies, with a rib pitch slightly larger for Dacron, as expected as its stiffness is lowered by 0.5 GPa. Furthermore, as the Young's modulus of Nylon and Dacron are comparable, it was expected to have the same amount of ribs on each side of the wing, in fact 12 ribs, as shown in Figure 7.43 and 7.41. Regarding Vectran, as its Young's modulus is ten times greater than that of Nylon, it is expected that the rib spacing would increase as the canopy would better resist the elongation. This is indeed validated as for Vectran, 7 ribs are required on each side of the wing as shown in Figure 7.42, compared for the 12 for Nylon and Dacron.

Rib Distribution Results

For the three materials listed in Table 7.9, the method of elongation will be used to evaluate the rib spacing distribution. In fact, this approach was considered more appropriate over the elastic deflection method and was observed to be more conservative as well in the verification and validation process detailed here above.

The allowable canopy deflection has been set to 0.01 m. From [6], a maximum deformation of 5% of the chord length in the center of cells of ram-air kite was measured. Applying this measure to the wing considered in this report, taking a chord length of 3 m to be conservative, this would result in a maximum deflection of 0.15 m. Thus, assuming a maximum allowable deflection of the canopy to 0.01 m seems acceptable as it falls below measurements on ram-air kite, having a more flexible structure than the wing designed for this project. For this reason requirement TEC-AIR-14 was defined, thus limiting the loss of aerodynamic properties due to the deformation of the canopy.

Performing the calculation of the rib spacing, provided with the lift distribution and the wing configuration from the aerodynamic department, the rib distribution along half a wing for the three materials considered for the canopy can be graphed. In fact, for Nylon-6 one can refer to Figure 7.41; for Vectran, Figure 7.42 provides the rib distribution; and for Dacron, please refer to Figure 7.43. Please note that the canopy thickness used for this analysis was set to 0.1 mm. To ensure that this thickness for the canopy is sufficient to transfer the aerodynamic loads without failing, the tensile yield stress in the skin was compared to the material yield strength and the canopy was shown to withstand the applied loads.

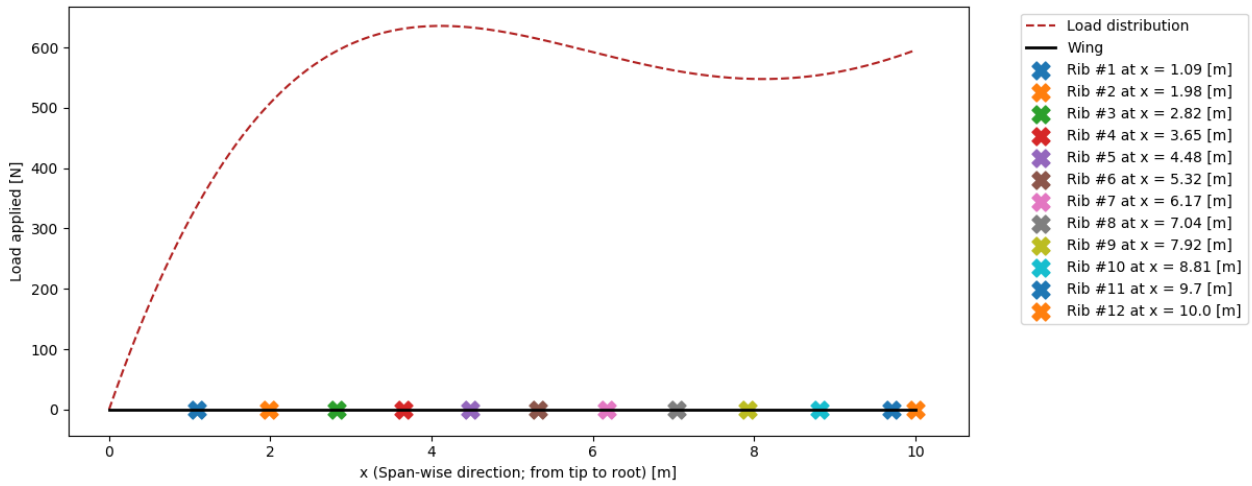

Figure 7.41: Rib distribution over half a wing for a Nylon-6 canopy (thickness of 0.1 mm)

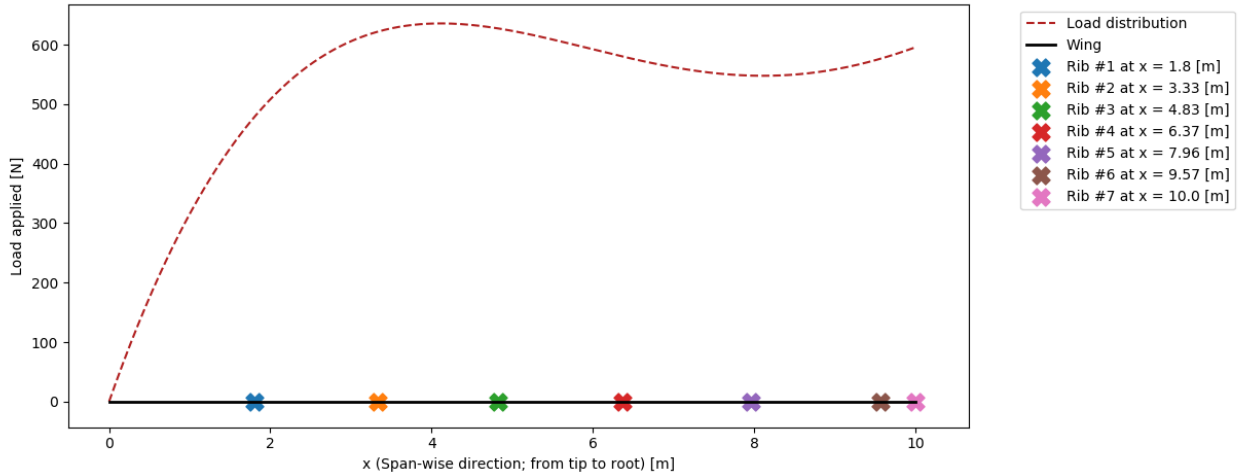

Figure 7.42: Rib distribution over half a wing for a Vectran canopy (thickness of 0.1 mm)

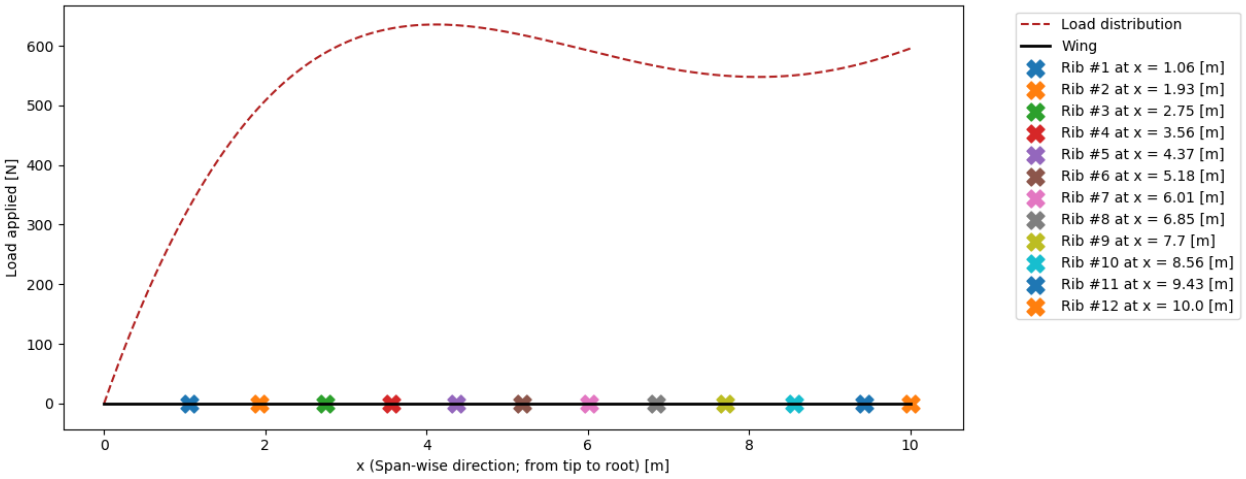

Figure 7.43: Rib distribution over half a wing for a Dacron canopy (thickness of 0.1 mm)

One can straightforwardly notice that the elongation method estimates that Nylon and Dacron both require 12 ribs along half a wing, whereas Vectran, with a Young's modulus a factor ten times greater, only requires seven ribs to limit the canopy deflection to the allowable level. It would therefore be attractive to select the Vectran as canopy material as it requires less ribs. However, one shall also consider the mass of the canopy given the density of the three materials and the wing surface area that has to be covered. In fact, given the wing area (i.e. 60 m^2), the thickness of the membrane (i.e. 0.1 mm) and the density of the materials as provided in Table 7.9, the mass of the canopy for the three skins can be estimated as follows:

Table 7.11: Summary of the masses of canopy for a wing area of 60 m^2 and canopy thickness of 0.1 mm

Canopy materials	Mass of the canopy kg
Nylon-6	13.56
Vectran	16.80
Dacron	16.56

To conclude, requirement TEC-AIR-14 is complied with as rib distribution is determined based on the allowable maximum deflection of the canopy, set to 0.01 m in the input of the model. Regarding the rib distribution, one would choose the Vectran canopy as it results in the least amount of ribs (i.e. 7 ribs on half a wing). Regarding the mass of the canopy, one shall prefer the Nylon-6 canopy as it proved to be the lightest (i.e. 13.56 kg). Hence, a trade-off has to be made between a heavier canopy or more ribs over the span of the wing, as more ribs leads to a lighter canopy, however it may result in a heavier solution as more ribs might weigh more than the extra mass of the canopy. Thus, the total mass of the ribs and canopy will be evaluated in subsection 7.3.7 as this section will evaluate the mass of the ribs for the three distributions shown in Figure 7.41, 7.42 and 7.43. The lightest combination of ribs and mass of the canopy will be the combination selected as the optimal configuration.

7.3.7. Rib Design

The ribs had to be designed to be able to transfer the aerodynamic load from the skin to the wing box. The dimensions of each rib depend on the local chord length and the amount of the resulting aerodynamic force that needs to pass through the rib structure. For simplicity of analysis and ease of assembly a truss structure was chosen to bear the load. In the model the forces apply to the pins that connect the trusses. However, in reality there would be an extra support shape with a flange that gives the shape to the canopy and

The longest possible trusses for the front and aft parts of the airfoil were chosen graphically as shown on the Figure 7.44. The thickest part of the airfoil at around 30% of the chord length is reserved for the wingbox. As we can see from the drawing, the aft truss structure extends to 84% of the chord and the front truss structure goes from the leading edge to the wingbox at 30%.

In order to calculate the forces on the four trusses, a following model is established: the trusses are assumed to be connected to the wingbox and to each other by pins, and the aerodynamic force is assumed to be applied to the tip of the structure. In reality, that is not the case, however, it was chosen to represent a pessimistic scenario.

Since two truss structures are present, it is necessary to identify which part of the force both of them carry. This was done by obtaining the pressure distribution over the airfoil and calculating which part of the aerodynamic force applies in front and behind the wingbox location.

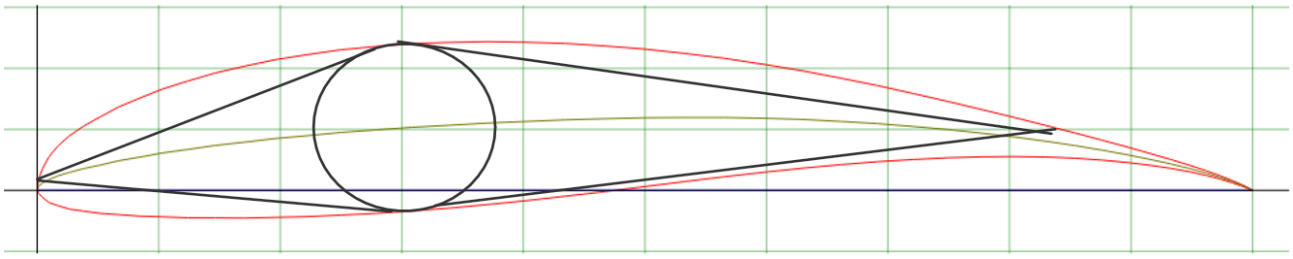

Figure 7.44: Rib structure: each black line represents a circular truss member, the black circle represents the wibgbox.

The code calculating the mass of the ribs is described in Figure 7.47.

Assumptions
The model assumes the following:

- The truss structure takes loads in tension and in compression.
- The pins connecting trusses transfer forces but not moments.
- The pin connecting the aft trusses is at 84% of the chord and the pin connecting the forward trusses is at 0% of the chord.
- The trusses attach to the wingbox through pins exactly at 30% of the chord, at its top and bottom.
- The loads apply to the pins that connect trusses to each other directly.
- The forward truss structure bears 48% of the aerodynamic force and the aft truss structure bears 52% of the aerodynamic force.
- The aerodynamic load applied to a section of the wing between two ribs is distributed equally between those two ribs.

At the current level of detail it was considered sufficient to simply include the main load bearing structure to estimate the weight and dimensions and omit designing the structures that transfer load from the skin to the trusses as well as the attachments of the trusses to the wingbox as they will be taken into consideration at a later design stage. The structure transferring the load from the skin to the truss structure will make it possible to design an even lighter truss structure since the load will be distributed in a more optimal way. This means that the end weight will likely be even lower than that predicted by the calculations. Of course, some more weight will, be added by creating the attachments to the wingbox, for which an extra 5% is reserved. This extra mass will allow for more flexibility in the future design process.

Another aspect that might affect the performance of the rib structure is the fact that there was insufficient time to evaluate the deflections of the rib. The deflection of the tip of the rib will be evaluated in future and it will have a direct effect on the final weight of the ribs if it turns out that the current structure allows for extensive flexibility.

One of the aspects that was not taken into account are the loads that will be applied to the structure during assembly. Since it will be assembled and launched on Mars, it is necessary to make sure that the loads that are expected to happen are much lower than those for which the structure is designed. For instance, it will need to withstand all the sideways loads that will be applied to it by the canopy during the assembly phase when the canopy will be attached.

The last but not the least, it was assumed that the forward part of the structure supports 48% of the load and the aft part supports 52%. This, of course, changes with the angle of attack and should be investigated further in order to make sure that the structure is strong enough for all angles of attack. There was only sufficient time to investigate the situation at $0°$, and further evaluations will show that the pressure distribution slightly differs for other scenarios.

Rib Sizing Methods

The model calculates the size of each of the four trusses of each of the ribs separately. The model obtains the data about the locations of the ribs from the code calculating the rib spacing. The code then uses a function to calculate the aerodynamic force applied to each of the section between the ribs. That load is assumed to be divided equally between adjacent ribs, which allows to calculate the loading on each rib.

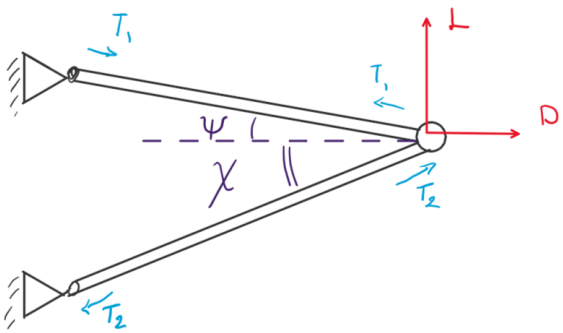

Figure 7.45: Truss structure model

After the loading on the rib in question in known, the code divides that loading into two parts, applying 52% of it to the aft part and 48% to the forward part. An equilibrium condition is used to calculate the forces on the trusses as illustrated in Figure 7.45. Equation Equation 7.45 is used to calculate the force on the upper truss and the Equation 7.46 to calculate the force on the lower truss. With a few modifications it is possible to calculate with the same equations the forces on the trusses of the forward truss structure and also the forces that would act on the structure if a smaller aerodynamic load would be acting in the opposite from the usual direction. Therefore, both the upper and the lower truss are designed to withstand both compression and tension, although for different loading scenarios. As it is highly unlikely that at any time of the operation the forces will be acting in the opposite direction, the forces are scaled down by a factor of 5 when applied in the opposite to the presented manner in order not to overdesign the structure.

$$T_1 = \frac{L - D \cdot \tan(\chi)}{-\tan(\chi) \cdot \cos(\psi) - \sin(\psi)} \tag{7.45}$$

$$T_2 = \frac{D - T_1 \cdot \cos(\psi)}{\cos(\chi)} \tag{7.46}$$

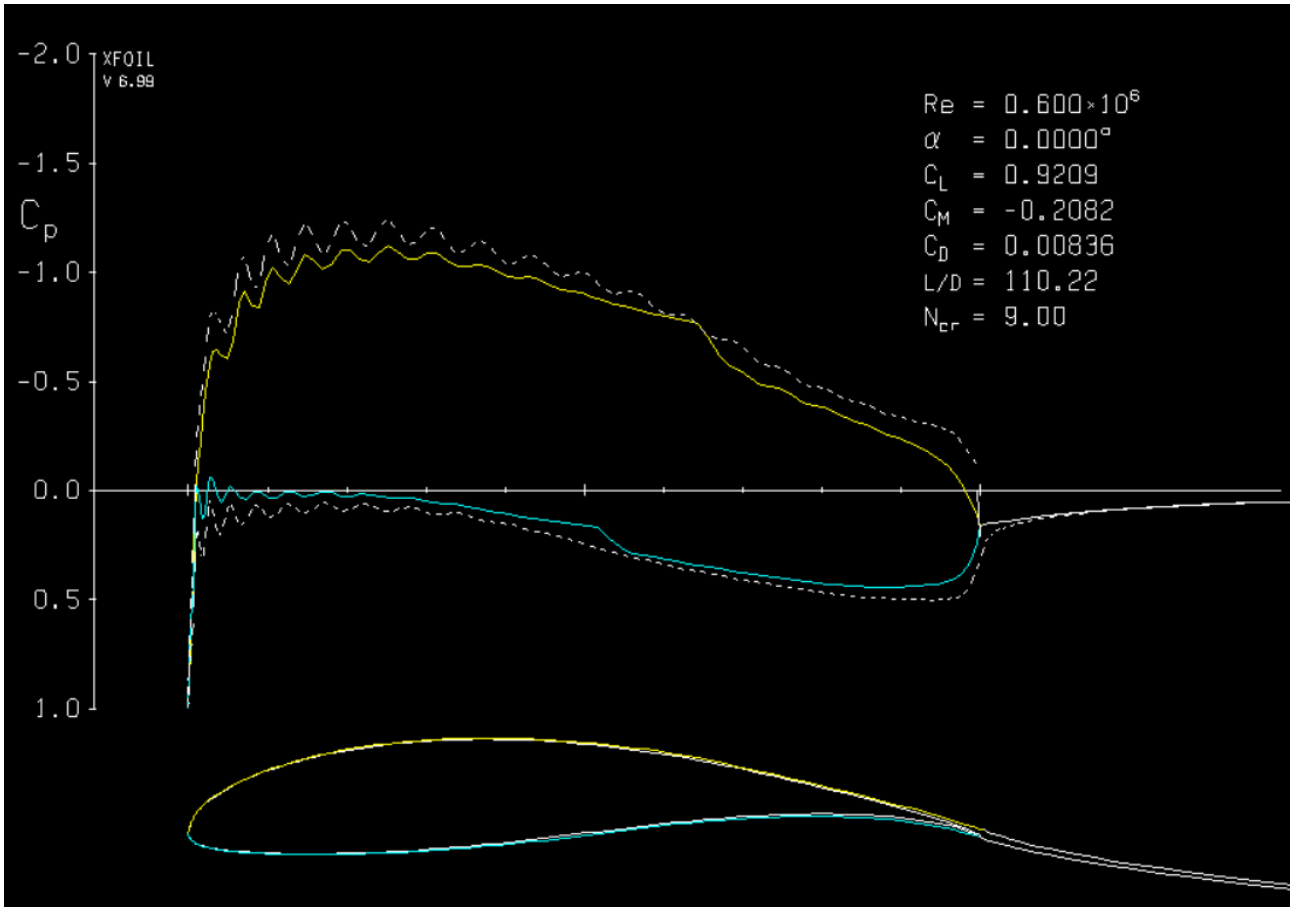

Figure 7.46: Pressure distribution of the Wortmann FX 63-137 airfoil at an angle of attack of $0°$

In order to make a decision as to how to divide the load between the forward and aft truss structures, a pressure distribution graph of the relevant airfoil shown in Figure 7.46 was investigated. It was concluded that about 52% of the force is applied to the aft part of the airfoil, which was used in the subsequent calculations.

Furthermore, a typical aerospace safety factor of 1.2 was applied to all loads.

After the program determines the loads that each truss member has to support, it iterates through a number of diameters going from 10 cm down and finds the minimum allowable thickness for each diameter in order to sustain the loads and resist failure in tension and column buckling. The program finds the optimal diameter in order to minimise the mass of the member while still fulfilling the requirements. Subsequently, the thickness is increased if necessary in order to match the minimum possible thickness of 0.88 mm for a single quasi-isotropic sheet of Carbon Fibre Epoxy. It is also checked that the diameter is indeed larger than the thickness taken twice, since such mistakes occurred during the development phase of the code.

After all the truss members are accounted for, the full weight of all the ribs is calculated.

The final step of the design was to check that the periodic loads that are present during the operation of the system do not go over the required limits. The critical loading case was the figure of 8 movement, since it occurs more than $1.7 \cdot 10^7$ times throughout the operation of the system, as shown in Equation 7.47.

$$N_{f8/5years} = 5 \cdot N_{f8/sol} \cdot N_{sol/year} = 5 \cdot N_{f8/cycle} \cdot \frac{N_{sec/sol} \cdot N_{sol/year}}{t_{reel-in} + t_{reel-out}} = 5 \cdot \frac{t_{reel-out}}{t_{f8}} \cdot \frac{N_{sec/sol} \cdot N_{sol/year}}{t_{reel-in} + t_{reel-out}} \quad (7.47)$$

Where $N_{f8/5years}$ is the number of figures of 8 done in 5 years if, in this context, a pessimistic assumption of constant operation is applied. $N_{f8/sol}$ denotes the number of figures on 8 per sol, $N_{sol/year}$ is sols in a year, $N_{f8/cycle}$ is the number of figure of 8 patterns flown in one cycle of winding and unwinding the power tether. $N_{sec/sol}$ is the number of seconds in a sol, $t_{reel-in}$ is the time that the reel-in phase of the pumping cycle usually takes, $t_{reel-out}$ is the time that the reel-out part of the pumping cycle usually takes. Finally, the t_{f8} denotes the time that it typically takes to complete one figure of 8. This is how the number of loading cycles in TEC-AIR-13 was calculated. In order to comply with it, the stresses were calculated and compared with the 422 MPa given for the fatigue[10].

Other loading cycles such as the reel-in and reel-out cycle or the landing and launching cycle were considered, however, they are more than 10 times less common, which makes them far less threatening to the system even though the changes in loading are more drastic in the other scenarios. It is recommended to investigate the other scenarios as well, but at this point of design it was considered premature. After the number of cycles was established, it was necessary to identify the differences in loads during one figure of 8 manoeuvre. From the simulations described in section 7.5, it became apparent that a maximum variation of 3 kN was experienced by the wing during the manoeuvre. Thus the stresses that result from the 8 kN and 5 kN loads were calculated and the maximum difference in stresses was found. Using Equation 7.48 provided by the Ashby Materials [20] the equivalent zero mean stress was calculated.

$$\Delta\sigma_{0mean} = \Delta\sigma(1 - \frac{\sigma_{mean}}{\sigma_{tension}}) \quad (7.48)$$

Where $\Delta\sigma_{0mean}$ is the equivalent amplitude of the stress if the mean was at zero stress, the $\Delta\sigma$ is the actual amplitude of stress calculated by applying the maximum and minimum expected loads to the structure, the σ_{mean} is the mean stress, an average of the maximum and minimum stresses, and the $\sigma_{tension}$ is the tensile yield stress. The resulting amplitude of the stress difference has turned out to be an order of magnitude lower than the required σ_e, endurance stress. This means that the design of the ribs already satisfied all the required parameters for the cyclic loading.

[10]https://www.ansys.com/products/materials/granta edupack[Accessed on June 20, 2021]

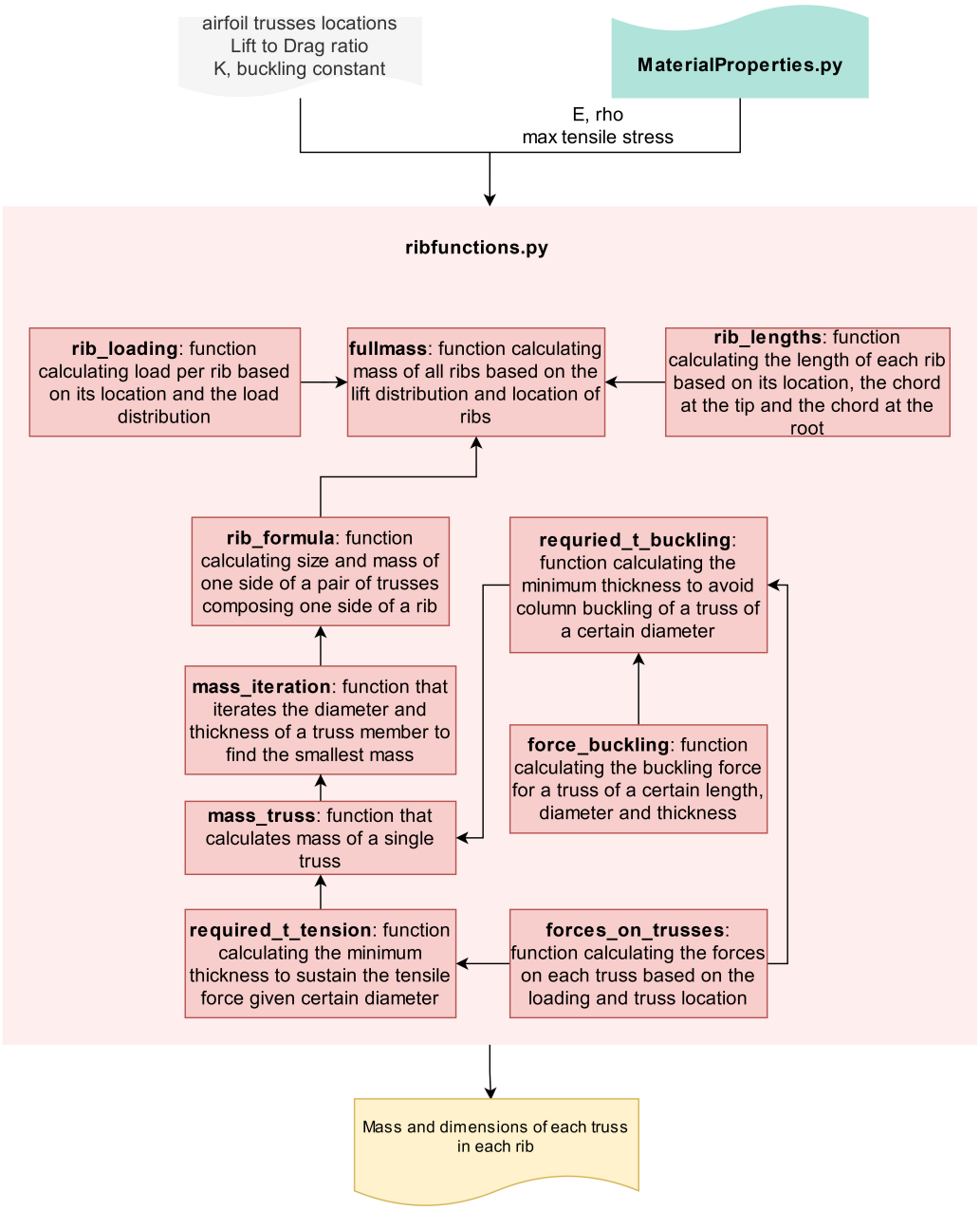

Figure 7.47: Code for rib design schematics

The Figure 7.47 describes the logic of the code that calculates the dimensions of the trusses. The names of the function are stated in bold, along with description of their purpose. The arrows go from the function that is used inside the function to which they lead in order to reflect the hierarchy in the code. The ”fullmass” function calculates the final mass and outputs all the dimensions of each truss present in the structure.

Verification of the Rib Code

The verification process went hand in hand with development of the model. At each stage each new function that was created was also tested with several inputs in order to ensure that it is doing what is expected. For instance, the function had to produce the result within the bounds of what can be expected by a reasonable engineer. That was the first test of whether the new part of the code is performing as expected. Furthermore, each part of the code was tested to give consistent results with various inputs.

For instance, it was expected that the steel structure will be the heaviest, followed by titanium and aluminium, and finally the carbon fibre was expected to be the lightest. When the piece of code gave different results it was assumed that something went wrong and an attempt to find a mistake was made.

Furthermore, the values of physical parameters were outputted in order to do a sanity check. This way it was discovered that for certain conditions the model would reduce the diameter of the truss member to below the double of the chosen thickness. This, of course, is physically impossible, so the code was wrong. That mistake

was fixed thanks to verification.

The following functions needed to be verified:

The **rib_lengths** function takes the locations of the ribs provided by the code for the rib spacing and calculates the length of each rib based on its location and information about the length of the chord at the root at at the tip. This function can be easily checked by hand.

$$l_c(x) = l_{root} - (l_{root} - l_{tip})\frac{0.5b - x}{0.5b} \tag{7.49}$$

Where $l_c(x)$ is the length of the chord to be calculated, the l_{root} is the length of the root chord, l_{tip} is the length of the chord at tip, x is the position of the chord in question and b is the span of the wing.

The **rib_loading** function takes the locations of the ribs as an input along with the function to calculate the lift distribution and turn it into a set of point loads applied at each wing section. The function that calculates the lift applied on the section was described and verified in thesubsection 7.3.6. After the lift on the section is calculated, the two equal parts of the lift are assigned to both ribs supporting that section. Each rib then carries a sum of half of the lift on the section to its left and half of the lift to its right. During the verification process it turned out that the lift was calculated to be the same for every section, which is not plausible. The investigation has confirmed that indeed an index iteration was missing. That made the end result of the rib mass go up by about 2kg.

The **forces_on_trusses** takes the Lift and Drag forces as inputs, along with the angles at which the truss members are positioned. The result is T_1 and T_2 which are the forces on the truss members. This function was verified by hand since it is a very simple calculation, described in Equation 7.45 and Equation 7.46.

The **force_buckling** calculates the minimum compressive load at which a column of a given diameter would buckle according to Equation 7.50.

$$F_{bck} = \pi^2 \frac{EI}{(K \cdot l)^2} \tag{7.50}$$

$$I = \pi \frac{(0.5d)^4 - (0.5d - t)^4}{4} \tag{7.51}$$

Where F_{bck} is the minimum force for column buckling, E is Young's modulus, I is the second moment of area for a cylinder, $K = 1$ is a constant reflecting the type of loading, l is the length of a column, d is its diameter and t thickness. The code is very easy to verify by hand since it is a straightforward calculation.

The **requried_t_buckling** uses the **force_buckling** function to calculate the required thickness to prevent buckling of a truss member of a certain length and diameter under a given load. It starts with a very small thickness and iterates, adding more and more thickness in order to find the minimum thickness at which the truss member will not buckle. It is impossible to repeat the calculations by hand, since there are too many of them, but it is possible to check the final result with Equation 7.50. If the force on the truss member is a little bit smaller than the one given by the equation, the code is verified.

The **required_t_tension** calculates the necessary thickness to sustain a tensile load with Equation 7.52. This can also be verified by hand.

$$t = \frac{F_t}{d\pi\sigma_{max}} \tag{7.52}$$

The **mass_truss** is a straightforward formula that takes the diameter, thickness and length of a truss member and calculates its mass based on the material properties, also easily verifiable by hand.

The **mass_iteration** takes into account the maximum compressive and tensile forces that are acting on the truss member and iterates through diameters, calculating the minimum thickness for each and the mass that results from it. Once the mass stops decreasing with decreasing diameter and starts increasing, the calculation stops at this local optimum and outputs the results for diameter, thickness and mass. It is impossible to verify it by repeating every calculation. In order to verify it, the function was made to output the smallest diameter and the diameter just after that to make sure that it gives reasonable values. The step size for diameter was tweaked in order for the adjacent values of masses to be different up to the third value after the decimal separator. Furthermore, the function outputs a warning if the diameter decreases below zero and makes an adjustment to diameter value if it becomes smaller than 210% of the thickness, since during the verification by inspecting the thicknesses and diameters this was discovered to be an issue in some situations. In the case when the

adjustment is needed the mass is no longer at the local optimum, but further modifications to the code are required in order to obtain the local optimum in this situation, too.

The **rib_formula** is one of the functions that are harder to verify since it makes use of all the aforementioned functions in order to calculate the dimensions of all four truss members in a rib. The function outputs the dimensions of each truss member. Since it was consistent with the outputs of subfunctions that were obtained previously, it was deemed to be accurate.

The **fullmass** simply goes over every rib and calculates its dimensions. Similarly to the **rib_formula**, it was considered sufficient to make sure that the output for each function is consistent with the outputs to similar entry conditions of the utilised subfunctions.

Validation of the Rib Model
In order to validate this model, prototypes of the ribs will be produced and tested to be able to withstand the required forces for a sufficient number of loading cycles. They will also be tested until failure to make sure that the ribs are not overdesigned. The ribs will be tested both separately and in an assembly, with canopy in tension.

Three main experiments will be conducted in order to validate the model.

In the first experiment, the ribs will be connected by pins to each other and to a test rack. The load will be applied directly to the pin connecting the tubes to each other. The setup will be very similar to what is described in Figure 7.45. The rib will be tested until failure. The pins and attachments will have to be designed in such a way that the truss members fail first to make sure that the trusses themselves are tested and not the attachments. The ultimate load will show whether the structure is underdesigned or overdesigned. If the ultimate load differs significantly from the one expected, the structure will be double-checked for manufacturing errors and the code will be checked for wrong assumptions.

The second experiment will be conducted with a more realistic prototype, however, more design steps have to be done before starting this experiment. This experiment will be possible after the supports for the canopy that connect to the truss members are designed. The experiment starts by assembling a simplified prototype of a section of the wing. This will be a straight section without any taper or sweep. First of all, the ribs are attached to a simplified wingbox. The ribs then are tested to withstand the sideways loads expected during assembly. If this step of the experiment goes well, the next stage includes attaching a canopy to the wing section assembly and putting it into a wind tunnel to simulate the real loads.

The third experiment will be designed to test that the fatigue requirements are indeed satisfied. The structure of the rib will be subjected to the required number of loading cycles in order to test that it indeed can withstand the repeated loading for 5 Martian years.

Rib Sizing Results
The code for the weight of the ribs was combined with the code for the rib spacing. This made it possible to choose the lightest option for the canopy in combination with ribs, since the number of ribs varies with the type of canopy material used. The results of the calculations show that the ribs are expected to weigh about 8 kg in total with the most accurate estimation of 8.24 kg after an extra 5% was added to account for future changes and design of attachments. The mass of each rib varies between 0.16 kg and 0.31 kg, while the diameter is typically between 1 and 3 cm and thickness is typically about 1.76 mm (twice a single quasi-isotropic layer of 0.88mm), showing that it is usually sufficient to have a single layer of quasi-isotropic carbon fiber.

The mass should be minimised in order to comply with CON-DG-03, so the lightest solution is chosen. The results can be seen in Table 7.12.

Table 7.12: Various canopy materials result in different weight of the canopy and ribs together

	Vectran	**Dacron**	**Nylon**
number of ribs	15	25	25
total rib weight, kg	6.57	8.05	8.24
canopy weight, kg	16.8	16.56	13.56
canopy+ribs weight, kg	23.37	24.61	21.80
wing weight, kg	81.1	82.3	79.5

Sensitivity In order to estimate the real range of the values that the mass of the ribs might take, a preliminary sensitivity study was performed. The following was done in order to estimate the effects of uncertainties on the final result for the rib weight:

- Decrease of the Young's modulus by 1%
- Decrease in the strength of Carbon Fiber Epoxy by 1%.
- Decrease of the lift to drag ratio by 5%.
- Increase in the total force by 1%.
- Shifting the resultant force to the back by 5%
- Shifting the resultant force to the front by 5%

The Table 7.13 demonstrates the effects of the changes in different values on the end weight of the ribs. The values that are known to be more reliable were changed only by 1% while the less reliable values were changed by 5%. We can see that all the changes are within 300 g, which is much smaller than the extra weight reserved for future changes. However, it would be necessary to further investigate the range of the Lift-to-Drag ratio that is expected along with the pressure distribution for various angles of attack. It has to be noted that it is impossible to compare the changes in the final weight between each other directly. However, we can see that the differences induced by a difference in the Lift over Drag ratio are quite small compared to those achieved by changing the total force even if the force is increased only by 1% and the Lift over Drag ratio is changed by 5%. This means that the safety factor that is put on the total aerodynamic force will probably account for possible deviations from the model in the Lift to Drag ratio. The largest concern would be the force distribution, since it is possible that at the larger angles of attack the force shifts to the back. Thus, this will be the first point of investigation in the further iterations of the design.

Table 7.13: Effects on the rib weight

	New rib weight, kg	**Change in** $\%$
E -1%	8.27	$+0.3\%$
$\sigma_{tensile} - 1\%$	8.24	0%
L/D -5%	8.23	-0.1%
Total force $+1\%$	8.27	$+0.3\%$
new force distribution: 0.57 front, 0.43 back	8.34	$+1\%$
new force distribution: 0.47 front, 0.53 back	8.03	-3%

7.3.8. Wing Transportation Mass and Volume Estimation

The total mass of the wing without safety factors was calculated in the previous section to be 79.5 kg, as shown in Table 7.12. However, it should be notices that no mass has been added for future reinforcements and changes, including the reinforcements needed at the root and attachment points of tethers.

In order for the system to comply with CON-DG-04, it is necessary to know what is the minimum possible transportation volume of the structures of the wing.

The transportation volume consists of three main parts, just as the wing does: the wingbox, the rib truss members and the skin. Also, the connecting parts need to be packed, but that is not taken into account here, since they can be packed in any part of the volume and they do not need to be divided.

First of all, the wingbox will have to be divided into separate parts, since it is impossible to transport it as a whole. Each side of the wingbox is divided into five parts which are fit inside each other. In total, there would be two tubes to transport, each with four sections inside them. Each tube is 0.5 m in diameter and 2.2 m in length. This makes the total volume of 1.1 m^3. The canopy has a volume of $60 \cdot 2 \cdot 0.0005 = 0.06$ m^3 since the packing of the canopy won't be ideal, the result is multiplied by 1.2. The resulting volume fits inside the smallest cylinder of the wingbox, which means that it does not further increase the transportation volume. The truss members of the ribs fit well inside the other wingbox and in the gaps between the two tubes, so the resulting volume is still 1.1 m^3.

7.3.9. Structural Recommendations

As the structural analysis of the wing performed in this project aims at providing a preliminary estimation of the dimensions of the structural as well as an initial mass estimation, several recommendations can be made to improve the accuracy of the estimations made here above. Here follows the general recommendations that were identified to improve in later stages of the design process.

- Structural additions should be accounted for at the points of applications of the tethers and the point of attachment between both sides of the wing.
- One shall consider the thermal loading the wing will experience on Mars in later design stages of this project. In fact, the low temperature experienced on Mars (i.e. around -50 to -100 $^{\circ}C$) and the fluctuation in those ranges of temperature shall be assessed thoroughly for a more refined design. Materials property were taken for -50 °C when the data was available in the Granta EduPack, as explained in subsection 7.3.3. Hence, requirement TEC-AIR-12 was not completely complied with.
- The structure of the wing as a whole has to be evaluated for performance under vibrations induced by the tethers. The tethers will have a significantly large range of frequencies that they might excite under loading from wind since their length changes constantly. This means that the structure of the wing should not get excited under any of the frequencies that the tethers might obtain during operation.
- The loadings from the accelerations of the mass of the wing should be checked, however, it is likely that they will be negligible compared to the aerodynamic loadings.
- More types of cyclical loadings shall be checked for all the parts of the structure.
- Regarding operation and logistics, the structure shall be designed to be divided into multiple parts in order to allow for assembly and transportation to Mars. To that end, the attachment interfaces have to be designed for.
- The manufacturing process shall be refined and the structure has to be adjusted in order to be possible to manufacture. For instance, considering the production of the carbon-fiber

7.4. Tether characteristics

The manner of calculating the tether thickness is an iterative process in which three main properties are to be considered, the yield stress, the bending fatigue and the creep fatigue. As the bending fatigue is proven to be the main fatigue mode determining the amounts of tethers to be taken towards Mars, SK78 Dyneema fiber is used, this kind of Dyneema is created especially to reduce bending fatigue [21].

Preliminary Assumptions

During the iteration the following things have been assumed: D_{drum}/d_{tether} will not increase bending cycles anymore above a ratio of 100 and this ratio could be used as the tether diameter is small enough. Secondly, it is assumed that SK78 will sustain three times more bending cycles [21]. Thirdly, SK78 has a minimal increase in bending cycles before failure of approximately 30 percent at a temperature of -60 °C. This is a conservative assumption [11]. This knowledge has been obtained by private contact with the rope testing facilities at the university of Stuttgart. Fourthly, as described in [21], it can be assumed that the reeling-out phase takes around 70 percent per cycle, while the reeling-in phase creates negligible tension. This leads to a factor of 1.42 increasing the lifetime of the tether. Lastly a coating with 10 wt% is assumed to ensure UV-protection, coating has been accounted for in the sizing of the cables below.

Yield Stress

By use of the performance model described in chapter 8, the maximum tensile force on the main tether has been calculated to be 12 kN. With a yielding stress of SK78 of 1.26 GPa [22] and a safety factor of 2, a minimum main tether diameter of 4.6 mm has been found. As the forces acting on the control tethers are unknown and to be computed in a dynamic model of the wing, a safe 2 mm diameter is chosen corresponding to a maximum tensile force of approximately 2 kN.

Bending Fatigue

The bending fatigue is characterized by Equation 7.54 [21]:

$$SSL = \frac{\frac{CTF}{1.33} * cycletime}{Bends - per - cycle} \tag{7.53}$$

In this equation SSL means safe service life, CTF means the amount of kite cycles the tether would withstand and bends per cycle is assumed to be 2. The factor of 1.33 is a safety factor. Filling in the various factors described in the assumptions 7.54 could be formulated in the following manner:

$$cycles_{life} = \frac{\frac{CTF}{1.33} * 1.42 * 3 * 1.3}{2} = 2.082 * CTF \tag{7.54}$$

[11] Private mailing-contact with Gregor Novak, [21-05-2021]

In this formula $cycles_{life}$ is the amount of cycles the cable would withstand before failure. CTF is approximated by use of 7.49 which describes the amount of cycles SK75 could withstand at a given tension. The line describing a drum over diameter ratio of 100 is approximated by equation 7.55

$$CTF = 11233.23 * (N/tex)^{-2.726} \tag{7.55}$$

Where the unit N/tex could be converted towards stress in MPa by multiplying N/tex with the density, 970 kg/m^3.

Miner's rule is used to estimate the bending limited lifetime of the main tether. This is done by the following formula:

$$\%_{failure} = \sum_{start}^{end} \frac{cycles}{cycles_{life}} \tag{7.56}$$

By use of the performance program described in chapter 8, for each cycle, which has its own tension, the amount of fatigue inflicted on the tether shall be computed. All these fractions are added as described in equation 7.56 to compute the total amount of tethers needed. A fraction above one shall mean multiple tethers are necessary.

The following assumptions have been made in the code describing the amount of tethers needed. First of all, a main tether diameter of 4.6 mm is used as required for the maximal tension force. Second, the amount of cycles per day has been calculated by dividing the airborne time by the average cycle time over the course of a full martian year.

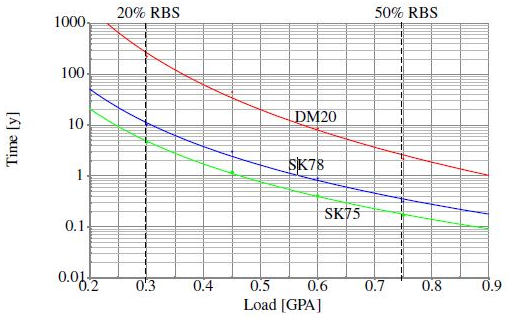

Figure 7.48: Safe Working Life for Dyneema fibers

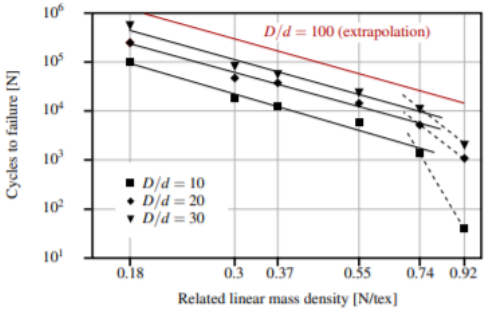

Figure 7.49: Bending fatigue Dyneema SK75

Creep Fatigue

After the thickness of the cable has been determined, it has to be verified that the creep fatigue will not decrease the required lifetime. The computed average stress in the main tether is computed to be 0.28 N/tex. By looking at Figure 7.48 and following SK78, the lifetime in years can be found for the average stress found in the previous step. It is important to notice that Figure 7.48 is applicable at 20 °C. It is stated in [21] that for every average temperature decrease of 10 degrees the safe lifetime found in Figure 7.48 is multiplied by 3. Combining this with an already abundant value of approximately 10 earth years leads to the conclusion that creep fatigue will not be an issue for the main tether. Considering the control tethers, a computed average stress is found by using the assumption that the control tethers together will take up 10% of the load on average. An average stress of 0.082 N/tex is found, again creep is not a limiting factor.

Results

This lead to a total amount of 2.7 main tethers needed throughout the entire mission. As no half tethers could be used, this number is rounded up to 3, adding another safety margin. Each main tether shall have a minimum lifetime of 3.14 earthly years. The control tethers are found to have a lifetime of approximately 50 years for the forces assumed. This long lifespan is caused by the over designing of the diameter to account for forces throughout the turns. As these forces are unknown these could not be used to calculate the true fatigue of the control tether. For this reason more research should be done towards the control tethers. As shall be stated in the performance analysis the tethers shall have a length of 1000 m, this results in a weight by multiplying it with a density of 0.98[12]. This is summarized in table 7.14. Note that only one control tether, of the two needed for the kite to fly, is taken into account.

[12]https://www.marlowropes.com/material-properties

	Diameter, mm	Weight, kg	Spares	Total weight, kg
Main tether	4.6	16.29	2	48.86
Control tether	2	3.08	0	3.08

Table 7.14: Tether dimensions

7.5. Power Characteristics

This section covers the aspects that are related to the power generation of the wind energy system. The focus will however be towards the ground station and its corresponding components and how these components interact with one another. This means that the conversion of mechanical power generated by the wing and transferred via the tether to electrical power will be discussed. The generation of mechanical power will be discussed in section 7.1. Ground station configuration, motor sizing, drum sizing and the power distribution system will be discussed in detail. The terms ”torque motor” and ”generator” represent the same component but the usage of these terms differ depending on the phase of the pumping cycle. During reel out, the term ”generator” is used and during reel in the term ”torque motor” is used.

7.5.1. Requirements

In Table 7.15 the relevant requirements used to guide the power design are included.

Table 7.15: Relevant requirements of power characteristics

Requirement Index	Requirement	Justification
TEC-GE-01	The generator shall have a 90% average efficiency	This requirement originates from system operation prerequisites
TEC-GE-02	The generator shall be able to provide a torque 1000 Nm	This requirement originates from system operation prerequisites
TEC-PS-01	The power storage system shall have a capacity of 50000 kWh	This requirement originates from system operation prerequisites
TEC-PS-02	The power storage system shall provide an output of 10 kW	This requirement originates from stakeholder needs and is to be complied with

7.5.2. Ground station configuration

The ground station is where the main power generating and control components are located. These components are as follows:

1. Motor controller / inverter - This functions to control the speed of the torque motor/ generator during the pumping cycle, launch and landing phases. The inverter also plays a critical role during the traction phase. The inverter sits between the generator and grid and regulates the amount of power to be transferred to the grid with the help of the external power management system.
2. Internal control unit - The function of this component is to regulate the flow of power from the buffer storage to the individual motors for them to perform their specific functions.
3. Torque motor / generator - This is the main motor that converts mechanical power from the tether to the electrical power during the traction phase of the the wing. During reel in, this motor switches roles and pulls in the tether to complete the pumping cycle. The selection of this motor is explained in subsection 7.5.3 subsection.
4. Control motors - These motors control the reeling in and reeling out of the control tether lines which are meant to control the flight path of the wing during the pumping cycle, launch and landing maneuvers.
5. Spool motor - This is a linear motor on which tether guides and pulleys are present. This linear motor is located parallel to the length of the drum (perpendicular to the spool direction) and allows for the even spooling of the tether on the drum.
6. Slewing motor - This motor is located at the bottom of ground station and is attached to the gear-ring of the slewing ring. This functions to rotate the entire ground station so that the maximum power can be generated with respect to the direction and speed of wind.
7. Brake actuator - The brakes require an actuation system to allow the calipers to pinch the disc. An electrical actuation system is chosen over a hydraulic one as the Martian environment does not facilitate the use of hydraulic fluids.

8. Buffer storage - The supercapacitor array is there to provide power to the individual motors during the pumping cycle. The main duty is during the pumping cycle, where some energy is siphoned during the traction phase and stored in the supercapacitor array. This energy is then dumped back into the torque motor to reel in the wing. The energy stored is also used to power the control motors, spool motor and slewing motor.

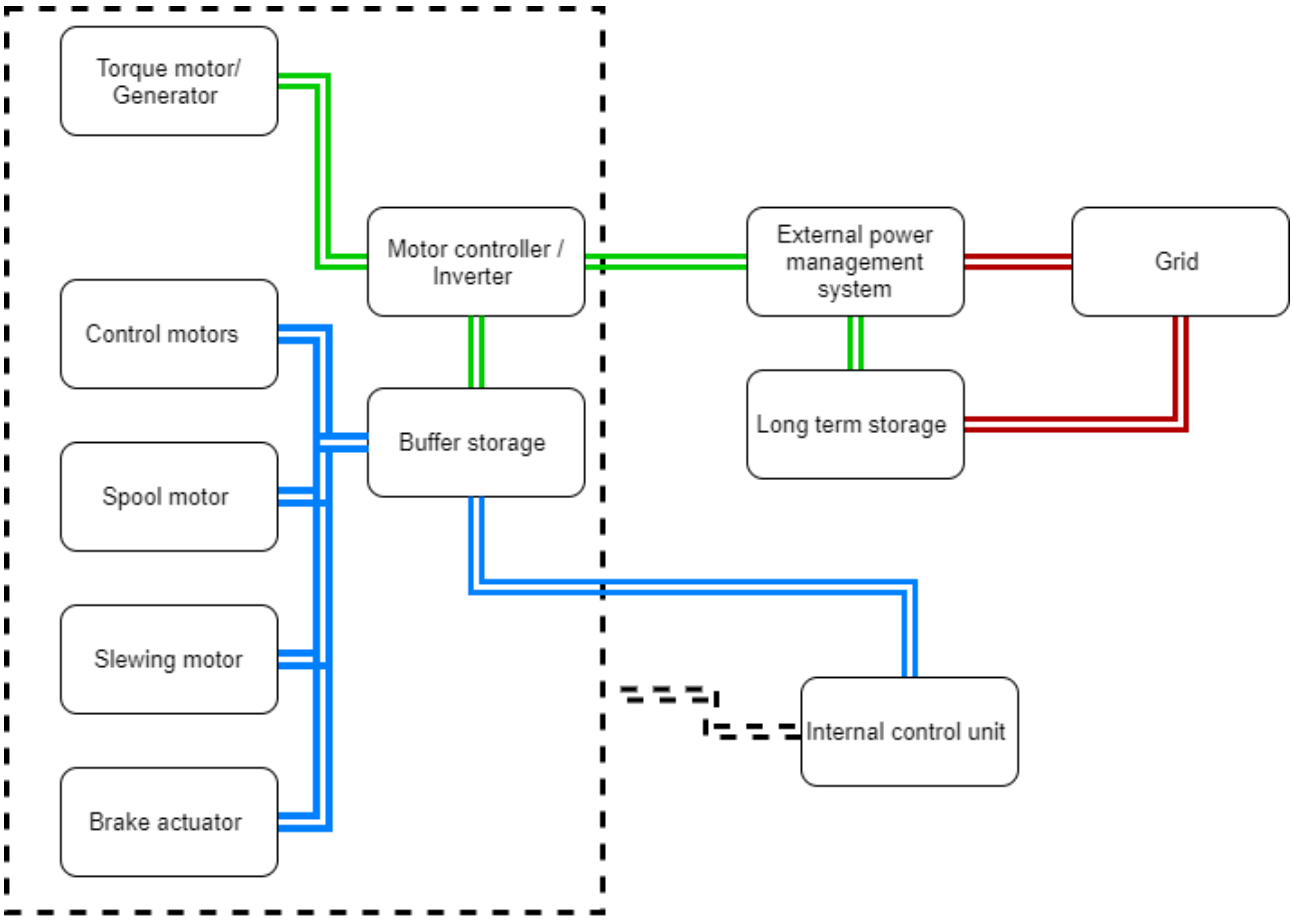

Figure 7.50: Electrical block diagram

Figure 7.50 shows the flow of power within the ground station and out to the long term storage and subsequently to the grid. The green lines indicate the high voltage power lines that connect the torque motor/ generator to the motor controller/ inverter to the buffer storage and the external power management system. During the traction phase the electrical output of the generator is unstable as the mechanical power transferred to the generator varies due to varying lift forces experienced by the wing. The motor controller/inverter stabilises the output to the external power management system which determines the load requirement of the grid and either channels all the power to the grid or channels some into the long term storage if there is an excess of power. If both the grid requirement is met and the long term storage full, the excess power is dumped via heat. The red power lines show the stabilised power that is channeled to the grid. The dotted lines around the ground station components represent the power control that the internal control unit has over the individual components. It ensures that the right amount of energy from the buffer storage is directed based on the load requirements.

It was decided that power production will only be performed by the torque motor and the two control motors will not generate any power. During reel out, the control tethers are reeled out of their drums and this has the potential to generate power via the same mechanism as the main tether. However, to achieve fast reaction times during the figure of 8 maneuver, it is critical that one control tether is reeled in and the other free to reel out without tension. This would enable the wing to bank at a faster rate and hence the radius of turn during the figure of 8 maneuver can be reduced. This enables more figure of 8 maneuvers to be performed during a pumping cycle and subsequently producing more power during reel out. To minimise tension of the free reeling tether, no torque should be induced in the control motors which means that no power generation load will be applied on the control motor. For this reason, no power will be generated by the control motors during the pumping cycle.

Due to the ground station having a freedom of rotation of 360°, normal power transmission wires will eventually

twist and potentially fail due to bending. To solve this, slip rings will be used which enables power to be transmitted from a rotating element to a fixed one. The power lines that are are connected to the external power management system from the motor controller are fixed to the ground and the slip rings are mounted on the axis of rotation of the ground station. The contact point between these 2 elements allows for a two way power transmission between the ground station and the rest of the power distribution infrastructure.

7.5.3. Motor Sizing

To fulfill the 10 kW nominal power requirement for the habitat and taking into the consideration the complementary power generation of the solar panel system, a motor with a rated power of 70 kW and peak power of 85 kW was chosen. A direct drive motor was determined to be ideal for this application as it allows for the drum to be directly connected to the motor, eliminating the need for a gearbox which has a significant impact on the total efficiency of the power generation system. A high torque, low speed motor fits the aforementioned needs of the ground station motor requirements. Looking at comparable motors on the market, an estimation of the mass of the motor was done using an interpolation of their respective masses [13]. With the derived trend-line, a mass of 293 kg was obtained for a torque motor of 70 kW rated power. However due to the space application and the timeline of the project, the mass of the motor was estimated to be around 250 kg with savings made with the use of lightweight alloys or composites for the housing and mounting. This improvements are expected to be made over the developmental period of the mission.

For the control motors, the power estimated for the motor to reel in the control tethers is 150W at a rotational speed of 40 rad/s. This power estimate was obtained by first determining the control requirements of the wing of which a distance of 7.07 m of control tether needs to be reeled in a time of 1.75 s during the figure of eight maneuver. With the mass of the kite determined to be 79.7 kg and one control motor estimated to carry a load of 10% of the total load, the control motor would require a power of 144.8 W. Taking into account the 10% nominal load that each control tether has to carry, an additional 500 W is need. Hence, a 650 W motor was thus selected to be the most suitable option. The summary of the motors selected and their corresponding parameters are summarised in the following table.

Table 7.16: Motor sizing

Motor	Rated power, kW	Rated torque, Nm	Rotational speed, rad/s
Torque motor	70.0	1100	63.6
Control motor	0.65	15.5	42.8
Spool motor	0.24	0.405	594.8

7.5.4. Drum Sizing and Buffer Storage Sizing

The drum size is determined using the relationship D/d which corresponds to the ratio of drum diameter to tether diameter. With a D/d value of 100 and main tether and control tether diameters being 4.6 mm and 2.0 mm respectively section 7.3. This corresponds to a main drum diameter of 0.46 m and control drum diameter of 0.2 m. However, to achieve take-off speeds for the kite, the main drum is sized to 0.6 m diameter which still fulfills the main tether creep stress and bending requirements.

In the midterm report [9] the selection of the the buffer storage system was done. The sizing of the buffer storage was done based on the the use of the stored energy for the motors as explained in subsection 7.5.2. The energy needs for each operations sums up to 184 Wh and the breakdown is as follows:

1. Reel in of main tether during pumping cycle: 167 Wh
2. Spool motor per pumping cycle: 2 Wh
3. Both control motors: 15 Wh

With a energy density of 9.5 Wh/kg for the supercapacitor buffer storage system, the mass is estimated to be 19.4 kg [23].

7.5.5. Efficiencies

To be able to accurately size the system, it is critical to consider the efficiencies of the different systems and components within the ground station. The components considered are of the the main power generation system and are as follows:

1. Torque motor efficiency: $\eta_{tqmotor} = 0.925$ The value of this efficiency is at the motor's rated power at 70 kW. This means that at lower power operations (lower loads) the, efficiency decreases as well. This is a

[13] https://hiwin.co.uk/wp-content/uploads/2017/06/Torque-Motors.pdf [Accessed on June 15, 2021]

result of the loses of the motor being assumed to be constant throughout the motor's operation. With the given efficiency and rated power, the loss is derived to be 5.25 kW. This means at the motor/generator's lowest operation, the efficiency is reduced to 0.825. This value is still relatively high as the operation at this generator load is minimal.

2. Motor controller/inverter: $\eta_{conroller} = 0.95$
3. Buffer storage: $\eta_{buffer} = 0.98$
4. Friction losses: $\eta_{friction} = 0.95$

The combination of these efficiencies are slightly different for the reel in and reel out phases of the pumping cycle. This is because, the efficiency of the supercapacitor buffer storage system is assumed to be only applicable when discharging during the reel in phase when energy is taken put of the buffer system and provided to the torque motors.

The total efficiency during reel out is:

$$\eta_{reelout} = \eta_{tqmotor} * \eta_{controller} * \eta_{friction} \tag{7.57}$$

This results in a reel out efficiency, $\eta_{reelout} = 0.834$

The total efficiency during reel in is:

$$\eta_{reelin} = \eta_{tqmotor} * \eta_{conroller} * \eta_{friction} * \eta_{buffer} \tag{7.58}$$

This results in a reel in efficiency, $\eta_{reelin} = 0.818$

DSE The pumping cycle efficiency was estimated to be 0.9. This value is relatively high when compared to Earth based systems currently in operation. This pumping efficiency is obtained from the following formula:

$$\eta_{pumping} = \frac{t_{out} * P_{out} - t_{in} * P_{in}}{t_{out} * P_{out}} \tag{7.59}$$

$$\eta_{pumping} = 0.9 \tag{7.60}$$

The reason for making the assumption of the pumping efficiency is the difficulty in calculating the actual pumping efficiency. This is because, the gliding performance of the wing during reel-in was difficult to estimate. Hence the assumption takes into account that the semi-rigid wing is able to achieve high glide ratios and hence the torque motor is not required to apply much force to reel in the wing and the main tether. Further research is recommended to be done on the gliding performance of the wing to obtain an accurate value for the pumping efficiency.

Taking into account the reel in efficiency, η_{reelin}, reel out efficiency, $\eta_{reelout}$ and $\eta_{pumping}$, the total electrical efficiency of the system can be determined. Since the efficiency of the system is dependent upon the lowest efficiencies of its elements, the total electrical efficiency is:

$$\eta_{electrical} = \eta_{reelin} * \eta_{pumping} \tag{7.61}$$

$$\eta_{electrical} = 0.736 \tag{7.62}$$

This total electrical efficiency value of 0.736 corresponds to the conversion of mechanical energy from the main tether to electrical energy into the grid.

7.6. Operation & Logistics

This section will go over the operation and the logistics of the AWE system. First, in subsection 7.6.2 the general mission is explained along with the transportation, Mars production and system installation phases. Next the operation of the system is discussed in subsection 7.6.3. This includes a detailed overview of the take-off and landing systems. After this subsection, the maintenance plan is evaluated in subsection 7.6.4. Finally the End-of-Life phase is discussed in subsection 7.6.5.

7.6.1. Requirements

In Table 7.17 the relevant requirements used to guide the operation and logistics design are included

Table 7.17: Relevant requirements of operation and logistics characteristics

Requirement Index	Requirement	Justification
CON-LE-01	The AWE system shall adhere to guidelines established by the resolution 2222 (XXI) of 19 December 1966 of the United General Assembly.	This requirement originates from stakeholder requirements as the space organizations are bounded by this law and are key stakeholders in the mission.
CON-LE-02	The mission shall not interfere with other missions that are to be in operation or already in operation.	This requirement originates from stakeholder requirements as conflicts could arise if this were to happen.
CON-SF-02	The AWE system shall not damage the Mars habitat while in operation.	This requirement originates from the risk analysis and stakeholder requirements considering ESA is a stakeholder.
CON-SF-03	The AWE system shall not damage the Mars habitat in case of failure.	This requirement originates from the risk analysis and stakeholder requirements considering ESA is a stakeholder.
CON-SF-04	The AWE system shall not hurt anyone while in operation.	This requirement originates from the risk analysis and stakeholder requirements considering ESA is a stakeholder.

7.6.2. General Mission

As discussed in the previous report [9], the mission will consist of five phases: transportation, Mars production, installation, operation and end-of-life. The transportation, Mars production and system installation will be explained in this section. The other two, system operation and end-of-life will be discussed in subsection 7.6.3 and subsection 7.6.5.

Transportation and Landing

First and foremost, the Airborne Wind Energy System will have to be transported to Mars. This phase is currently being researched and developed by another DSE group (DSE group 7). Thus, a quick summary of their current developments will be given. As the AWES will not be transported on the first transfer to Mars, it can be assumed that the Interplanetary Transportation System is already assembled and in orbit around Earth. First the ITS will need to be refueled using multiple launches from Earth. On the last launches, the payload, including the AWES, will be transported to the ITS as well. Once the transfer window to Mars is open, the ITS will transfer the payload to Mars. Once the spaceship arrives, the Mars lander detaches and starts it descent to the Martian surface. Meanwhile, the ITS, now without payload, will start its circularisation burn. Finally, when the lander has touched down on Mars, the payload can be unloaded and new payload from Mars can be sent back to the ITS to be transported back to Earth.

Mars Production

As the transfer to Mars takes quite a while (around seven months), the Mars production phase can already be started while the system is still being transported. This is also possible due to the fact that the 3D printer from the Rhizome project will already have been transported to Mars on a previous transfer. Thus additive manufacturing shall be used to produce various parts of the system, for example the ground station housing/shielding.

System Installation

Once the system has been transported to Mars, the installation phase may commence. First, the astronauts and/or robots will have to unload the system from the lander module. Once this is done, all parts need to be brought to the site where the system will operate. Finally the astronauts/robots assemble the system and install it at the operation site. Once they are done the operation phase can begin. It should be noted that this installation phase should be done in a couple of days. As the astronauts will arrive on Mars at the same time as the AWE system, enough stored energy should be available to sustain them during the time AWESOM is being installed. This energy can either be transported to Mars, or produced using solar panels previously installed during an earlier phase of the Rhizome project. The power production using solar panels was researched last year [2].

7.6.3. System Operation

After the system is installed, the generation of power can start. Note, due to the changes in wind speed throughout the year, the optimal time to start flying would be during the autumn. This is due to the high wind speeds experienced during this season (as found in chapter 2), allowing the system to store enough power to be able to deliver enough power during the seasons which experience lower wind speeds. First the AWES is rotated so that the kite will fly in the most optimal direction with respect to the wind and thus generate the most power. Once in position, the take-off of the kite can commence. This operation is explained in more detail in the next subsection. Once the kite is in the air, power will be generating by flying in a pumping cycle. This means that the kite will first fly away from the ground station, thus reeling out the tether. This turns the generator causing it to generate power. During this reel-out phase, the kite will fly in the figure eight pattern as explained in subsection 7.2.2. This maximises the power generated while preventing the tethers from getting entangled. Once the kite has reached the maximum distance from the ground station, the reel-in phase will start. During this phase power is consumed instead of produced. Thus, to maximise the nominal power generated, the power used during the reel-in phase should be as minimal as possible. One of the ways this can be achieved is to let the kite glide back to the ground station. This will allow the tether to slack as less tension is applied to it. This in turn makes it easier for the motor to reel the tether back in, thus requiring less power. Finally, when the wind velocity is either too low or too high, or maintenance is required, the kite will land back at the ground station. This is also further explained in more detail in the next subsection.

Take-Off and Landing System

Some of the most critical maneuvers performed by the AWE system are the take-off and landing operations. There are various ways to carry out these maneuvers. To evaluate which of these methods would be the best, a trade-off was made.

For take-off the design options identified were:

- Horizontal runway: A runway is made either by carving the regolith, removing boulders and making an overall smooth surface, or by manufacturing it using additive manufacturing or bringing it from Earth. By putting the kite on some sort of sled and reeling in the main tether, a take-off speed can be achieved.
- Bungee launch: A bungee launching system involves an elastic band and a sloped up runway. Attaching the kite to the elastic band, and stretching it so the kite is placed at the bottom of the runway, the kite can be launched by releasing the elastic band.
- Geography: A take-off based on geography requires the AWE system to be located on a slope of some sort. Then by throwing the kite of the slope, it can achieve a high enough velocity to produce enough lift to stay airborne.
- Balloon: Using a balloon attached to the kite surface, the kite can be brought to a parking altitude. Here it can be released, and gain enough velocity from falling to generate enough lift to stay airborne.
- Pressurised canister: Using a pressurised gas, the kite can be shot into the air, providing it with a high enough velocity to stay airborne.
- Mast: The tether will be guided through a hollow mast at an angle of 45 °. Thus, the kite will hang off the edge of this mast. To take off, the kite should be moved backwards, thus extending the tether, by either an automated railing system, robots or the astronauts. When in place, the main tether can be reeled in, thus providing the kite with a velocity to take off.

Trade-off Criteria for Take-off Systems

The criteria chosen for the take-off systems and its corresponding weights will be explained in the section. The criteria are as follows:

- Kite survivability - Weight (5) - This is a critical criteria as it gauges the magnitude of damage that the wing would be subjected to during the the take-off maneuver. With every take-off maneuver, if the wing is to endure a small amount of damage, this could add up and result in a catastrophic failure of wing.
- Extra payload weight - Weight (4) - The additional components of the take-off system would contribute to the total mass of the payload and this is important as it has a mass penalty to the total mass budget. A heavier take-off system would lead to other components having to be penalised in terms of mass.
- Location from habitat - Weight (4) - The location from the habitat is important as access to the wind energy system is important for take-off operation and maintenance. Also the further the energy system is from the habitat the longer the power transmission cables would need to be resulting in power losses, making the system less efficient.

- Installation complexity - Weight (3) - Since the the wind energy system would need to provide power to the habitat, the installation complexity is important in determining the installation time and subsequently the time it takes to provide power to the habitat. The higher the complexity, the longer it takes to start powering the habitat.
- Energy consumption - Weight (3) - The energy consumption of the take-off is less critical as a criteria as this maneuver has a low frequency with respect to nominal operation of the the system. However, some systems do consume more energy than their peers during take-off.

Table 7.18: Trade-off table for take-off design options.

	Kite Survivability (5)	Extra Payload Weight (4)	Location from habitat (4)	Installation Complexity (3)	Energy Consumption (3)
Horizontal Runway					
Bungee Launch					
Geography					
Balloon					
Pressurised Canister					
Mast					

For the landing maneuver the following design options were found:

- Runway horizontal landing: Using the same runway from the take-off design options, the kite can also land on it. The runway would include arresting wires to catch the kite by a tailhook. Note that this option is only really viable with the horizontal runway take-off option.
- Soft crash: The kite will fly in a figure eight pattern parallel to the ground, slowly decreasing its velocity. This ensures that when touching down, the kite will sustain as minimal damage as possible.
- Parachute soft crash: A parachute is attached to the kite to deploy when it needs to land. This will ensure the kite will touch down as slow as possible, minimizing any possible damage to the kite.
- Water landing: A water landing is made either by additive manufacturing or by excavating part of the surface. This is then filled in with a liquid, for example melted water from the Martian ice. This will allow the kite to land on a softer surface, minimizing damage.
- Glide landing: Like on the runway, the kite will glide down, stalling just above the ground. This will reduce the velocity of the kite, allowing it to land on the Martian surface.
- Mast: Like the Mast option for take-off, the kite will be attached to an angled mast. To land the kite, the tether will be reeled in. This allows for the kite to hang off the mast, thus causing no damage to the kite surface as it will not touch any surface.

Trade-off Criteria for Landing Systems

The criteria chosen for the landing systems and its corresponding weights will be explained in the section. The criteria are as follows:

- Kite survivability - Weight (5) - Similar to that of take-off.
- Landing control - Weight (5) - The ability to control the wing during landing is critical to both the kite survivability as well as the safety of the habitat.
- Extra payload weight - Weight (4) - Similar to that of take-off.
- Installation complexity - Weight (3) - Similar to that of take-off.
- Extra weight on kite - Weight (3) - The extra weight induced by the landing system of the kite is not very critical as most landing systems are ground based. However, the parachute is the only system that would be onboard the wing, resulting in additional weight.

Table 7.19: Trade-off table for landing design options.

	Kite Survivability (5)	Kite Control During Landing (5)	Extra Payload Weight (4)	Installation Complexity (3)	Extra Weight on Kite (3)
Horizontal Runway					
Soft crash					
Parachute Soft Crash					
Water Landing					
Glide Landing					
Mast					

Sensitivity Analysis of L&L Trade-offs

To verify that the results from both the take-off and landing trade-offs are valid, a sensitivity analysis was made. This was done by first checking if the weights used for the different criteria make sense for the design. Then the trade-offs were also verified by removing a criterion one by one, to see the influence of a particular criterion.

The most important criteria according to the weights are the kite survivability and the control during landing. This makes sense, as repairing the kite is very expensive due to the limited resources available on Mars. This also counts for the control during landing, as the better it controls, the less likely it is to crash. Although still important, installation complexity, energy consumption and extra kite weight are relatively less important. This is due to the fact that these criteria can be compensated for using different subsystem designing.

Removing different criteria resulted in somewhat different ranking. For take-off, the mast design is still the best option for the majority of cases. However, when removing the location from habitat criterion, geography would be considered better, and when removing the installation complexity, the horizontal runway would come out on top. Nonetheless, these criteria are considered important, meaning they can not just be removed during the actual trade-off. Thus, the mast design is still considered the best take-off option.

For the landing design trade-off, the mast design is still considered the best even when removing any of the criteria. Thus, this design is the best choice.

Final Take-off and Landing Configuration

After performing the trade-off for both take-off and landing, the mast concept is chosen as the most suitable method for both maneuvers. Utilising the same concept for both maneuvers also reduces the mass of the payload and the complexity of the system as only one system has to be installed. The final configuration of the take off and landing can be seen in the figures below:

Figure 7.51: Landing and parking configuration

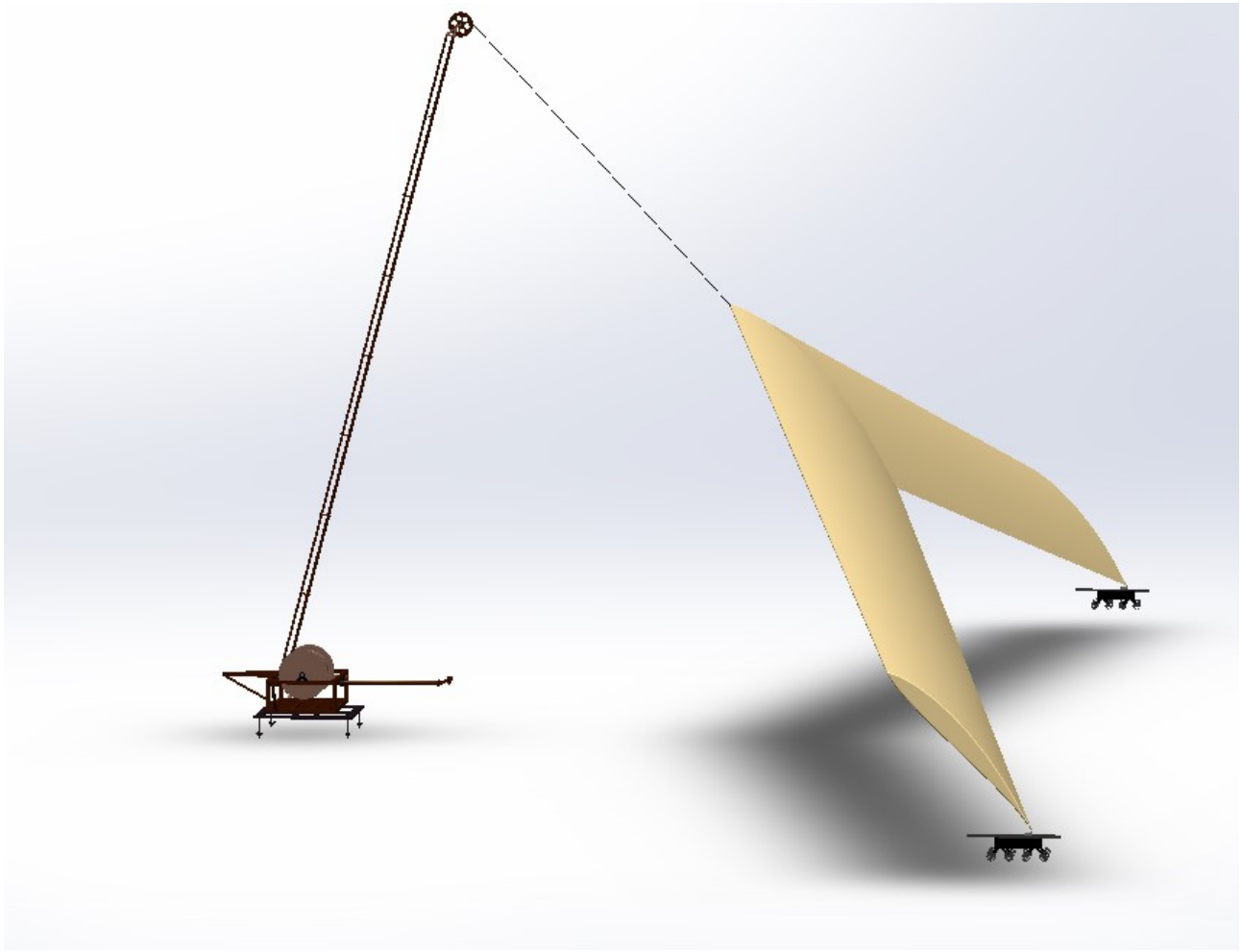

Figure 7.52: Take-off configuration

Looking at Figure 7.51, the main components of the mast concept are the rotating ground station, the anchoring platform, the vertical mast and the horizontal boom. The anchoring platform is secured to the ground via regolith anchors. The ground station is attached to the anchoring platform via a slewing ring which enables 360°of rotational freedom. The vertical mast and horizontal boom are free to rotate with the ground station in either direction depending on the wind conditions. Through the vertical mast and the horizontal boom, the main tether and control control tether lines are fed through and are guided via pulleys and rope guides. The vertical mast is angled at 75 degrees from the ground to provide enough clearance for the wing from the mast itself during the landing phase. To reduce the bending loads at the root of the mast, tension lines are attached from supporting beams to the vertical mast to transfer loads. The ends of the horizontal boom are located at the same distance as that of the end of the vertical mast. This design choice provides clearance for the wing from the ground station. In Figure 7.52, the modified rover is used in the take-off phase that will be explained further. The assumption for this is that an existing rover on Mars that was used in the initial phase of the RHIZOME project [24] is decommissioned and modified and used as a platform on which the wing will sit on during the take-off sequence.

The take-off sequence is initiated with the main drum reeling out a short length of tether and lowering the wing onto the modified rover. The drum and rover are simultaneously rolled back and the length of the tether is extended. To lift the wing into the air, the tether is reeled in at 20 m/s and the control tethers are used to increase the angle of attack the wing. This step ensures that the wing will have a higher relative wind speed and be able to lift into the air. The figure eight maneuver and traction phase is then commenced. The landing sequence begins with the wing pitching up midair using the control tether lines and gliding down towards the ground station. When the wing is close to the ground station, the control control tether lines are reeled in more to pitch up the wing and make it stall. The parking position is then achieved with the wing in a vertical position above the ground as seen in Figure 7.51.

7.6.4. Maintenance

As found in the previous report [9], it is crucial that the airborne wind energy system is regularly maintained, as it will ensure that the system will stay operational during the required life span of five Martian years. The maintenance strategy of the AWES involves three main steps, failure detection, intervention and and reparation. As the resources for reparations or replacement of parts is very limited, it is crucial to have a well performing failure detection in place. This is to ensure a failure is detected very early on, thus preventing it from becoming a bigger and bigger problem further down the line, which would increase the amount of resources needed to repair it.

Failure detection can be done in multiple ways, however it is first important to analyse what detection mechanisms may be used and how they can be used to prevent undetected failures snowballing into a system-wide failure without much remedy. Vibration-sensors may be placed on the generator to detect off axis rotations and vibrations of loose/damaged components. Strain gauges can be implemented to detect possible damage in the tether or kite, although this poses the problem of having to power these airborne devices. Though they would help to monitor the loads experienced and judge if damage may have occurred without on site inspection, it will likely not be worth it to install a system to power them. The new technology of thermography may be used instead. This involves using infrared radiation to detect faults/failures in the ground station's electrical and mechanical components visually rather than by using vibration measurements. Although this technology is not yet fully proven in the field, by the time of launch the technology may have developed enough to be of great use. Temperature sensors are also vital to monitor the status of the ground station and detect any occurrence of over- or underheating and schedule an intervention to visually check for damage. Lastly, lubrication analysis devices may be used in the generator, direct drive shaft and drum to make sure the lubrication is not contaminated or insufficiently applied.

All of the aforementioned failure detection mechanisms should be used as much as possible in order to maximise the amount of information gathered before any intervention by the astronauts, as often visual inspection will require large amounts of downtime (especially if the generator needs to be opened up). Additionally, a quick overview of the health status of the system may be provided by the various sensors which will allow more regular checkups on the AWES and earlier failure prediction before other components are damaged. Hence, the main strategy used for maintenance will be condition based maintenance. Failure model predictions and regular checkups are still viable options and should be used in combination with condition based maintenance.

In order to ensure that the required maintenance can be performed, spare parts are required. Although some maintenance will be performed using in-situ materials and additive manufacturing, many parts would need to be transported from Earth alongside the main system. Since this would add more weight to the total mass that has to be transported from Earth, it is vital to analyse what spare parts are critical to bring from Earth and which can be produced on Mars in order to minimise the amount of spare parts transported from Earth due to high costs. The main spare parts that will have to be taken from Earth include: multiple spare tethers and control tethers, and either a full extra kite or some parts such as the membrane to repair it.

7.6.5. End-of-Life

As stated in the previous report [9], multiple options are available for the end-of-life of the system. The first one is a possible life extension. This can be considered when the system is still able to provide enough power to the habitat. Life extension may involve the replacement or repair of some parts as well as the upgrade of certain subsystems for more efficient operation using new technologies. If this is not an option anymore, each of the different parts of the airborne wind energy system should be evaluated for the possibility of re-using, recycling or up-cycling. For example the mast used for take-off and landing could be reused in the structure of another system or the habitat itself. Furthermore, the motor-generator could be taken apart to use different parts of it in other mechanical systems. The system should be designed such that this will be possible for many of the other parts as well, to ensure a greater sustainable system. The parts which can not undergo any sustainable process will be disposed off in a manner which damages the environment the least. This can for example be done by storing them for possible future usages, or bringing them back to Earth.

7.7. System Characteristics Results

In this section the results from the design process are summarised with the use of Table 7.20. In the table the first column lists all subsystems in bold and its elements below it and the second column gives a brief description of what the chosen design option for that element is. The third column describes the important dimensions and the volume that the system or element will take up in the spacecraft and the fourth column lists the mass of that system or element. Each subsystem volume or mass is the sum of its composing elements. The wing volume is an exception in this due to the fact that the wingbox can be used as storage for smaller components when packing for transportation.

Table 7.20: Results of the preliminary design stage for each subsystem (bold) and it's elements with its dimensions and mass

Sub-system	Chosen Design Option	Dimensions	Mass, kg
Wing	**Swept flying wing; Wortmann FX 63-137 airfoil**	S = 60 m^2; b = 20 m; MGC = 3.0 m; AR = 6.67; Taper ratio = 1.4; Λ_{LE} = 16.96; **V = wingbox volume = 1.1 m^3**	**79.5**
Canopy	Nylon-6 membrane	±2.2 □S = 132 m^2; t = 0.1 mm; V = 0.066 m^3	13.56
Ribs	Q.I. Carbon Fiber Epoxy truss structure	Truss thicknesses range1-3 cm depending on spanwise location, lenghts range from	9.94
Wingbox	Q.I. Carbon Fiber Epoxy circular wingbox	Diameter range 48 cm (root) - 34 cm (tip) t = 18 mm at root, t = 10 mm at tip section; V = 1.1 m^3	57.7
Tether	**Dyneema rope** (3)	l = 1000 m; t = 4.6 mm; **V = 0.0499 m^3 (3)**	**48.86 (3)**
Control Unit	**On-ground system with control tethers, figure-of-eight pumping cycle**	**V = 0.03133 m^3**	**28.76**
Control Pod	Pod with main computer, flight path computer and telecom and transmitter receiver inside .	V = 0.025 m^3	20
Control Tethers	2 x Dyneema rope	l = 1000 m; thickness = 2 mm; V = 0.0063 m^3	6.16
Sensors	Visual camera on ground station, angle sensors and torque sensing by motors and wind-speed sensor	-	<1.0
Actuators	Servo motors	-	1.6
Ground Station	**Carbon fiber composite structure, with a pole to attach the wing to and a slewing system to point to the optimal direction and the power generation and distribution system integrated**	**V = 0.3171 m^3**	**518.4**
Structure	Carbon fiber	Pole length = 8.5 m; box height = 0.4 m; box length = 0.75 m; box width = 1.1 m; volume of components = 0.045 m^3	150
Motor/Generator	Electrical direct drive torque motor with 70 kW of rated power	V = 0.07 m^3; height = 0.21 m; radius = 0.325 m	250
Drum	Carbon fiber composite	Diameter = 60 cm; length = 60 cm; V = 0.2309 m^3	15
Motor Controller/ Inverter	Small computer that regulates the functioning of the motor/generator	V = 0.012 m^3	4.5
Internal Control Unit	Small chip	-	-
Buffer Storage	Supercapacitor	V = 0.012 m^3	19.4
Slewing System	Slewing ring below the ground station with small motor	V = 0.0155 m ^{3}	70
Brake Actuator	Disk brake	V = 0.00171365 m^3	9.5
Total		**V = 1.49833 m^3**	**675.52**

8

Performance Analysis

Having decided on all the design choices, an analysis needs to be made in order to check how the design will perform and if the requirements are met. In this chapter, the model built to assess the performance of the designed system will be presented. Firstly, the model will be described in section 8.1. Then, the underlying calculations will be explained in section 8.2. Before moving further, the model will be verified and validated in section 8.3 to ensure that there are no errors in the code or that the code outputs what is required. Finally, the results will be presented in section 8.4.

8.1. Model Description

A Python model of the system was built in order to assess how much power is produced by the system over the time. Since one of the main requirements (TEC-PS-02) is to provide 10 kW power output, it is crucial to prove that the designed system can produce enough power.

In order to build the software model for the system, a step by step plan was followed. Firstly, a simulation for one figure of eight motion was developed. Subsequently, this simulation was extended to one pumping cycle. After this step, this pumping cycle simulation was extended to simulate the behavior throughout the day. Consequently, the simulation was improved to be for the power production during the whole year. The first two steps, the figure of eight and pumping cycle simulations, make the basis of the model. In the next section, the logic and calculations of the simulation will be explained.

8.2. Calculations

As explained in subsection 7.2.2, a down-loop figure of eight flight trajectory has been chosen for operation. As shown in Figure 7.8, the reel-out phase consists of figure of eight motions of the wing while also climbing up. The instantaneous power production depends on many parameters during one figure of eight motion. To be able to build a model for this motion, the motion itself together with the change of parameters should be modelled.

The desired outcome of the simulation is the power generated by the pulling force of the wing. This pulling force is due to the lift generated by the wing, and the amount of lift depends on several parameters, and its formula is:

$$L = C_L \frac{1}{2} \rho v_{k,\tau}^2 S \tag{8.1}$$

The C_L and S depend on the wing design, while ρ depends on the environment. At this point, it is necessary to calculate the tangential speed of the wing ($v_{k,\tau}$). This speed is used for the calculation of the lift force because it is assumed that the wind speed in the direction of flight is negligible. According to [25], this speed can be calculated using a factor, λ. This factor is defined as follows:

$$\lambda = \frac{v_{k,\tau}}{v_w} \tag{8.2}$$

In order to calculate this factor, the orientation of the wing and its trajectory is necessary to know. This orientation can be represented by three angles: elevation, azimuth and course. These angles are shown in Figure 8.1.

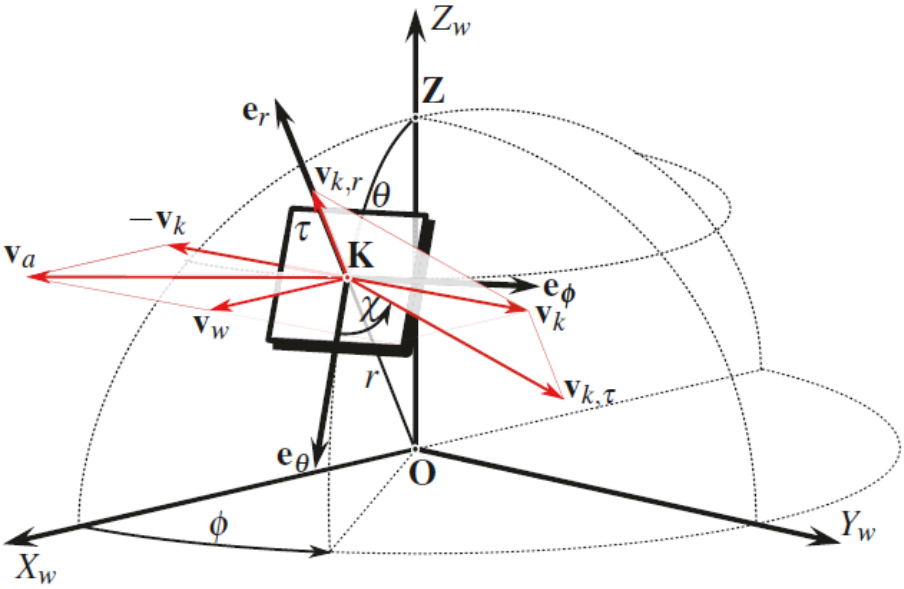

Figure 8.1: Orientation of the wing in terms of elevation, azimuth and course angles.

Now that the angles are defined and visualised, the formula for the lambda factor can be presented.

$$\lambda = a + \sqrt{a^2 + b^2 - 1 + \left(\frac{L}{D}\right)^2 (b - f)^2} \tag{8.3}$$

where a and b are defined as:

$$a = \cos(\theta)\cos(\phi)\cos(\chi) - \sin(\phi)\sin(\chi) \tag{8.4}$$

$$b = \sin(\theta)\cos(\phi) \tag{8.5}$$

It is seen that the calculation of lambda requires the values of L/D and f as well. L/D is found by dividing the lift coefficient C_L and drag coefficient C_D. For the model, the coefficient values are taken for the optimal L/D point, and the drag coefficient is corrected for the tether drag. The correction is done by adding the drag on the wing that is induced by the main tether and control tethers as follows:

$$C_{D_{corrected}} = C_{D_{wing}} + \frac{C_\tau l_{tether} d_{tether}}{4S} + \frac{2C_\tau l_{controltether} d_{controltether}}{4S} \tag{8.6}$$

The lift coefficient also has to be corrected due to the compressibility effect. This is done using the Prandtl-Glauert rule as seen below which is applicable in the speed region between a Mach number of 0 to 0.5 which holds for AWESOM as the tangential kite speed was limited to 120 m/s in section 7.1. [26]

$$C_L* = \frac{C_L}{\sqrt{1 - M^2}} \tag{8.7}$$

Before moving further into the development of the model, it is important to analyse the assumptions made for the formulae above along with their effects on the model. The assumptions are listed below together with some elaboration on them and how they are incorporated in the design process.

- **Sagging of the tether is neglected.** Due to this assumption, the radial component of the wing's velocity can be accepted as the tether velocity of reeling out. This assumption is not expected to have a big impact looking at the existing systems on Earth. Therefore, no further action is done on this matter.
- **Constant C_L & C_D.** This assumption is made to simplify the problem as the aerodynamic coefficients change with the angle of attack but it is hard to estimate the angle of attack at each location. For the design of the AWESOM, the aerodynamic performance of the chosen airfoil is analysed in detail as seen

in section 7.1. This makes it possible to assess how the aerodynamic performance is affected by the change of angle of attack. Moreover, the angle of attack can be controlled by the control subsystem. Therefore, even though these preliminary calculations did not incorporate this dynamic relationship, it was taken into account during the scope of the design.

- **Steering of the wing is neglected.** This means that the forces experienced on the system due to the steering are neglected. In the model, some corrections are applied to the calculated power output to account for the steering. For example, the banking angle changes the line of direction of lift force which affects the force on the tether for power generation. Therefore, the effects of this assumption are analysed sufficiently.
- **Internal and gravitational forces are neglected.** The effects of these assumptions were estimated throughout the design process, and even though they are not implemented on the model itself, the structural design of the wing is done considering the effects of these forces, not overlooking their contributions.

At this point, it is possible to calculate the lambda factor and hence the tangential speed of the wing. However, there are some limitations that has to be incorporated in the model. For example, there is a maximum speed of 120 m/s which is dictated by the turn radius and structural strength of the wing. Another limitation is dictated by the generator, namely its peak power. Since the generated power is within a very large range due to the wind speed fluctuations throughout the year, the generator was chosen to be custom designed for AWESOM. This generator will be made to have a peak power of 85,000 W and a rated power of 70,000 W. As explained in section 7.5, the efficiency of the motor above 15% of its nominal power is very high, so the loss is not incorporated in the simulation as it is assumed to be negligible.

As explained at the start of this chapter, the first step is to model the power performance during one figure of eight motion. In order to do this, the angles of elevation, azimuth and course have to be defined. These angles are defined for eight distinct points on the trajectory which can be seen in Figure 8.2. The elevation is assumed to be constant at 30°at each point. Azimuth angle was calculated using the turn radius which determines the total length of one figure of eight. The course angle is dependent on the orientation of the wing within its course of motion. This angle for each point can be seen on the figure as well.

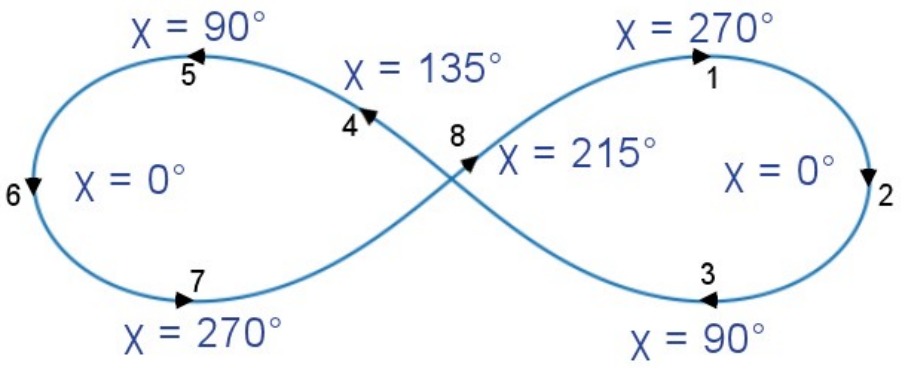

Figure 8.2: Points on figure of eight trajectory.

Having defined the angles for each point, now the power calculations can be applied to each point. For the specific points of 2 and 6, the calculated power is corrected for the banking angle as the lift force is not parallel to the tether direction anymore. At this point, the aforementioned limitations have to be implemented as well. First, the power output and the wing's tangential speed is calculated. If they are above the limits, then some correction process is initiated. For the tangential speed, the value is lowered below the limit by changing the angle of attack. By increasing the angle of attack, it is possible to decrease the lift-to-drag ratio while also increasing the lift coefficient. The first one of these lower the tangential speed which reduced the generated lift and hence the power. However, the increase in lift coefficient is beneficial for higher lift. For the power, any power output higher than the peak power output of the generator is lowered to the peak number since that limit is not possible to stretch. The high values of power are directly related to high tangential wing speeds as well so lowering them will be possible again by increasing the angle of attack. The relationship between the lift to drag ratio and the angle of attack can be seen in Figure 8.3.

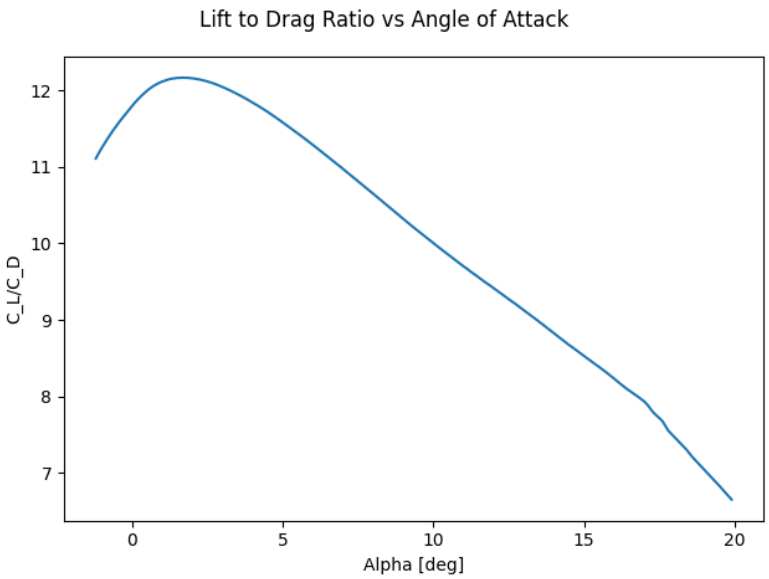

Figure 8.3: Change of lift to drag ratio over different angles of attack.

With these values, the power calculations for one figure of eight is complete. The next step is performing the calculations for one full pumping cycle which consists of many figures of eight. For this, the altitude change is needed, which can be calculated as follows:

$$\Delta h = v_t t_{figure} \sin(30^\circ) \tag{8.8}$$

The parameter t_{figure} represent the time it takes to complete one figure of eight. The sine correction follows from the elevation angle, and the tether speed is calculated using the reeling factor. After each figure of eight motion, the altitude is updated using the above formula, and the figure of eight calculations were run again. This iteration starts at the initial altitude and stops at the final altitude. When the final altitude is reached, the model moves on to the next hour of the day. For estimating how much power is generated per cycle, average of every point of each figure of eight motion within that cycle is used. Similarly, the average of all the cycles per day is used as an estimate of the power generating capacity of the system.

8.2.1. Time Correction

The model continues by cycling through 361 (0-360) different solar longitudes. Thus, to calculate the total energy produced over a year, a time correction is needed. The eccentricity of the Martian orbit causes the lengths of the months to be longer or shorter depending on the time of the year. The model incorporates this by taking the average power produced on a day at a certain solar longitude and multiplying that by the amount of days in that month and dividing by the amount of solar longitudes in that month. The amount of days in every month can be seen in Table 8.1. The total amount of energy produced in a day i and in month j:

$$E_{total-i} = P_{average-i} * t_{Martian-day} * \frac{N_{days-j}}{N_{ls-j}} \tag{8.9}$$

Where $E_{total-i}$ is the average total energy produced in those days,$P_{average-i}$ is the average power of the 24 Martian hours at that solar longitude, $t_{Martian-day}$ is the length of a Martian day in Earth hours, 24.62 hours. N_{days-j} is the amount of days in that particular month and N_{ls-j} the amount of solar longitudes in that month (31 for the first month, 30 for the others).

Table 8.1: The amount of days in the different months.

Month Number	Solar longitude	Amount of days
1	0 - 30	61
2	31 - 60	66
3	61 - 90	66
4	91 - 120	65
5	121 - 150	60
6	151 - 180	54
7	181 - 210	50
8	211 - 240	46
9	241 - 270	47
10	271 - 300	47
11	301 - 330	51
12	331 - 360	56

8.3. Verification & Validation of the Model

Verification and validation (V&V) is done to check whether the software program meets specifications and requirements so that software fulfills its intended purpose. Verification is the evaluation of whether or not a product, service, or system complies with a regulation, requirement, specification, or imposed. Validation is the assurance that a product, service, or system meets the needs of the customer and other identified stakeholders[1].

To perform software verification for the AWESOM project, unit tests and systems tests were performed on all scripts of code used for performing calculations. During unit testing, a 90% line coverage was achieved for most scripts and during system testing, the integrated system was evaluated.

There are two ways to perform software validation: internal and external. During internal software validation, it is assumed that the goals of the stakeholders were correctly understood and that they were expressed in the requirement artifacts precisely and comprehensively. If the software meets the requirement specification, it has been internally validated. External validation happens when it is performed by asking the stakeholders if the software meets their needs. External validation is not possible for this project as there is no direct line of communication between the group's members and the stakeholders. Therefore, the main focus will be on verifying all the programs and software associated with the project. Although Validation will not be explicitly performed, various approaches will be discussed with a special emphasis on the most widely used strategies.

In Table 8.2, the results of multiple unit tests are shown. These tests were performed by first computing the desired property using an analytical approach and then comparing these analytical results to the computed results. If any discrepancies arise during this process, the code is immediately rectified and re-checked again. This process goes on until a desired amount of coverage is achieved. For this project, the desired code coverage is set between 85% to 90%.

[1] https://en.wikipedia.org/wiki/Software_verification_and_validation[Accessed on June 18, 2021

Table 8.2: Verification tests for the functions used in the model.

Unit/Function	Input	Expected Value	Calculated Value	Error
f_ab(theta, phi, chi)	1,1,1	a = -0.55, b = 0.45	a = -0.55, b = 0.45	0,0
f_ab(theta, phi, chi)	0,0,0	a = 1, b = 0	a = 1.0, b = 0.0	0,0
f_ab(theta, phi, chi)	-1,-1,-1	a = -0.55, b = -0.45	a = -0.55, b = -0.45	0,0
f_lambda(L_to_D,f,a,b)	20,1,5,4	65.3	65.3	0.0
f_lambda(L_to_D,f,a,b)	0,1,0,1	0	0.0	0.0
f_lambda(L_to_D,f,a,b)	-20,1,-5,4	55.3	55.3	0.0001
f_tangential_speed(v_w, lambda_factor)	100, 0.5	50	50	0
f_tangential_speed(v_w, lambda_factor)	100, 0.0	0	0	0
f_tangential_speed(v_w, lambda_factor)	-100, 1	Err	Err	0
f_Mach_correction(C_L, v_k_tangential, T)	1.7, 100, 273.15	1.829	1.829	0.0
f_Mach_correction(C_L, v_k_tangential, T)	1.7, 100, 0	Err	Err	0.0
f_Mach_correction(C_L, v_k_tangential, T)	1.7, 8.3, 273.15	19.1	19.1	0.0
f_weight(m_wing,..., l_tether)	60, 0.005, 0.001, 600	264.2914	264.30	0.0086
f_weight(m_wing,..., l_tether)	0, 0.005, 0.001, 600	Err	Err	0.0
f_weight(m_wing,..., l_tether)	60, 0.0, 0.0, 100	223.26	223.26	0.0
f_power_required(v_reelin,..., eta_reelout)	5,6,600,0.5,0.2	220.0	220.0	0.0
f_power_required(v_reelin,..., eta_reelout)	0,0,100,0.5,0.2	Err	Err	0.0
f_power_required(v_reelin,..., eta_reelout)	1,1,1,-1,-1	2.0	2.0	0.0
f_power(C_L_corrected,..., eta_reelout)	1.8,0.015,100,50,60,120,0.5	360900.0, 6015.0	360900.0, 6015.0	0,0
f_power(C_L_corrected,..., eta_reelout)	0,0.015,100,50,0,120,0.5	0.0, 0.0	0.0, 0.0	0,0
f_power(C_L_corrected,..., eta_reelout)	-1,0.0,0,50,60,120,0.5	Err, Err	Err, Err	0,0
f_angle_check(theta, phi, L_to_D, f)	0.523599,1.0472, 20 , 0.3	True	True	0.0
f_angle_check(theta, phi, L_to_D, f)	0.523599,1.0472, 10 , 0.1	False	False	0.0

8.4. Results

The main goal of developing the described performance model was to provide results on how much power the designed AWE system is capable of producing. In this section, the most important results will be presented with the help of visuals. The presented results are the output of the model for the following set of parameters in Table 8.3 as input. The table also presents what the source of each number is.

Table 8.3: Input parameters for the model.

Parameter	Value	Source
Reeling factor (f)	1/3	Literature
Wing surface area	60 m^2	Aerodynamics
Wing mass	79.7 kg	Structures
Tether diameter	4.6 mm	Structures
Control tether diameter	2 mm	Structures
Reel-in speed	12 m/s	Power
Initial altitude	105 m	Control
Final altitude	365 m	Control

Literature means the number is chosen according to research and existing systems. The rest of the sources are departments, and their design results are all presented in chapter 7. Most of them are direct results such as wing surface area or mass. The initial and final altitudes follow from the turn radius and how much clearance it requires.

The main results of the model is the yearly power output which can be seen in Figure 8.4. The x-axis shows the year in terms of solar longitude which does not directly correspond to days as explained in subsection 8.2.1. As stated in the legend, the blue line shows the electrical power output of the system throughout the year. The orange line is the required electrical power output to provide 10 kW of power to the habitat. The calculation of this required power is presented in section 7.5.

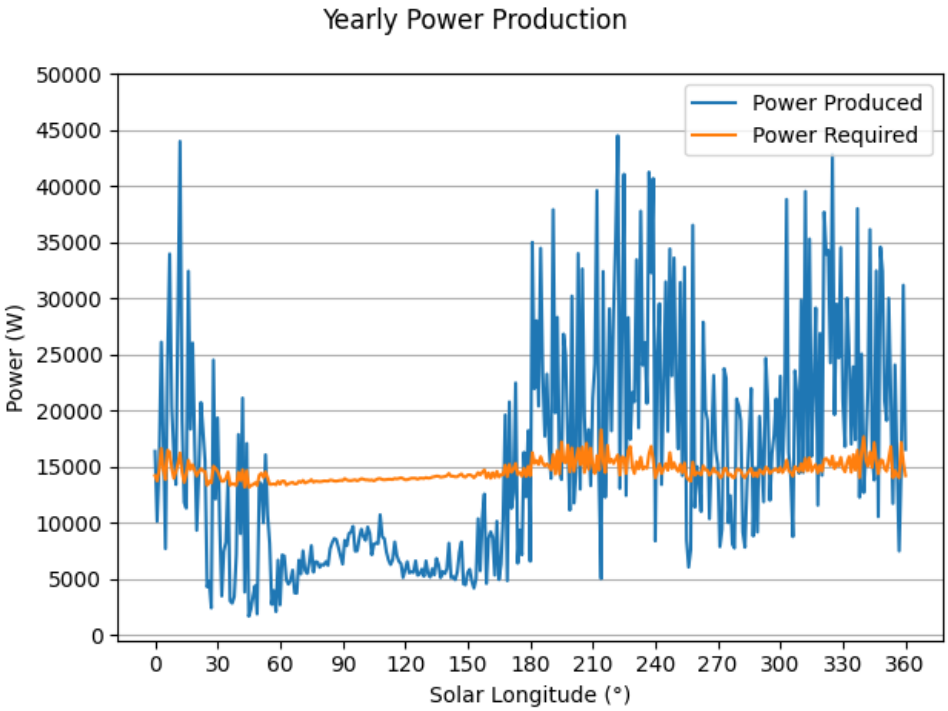

Figure 8.4: Electrical power output per one year.

This graph can also be presented in a different way by showing the difference between the produced power and the required power. This change in this excess amount throughout one year can be seen in Figure 8.5. In this figure, the green part of the curve represents positive excess power while red part represents the negative excess. This graph helps showing the balance between these two parts, since it is required to save enough energy when there is positive excess power to be able to use it when the excess is negative, which means extra energy is needed from the long term storage.

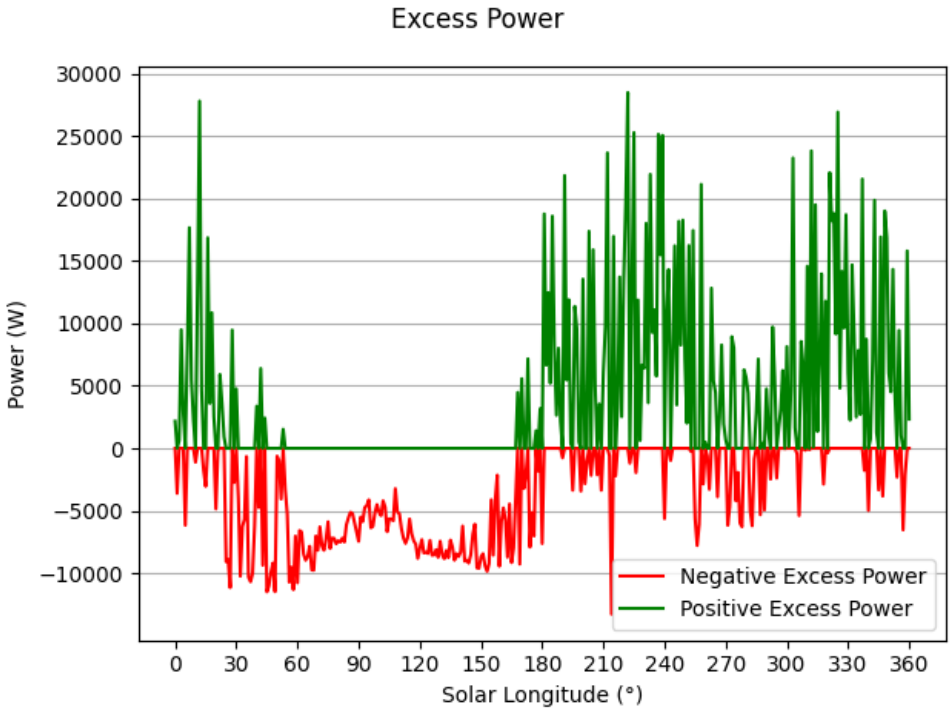

Figure 8.5: Excess power throughout one year.

Although the main goal of this simulation was to calculate the power generation capacity of the system, there

is other useful information that can be obtained from the outputs of the model. One example of this is the force carried by the main tether. This information is of use since it can show if the tether is designed adequately to survive the loading on it during the whole operation. The variation in force on the main tether can be seen in Figure 8.6. The curve represents the daily average force on the tether throughout one Martian year.

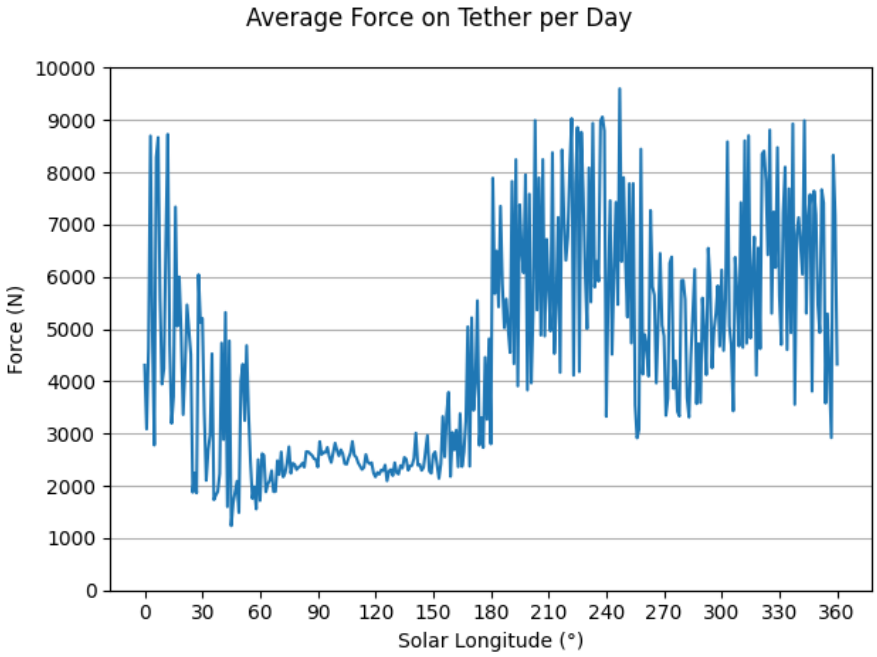

Figure 8.6: Average force experienced by the main tether per day of year.

The maximum daily average seen on this plot is 9603 N. The maximum force on tether at any time is limited to 12000 N which is dictated by the control unit. Therefore, it was established that the chosen diameter of the main tether was thick enough to survive the forces experienced during operation. This conclusion takes into account the fatigue as well as the tensile force on the tether. Moreover, this proves that the requirement TEC-AIR-07 is complied with.

With the outputs of the model, tangential speed of the wing throughout the year can also be plotted. This plot is seen in Figure 8.7.

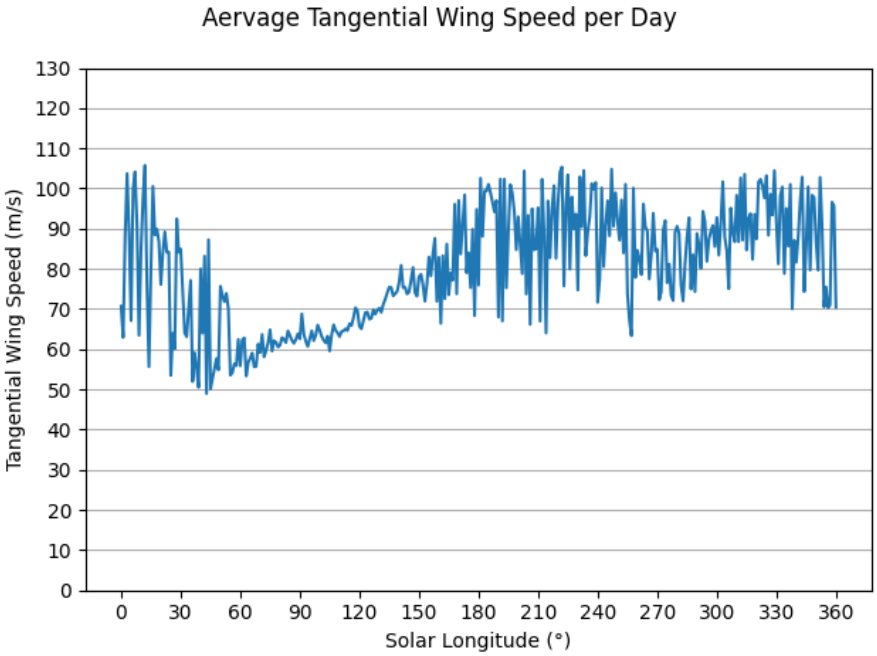

Figure 8.7: Average tangential wing speed per day of year.

As seen in the plots of tether force and tangential wing speed, they directly relate to each other. This comparison acts as a verification of the model as well.

Until this point, the model of the system was used to calculate how much power is generated. However, the power performance of the system is also dependent on some other parts of the system which required energy. One significant energy draining part is the control actuators. As explained in section 7.5, the control actuators use 1.4 MWh of energy per year. Another energy draining part is landing and launching processes. When the wind speed is below a limit, the wing cannot generate enough lift force to counteract its weight. To avoid crashing, the wing should be able to safely land during the low-wind periods and re-launch once the wind speed is sufficient again. According to the calculations in section 7.6, each launch uses 5.3 Wh of energy while each landing uses 2 Wh, adding up to 7.3 Wh per landing and launching. Knowing this, the only necessary information is how often the wind speeds go below the required value. According to the model, the minimum wind speed the wing can stay airborne is 4.46 m/s which complies with the requirement TEC-AIR-11 to have a maximum of 5 m/s for this. Then, the model is used to determine how often the wind speed is actually below this number. The consecutive hours were counted as one single landing and launching since the wind speed stays below the cut-in speed for the whole period. This evaluation led to 287 landing and launching cycles per year. This equals to a total required energy of 2095.1 Wh, which is very low compared to the energy generation, but still added to the total energy requirement.

The simulation also output the cut-out speed, which is 22.8 m/s. This speed complies with the requirement TEC-AIR-08.

All in all, the total energy produced by the system equals to 241.51 MWh. The total required energy is 233.852 MWh, which includes energy required due to losses, reel-in phase and also for control actuators and landing & launching activities. This means there is 3.2% extra energy produced by the system. This small extra amount can be treated as a safety factor, and can be used in case of emergencies. The summary of this evaluation can be seen below in Table 8.4.

Table 8.4: Summary of simulation results in terms of energy.

Energy	Amount per year, MWh
Required for landing & launching	0.002
Required for control	1.40
Required for the habitat	232. 45
Total required	233.852
Total produced	241.51
Excess	7.658

At the end of this performance analysis, it is seen that the designed system is capable of producing enough power, complying with the key requirement TEC-PS-02.

8.5. Sensitivity Analysis

No simulation is ever going to be as complex as reality. This means, the resulting power performance of the real system will differ from the model's outputs. However, it is still crucial to build and evaluate the model in order to understand what is to be expected from the actual system. One aspect the model can aid the actual system's design and production is by analysing which input parameters the system's output is sensitive to. This information shows which parameters should be given special attention during the design and production process.

In order to determine which parameters the simulation model is sensitive to, the parameters can be altered and the change in power production output can be observed. As an example procedure, below in section 8.5, the sensitivity towards the wing mass parameter can be seen. Visibly from the values, just the mass of the wing does not have a significant effect on the average power output per day. If there is a minor mistake in the wing sizing, this would only affect the power production slightly. Therefore, wing mass does not belong to sensitive parameters.

Table 8.5: Sensitivity of power output towards change in wing mass.

Wing Mass, kg	Average Daily Production, W
79	15401
80	15392
85	15342

A similar procedure was applied for other parameters as well. In the end, the following parameters were found to be sensitive: tether diameter, reel-in speed, altitude range, wing surface area, pumping efficiency, reeling factor and tether density.

Among these parameters, the tether diameter, altitude range, and tether density are directly related to the tether weight, which has a big impact on the power production. Due to 30° elevation from the ground, the tether length is twice the altitude. This results in a long tether which increases the weight carried by the wing significantly. On another note, the altitude range which the system operates in between also affects the wind speeds the wing is experiencing. Since the high and low wind regions are not regular as presented in chapter 2, the change in initial and final altitudes for one cycle can have a big impact on the power output values.

The reel-in speed is among the sensitive parameters due to its effect on the required power output. This is due to the way the model calculates the power requirement to provide 10 kW output, which is explained in detail in subsection 7.5.5. The same part (Equation 7.59, Equation 7.60) explains the pumping efficiency as well. This number was assumed to be constant due to the complexity of implementing its dynamic behavior in the model within the limited time. The change of this number has a significant effect on the power production results, hence its location among the sensitive analysis.

The final two of the sensitive parameters are wing surface area and the reeling factor. Reeling factor is sensitive since it indirectly affects the tangential velocity of the kite which has a direct impact on the lift generated by the wing. The wing surface area is also sensitive due to its direct effect on the lift generation.

In the end, the sensitivity analysis was useful because it showed the design team which parameters need to be chosen very carefully. Any small change in these parameters can affect the power output significantly. Therefore, it is crucial to use correct values for these parameters.

8.6. Recommendations

Especially considering the limited time the design team had for the whole conceptual design, it was expected that not all the calculations within the simulation are completely realistic. This is why several assumptions were made, and they naturally have some effects on the accuracy of the results. Therefore, the main recommendation for the next design phase is to create a more accurate model of the system.

Apart from the assumptions there are also some details which were not implemented due to limited time and resources. One of these details is changing elevation angle. Currently, the simulation assumes constant elevation angle during operation. However, especially due to the trajectory having a significantly big turn radius, the elevation angle cannot actually stay constant. This is expected to have some effect on the power production performance, but it was not possible to implement during the limited time present for the preliminary time. Therefore, it is expected to be implemented in the detailed design phase.

Another detail lacking from the simulation is the generator efficiencies. Since development team did not have sufficient experience or knowledge on this topic, it was a real challenge to implement the change in generator's power conversion efficiency depending on where within the power range it is operating. Therefore, it was only assumed that the generator had a maximum and minimum rated power, and within these two values, the conversion efficiency was assumed to be constant. This is also expected to have an impact on the results of the simulation, and it is a valuable addition for the detailed design phase.

9
Interface Design

9.1. Hardware & Software Interface

This section shows the overview of both the hardware and software components that are to be used in the AWE system. This is done with the help of a hardware and a software block diagram (Figure 9.1 and Figure 9.2). The hardware block diagram is explained in subsection 9.1.1 which is followed by an explanation of the software block diagram in subsection 9.1.2.

9.1.1. Hardware

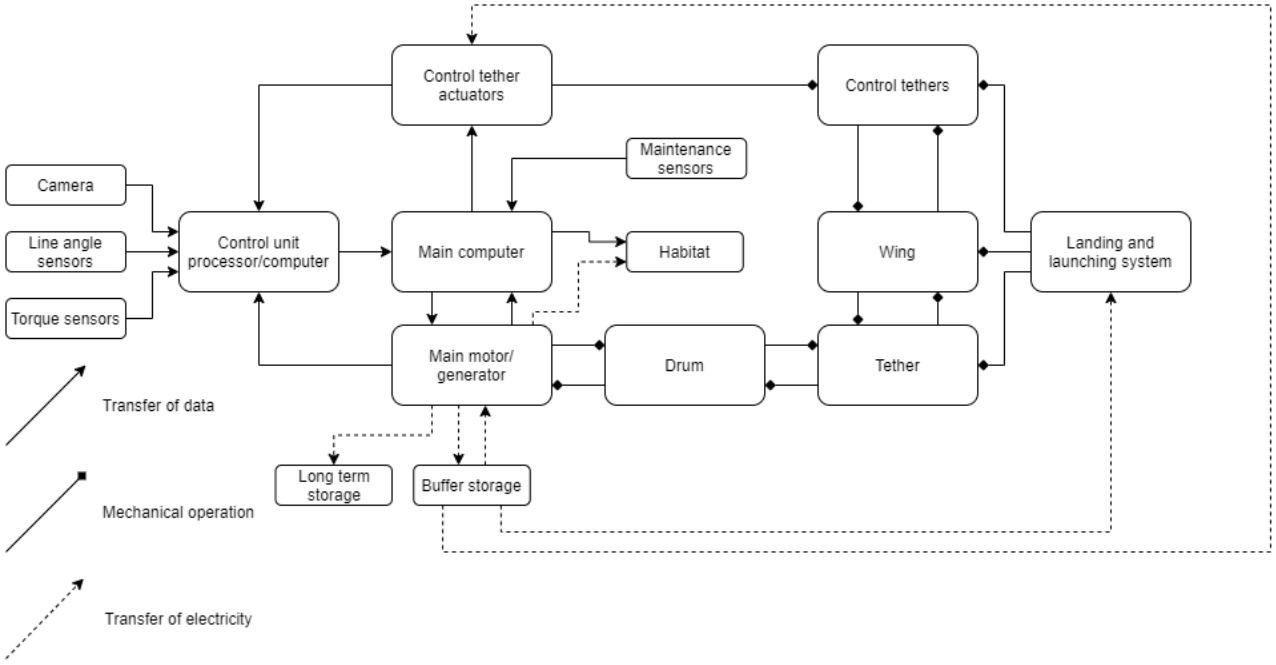

Figure 9.1: Hardware block diagram

The hardware block diagram shows the different parts of the system along with the interactions between them. It starts on the left with the data transfer between the sensors, the control unit and the main computer. This part is also shown in more detail in the software block diagram, which is explained in subsection 9.1.2. The data from the main computer is then transferred to the control tether actuators and the main motor/generator. Furthermore, the main computer also receives data from the generator and from the maintenance sensors. The data from the generator indicates the total power that is being generated. From the maintenance sensors, the main computer receives any data regarding possible failures or damage of the different subsystems. Both the generator data and the maintenance data is sent to the habitat, after being processed by the main computer. Using the input from the main computer, the actuators are able to manipulate the control tethers in order to control the wing. Similarly, the main motor is able to turn the drum to control the main tether and thus control the wing. It should be noted that the wing also influences the tether and control tethers, as during normal operations, the wing will fly away from the ground station pulling the tether and control tethers and reeling them out further. This also means that the tether turns the drum, which in turn turns the generator and thus generates power. This is shown in the diagram by the operation arrows between these subsystems. It should be noted that the motor and generator are one single block. This is due to the usage of a motor-generator, a system which is both able to be used as a motor to reel the tether in, and a generator which produces electricity when the tether reels out. The power generated is then transferred to the long term storage, the buffer storage, and the habitat itself. As the buffer storage is used to power most of the different motors used in the AWE system,

electricity transfer lines are drawn between it, the main motor, the landing and launching (L& L) system, and the actuators. Finally, the L&L system is connected to the control tethers, the wing and the tether, as all these parts are influenced during the landing and/or launching phases.

9.1.2. Software

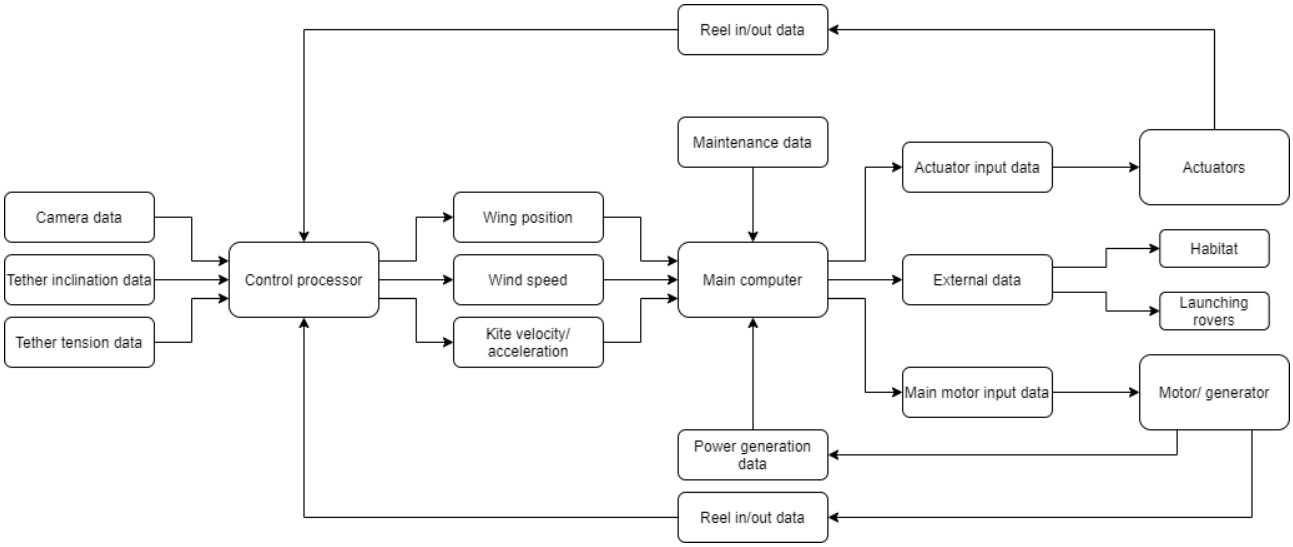

Figure 9.2: Software block diagram

As stated in subsection 9.1.1, the software block diagram shows the transfer of data between the different subsystems in greater detail. First the data from the different sensors is transferred to the control unit processor. This processor uses the sensor data to calculate the different parameters used to control the wing, such as the wing position, wing velocity, wind speed etc. These control parameters are then sent to the main computer, which uses this data to determine how the different motors should be used to control the wing to fly the correct flight path. The main computer, transmits these input data to both the actuators and the main motor. While in operation, the actuators and the main motor sent their respective reel in and reel out data to the control processor, to allow for a more accurate calculation of the different control parameters. Furthermore, the generator also sends data of the amount of power that is being generated to the main computer. This data, along with the maintenance data is processed and then transmitted to the habitat. Finally, during landing and launching, the main computer also needs to send data concerning the wing position, velocity etc. to the rovers used during these two phases.

9.2. Communication Flow Diagram and Block Diagram

PID controllers have been used in Williams et al. [27] and Fechner [28]. Williams et al. [27] developed a unified kite-winch controller based on the rate of change of the angle of attack, roll angle, and tether length to control the position and trajectory of the wing. The simulations included steady and unsteady wind conditions, showing good control of the three desired parameters, yet no consideration for non-linear behaviour is taken and, practically speaking, precise measures of the rate of change of the angle of attack are difficult to obtain[13]. Fechner [28] proposes a PID controller with nonlinear dynamic inversion (NDI), controlling only the heading angle as depicted in Figure 9.3.

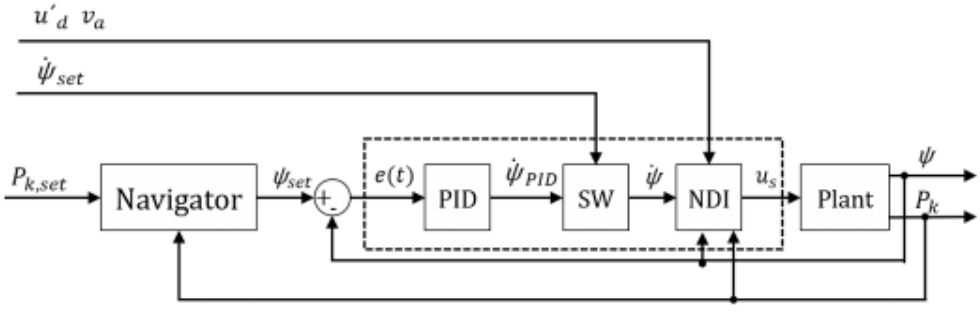

Figure 9.3: Control Block Diagram

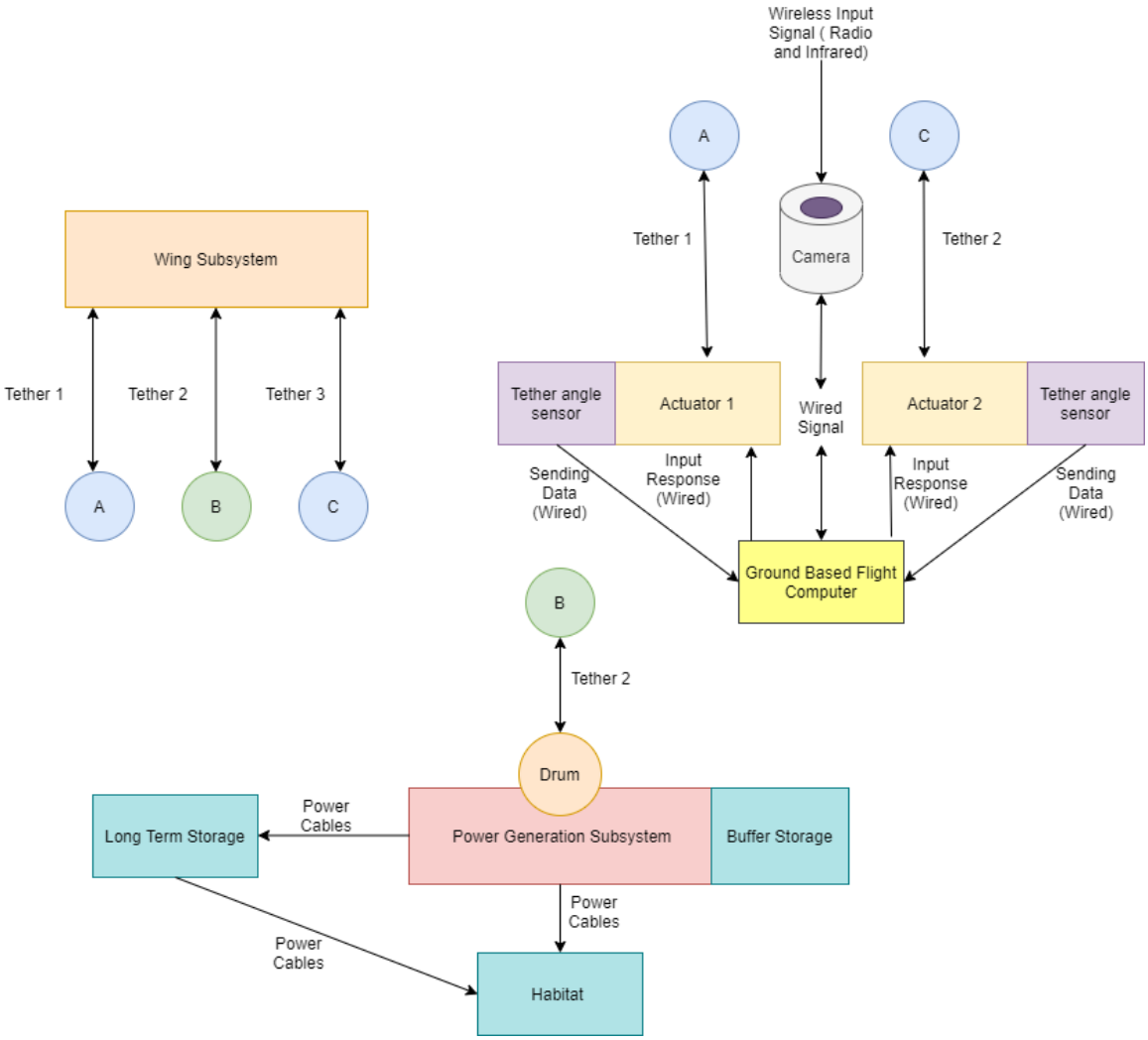

Figure 9.4: Communication block diagram

The communication flow diagram shown in Figure 9.4 shows the flow of information between subsystems and internal components. The direction, medium of transmission and content of each transmitter-receiver pair will be further elaborated upon in this subsection. The entire system can be divided into two categories:

- **Airborne Units:** Consists of all the subsystems present airborne during normal operations. This includes the wing and tether subsystems. Although the airborne unit has no electrical component on-board, the tether acts as a physical medium between the wing subsystem and the control unit and power generation subsystems. The control unit only exerts its influence on the control tethers and vice versa, whereas the main tether only exerts its influence on the power generation unit and vice versa. The airborne units operate mostly during the reeling-in and reeling-out phases of the mission. During the reel-out phase, the lift generated by the wing subsystem creates tension in the tether. This tension produces a torque to generate electrical energy. During the reel-in phase, the buffer storage unit provides the required energy to wind the tether back to its original position.
- **Ground-based Units:** Consists of all subsystems present on the Martian surface during normal operations. This includes the Control Unit, Power Generation, Buffer Storage, Long Term Storage and Power Distribution subsystems. The control unit consists of all the sensors, actuators and computers used to pilot the wing. The sensors used for control are the camera, tether angle sensor and wind speed sensor. The camera in always pointed towards the wing to determine its position and velocity. The tether angle sensor is also used to verify the camera's recordings and report anomalies. The wind speed can be computer by the camera, however, an additional wind speed sensor is place on the ground station to know the direction and strength of the wind at any instance in time.

9.3. Data Handling

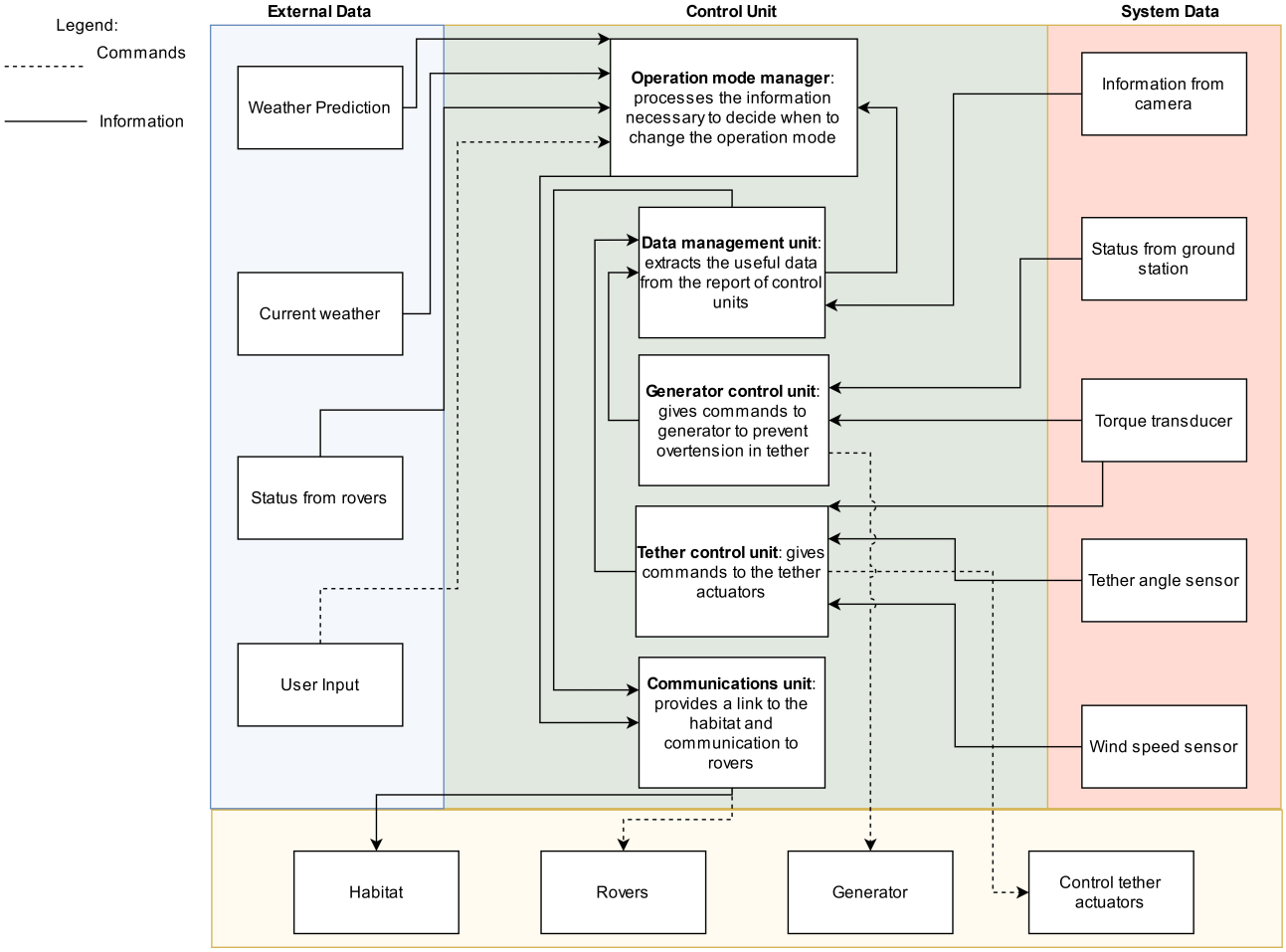

Figure 9.5: Data handling diagram

Figure Figure 9.5 shows how the inputs and outputs of the control system with two main decision algorithms that the control unit runs.

The Command Unit models the state of the system and gives commands to different parts of it constantly throughout the airborne part of operation. It needs to have the moment-to-moment data from the sensors in order to take correct decisions about the next inputs to the system.

The different part of the system receive commands from their own command unit, since this helps to process the information faster. There is a special unit dedicated to control of the tethers in order to steer the system and a special unit to control the generator. Each sub-unit receives information from the relevant sensors. The Communications unit provides for a downlink to the habitat and gives commands to the rovers if the system transitions to a different state in launching or landing. The data management unit extracts the most useful data and sends it to the operation mode manager and to the communications unit whenever required.

10

Risk Assessment

To minimise the failures and required maintenance of the system, a risk assessment was executed. The first step is to set up a scale to quantify the risk scores and to decompose and identify the system components which was done in section 10.1. Next, a Failure Mode Effects & Cause Analysis (FMECA) was done to determine how and why a component fails and what the consequences are in subsection 10.1.1, these risks are then quantified using the scaling set up before. Additionally, a risk mitigation strategy was created to reduce the likelihoods and impacts of the risks in section 10.2. Finally, all risks were plotted according to their frequency and severity scores in section 10.3.

10.1. Risk Quantification & System Identification

In Table 10.1 the risk categories are quantified. The risk consists of 2 elements, a frequency score and a severity score, where frequency indicates the likelihood or time to failure and severity indicates the consequence of a failure, the final risk score is the product of these 2 scores. It has to be noted that a logarithmic scale was used to differentiate the categories.

Table 10.1: Frequency and risk categories, in logarithmic manner.

Category	**Score**	**Frequency**	**Severity**			
			Safety	**Cost, €**	**Power loss, %**	**Downtime**
Very high	5	Less than 3 days	Multiple fatalities	10 - 100 M	95 - 100	1 year - permanently
High	4	3 days - month	Single fatality	1 - 10 M	85 - 95	Month - year
Moderate	3	Month - 1 year	Serious injuries	100k - 1 M	60 - 85	Week - month
Low	2	1 - 10 years	Lost time incident	10k - 100k	40 - 60	12 hours - week
Very low	1	10 - 100 years	Unsafe situation	1k - 10k	0 - 40	0 - 12 hours

The power loss and downtime are combined into a single severity score called energy lost, this score is calculated in the following way: multiply the power lost score by the downtime score, then divide this number by 5 to scale the number to 5 again, this was done because the impact of both of these categories depend on the other. The final severity is the score of the highest category, so if a failure mode has a score for safety of 3 and a score for cost of 4, then the severity score chosen will be 4. This is due to the logarithmic scale, which means that the 4 will be 10x worse than a score of a 3 and will thus be negligible in comparison. If 2 scores are the same then it might be better to give it a score of 1 higher, if the scores are on the high end of their respective range. Finally the frequency and severity are used to plot the risk map in section 10.3. In Table 10.2 the systems, subsystems and their components and elements are identified, these are used in the following section to determine the failure modes.

Table 10.2: System decomposition & identification

System decomposition				
System	**Subsystem**	**Component**	**Element**	**Identifier**
Airborne system	Kite	Membrane	-	1.1.1
	Kite	Structure	Ribs	1.1.2.1
	Kite	Structure	Wingbox	1.1.2.2
	Tether subsystem	Tether	-	1.2.1
	Tether subsystem	Attachment point to kite	-	1.2.2
Ground station	Mechanical connection	Drum	-	2.1.1
	Mechanical connection	Direct drive shaft	-	2.1.2
	Power generation	Generator	Alternator	2.2.1.1
	Power generation	Generator	Lubrication system	2.2.1.2
	Power generation	Generator	Cooling/exhaust	2.2.1.3
	Structure	Anchoring	Frame	2.3.1.1
	Structure	Anchoring	Bearing	2.3.1.2
	Structure	Kite mast	Beam	2.3.2.1
	Structure	Kite mast	Tension lines	2.3.2.2
Control system	Control computer	-	-	3.1
	Actuators	Bridle lines	-	3.2.1
	Actuators	Control motor	-	3.2.2
	Sensors	Force sensors	-	3.3.1
	Sensors	Cameras	-	3.3.2
	Sensors	Angle sensors (Tether angle)	-	3.3.3
Electrical system	Buffer storage	Super capacitors	-	4.1
	Grid connection	Cabling	-	4.2.1
	Grid connection	Transformer	-	4.2.2
Mission operations	Production	On-Earth production	Part manufacturing	5.1.1.1
	Production	On-Earth production	Assembly	5.1.1.2
	Production	On-Mars production	-	5.1.2
	Transport	Launcher take-off from Earth	-	5.2.1
	Transport	Landing on Mars	-	5.2.2
	Installation	-	-	5.3
	Operation	Kite take-off	Rover	5.4.1.1
	Operation	Kite take-off	Winch launch	5.4.1.2
	Operation	Kite landing	-	5.4.2
	End-of-life operations	-	-	5.5

10.1.1. Failure Modes Effect & Cause Analysis

In Figure 10.1,10.2 and 10.3 the FMECA of the different systems can be seen using the identifiers defined in section 10.1, the a and b relate to different outcomes or failure modes for certain component or element.

Airborne System

For the airborne systems it can be seen that the most critical risks involve as final effect the kite falling to the ground, this risk is so big due to the high loading on the wing and big impact of the risk. If the kite were to fall to the ground it would not be able to produce any power until the kite is either repaired or replaced, impact of the kite could seriously injure someone or even be fatal while cost could be enormous.

Ground Station

For the ground station the biggest risks involve the generator. The most critical risk is damage to the alternator which is most commonly caused by erosion due to ball bearings inside the generator. The alternator is a very expensive part of the generator and a damaged alternator will not be able to produce power and can pose a potential hazard to the person performing maintenance.

Control System

The most critical risk regarding the control system are the control computer, control lines and the control actuators. The hardware faults in the control computer are especially hard to repair causing a long downtime. The risks regarding the control lines and actuators can make the kite uncontrollable. This creates a safety hazard and if the kite crashes can create a long downtime and high power loss.

Electrical System

The electrical system risks relate to the short term storage and the electrical cabling. The short term storage can be prone to failure due to fault currents or extreme temperatures. If the short term storage loses too much functionality it might not be possible to reel-in anymore, making it impossible for the system to generate power. If cabling is damaged, due to fault currents or erosion, it might not be possible to transfer electricity to the actuators, storage or the electrical grid.

Mission Operation

Finally, the risks regarding the mission operation are presented in Figure 10.3. The biggest risks are faults in assembly and risk relating to the installation and operation of the system. If faults in assembly are not found before final assembly of the system on Mars, this can lead to damage to the system, reduced power output or the system not working at all. During operation the faults can happen during take-off of the kite, if the rovers are not able to hold the kite or release it prematurely, then the kite might not be able to get enough velocity and fall to the ground, damaging the system.

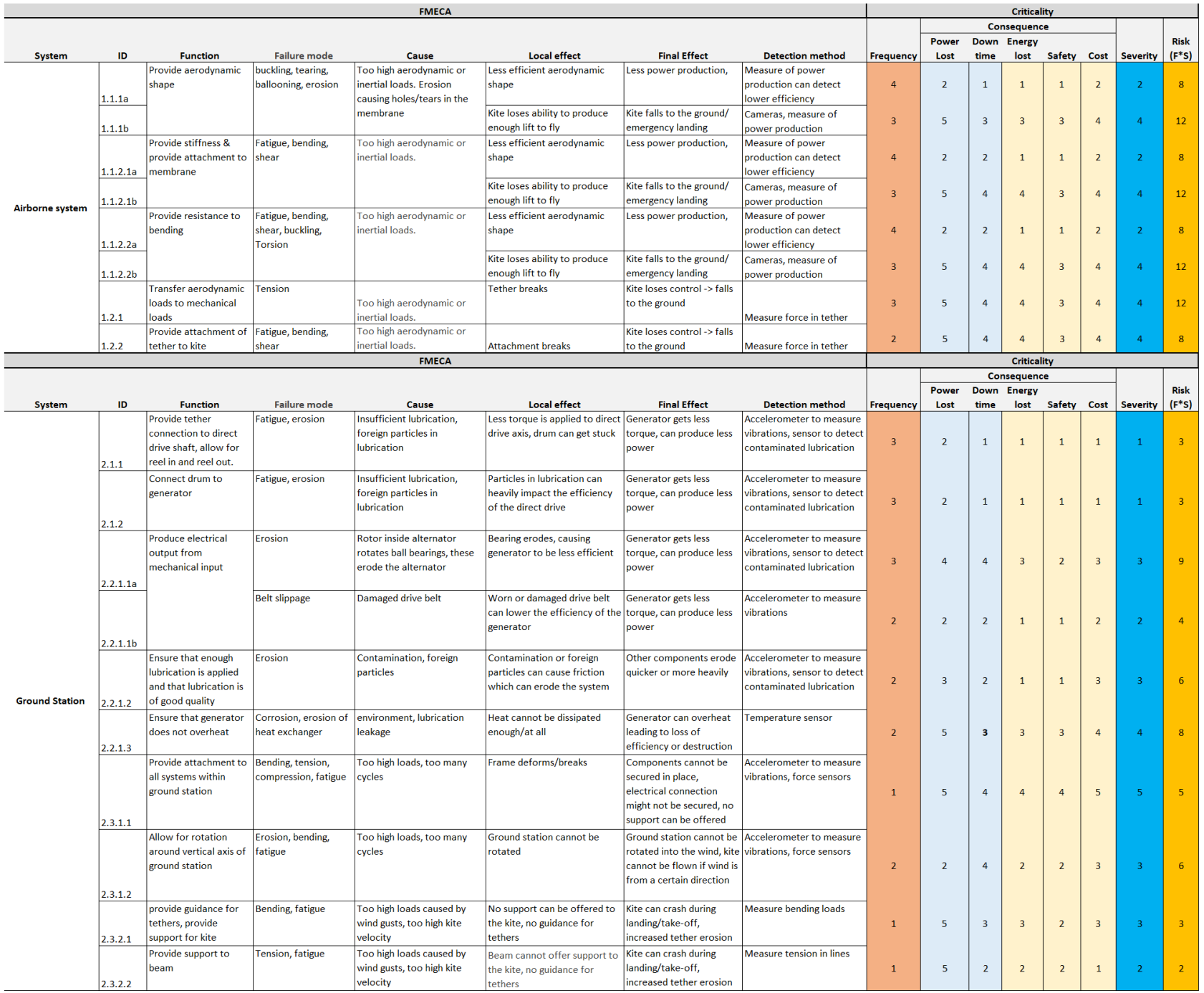

FMECA								Criticality							
									Consequence						
System	ID	Function	Failure mode	Cause	Local effect	Final Effect	Detection method	Frequency	Power Lost	Down time	Energy lost	Safety	Cost	Severity	Risk (F*S)
Airborne system	1.1.1a	Provide aerodynamic shape	buckling, tearing, ballooning, erosion	Too high aerodynamic or inertial loads. Erosion causing holes/tears in the membrane	Less efficient aerodynamic shape	Less power production,	Measure of power production can detect lower efficiency	4	2	1	1	1	2	2	8
	1.1.1b				Kite loses ability to produce enough lift to fly	Kite falls to the ground/ emergency landing	Cameras, measure of power production	3	5	3	3	3	4	4	12
	1.1.2.1a	Provide stiffness & provide attachment to membrane	Fatigue, bending, shear	Too high aerodynamic or inertial loads.	Less efficient aerodynamic shape	Less power production,	Measure of power production can detect lower efficiency	4	2	2	1	1	2	2	8
	1.1.2.1b				Kite loses ability to produce enough lift to fly	Kite falls to the ground/ emergency landing	Cameras, measure of power production	3	5	4	4	3	4	4	12
	1.1.2.2a	Provide resistance to bending	Fatigue, bending, shear, buckling, Torsion	Too high aerodynamic or inertial loads.	Less efficient aerodynamic shape	Less power production,	Measure of power production can detect lower efficiency	4	2	2	1	1	2	2	8
	1.1.2.2b				Kite loses ability to produce enough lift to fly	Kite falls to the ground/ emergency landing	Cameras, measure of power production	3	5	4	4	3	4	4	12
	1.2.1	Transfer aerodynamic loads to mechanical loads	Tension	Too high aerodynamic or inertial loads.	Tether breaks	Kite loses control -> falls to the ground	Measure force in tether	3	5	4	4	3	4	4	12
	1.2.2	Provide attachment of tether to kite	Fatigue, bending, shear	Too high aerodynamic or inertial loads.	Attachment breaks	Kite loses control -> falls to the ground	Measure force in tether	2	5	4	4	3	4	4	8

FMECA								Criticality							
									Consequence						
System	ID	Function	Failure mode	Cause	Local effect	Final Effect	Detection method	Frequency	Power Lost	Down time	Energy lost	Safety	Cost	Severity	Risk (F*S)
Ground Station	2.1.1	Provide tether connection to direct drive shaft, allow for reel in and reel out.	Fatigue, erosion	Insufficient lubrication, foreign particles in lubrication	Less torque is applied to direct drive axis, drum can get stuck	Generator gets less torque, can produce less power	Accelerometer to measure vibrations, sensor to detect contaminated lubrication	3	2	1	1	1	1	1	3
	2.1.2	Connect drum to generator	Fatigue, erosion	Insufficient lubrication, foreign particles in lubrication	Particles in lubrication can heavily impact the efficiency of the direct drive	Generator gets less torque, can produce less power	Accelerometer to measure vibrations, sensor to detect contaminated lubrication	3	2	1	1	1	1	1	3
	2.2.1.1a	Produce electrical output from mechanical input	Erosion	Rotor inside alternator rotates ball bearings, these erode the alternator	Bearing erodes, causing generator to be less efficient	Generator gets less torque, can produce less power	Accelerometer to measure vibrations, sensor to detect contaminated lubrication	3	4	4	3	2	3	3	9
	2.2.1.1b		Belt slippage	Damaged drive belt	Worn or damaged drive belt can lower the efficiency of the generator	Generator gets less torque, can produce less power	Accelerometer to measure vibrations	2	2	2	1	1	2	2	4
	2.2.1.2	Ensure that enough lubrication is applied and that lubrication is of good quality	Erosion	Contamination, foreign particles	Contamination or foreign particles can cause friction which can erode the system	Other components erode quicker or more heavily	Accelerometer to measure vibrations, sensor to detect contaminated lubrication	2	3	2	1	1	3	3	6
	2.2.1.3	Ensure that generator does not overheat	Corrosion, erosion of heat exchanger	environment, lubrication leakage	Heat cannot be dissipated enough/at all	Generator can overheat leading to loss of efficiency or destruction	Temperature sensor	2	5	**3**	3	3	4	4	8
	2.3.1.1	Provide attachment to all systems within ground station	Bending, tension, compression, fatigue	Too high loads, too many cycles	Frame deforms/breaks	Components cannot be secured in place, electrical connection might not be secured, no support can be offered	Accelerometer to measure vibrations, force sensors	1	5	4	4	4	5	5	5
	2.3.1.2	Allow for rotation around vertical axis of ground station	Erosion, bending, fatigue	Too high loads, too many cycles	Ground station cannot be rotated	Ground station cannot be rotated into the wind, kite cannot be flown if wind is from a certain direction	Accelerometer to measure vibrations, force sensors	2	2	4	2	2	3	3	6
	2.3.2.1	provide guidance for tethers, provide support for kite	Bending, fatigue	Too high loads caused by wind gusts, too high kite velocity	No support can be offered to the kite, no guidance for tethers	Kite can crash during landing/take-off, increased tether erosion	Measure bending loads	1	5	3	3	2	3	3	3
	2.3.2.2	Provide support to beam	Tension, fatigue	Too high loads caused by wind gusts, too high kite velocity	Beam cannot offer support to the kite, no guidance for tethers	Kite can crash during landing/take-off, increased tether erosion	Measure tension in lines	1	5	2	2	2	1	2	2

Figure 10.1: Airborne subsystem and ground station FMECA

FMECA								Criticality							
									Consequence						
System	ID	Function	Failure mode	Cause	Local effect	Final Effect	Detection method	Frequency	Power Lost	Down time	Energy lost	Safety	Cost	Severity	Risk (F*S)
Control System	3.1a	Calculate kite position, heading and velocity and correct actuation plan	Hardware faults	Inherent defects in manufactured items.	Reduced or no functionality of computer	Wrong or no calculation of kite pos/speed	Only detectable/solvable before launch from Earth	2	5	4	4	2	4	4	8
	3.1b		Software faults	Inherent defects in the software programming.	Non-functioning of calculation scheme	Wrong determination of kite pos/speed	Verification of the software during maintenance	3	4	1	1	2	1	2	6
	3.1.c		Systematic faults	Personnel error, environmental conditions and design faults	Non resolved problems in hardware/software or too extreme temperature to operate	Not operational for some period	Clear checklist for maintenance and a temperature range for during operations.	2	5	2	2	1	2	2	4
	3.2.1	Allow indirect actuation from the ground by the control	Tension, fatigue	Overloading or too many cycles	One or both bridles break	Wing becomes uncontrollable and crashes	Force sensing and staying well below the maximum amount of cycles	2	5	2	2	4	4	4	8
	3.2.2a	Pulls on bridles to indirectly actuate the wing from the ground	Over loading	Excessive load or phase unbalance	Burn out of one or more coils	Motor no longer functional	Visual inspection of coils	2	5	2	2	4	3	4	8
	3.2.2b		Over cycling	On/off cycling continues at max operating temperature	Destroys insulation of the coils, shorting the windings	Motor no longer functional	Heat monitoring	2	5	2	2	4	3	4	8
	3.3.1	Sense the forces applied on the tether and bridles	Software faults	Defect in the software	Incorrect or no current-to-torque calculation	Burn out the generator/applying too little force to tether or bridles	Health monitoring checks	2	5	1	1	2	3	3	6
	3.3.2a	Tracking of the position of the kite	Parts/assemblies damaged	Dust erosion	Decreases the lifetime	Camera might not operate the whole project life cycle	Health monitoring checks	1	1	3	1	1	2	2	2
	3.3.2b		Camera vision blocked	Dust storm/dust accumulation	No clear vision of the wing	Incorrect to no tracking of the wing position/velocity	Detection through decreased camera vision	3	1	1	1	2	1	2	6
	3.3.2c		Deviation of pointing direction	Vibrations of attachment point	Not the whole operational area is visible	No tracking possible for some areas	Inspection of video footage	2	1	1	1	2	1	2	4
	3.3.3	Measuring the angle of the tether with the horizontal and vertical	Parts damaged	Fatigue	Doesn't measure the angle correctly	No determination of kite position with this method	Inspect by testing the functionality directly	1	1	3	1	1	2	2	2

FMECA								Criticality							
									Consequence						
System	ID	Function	Failure mode	Cause	Local effect	Final Effect	Detection method	Frequency	Power Lost	Down time	Energy lost	Safety	Cost	Severity	Risk (F*S)
Electrical system	4.1	Provide the system with power for reel in and actuator activation	Fatigue, electrical failure	Too many cycles of charging, fault current	No power can be provided to actuators or reel in of kite	Loss of power production	Measure power provided	3	4	3	2	3	2	3	9
	4.2.1	Provide power from a storage facility or production facility to other systems	Electrical failure, erosion	Erosion of the wiring due to wind/environment, frequent fault currents	No power can be delivered to other systems or habitat	No power delivered to habitat	Measure voltage, current and resistances	3	3	2	1	3	1	3	9
	4.2.2	Transform power from one voltage and current to another.	Electrical failure, erosion	Electrical failure can be caused by the breakdown of the insulation due to thermal degradation. This can be caused by exceeding lifetime or frequent fault currents	Power cannot be transformed to correct voltages & currents.	Correct power cannot be delivered to other systems, this can damage them or they can't function	Measure voltage, current and resistances	2	3	3	2	3	1	3	6

Figure 10.2: Electrical system and control system FMECA

FMECA								Criticality							
									Consequence						
System	ID	Function	Failure mode	Cause	Local effect	Final Effect	Detection method	Frequency	Power	Down	Energy	Safety	Cost	Severity	Risk (F*S)
Mission Operation	5.1.1	Produce components	Defective part	Bad quality control, inconsistent manufacturing quality, defective machine, human error	Part does not carry out effectively its intended purpose	Defective part leads to the malfunctioning of its corresponding subsystem	Quality control during the production cycle and at the end	3	1	2	1	1	3	3	9
	5.1.1.2a	Assemble as much as possible on earth for further simple assembly on Mars	Badly assembled assembly	Human error, defective part	Assembly is faulty	Leads to extended setup time on Mars	Quality control during the assembly cycle and at the end	2	2	3	1	1	3	3	6
	5.1.1.2b					Useless assembly on Mars		1	5	4	4	3	4	4	4
	5.1.2	Produce necessary parts on Mars	Defective part	Bad quality control, inconsistent manufacturing quality, defective machine, human error	Part does not carry out effectively its intended purpose	Defective part leads to the malfunctioning of its corresponding subsystem	Quality control during the production cycle and at the end	3	1	2	1	1	3	3	9
	5.2.1	Take-off from Earth	Parts/assemblies damaged	Loads during take-off	Damaged assemblies/parts do not carry out intended purpose	Defective part/assembly leads to the malfunctioning of its corresponding subsystem	Secure payload attachment	2	2	2	1	1	3	3	6
	5.2.2	Landing payload on Mars	Parts/assemblies damaged	Loads during landing	Damaged assemblies/parts do not carry out intended purpose	Defective part/assembly leads to the malfunctioning of its corresponding subsystem	Secure payload attachment and pre-launch load tests	2	2	2	1	1	3	3	6
	5.3	Assemble and install the AWES system	Parts/assemblies damaged, badly-installed AWES	Human error, defective part, defective assembly	AWES does not function correctly	Decreased power production/loss of functionality	Quality control during the assembly and at the end	2	2	2	1	1	3	3	6
	5.4.1.1	Rover provides a platform for kite take-	Rover stops working	Age, crashes into object	Rover cant position kite for take-off	Kite can't take off/needs assistance from habitat	Test ride rover	2	4	3	2	1	3	3	6
	5.4.1.2	Launch the kite	Insufficient force provided by reel in	Age, wear-and-tear, faulty assembly/part	Kite does not reach desired velocity	Kite can't take off and falls to the ground	Test reel in mechanism before usage	2	4	3	2	2	3	3	6
	5.4.2	Land the kite safely when wind speeds are too low	Bending, tension, compression, fatigue	Faulty design, manufacturing error, assembly error, age	Landing structure breaks	Kite can't take off and falls to the ground as well as no more launch and lading system. No more empower generation from AWES	Load and deformation sensors in landing structure, routine inspections, manufacturing and assembly quality control	1	5	3	3	2	3	3	3
	5.5	Disposal/reuse/recycle /life extension of AWES	EOL not executed	Human error, wrong estimation of reusability/recyclability/life extension	Excess waste material	Life extension/ not possible/disposal/reuse/recycle	Re-evaluation of EOL plan throughout the lifetime of AWES	2	N/A	N/A	N/A	N/A	3	3	6

Figure 10.3: Mission Operation FMECA

10.2. Risk Mitigation

Now that risks have been identified and their causes and effects presented, a risk mitigation strategy can be made to reduce the likelihood and impact of the risks.

In Figure 10.4 the mitigation strategy for the airborne system can be seen, the main strategy here is to implement a safe mode, this means that the kite will return to a certain altitude and orientation during wind gusts such that the aerodynamic forces on the kite are minimised. Wind gusts of more than 22.8 m/s as determined in 8.4 would result in this situation. On average this would happen less than 1% of the time, but in late autumn this can occur up to 2.5% of the time according to subsection 2.5.3. Furthermore, the kite can be visually inspected once every month to detect holes and tears on the canopy, this can be done during times when the kite cannot fly due to low wind speeds.

Risk mitigation						
System	ID	Risk mitigation strategy	Outcome	New Frequency	New Severity	New Risk
Airborne System	1.1.1a	Safe mode (parking altitude) during wind gusts in order to reduce lift force and loads on kite, visual inspection by rovers to detect holes/tears during launching.	Early detection of holes/tears reduces impact. Limiting the high aerodynamic forces reduces the impact on the structure, thus increasing lifetime	3	2	6
	1.1.1b			2	3	6
	1.1.2.1a			3	2	6
	1.1.2.1b			2	3	6
	1.1.2.2a			3	2	6
	1.1.2.2b			2	3	6
	1.2.1	When the measured force in the tether is too high, the drum "lets go" of the tether for a short duration to reduce tether force	Reducing the frequency & duration of really high forces increases lifetime of tether	2	3	6
	1.2.2			1	4	4

Figure 10.4: Airborne System Risk Mitigation

In Figure 10.5 the mitigation strategy for the ground station is presented. This strategy mostly focuses on early detection of failures with the sensing of vibrations of the ground station and components and the sensing of contamination of lubricants. This mostly reduces the frequency or likelihood of a failure because the failure is caught before it can inflict significant damage.

Risk mitigation						
System	ID	Risk mitigation strategy	Outcome	New Frequency	New Severity	New Risk
Ground Station	2.1.1	When vibrations increase to an excessive amount, contaminated lubrication can be removed and new lubrication can be applied.	Lower frequency of failure, parts erode slower	2	1	2
	2.1.2			2	1	2
	2.2.1.1a			2	3	6
	2.2.1.1b	Accept risk	-	2	2	4
	2.2.1.2	Measure contaminants and particles in lubrication to determine faults.	Contaminants can be detected before they can pose a hazard to other systems, thus decreasing frequency.	1	3	3
	2.2.1.3	Shield heat exchanger from environment and lubrication leakage	Prevents the erosion/corrosion of heat exchanger	1	3	3
	2.3.1.1	Perform monthly checks on structure to ensure no cracks are forming, that structure can still perform its function	Reduces impact of failure	1	4	4
	2.3.1.2	Install shielding to prevent dust & debris from getting into the bearing, perform monthly check to prevent damage from accumulating	Failure is caught in the early stages of development, frequency decreased	1	3	3
	2.3.2.1	Accept risk	-	1	3	3
	2.3.2.2	Accept risk	-	1	2	2

Figure 10.5: Ground Station Risk Mitigation

In Figure 10.6 the mitigation strategy for the control system is presented. A few risks here are accepted because of their low frequency and severity. Others are mitigated by applying safety factors and using multiple sensors to introduce redundancy such that a single failure is not fatal to the system. For harder to detect failures routine inspections are done monthly.

Risk mitigation						
System	ID	Risk mitigation strategy	Outcome	New Frequency	New Severity	New Risk
Control System	3.1a	Failure prediction models, failure detection systems, routine inspections	Early failure detection/pre-failure part replacement	1	4	4
	3.1b	Accept risk	-	3	2	6
	3.1c	Accept risk	-	2	2	4
	3.2.1	Failure prediction models, failure detection systems, routine inspections	Early failure detection/pre-failure part replacement	1	4	4
	3.2.2a	Apply large safety factor on the acceptable force on the motor and check regularly to ensure all coils are in good condition	Lower chance of complete overloading and phase unbalance	1	4	4
	3.2.2b	Design cooling system so that over cycling does not come close to occurring during operations	The chance that over cycling occurs becomes small enough to accept the	1	4	4
	3.3.1	Accept risk	-	2	3	6
	3.3.2a	Accept risk	-	1	2	2
	3.3.2b	Use angle and force sensors as a backup system	System redundancy makes failure acceptable	3	1	3
	3.3.2c	Accept risk	-	2	2	4
	3.3.3	Accept risk	-	1	2	2

Figure 10.6: Control System Risk Mitigation

The electrical system risk mitigation is presented in Figure 10.7, the main strategy is to measure voltage and current outputs to detect any irregularities. Furthermore the cabling is run underground whenever possible to reduce the impact of erosion due to the environment.

Risk mitigation						
System	ID	Risk mitigation strategy	Outcome	New Frequency	New Severity	New Risk
Electrical System	4.1	Measure voltage & current outputs to determine when the supercapacitors are losing efficiency, when efficiency is degraded beyond a certain level, replace supercapacitors.	This will prevent the supercapacitor from burning out beyond the point where no power is left for reel-in.	2	2	4
	4.2.1	Run wiring underground when possible, this will reduce the impact of the wind on erosion, this will also reduce safety impact due to exposed wires. Exposed wires can be inspected to determine damage.	Frequency of failure due to erosion goes down, safety impact goes down, earlier detection leads to replacement before failure happens.	2	2	4
	4.2.2	Measure of voltage & current can indicate when the transformer is degrading, thus indicating that replacement is necessary.	Early replacement decreases impact due to failure	2	2	4

Figure 10.7: Electrical System Risk Mitigation

Finally in Figure 10.8 the risk mitigation strategy for the mission operation is presented. In production the implementation of quality control and non-destructive testing will reduce the likelihood of production and assembly faults. The risks regarding the rover are hard to mitigate since the rovers are already there and are reused after their original life span ended. However, the rovers do not have to perform very difficult or challenging tasks and repair is still possible so this should not pose an unacceptable risk.

Risk mitigation						
System	ID	Risk mitigation strategy	Outcome	New Frequency	New Severity	New Risk
Mission Operation	5.1.1	Quality control and the use of non-destructive testing	Early defective part detection and replacement	2	3	6
	5.1.1.2a	Quality control and the use of non-destructive testing	Early detection of defective assembly	1	3	3
	5.1.1.2b	Quality control and the use of non-destructive testing	Early detection of defective assembly	1	2	2
	5.1.2	Quality control and the use of non-destructive testing	Early defective part detection and replacement	2	3	6
	5.2.1	Pre-launch tests	Verification of launch load endurance	1	3	3
	5.2.2	Pre-launch tests	Verification of landing load endurance	1	3	3
	5.3	Quality control and the use of non-destructive testing	Early detection of bad assembly	1	3	3
	5.4.1.1	Accept risk	-	2	3	6
	5.4.1.2	Failure prediction models	Know when the launching mechanism needs a repairs/inspection	2	2	4
	5.4.2	Failure prediction models and non-destructive testing	know when the take-off mechanism needs a renovation/inspection and detect failure early on before it becomes more catastrophic	1	2	2
	5.5	Accept risk	-	1	2	2

Figure 10.8: Mission Operation Risk Mitigation

10.3. Risk Map

The risks identified in subsection 10.1.1 and section 10.2 have been plotted in Figure 10.9 according to their respective frequency and severity score.

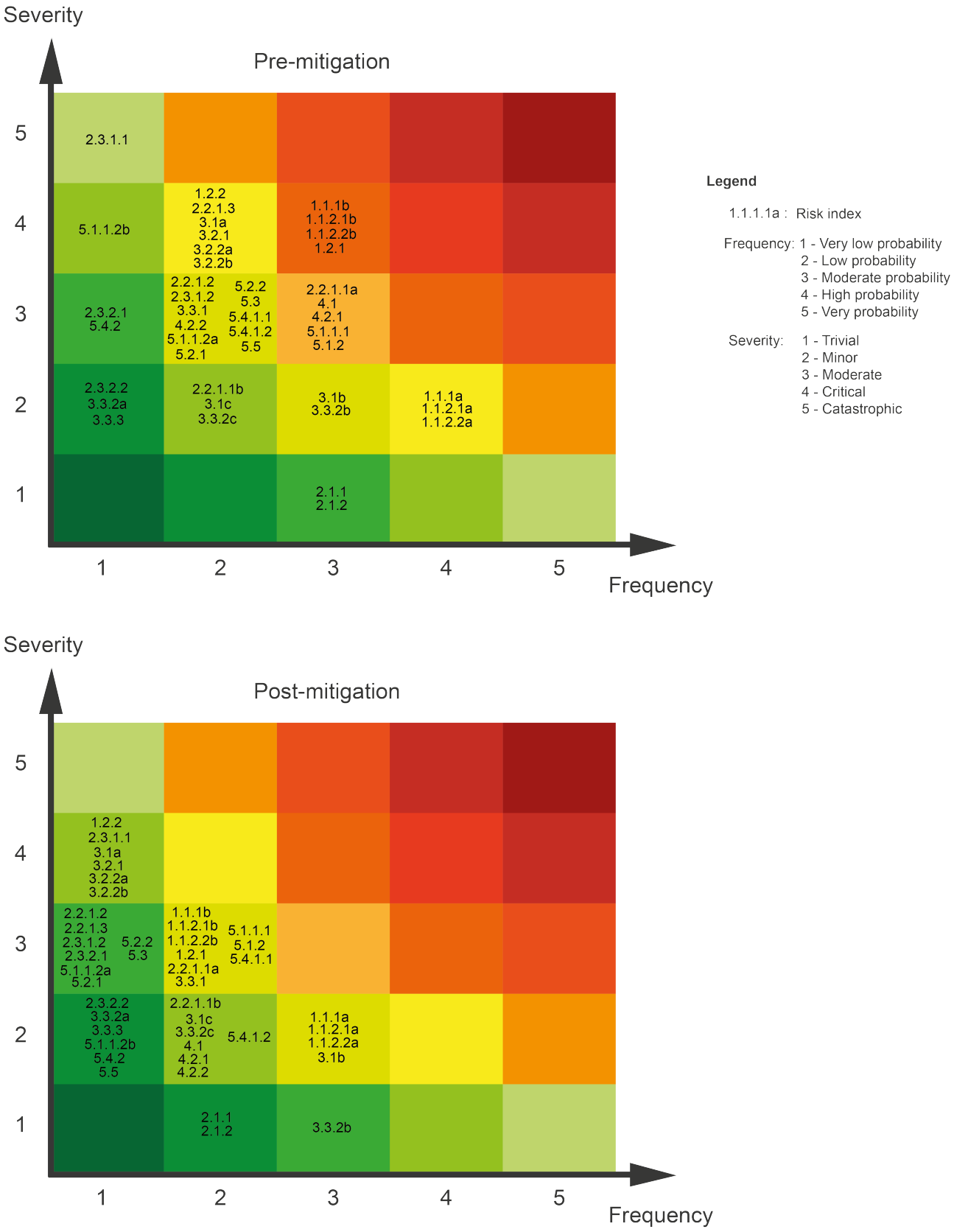

Figure 10.9: Pre- and post mitigation risk maps

11

Verification & Validation

This chapter will present the verification and validation steps taken for AWESOM's system design and performance analysis. First, requirement verification will be performed in section 11.1. Then, the code verification will be presented in section 11.2. The chapter will be concluded with the validation strategy in section 11.3.

11.1. Requirement Verification

In this section, the requirements will be checked for completion and supported with a justification statement. This will be done within a compliance matrix which can be found in Table 11.1.

Table 11.1: Compliance matrix

Requirement	Compliance	Justification
CON-LE-01	Yes	The designed system is within these legal guidelines.
CON-LE-02	Yes	There is no other mission within the knowledge of the design team that AWESOM could interfere with.
CON-CT-01	Yes	The final cost of the preliminary design of AWESOM is 114,195€ which is below 500,000€.
CON-TM-02	Yes	AWESOM's preliminary design was completed by 10 students within 10 weeks.
CON-SF-02	Yes	AWESOM was designed in a way that would not damage its environment during operation.
CON-SF-03	Yes	The system will be placed far enough to comply with this requirement.
CON-SF-04	Yes	The system is autonomous, so there is no need for astronauts to be present around during operation.
CON-DG-01	No	The final mass of the system is 641.41 kg which is above the 200 kg requirement.
CON-DG-03	Partially	Rib design takes into account the repeated loading, but there are still other components which need to be tested on this. The design team expects that all components comply with this requirement.
CON-DG-04		subsection 7.3.8
TEC-AIR-01	Yes	The system can release the tether to reduce the force on it in case of a significant wind gust.
TEC-AIR-07	Yes	The control system is designed to maintain maximum of 12000 N, and the tether is designed to be able to bear this load.
TEC-AIR-08	Yes	The cut-out speed is 22.8 m/s as calculated by the simulation.
TEC-AIR-09	Yes	The system can release the tether to reduce the force on it in case of a significant wind gust.
TEC-AIR-11	Yes	The simulation outputs a minimum wind speed of 4.46 m/s for the wing to stay airborne.
TEC-AIR-12	Partially	Materials properties for temperature ranges of -190 °C to 20°C were not available for all materials considered (c.f. subsection 7.3.9).

TEC-AIR-13	Partially	Only the ribs were checked to comply with this requirement due to insufficient time. However, the ribs were way below the required values, so it is likely that the rest of the structure will withstand those loads as well. The results can be found in subsection 7.3.7
TEC-AIR-14	Yes	The rib spacing distribution has been designed to limit the canopy deflection to 0.01 m (c.f. subsection 7.3.6).
TEC-AIR-15	Yes	The twist computed was found to be 0.08 radians.
TEC-AIR-16	Yes	The deflection computed was found to be 5 cm in total
TEC-CL-05	Unknown	This thermal analysis is not performed yet.
TEC-GE-01	Yes	The generator has an average efficiency of 92.5%.
TEC-GE-02	Yes	The generator can provide a torque of 1100 Nm.
TEC-GE-07	Unknown	This thermal analysis is not performed yet.
TEC-GE-08	Unknown	This has not been analysed yet.
TEC-PS-01	Yes	The storage was sized according to this requirement.
TEC-PS-02	Yes	The simulation outputs sufficient power output.
TEC-PS-09	Unknown	This has not been analysed yet.
TEC-PS-10	Unknown	This has not been analysed yet.

The most alarming requirement compliance is the one regarding the mass budget. The 475.52 kg overshoot of the mass budget is mainly due to the ground station which contributes 518 kg. 250 kg of the ground station mass is as a result of the generator used which needed to be of considerable size due to the high variability of wind as shown in section 2.5. More specifically, in order to generate enough energy to compensate for low wind periods, the generator must be able to output high quantities of power during the very high wind speed periods and still produce some power during low speed seasons. This is independent of the wing design to a certain extent as the generator must be able to produce high levels of power when high wind speeds happen which lead to the high rated power output of the generator of 70 kW which in turn lead to a high mass. The majority of the rest of the weight of the ground station was due to the landing and launching structure. However, in order to launch and land the kite in an automated manner with minimal human aid, such a system was needed. The human intervention of the launch and lading system would costs thousands of euros as each hour of an astronaut is worth very much. Additionally, it would take up hours of their day which they could be dedicating to other important tasks. Other systems such as fully flexible ram air kites would need massive ventilators to inflate the kite or large structures to allow a relative wind velocity for the system to take off, alike the one used here. Hence, regardless of the kite system chosen it is firmly believed that the mass of the ground station would not be significantly altered.

11.2. Code Verification

Verification is an essential step while developing any computational model. This step aims at confirming that the model has been developed correctly, verification thus answers the question 'is the computational model correct?'. To verify the models developed in for this project, their diverse modules will be independently tested through unit tests, and the complete code will be verified through system tests. The unit test are meant to verify sections of a model, while system tests aim at verifying that the individual modules function as a whole.

The various computational models developed were verified in their respective sections. Here follows an overview of the sections were verification was performed:

- Regarding aerodynamic characteristics, the verification performed on the airfoil analysis code is presented in subsection 7.1.5.
- Regarding the structural analysis of the wingbox, the verification of the model developed is performed in subsection 7.3.5.
- The rib spacing model was also verified in subsection 7.3.6.
- The verification of the rib design method was performed in subsection 7.3.7.
- Finally, the verification of the performance model was performed in section 8.3.

11.3. Validation

Besides verification, validation of a computational model is the following important step. In fact, once a model was shown to be implemented correctly through verification, validation shall be perform in order to confirm that the model chosen appropriately represents the system considered. In fact, validation shall answer the question 'is the computational model the right model?'.

Validation can be performed by comparing computational predictions to experimental observations. Due to project constraints, access to experimental results was not achievable. Nevertheless, validation processes were planned for the various models developed. Please find here below an overview of the sections were validation was performed:

- For the structural analysis of the wingbox, the model developed was validated in subsection 7.3.5.
- The rib spacing model was also validated in subsection 7.3.6. As experimental results were not available to fully validate the model, in addition to a presentation of validation tests that could be performed in a later stage of the design, the assumptions made to derive the rib spacing model were also evaluated.
- The validation of the rib design method was performed in subsection 7.3.7.
- Finally, the validation of the performance model was performed in section 8.3.

12

Sustainable Development Strategy

In this chapter, the sustainable strategies chosen during the various phases of the mission are discussed. Sustainable development aims at integrating the economic, social and environmental objectives of society, in order to maximise human well-being in the present without compromising the ability of future generations to meet their needs. This means seeking mutually supportive approaches whenever possible, and making trade-offs where necessary. The pursuit of sustainable development thus requires improving the coherence and complementary of policies across a wide range of sectors, to respond to the complex development challenges ahead[1]. Each section in this chapter will treat one of the three sustainability aspects. section 12.1 will discuss the strategies and methods related to the environmental aspect, followed by section 12.2 regarding the economic aspect. Finally, the social aspect of sustainability will be treated in section 12.3.

As a general remark, please note that for space applications, sustainable approaches might not be achievable. For instance, the use of sustainable materials as defined in subsection 12.1.2 might not be able to achieve performance requirements compared to the conventional aerospace materials. Hence, the sustainable approaches, methods and strategies discussed in this chapter are mainly guidelines for this project instead of hard requirement on the design.

12.1. Environmental Aspect

For a sustainable design, both the materials used and the manufacturing processes employed should adhere to the sustainable philosophy as much as possible. In this section, the environmental dimension of sustainability will be treated for both begin-of-life and end-of-life of the system. In subsection 12.1.1 and 12.1.2 the production methods and materials to be used will be considered, followed by the end-of-life strategies in subsection 12.1.4.

12.1.1. Sustainable Production Methods

As sustainable production methods, this project will aim at applying the lean philosophy. In fact, the lean philosophy is not a method, rather a way of thinking in which the focus is set on eliminating the waste in a process. This philosophy is therefore interesting to be applied in the context of sustainable production and manufacturing. Lean production and manufacturing refer to the use of systematic methods to reduce costs by eliminating waste and non value-adding activities, while delivering customer-focused products, on time. Without explicitly targeting environmental outcomes, namely by reducing material waste, lean efforts can yield substantial environmental benefits [29].

Prior to selecting appropriate lean methods, it is important to note that several forms of waste can be identified in the lean methodology. Among the most relevant to this project, one can identify the following waste creating activities [29]:

- **Waiting time:** Delays are important consideration for space technologies, specifically for missions to another planet, such as Mars, as launch windows might not allow much delay. Hence, waiting time in the design and production process shall be properly planned for. Other important approaches to limit waiting time, thus delays, is through the use of proper workload and efficient manufacturing techniques.
- **Transportation and movement:** As the lean methodology aims at optimizing value creating activities, transportation of all kind (i.e. of parts, personnel or machines) shall be limited as this is not creating any value. Recommendations to avoid waste of this kind is through proper manufacturing facility layout, thorough understanding and planning of process flow, and consistent working methods.
- **Rework:** Rework is the extra work done because the first time a defective product was made [29]. Space technologies often have very little room for error during operation. Even the qualification models need to be built without any significant error as they can cause a huge amount of waste if the test ends up useless and needs to be repeated. The Martian AWE system is no exception in these regards. Through the use of scarce materials and expensive production processes, extra work is required on a system because the defects and inaccuracy are to be avoided. Methods to avoid rework is through process monitoring,

[1] https://www.oecd.org/dac/environment-development/1899857.pdf [Accessed on April 20, 2021]

quality control, appropriate training and equipment, as well as preventive design against the occurrence of defects.

Lean manufacturing has a multitude of approaches that can be applied depending on the project conducted. From the previous recommendation on how to limit waste production, several methods can still be identified in order to adopt a lean philosophy in the production process. Production planning is for instance an important method. This involves identifying all the production methods for each component used in the system. Apart from this, it also identifies the cost per unit time, total processing time taken, level of sustainability, and types of production methods. Secondly, transportation on Earth between different suppliers and manufacturers has to be optimised so as to save the energy and reduce the impact on climate and minimise other types of pollution associated with transportation. Finally, maintenance stages have to be appropriately planned for. Maintenance phase of the mission involves inspection of the entire system and its sub-systems. These inspections are done to check for any local buckling/failure that has occurred in the structure. The frequency of the maintenance cycles have to be calculated to prevent unnecessary interruptions.

12.1.2. Sustainable Materials

Sustainable materials can take multiple definitions. From literature, certain key characteristics of sustainable materials can be identified. From [30, 20], sustainable materials:

- shall be abundant or rapidly renewable materials;
- shall be chemically safe;
- shall have recycling, as well as reusability potential;
- shall not use resource-intensive production methods.

The characteristic about reusability and recycling potential of sustainable materials is treated in subsection 12.1.4. Furthermore, the production methods were treated here above in subsection 12.1.1. The remaining two characteristics of sustainable materials are detailed here after, namely on how those can be incorporated into the design of a Martian airborne wind energy system.

Regarding the use of abundant or rapidly renewable materials, in-situ resources and the access to additive manufacturing from regolith within the Rhizome project is an important consideration. In fact, using Martian soil as building block to create structure for the AWE system might have several benefits. This possibility will be investigated in further detail in a later stage of the project, but this technology was envisioned to be used in shielding or other secondary structure of the AWE system. Indeed, the use of in-situ materials, being abundant resources might help in limiting the use of scarce materials from Earth and in reducing the amount of mass to be transported to the Martian habitat. These are indeed important improvements towards a more sustainable design.

The second characteristic of sustainable materials as defined here above is that they shall be chemically safe. Several techniques and methods can be used to assess materials health. For this project, the chemical database of *Pharos Chemicals* can be used [2]. From this database, chemicals can be compared based on their health and hazardousness using different scores (e.g. regarding carcinogenicity, corrosivity, physical reactivity or flammability). Besides, this database gives *GreenScreen* hazard rating[3], providing a score on a scale of one to four based on the various hazard categories listed previously. Please note that the use of non-toxic materials and chemicals is coupled to the third aspect of sustainability, namely the social aspect discussed in section 12.3, since the production and operation of the system shall not harm anyone, non-toxic materials are preferred.

To help in sustainable material selection, resource cataloging shall be used. Through resource cataloging, a database of materials is created containing the cost, availability, GreenScreen scores, and usage of every component used in the mission. This is done to ensure a thorough overview of the resources used is documented and the sustainable options are considered.

12.1.3. Sustainability on Mars

Sustainability on Mars can not be approached in the same manner as on Earth as the resources available differ, the impact on the environment also differs and consequently a different analysis is needed of what it actually means to be sustainable on Mars.

Firstly, the resource used for energy production as mentioned before is the wind, this aspect is sustainable as the wind resources infinite and will always provide power. The only resource currently planned to be used and

[2] https://pharosproject.net/ [Accessed on May 17, 2021]

[3] https://www.greenscreenchemicals.org/ [Accessed on May 18, 2021]

obtained from Mars is regolith and the usage is very low and hence can be deemed sustainable especially as there is an abundance of regolith on Mars in comparison to how much would be used.

An aspect that can be regarded as non-sustainable is waste disposal of the components after they have been used for their intended purpose at the end of life or if they break and need replacement. On earth, processes such as recycling would be used in order to make use of the waste material generated by the system. However, every hour of an astronaut and every kilo of equipment brought to Mars costs vasts amount of money and for such a high risk and cost mission is not a priority and is basically impossible as recycling equipment is terribly heavy and requires huge amounts of energy not available from the energy generation system. This lack of infrastructure makes the usage of recycling virtually impossible without sending old or broken components back to Earth to recycle, which creates more damage to environment and costs than recycling would ever bring in. Hence, it is safe to say the current sustainability plan is as good as it can get in the Martian context without sabotaging the economic viability of the project.

12.1.4. End-of-Life Strategy

Sustainable methodologies consider full product life cycles, from begin-of-life to end-of-life. Sustainable product design aims at changing the traditional linear economy to a circular one. Linear economy, often referred to as the make-use-dispose consumption approach is in contrast with the circular approach where a product is used as long as possible and life extension methods are designed for at the end-of-life. The circular philosophy relies on the reduce-reuse-recycle approach. In this design project, waste will be reduced during production as discussed in subsection 12.1.1, and the system will be designed to be reused and recycled at end-of-life. Strategies to do so is discussed in this section.

Regarding reusability, several components of the AWE system could be reused. For instance, the motor and drums could find other applications for the Martian habitat, namely for new power system or to drive some vehicle. Other structural elements of the ground station could find application as construction material for new generation AWE system, or within the Mars habitat. Reusability of other components (e.g. gearbox else recycle, control unit, supercapacitors, spindle, long term storage in most forms should also be reuseable.) could also be considered, depending on wear, else recycling would be considered.

Next to reusing components at end-of-life, one last option before discarding components would be to recycle them. Recycling the materials of the tether for instance could be used to produce other parts, possibly to produce new composites. Besides, the kite membrane and its structure could also be re-purposed.

Please note that further detailed analysis of end-of-life strategies will be possible once a material database is documented. Further investigation will then be needed to specify which component shall be recycled, or preferably reused. It is also important to keep track of the lifetime of all components in the system and update the information on recycling and environmental impact of production as the information comes in. This will help the team to make sure that the target for the environmental aspect of sustainability is met.

12.2. Economic Aspect

The market analysis performed in the Baseline Report highlighted that this project opens new perspective for both space exploration and for the renewable energy sector. Furthermore, the market analysis showed that there are currently no direct competitors on the market for an airborne wind energy system on Mars [10]. Therefore a successful design would likely be relevant for the coming years. Even when this is not the case, the acquired knowledge on the topic and the publicity gained from being the first to achieve this will make this project team interesting for future investors and recruiters.

Furthermore, research and development in the aerospace industry often lead to improvement in quality of life on Earth [31]. In fact, space exploration has benefited life on Earth in several sectors such as health, education, communication, but also Earth monitoring, and many more. Hence, research and development performed on the airborne wind energy system on Mars shall surely benefit other fields, possibly improving wind energy production back on Earth. Regarding AWE systems the project will, as it is designed for Mars, improve knowledge on application in extreme operating conditions. Another advantage for the AWE sector in general will be the hype that is created when the system shows to perform as expected, combined with the trust in the concept from the fact that it even works on Mars. The main sustainability benefit in other areas is the fact that the project brings the human race closer to being a multi-planet species, which could potentially save us from extinction.

12.3. Social Aspect

The social aspect of sustainability shall consider the impact of the design on the stakeholders, namely any party affecting or affected by the airborne wind energy system. The following topics related to social sustainability

were identified:

- **Materials sourcing:** All the resources shall be supplied ethically. Documentation on every product type has to be created stating where it is sourced and how it affects the people that live in the areas involved with production of the system. This point can also be linked to the materials health assessment discussed in subsection 12.1.2 as chemically hazardous materials shall be avoided in a sustainable design. However, it must also be considered that sometimes the companies where off-the-shelf products are purchased from are not transparent regarding their production processes. This introduces a limitation on the confidence of AWESOM in ethical material sourcing.
- **Legislation:** Regarding the project design, compliance with space legislation shall be constantly monitored for the fulfilment of the mission. It is key to ensure the ethics of the design and production, as this would influence public opinion and thus potential financial support of the project, but would also influence the opportunity of performing the mission. This consideration is directly linked to requirement CON-LE-01, specifying that the AWE system shall adhere to the treaty on Principles Governing the Activities of States in the Exploration and Use of Outer Space by the United Nations[4].
- **Educational benefits:** As explained in the stakeholder characterisation performed in the baseline report, TU Delft was shown to be an important partner in this project. [10] In fact, this project is part of the AE3200 Design Synthesis Exercise (DSE) course, provided at TU Delft during the third year of the Bachelor of Science in Aerospace Engineering. The DSE aims at providing students with aerospace system design and multidisciplinary work experience. This project therefore has great educational value as it immerses the team members at stake for ten weeks in a full-time design exercise.

12.4. Compliance with Sustainability Goals

This section aims to analyse to what degree the sustainability goals have been met. Three different aspects will be analysed, the usage of sustainable resources in subsection 12.4.1, the sustainable methods that are used for production will be presented in subsection 12.4.2 and the sustainability during end-of-life operations will be discussed in subsection 12.4.3.

12.4.1. Usage of Sustainable Resources

The implementation of sustainable resources in the design mostly played a secondary role, this is due to the tight technical requirements and high performing materials that come with it. The high power requirement means that the aerodynamic load on the wing is relatively high, leading to high structural loads and thus requiring a strong structure. This results in a wing box that needs a high performing material to reduce the weight while still being able to resist these loads. In some cases it is impossible to use abundant materials, for instance the generator requires rare earth metals such as neodymium and praseodymium for the production of permanent magnets [32].

Furthermore, the main and control tethers will be made out of Dyneema, a polyethylene fibre. This fibre offers high strength properties, but the fibres are mainly produced out of petroleum and natural gas, a non renewable resource. Furthermore, these fibres are not biodegradable and while recycling is possible, the added coating and gel makes the recycling extra difficult.

12.4.2. Sustainable Production Methods

In order to produce the product in a sustainable manner, the team will adhere to the lean manufacturing philosophy. The main way to optimise production process for this system is outsourcing. This is due to fact that setting up a new production line for such a low volume is not worth it, as it takes more time to set up than the actual production would take and costs more as well. All components that allow it, will be produced by known custom part manufacturers who will produce quicker and cheaper than when produced by the team itself.

In order to reduce waiting and storage time, a plan will be made with a schedule on when orders have to be placed, which is based on information on delivery times and the production schedule.

To keep transportation and movement to a minimum, components are ordered from companies that are located close to the production site, meaning European companies will be given preference. Ideally the production site would be close to the launch site but this will not be a possibility as the closest launch site for large missions is in the east of Russia. Therefore it will be cheaper and safer to ship the components to 'Centre Spatial Guyanais', the ESA launch site in French Guyana.

In order to not have to rework components at a later stage, the design made in this report will have to be refined

[4] https://www.unoosa.org/oosa/oosadoc/data/resolutions/1966/general_assembly_21st_session/res_2222_xxi.html[Accessed in May 18, 2021]

and iterated. Then during production, lots of tests will have to be done to verify that each component does what it should do and can withstand the expected loads.

12.4.3. End-of-Life Reusability

In order to make the Rhizome mission more sustainable as a whole, a lot of progress can be made by maximizing the end-of-life reusability of the systems used. This can potentially lower the costs of sustaining the habitat by a lot since it means less material has to be transported from Earth to Mars, which is by far the costliest aspect of the mission. For the non-reusable components an analysis will be made to determine if recycling is optional, which considers the possible application of the recycled material, the availability of recycling-infrastructure and in the case of a very precious material the options for bringing recycling infrastructure for it.

Out of the reusable components there are some that are reusable as they are whereas for other components some refurbishing is required. The items that will likely be reusable are those that experience little to no fatigue and can therefore be assumed to be new components for their next application. Among these items are the wing structure, the electric grid and the drum that is used for winding the tethers. The wing structure can be reused for construction of a new AWE system, given that no heavy crashes happened during it's lifetime. Before reusing it, the electric grid has to be checked for defects in connections or wires, but can then be completely reused for application in a new energy system. The drum also does not experience unacceptable wear and can therefore be used for the same application in a new system as well. Important items that can be refurbished are the generator and the ground station. The coils in the generator to experience wear due to the heating that occurs with each cycle, but are easily replaceable. The ground station will be completely reusable except for some parts that might experience higher loads such as the pole, which at least needs to be well inspected but might need to be completely replaced. Lastly there are some materials such as the membrane of the wing which can be used for household applications, but those will not be considered as they are not important for the scientific goals set by the team even though they might also reduce the payload that has to be brought to Mars.

In terms of recycling, the fact that the system will operate on Mars next to being made for the most part out of carbon-fiber composites complicates this to a level that it will very likely not occur at all. On Earth a recycling method for supercapacitors is available which makes a large part of them reusable [33]. In this method it is presented that a facility with a recycling capacity of 100 kg/h can produce 93 kg of usable material out of the input supercapacitors using only 58.5 kWh. However, this method has only been tested in a lab. In an actual recycling plant these efficiencies will not be achieved and thus recycling will be either more energy intensive or less of the original material can be retrieved. Furthermore, this assumes that a supercapacitor recycling facility will be available on Mars. This is highly unlikely as it requires the Earth-to-Mars transportation of too much infrastructure for too little benefit.

From the analysis in this chapter it can be concluded due to the constraints that come from having to operate on Mars, only a small part of the sustainable development goals can actually be achieved. It is not possible to make any compromise regarding structural integrity, life cycle or performance as this would mean that to ensure a working system for the whole system life cycle, much more material has to be transported to Mars. This is not even desirable from a sustainability perspective as it will add an enormous amount of extra fuel that has to be burned for transport. However, this makes it even more important for the continuation of the production process to optimise the reusability of the systems components as this actually decreases the amount of Earth-to-Mars trips that have to be made.

13

Production Plan, Manufacturing & Assembly

The production and assembly of the AWES is critical for it to function properly - an adequate plan will allow for a lower likelihood of failure and a higher efficiency in order to save costs and time. First, this chapter will provide an overview of the production plan for AWESOM through a visual representation in section 13.1. Secondly, in section 13.2 the manufacturing techniques used for the parts produced on earth are elaborated upon. Conversely, in section 13.3 the manufacturing techniques used to produce components on Mars are discussed. In section 13.4 the methods used in order to assemble parts are discussed where as in section 13.5 a look is taken at the assembly process used on Mars.

13.1. Production Plan

Figure 13.1 gives a visual overview of the plan for the production of the AWES. Each colour and shape of an element is linked to what of part or process of the AWES production is in question. The legend can be found in the top right of the figure.

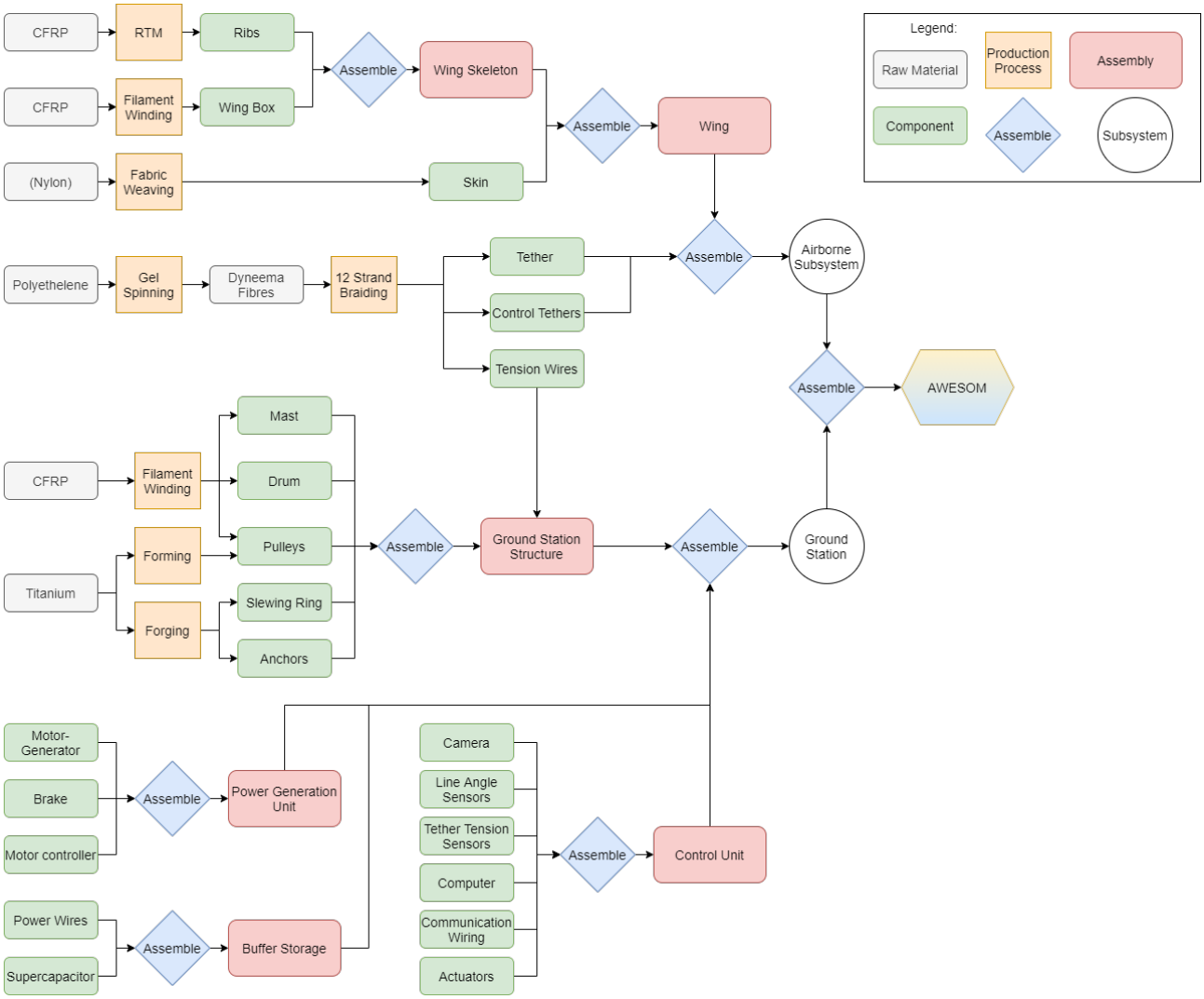

Figure 13.1: Production Plan of AWESOM

13.2. Part Manufacturing on Earth

As seen in Figure 13.1, the main material used in the AWE system is carbon fiber reinforced polymer (CFRP). This is due to its great strength performance while also having a very low weight [1]. As minimizing the mass of the systems is one of the most important tasks, this last characteristic was of utmost importance in choosing CFRP. Due to the fact that a lot of different parts will be made from carbon fiber, different manufacturing techniques should be considered and used. It should be noted that use of regolith was evaluated for the components of the ground station as well. However, since these components need to carry tensile forces and 3D printed regolith components are not able to survive this, this material option was discarded.

One of the most used manufacturing techniques for carbon fiber used for the airborne wind energy system is filament winding. This process consists of loading rolls of carbon fiber onto spools and threading them through a winding machine. It is then picked up and wound around a rotating mandrel. This method is used to create the cylindrical parts, such as the wing box, mast, drum and pulleys [2]. Thus, filament winding is the best way to produce these parts. Other components such as the platform of the ground station structure should be constructed using Vacuum Infusion Moulding (VIP) due to its relatively high possible fiber-to-resin ratio and therefore also its higher strength and stiffness despite being slightly more complex and costly [3]. Since high cost and complexity are standard issues within the space industry, let alone habitat design for Mars, it can be assumed that these high level technologies will be available to the AWESOM project. VIP involves using a vacuum to suck the resin into the mould by making use of the pressure differential[4].

Another material that is widely used throughout the design is titanium. Two manufacturing techniques were identified to be used in the production of the different parts of the AWE system. The first method is forming. Although different forming techniques exist, the preferred method for this system is hot forming as titanium can often not be formed through cold forming and is good for small series of products [5] [34]. During hot forming, the titanium is heated to extreme temperatures and formed in a press. This method is primarily used for the production of the pulley bearings, slewing ring and the anchors. This process is chosen due to its high accuracy, complex shape tolerance, and high surface profile tolerance.

Another manufacturing technique used for some titanium parts is forging. Using blows of a hammer, the titanium is forged into the desired shape [35]. This process is used for parts such as the slewing ring and the anchors. This particular process is used due to the large number of slewing rings produced and the need for the high strength which is not achieved through other methods such as casting.

For the wing membrane, nylon is used. The nylon filaments are woven into the fabric used. This is done by repeating the following steps: first, the thread ends are separated to form a clear space where the pick can pass. After, the pick is propelled across to lay other threads perpendicular to the first [6]. This is repeated until a full fabric is made achieving a quasi-homogeneous fabric structure.

The final manufacturing method used is for the production of the different tethers and tension lines. These parts are made from Dyneema fibers. These fibres are made using polyethelene, which is made into Dyneema fibers by gel spinning. Here, the fibers are drawn, heated, elongated and cooled, which leads to high crystallization and low density. These Dyneema fibers are then made into wires by 12 strand braiding, which allows for a high strength-to-weight ratio[7].

13.3. Part Manufacturing on Mars

As stated in subsection 7.6.2, some parts may be produced using additive manufacturing on Mars itself. Simple parts of the system such as the shielding/housing to cover the generator will be able to be produced with the 3D printer provided by the Rhizome project. This saves quite some weight and volume that would otherwise be needed to be transported from Earth. Furthermore, producing parts on Mars will increase the sustainability of the system, as no emissions will be produced on Earth for these parts. Some of the components used will be produced out of CFRP or titanium which require very large and heavy machinery and equipment in order to produce which can not be assumed to be available on Mars. Therefore, despite the in-situ production of parts being extremely useful in terms of mass budget requirement satisfaction, it is not feasible to produce any of the CFRP or titanium components.

[1] https://studymoose.com/advantages-and-disadvantages-of-carbon-fibre-reinforcement-polymer-essay [Accessed on June 22, 2021]
[2] http://compositeslab.com/composites-manufacturing-processes/open-molding/filament-winding/ [Accessed on June 22, 2021]
[3] https://www.performancecomposites.com/about-composites-technical-info/125-resin#:~:text=Vacuum%20Infusion%20is%20also%20an,Higher%20strength%20and%20stiffness [Accessed on June 22, 2021]
[4] https://www.performancecomposites.com/about-composites-technical-info/125-resin#:~:text=Vacuum%20Infusion%20is%20also%20an,Higher%20strength%20and%20stiffness [Accessed on June 22, 2021]
[5] https://www.jmpforming.com/blog/hydroforming/cold-forming-vs-hot-forming-metal-parts.htm [Accessed on June 22, 2021]
[6] https://en.wikipedia.org/wiki/Weaving[Accessed on June 22, 2021]
[7] https://www.dsm.com/dyneema/en_GB/our-products/dyneema-fiber.htmlAccessed on June 22, 2021]

Comparison of AM approaches proposed for 3d-printing of lunar regolith.

AM method	Energy consumption	Dimensions, weight & scalability	Low-G capability	Autonomy	Consumables (per 100 kg)	Printing speed	Printing precision	Compressive strength	Flexural strength	Pre-treatment	Post-treatment	Readiness level
CCC	Low (only moving parts)	<36 m^3 <4500 kg (ACES-3), easily scalable	WR-FPC	Goal: 3 operators, now 6	35 kg of cement binder and water + IGPD	12.7 m/mim 13.1 L/min	3.2 mm	48 MPa [a]	NR	Sv, Hm	–	1:1 habitat prototype constructed
BJ	Low (only moving parts)	~80–100 m^3, incl. binder material, ~5000–8000 kg, easily scalable	WR-FPC	Potentially good	25 kg of inorganic binder (Mg salts solution) + IGPD	6–12 m/min	0.5 mm	17–20 MPa	1.5–3.5 MPa	Sv	Cl	1:1 habitat building block (1.3t), vac. tested sampl.
IJ	~50 kW h [b]	Compact, SLFS	Applicable	NR	25–30 kg of organic admixture + IGPD	0.3–0.36 m/min	0.5 mm	18 MPa	250% [c]	Sv, Hm	Db + Snt	1–2 cm printed samples
SSLS	Low (only moving parts)	8.4 × 6.4 m <<14,500 kg <(ATHELETE), scalable	WR-MPP	Good	0	2.8 m/min	20 mm	2.5 MPa	0.55 MPa	–	–	10–20 cm samples of diff. shape, ½vac. tested sampl.
SMWS	540–684 kW h/m^3 [d]	8.4 × 6.4 m <<14,500 kg <(ATHELETE), scalable	WR-MPP	Good	0	NR	1–2 cm (?)	NR	NR	–	–	NR prints
SSS	~50 kW h*	Potentially compact and light, SLFS	Applicable	Potentially good	0[e]	NR	Few mm	NR	NR	Sv	Cl + Snt	Few-cm samples sintered
SLM	Few MW h/m^3 [f]	RCL-HS	WR-MPP	Good	0	3 m/min	0.2 mm	22.7 MPa[g] <34.1 MPa[h]	NR	Sv	Pls	Few-cm samples of complex shape
LENS	2317 MW h/m^3 [i]	RCL-HS	WR-MPP	Good	IGPD	1.2 m/min	1.65 mm	NR	NR	Sv	Pls	Few-cm samples of complex shape
DLP	~50 kW h*	Compact- SLFS	WR-FPC	NR	15–30 kg of photopolymer	NR	0.025 mm	428 MPa[j] 55 MPa[k]	129 MPa (air) 24 MPa (Ar)	Gr, Sv, Hm	Cl + Db + Snt	Few-cm samples of complex shape
SLA	~50 kWh *	RCL-SLFS	WR-FPC	NR	10–15 kg of photopolymer	NR	0.01 mm (Ceramaker 900)	NR	NR	Gr, Sv, Hm	Cl + Db + Snt	Few-cm samples of complex shape

Figure 13.2: Additive Manufacturing Methods for Regolith [36]

Some of the additive manufacturing methods for regolith shown in Figure 13.2 were explored in greater detail. These were: Binder Jetting (BJ), Selective Solar Light Sintering (SSLS) and Selective Laser Melting (SLM).

BJ using regolith can primarily be used to produce wall structures to shield other subsystems from cosmic radiation, dust and micro-meteoroids [36]. Further, compared to metals, the regolith wall structure is able to resist very high temperature fluctuations, which is of utmost importance for structures build on Mars. In Figure 13.2 it can be seen that BJ manufacturing using little power compared to the other additive manufacturing methods, which is very important to the mission. Finally, the produced structure is also capable of resisting loads. From Figure 13.2, it can be seen that structures build using the BJ method have a compressive strength of 17-20 MPa and a flexural strength of 1.5-2.5 MPa. One of the disadvantages of this production method is the need for a binder material. This adds extra weight to the payload and limits the amount of parts that can be produced without a resupply.

SSLS is very beneficial in the sense that it does not require MW of energy from the grid since it uses concentrated energy from sunlight in order to melt the regolith and perform the additive manufacturing process. However, the issue regarding this method is that the Martian atmosphere is relatively effective at blocking radiation and sunlight from the sun where as this method was explored in [36] for lunar applications.

SLM is a technique similar to SSLS, due to it also being a Powder Bed Fusion technique. Compared to SSLS it produces parts with a much higher precision, providing a sub-millimeter resolution. However, it uses quite a lot of power, which is especially a problem due to it needing power from the habitat power storage instead of being able to use an external source such as sunlight. In Figure 13.2 it can be seen that the SLM method uses a few MW per cubic meter. Thus, this additive manufacturing method is best used to produce small, detailed parts.

13.4. Assembly of Parts on Earth

Assembly on Earth will be kept to a bare minimum due to the maximum volume requirement for the launcher only allowing a maximum of 3 m^3. Only complex sub assemblies such as electronic control systems will be assembled on earth. With the help of practice and a detailed guide, the majority of AWESOM will be constructed on Mars.

13.5. Assembly of Parts on Mars

In this subsection the various assembly stages are elaborated upon by explaining what sort of methodologies will be involved.

Firstly, in order to join the ribs and the wing box to generate the wing skeleton the two components will be joined using epoxy adhesive. The wing skeleton and the skin will be joined using adhesive tape as well as stitching as very high maximum loads can be reached with said joining method and can easily be fixed in comparison to other methods such as gluing or ultrasonic welding [16].

The tethers will be attached to the wing via a hooking mechanism which allows for rapid and simple replacement if the tethers need to be changed.

The motor-generator, the break and the motor controller will be connected via mechanical fasteners such as screws or nuts and bolts. The electrical systems will be connected via plugs and mechanically fastened to the structure therefore allowing the buffer storage to be constructed together with mechanical fasteners to secure it to the ground station. The control unit will be assembled using the same mechanisms as for the power generation unit and the buffer storage. The ground station structure will use epoxy adhesive in order to join the CFRP components and mechanical fasteners for the titanium components. Titanium components will be joined to CFRP components via mechanical fasteners. Subsequently, having constructed the ground station structure, the power generation unit, the buffer storage and the control unit, the ground station can be made by joining all the assemblies using mechanical fasteners leading to the ground station being complete.

To finish of the construction of the AWES system, the airborne subsystem and the ground station will be joined via the tethers being attached to their corresponding drums leading them through the appropriate pulley systems.

14

RAMS Analysis

RAMS is an acronym for Reliability, Availability, Maintainability, and Safety, commonly used to characterise a product or system[1]. Reliability refers to the ability of the system perform a specific function and may be given as design reliability or operational reliability. This can also include redundancies in the system, such as extra sensors to verify value to enhance the reliability. Availability is the ability to keep a functioning state in the given environment. As the Martian environment is hostile towards organic and inorganic substances, additional care is taken to ensure the system is available whenever required. Both reliability and availability are elaborated upon insection 14.1. Maintainability is the ability to be timely and easily maintained (including servicing, inspection and check, repair and/or modification). It is preferred to have a system that requires little to no maintenance and checks. Therefore, is it essential to know the reliability and durability of the components beforehand to plan these inspections. This is discussed in section 14.2 Safety is defined as ability not to harm people, the environment, or any assets during a whole life cycle. As the AWESOM project is not the first mission to Mars, existing missions chartered previously must not be interfered with. Additionally, the system must not harm anyone handling it during construction and maintenance. This is explained in section 14.3.

14.1. Reliability and Availability

In Table 3.1, the requirements stated by the stakeholders, key people and organisations complying with the reliability and availability aspect of the system as a whole and individual subsystems can be identified. It is essential for every subsystem to function reliably during the mission to prevent unexpected failures. Additionally, the interfaces of these subsystems must also perform as expected and ensure the signals/data is sent to the target destination without any interference. For the system to produce an average power of 10kW, it is essential to know the optimal periods at which power can be produced. Therefore, the system has to be available and ready during these periods. After the periods when the system would be grounded are known, measures can be taken to ensure adequate supply of power until the system is airborne. Reliability and Availability are both interdependent of each other. If a system is very reliable, it will be available during adverse conditions and vice versa. A more reliable system would also experience fewer interruptions for maintenance and safety related activities. Availability can also mean access to advanced technological advancements and using it to enhance the system performance.

14.1.1. Airborne System

In the list below the mission requirements along with steps taken to ensure reliability and availability of the airborne systems can be found:

- **TEC-AIR-01: The airborne system shall be able to withstand 25 m/s wind gusts.** When wind gusts are over the maximum limit, the wing will enter a safe mode, as discussed in section 10.2.
- **TEC-AIR-06: The kite shall withstand TBD N/m2 of tensile stress.** In order to verify this requirement, several scripts of code were written in Python to estimate the maximum loads acting on the wing during operation.
- **TEC-AIR-07: The tether shall withstand 12000 N of tensile force.** In order to verify this requirement, several scripts of code were written in Python to estimate the maximum loads acting on the wing during operation. Using these loads and knowing all the forces acting on the kite, the maximum tension generated in the tether was estimated.
- **TEC-AIR-08: The airborne system shall have a cut out speed of 20 m/s during nominal operation.** The kite can produce power up to wind speeds of 22.8 m/s as discussed in section 8.4, so the limit cut-out speed of 20 m/s is met.
- **TEC-AIR-09: The tether shall be able to withstand 25 m/s wind gusts.** In order to verify this requirement, several scripts of code were written in Python to estimate the loads acting on the wing at varying

[1] https://en.wikipedia.org/wiki/RAMS [Accessed on June 17, 2021]

wind speeds. Using these loads and knowing all the forces acting on the kite, the tension generated in the tether was estimated.

- **TEC-AIR-11: The airborne system shall be able to stay airborne(cut in speed) at 2.5 m/s wind speed.** In order to verify this requirement, several scripts of code were written in Python to estimate the loads acting on the wing at varying wind speeds. The model calculated a wind speed of 2.5 m/s to safely take-off before generating power.
- **TEC-AIR-12: The airborne system shall withstand 3340 cycles of temperature fluctuation from -190°C to 20°C.** The materials chosen for the airborne system were influenced by this requirement.

The aerodynamic and structural requirements were verified using unit and system tests. The ground station, control and electrical systems had to be verified by reading existing literature on similar systems or by performing analytical calculations as no code was written or software was used for their corresponding calculations. This was mainly attributed to insufficient time for writing script and performing these tests.

14.1.2. Ground Station System

In the list below the mission requirements along with steps taken to ensure reliability of the ground station system can be found:

- **TEC-GE-01:** The generator shall have a 90% average efficiency.
- **TEC-GE-02:** The generator shall be able to provide a torque 1000 Nm.
- **TEC-PS-10:** The voltage of the generator shall be matched to the voltage of the power storage system.

14.1.3. Control System

- **TEC-CL-04:** The control system shall have a response speed of 10 ms.
- **TEC-CL-05:** The control system shall withstand 3340 Martian temperature fluctuation cycles from 190°C to 20°C.

14.1.4. Electrical System

- **TEC-GE-07:** The connecting wires shall be able to withstand 3340 Martian temperature fluctuation cycles from -190°C to 20°C.
- **TEC-GE-08:** All electric connecting points shall be protected against cyclic loading.
- **TEC-PS-09:** All electric connecting points within the power storage system shall be protected against cyclic loading.
- **TEC-PS-01:** The power storage system shall have a capacity of TBD kWh.
- **TEC-PS-02:** The power storage system shall provide an output of 10 kW.

14.2. Maintainability

Throughout the lifetime of the system it is inevitable that failures happen. It is thus of utmost importance that a strategy is present to repair a system when faults happen. There are 2 main types of maintenance, scheduled and non-scheduled maintenance. Scheduled maintenance entails all maintenance that are scheduled before hand, while non-scheduled maintenance consists of maintenance that is instigated after an indication of failure. For scheduled maintenance the main goal is thus to catch a failure formation in its early stages, before a failure mode can be reached.

Airborne Subsystem

- **Kite maintenance** will be done once every 4 weeks and is thus a scheduled maintenance. The kite will be analysed after the kite has to land due to a period of low wind, this happens almost every day and thus this otherwise useless time can be used to examine the kite. Furthermore, After the kite has had to instigate the ”Safe mode”, non-scheduled maintenance will be done. The powerful wind gusts can cause damage to the canopy and structure of the kite and doing this maintenance afterwards ensures that the kite will not be flown with these flaws.
- **Tether maintenance** is a little more difficult to do. This is due to fact that at the moment the kite is grounded that the tether is mostly rolled up on the drum. Furthermore, the part that gets the most erosion is the lowest part of the tether, that is getting reeled in and out a lot. While in contrast the upper part of the

tether almost never makes contact with the drum which is what causes this erosion. One way of increasing the lifetime of the tether is by measuring the torque produced by the drum, this can be translated to the tension in the tether. If this tension exceeds a certain threshold, then the drum ”lets go” and releases the tether a little bit to reduce the tension in the lines. Furthermore, a spare tether will be taken to Mars and after 2.5 Martian years (half the total lifetime of the system) the tether will be replaced regardless of the condition of the tether at that point in time.

Ground Station

- **Drum, drive shaft and generator maintenance** will be done in the same way as the tether. Non-scheduled maintenance will be used by detecting vibrations or insufficient lubrication using accelerometers. Furthermore, impurities in lubrication can be found. This can give a good indication of when a failure has happened or will happen soon. Furthermore certain failures such as alternator bearing erosion make a lot of noise and can be audibly heard, this can also work as an indication of failure.
- **Structure** maintenance will mostly consist of check ups on the frame, rotating bearing, mast and tension lines. This is done to ensure that all components are working and can function properly.

Control System

- **Control Maintenance** will consist of scheduled maintenance, where every 4 weeks the actuators and control computer will be checked for flaws and failures, as well as non-scheduled maintenance, where the behaviour of the kite and power output of the system will be examined to determine whether or not the kite is making optimal movement. This can indicate a failure to, but not limited to, the control actuators or computer.

Electrical System

- **Short term storage maintenance** will be non scheduled maintenance, the voltage and current of the supercapacitors will be measured and these can indicate the deterioration of the system. If it is visible that these values change from the nominal values, the supercapacitors will be inspected, as well as the cabling and transformers that are connected to them as these can also be faulty and cause the change in output.

14.3. Safety

The final step of the RAMS analysis is to determine the safety of the system and any precautions that have to be taken for safe production, installation operations & maintenance.

Production

During production proper safety precautions have to be taken to ensure that no injuries happen. This is for both part production and assembly as tools and heavy equipment can seriously injure the workers if they are not handled properly. Furthermore, if an injury does occur, first aid has to be available on site, as well as certified first aid responders. Finally, precautions regarding fire hazards have to be taken as during some of the production processes high temperature processes such as forging are used.

Installation

For the installation on Mars, guidelines will be given to ensure that the correct steps are taken. Additionally, before the system arrives, the astronauts will be shown a demonstration of how to build the system, such that they are familiar with the process. This in combination with protective clothes during installation such as hard hats, gloves, reflective durable clothes will ensure that no unnecessarily dangerous situation arises.

Operations & Maintenance

During operation there are a few potential hazards, the first being the fact that if the kite loses control in any way that it could come crashing down and injure someone in the proximity. Though this is not very likely, precautions have to be taken to ensure that the likelihood is minimised, this was done already in section 10.2. Another potential safety hazard is related to the electrical system. There is an inherent danger connected to working with electrical systems that can really come to light when maintenance is needed. Exposed electrical cables, fault currents and electrical overloading can pose a direct safety hazard to anyone close to it. One positive about the thin, oxygen deprived atmosphere is the fact that it can’t sustain open fires or combustion that would otherwise be a potential result of electrical failures.

15

Financial Analysis

This chapter will go over the financial aspects of the AWESOM mission and development. First, in section 15.1 a cost breakdown is given for both the production of the system, as well as the development of the system. Afterwards, the return of investment and operational profit of the system is discussed in section 15.2.

15.1. Cost Breakdown Structure

The cost breakdown structure was made using Table 15.1. It shows an overview of the costs related to the development and production of the AWESOM system. These values were then put into a diagram to show a more visual overview (Figure 15.1).

Type of cost	Cost in €	% of total budget
Raw material cost	17,909	3.6
Manufacturing cost	4,286	0.9
Generator	15,000	3
Buffer storage	5,000	1
Sensors	2,000	0.4
Control unit	20,000	4
Maintenance cost	50,000	10
Total system cost	114,195	22.8
Labour cost	13,000,000	-
Testing cost	100,000	-
Unexpected cost	25,000	-
Total development cost	13,239,195	-

Table 15.1: Cost breakdown of the development of AWESOM

The raw material cost encompasses the amount of money needed to buy the materials needed for the AWE system. These materials were identified in the production plan (section 13.1) and were found to be: Carbon Fiber Reinforced Polymer (CFRP), titanium, nylon and Dyneema. As CFRP would be the most used material, it was expected to be the most expensive part of the raw material cost. The amount of CFRP needed for the whole AWE system was estimated to be around 229.09 kg. The material costs according to Granta Edupack are found to be approximately 50 € per kg [1], thus resulting in a raw material cost of the CFRP of 11455 €. The second material to be considered is titanium. Most of the titanium used in the system is used for the slewing ring. As this will have a volume of around 0.0155 m^3 [2], the cost of titanium for the slewing ring will be 2672 €. This cost is based on the price per kg of grade 5 titanium, the most used type of titanium in aerospace. Adding a bit extra for the smaller titanium parts the total titanium cost would be around 2800 €. The next material is nylon. This is only used for the wing, thus 120 m^2 would be needed. With a specific cost of 16.67 € per m^2, the total nylon cost becomes 2000 €. Finally, the cost of the Dyneema was found using the needed tether and control tether length and diameter, along with the length and diameter of the tension lines. Using a diameter of 4.6 mm for the main tether and tension lines and 2 mm for the control tethers. Further the length of the main tether and the control tethers is 1000 m and for the tension lines 5 m. This results in a total Dyneema cost of 1654 € [3]. This was found using the source and a raw material cost percentage estimate of 85%.

The manufacturing cost was calculated by looking at the different manufacturing procedures as found in chapter 13. The total cost was found to be 4286 €. A detailed overview of these calculations per subsystem are presented in subsection 15.1.1.

[1] https://www.ansys.com/products/materials/granta-edupack [Accessed on June 21, 2021]

[2] https://shop.eriks.nl/en/bearings-slewing-rings/four-point-contact-bearing-without-gear-teeth-vlu200414-rr-14191806/ [Accessed on June 22, 2021]

[3] https://linysyntetyczne.pl/dyneema-ropes-per-meter [Accessed on June 22, 2021]

The next cost types are individual subsystems and parts that are bought directly. The generator was found to cost 15,000 € [4]. It is expected that the generator for the AWE system will be a custom made generator, using more expensive materials. Thus the cost is expected to be higher than conventional generators that are currently being used. The cost of the buffer storage was found using the needed capacity found in subsection 7.5.4 and comparing it to existing supercapacitors. Thus the cost for the buffer storage was found to be 5,000 € [5]. Next the cost of the sensors used for controlling the wing was calculated. The sensors consist of a camera, line angle sensors and tether tension sensors as found in subsection 7.2.5. The most expensive sensor is the camera, priced at 1850 €, based on existing cameras [6]. Adding the cost of the other sensors, the total cost of the sensors was found to be around 2000 €. Finally, the cost of the control unit was found by comparing it to already existing designs. Eventually, the cost was found to be 20,000 €.

The last part of the total system cost is the maintenance cost. This was defined as the cost of the spare parts needed to be transported to Mars to be able to perform maintenance and carry out repairs. By researching other space mission, a value of 10% of the total budget was found to be a good estimate, thus equalling to 50,000 €.

The last four costs stated in Table 15.1 are related to the development of the system. As the budget as stated by the requirements only counts for the production of the system, these costs do not count towards the budget of 500,000 €. First, labour costs were considered. These consist of both the payroll of the engineers designing and building the system, as well as the astronauts assembling the system on site and performing maintenance, for 10 years of development and operation. Furthermore, it was estimated that 10 engineers would be needed for the development of the system, along with 10 astronauts that would be working in the Rhizome project. Thus, the total cost was estimated to be around 13,000,000 €. Next, the testing cost was considered. By looking into current and previous space missions, a value of 20% of the total budget was found to be sufficient, corresponding to a cost of 100,000 €. Finally, any unexpected costs should be accounted for. Thus, a value of 5% of the total budget was allocated to this cost, corresponding to 25,000 €.

15.1.1. Manufacturing Cost

This section gives a more detailed look at how the different manufacturing costs were computed. This was done for the wing, wires and the ground station structure.

Wing

The wing roughly consists out of three main parts, the wingbox, the ribs and the nylon canopy. The wingbox and the ribs are assumed to be made out of tubes, the price of which is estimated by looking at carbon fiber producers. The ribs consist of 4 small tube with a diameter of approximately 3 cm and a thickness of 1 to 3 mm. The length of the different tubes are around 2 and around 0.5 meter throughout the wingspan. In total 24 ribs are needed along the wingspan. A comparably sized tube was used to compute both the percentage of manufacturing costs and material costs to the total cost. A tube of 2 meter with an outer diameter of 3 cm and an inner diameter of 2.7 cm costs approximately 90 € [7]. Again using the material cost of 50 € per kg. Using a density of 1500 kg/m^3 this leads to a 89.5 % material cost. Since a total weight of 8 kg is needed this would result in a total estimated cost of 447 € of which around 47 € corresponds to the manufacturing cost.

The wingbox is a tube with an approximate radius of 45 centimeter and a thickness of 1 to 2 mm along the two wings. In order to assess its costs the same ratio as used for the ribs is applied to the wingbox. The wingbox total weight is 56.4 kg, an estimated total cost of 3150 € is computed consisting of an approximate material cost of 2820 € and an approximate manufacturing cost of 330 €.

The canopy costs are estimated by established contact with a sail production company. This company gave us an estimation of the costs of a nylon sail with a thickness of 0.1 mm, exactly the thickness used in this design. The costs of material were around 25 € per 1.5 m^2 whereas 3 full working days of around 500 € per day was expected to create the 120 m^2 sail. A total cost of the canopy was found to be around 3500 € [8].

Dyneema Wires

As the main tether, control tethers and tension lines are all manufactured the same way, the manufacturing cost only scales with size. Because a raw material percentage estimate of 85% was used previously for the cost of

[4] https://www.aeroexpo.online/prod/mgm-compro/product-171210-31055.html [Accessed on June 21, 2021]

[5] https://www.digikey.nl/product-detail/en/eaton---electronics-division/XL60-2R9348W-R/283-XL60-2R9348W-R-ND/10441149[Accessed on June 21, 2021]

[6] https://www.cameranu.nl/nl/p3189297/z-cam-e2-m4-4k-cine-camera-mft-mount?bgid=39342-AGI-119921801004-ASI-299965445940-3189297&gclid=CjwKCAjw8cCGBhB6EiwAgORey5rSpwGpS70oX5ECnfQ3m4R70PxYbxBsZchSCdVuG2Z5oID0liMDDhoCeW8QAvD_BwE[Accessed on June 21, 2021]

[7] https://www.carbonwebshop.nl/carbon-high-performance-buizen-rond#filter:f8cae627fd60d005d771ff4777237cd9[Accessed on June 21, 2021]

[8] Phone conversation with 'de Zeilerij'

the different tethers, the manufacturing cost would be the remaining 15%. This corresponds to a total cost of 292 €.

Ground Station
The ground station manufacturing cost consists of the manufacturing cost of all the carbon fiber parts, as well as the manufacturing cost of the slewing ring and the other titanium parts. As a manufacturing cost percentage of around 10.5% was found for the carbon fiber wingbox, this will also be used for the ground station. This is due to the fact that most of the carbon fiber parts in the ground station are also tubes. Thus, the manufacturing cost of carbon fiber parts in the ground station would become 917 €.

For the slewing ring and other titanium parts a conservative estimate of 30% of the total cost was made for the manufacturing cost. This corresponds to a cost of 1200 €.

Combining these values, the total manufacturing cost of the ground station was found to be 2117 €.

15.1.2. Visual Overview
This subsection shows the cost breakdown structure in a diagram format. All costs shown in Figure 15.1 correspond to the previously calculated costs shown in Table 15.1. It should be noted that these costs are preliminary estimates and are subject to change. Changes might occur due to for example supply shortages, new production methods, payroll increases, etc.

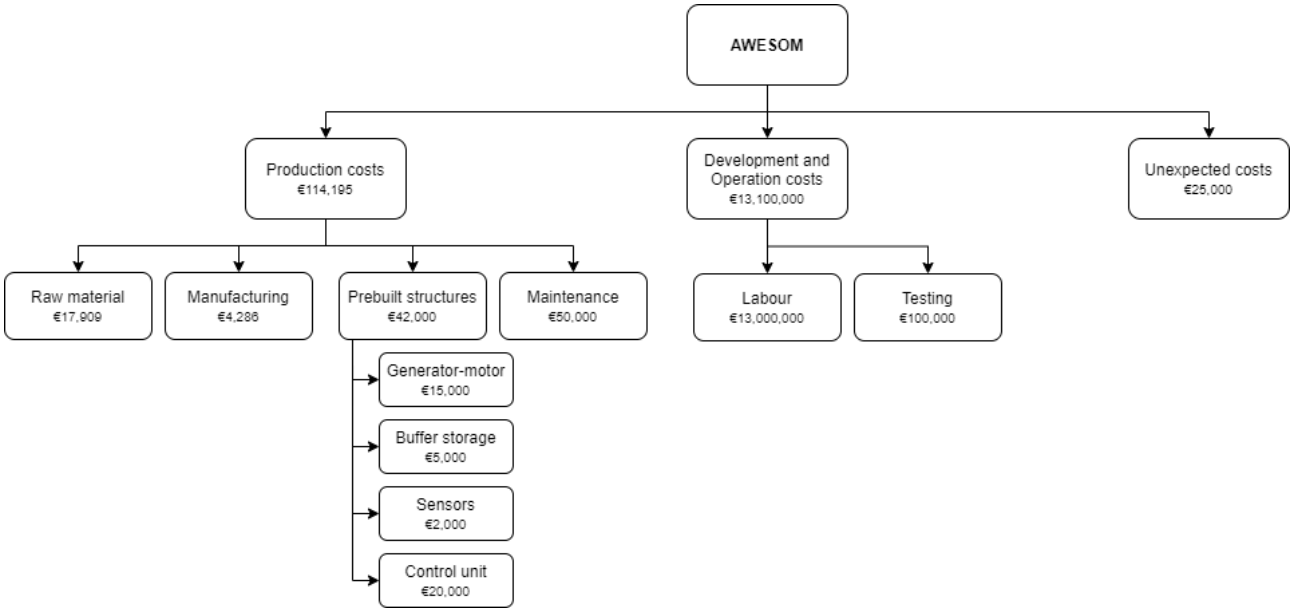

Figure 15.1: Cost breakdown structure of AWESOM

From this overview, it can be seen that less than 25% of the budget is estimated to be used for the production of the current design. This means that more expensive, higher performance materials and manufacturing processes could be used. This would make the design more efficient, lighter and overall improve the performance. Further, the leftover budget could even be spend on research into completely new materials.

15.2. Return of Investment & Operational Profit
Any project or mission has to have a return of investment. If not, there would be no point to developing it. However, this return of investment is not always in the form of money. Most space missions are still scientific in nature, in stead of commercial. Thus, their value and return of investment are in the form of education and and scientific breakthroughs. This is also the case for AWESOM. As it is not a commercial product, the ”profit” would be the additional research developments. Major breakthroughs are expected in the fields of airborne wind energy, Mars exploration and Mars habitation. These new developments would also encourage more people to study and research space exploration and extraterrestrial habitation. Thus, the return of investment of AWESOM would be the scientific breakthroughs and educational value in space exploration, Mars habitation and airborne wind energy.

16

Future of the Project

This chapter discusses the plans laid-out by the group to ensure the project is still underway after the DSE period concludes. By the end of the DSE, only the design choices made will be finalised. To ensure the designed system is manufactured, assembled, tested, and deployed, a Gantt chart is utilised in section 16.1 to show the timeline of all events leading up to the deployment and operation of the system. Additionally, a logic diagram is present in section 16.2 to give a schematic representation of the design and development flow of the project.

16.1. Gantt chart

Shown in Figure 16.1 is the Gantt chart briefly explaining the timeline of the project once the DSE has come to an end. The Gantt chart is present in addition to the logic flow diagram to specify the timelines of future stages of the project. The future stages of the mission are divided into 4 phases. These are namely: preliminary design phase, qualifying model development, flight model development, launch campaign.

The preliminary design phase involves defining a overarching AWESOM system and its functional efficacy. This phase will allow to bridge the gap between the design concept and the detailed design phase. The phase allows the exploration of creative ideas with higher levels of flexibility when it comes to making design changes. Later on, the detailed design is elaborated in this phase making ideas and concepts more concrete and preparing for the next step.

The qualifying model development phase looks at making sure the various levels of AWESOM are tested bottom up; starting with coupon tests all the way up to full assembly tests. Additionally, software will be developed and verification and validation of the software and the tests will be done in parallel. The design will be iterated if errors are detected. Having done tests on sub-parts of the AWESOM system, the following phase looks at the performance on a more complete scale.

The third phase named flight model development and dives into the analysis of how the whole system works via performing flight tests. If all is well and the verification and validation process yields a positive outcome, the final system is presented and integrated together to make sure all subsystems work smoothly with one another.

Once all systems have been integrated into the flight model, phase four titled: 'launch campaign', shall follow. In this final phase, estimated to span over half a year, the system will be tested and prepared for launch. The two main activities in the launch campaign are a pre-launch testing of the system and an integration of the payload on the launcher. From this step onward, the responsibility of the project will be passed on to the launcher contractor for a safe transportation of the payload to Mars and to ESA for the operation of the AWESOM system.

The critical path indicated by the red line shows the longest possible time taken to complete the project according to the Gantt chart devised. This is important to indicate which special attention must be payed to them in order to finish without delays. Even if the project is completed on time, the launch of AWESOM heavily depends on the development and launch of the Rhizome project. If this is delayed then the need for AWESOM will also be delayed and hence causing project delays. The same could work vice-versa putting AWESOM on a tighter schedule if the Rhizome project is launched early or AWESOM experiences delays and is not on time for the intended launch date of Rhizome. Another possibility of the project not being carried out as intended in the Gantt chart is if there are issues with the launcher module or the launcher fails causing AWESOM to be lost and not used for its intended purpose.

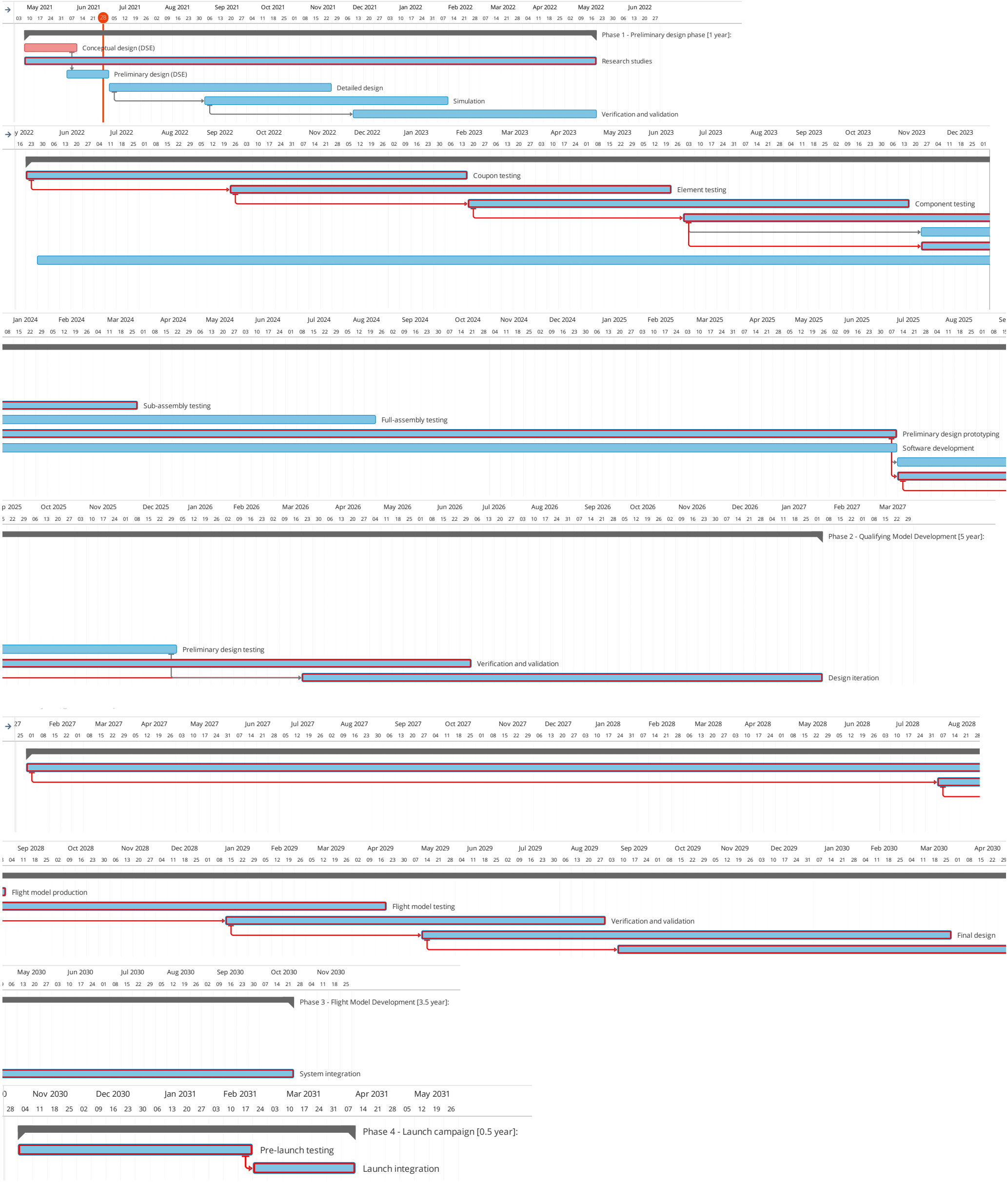

Figure 16.1: Gantt chart of the project milestones in the coming ten years

16.2. Design and Development Logic

Shown in Figure 16.2 is the logic diagram obtained after performing an in-depth study of the different phases mentioned in Figure 16.1. The main purpose of the logic diagram is to explain the steps taken to ensure the success of the project once the DSE has concluded. involved in reaching the end of each process. While the Gantt chart mainly describes the timeline of events, the logic diagram explains the step by step approach to reach the end of every event. It displays which steps shall be conducted concurrently, which are performed in series, or even where iterative processes shall be performed. Figure 16.2 features the same 4 phase as the Gantt chart however highlights iterative processes in yellow, the various phases in orange and the combination of branches with a red circle with a plus-sign on the inside. Standard steps in the project are designated by white boxes.

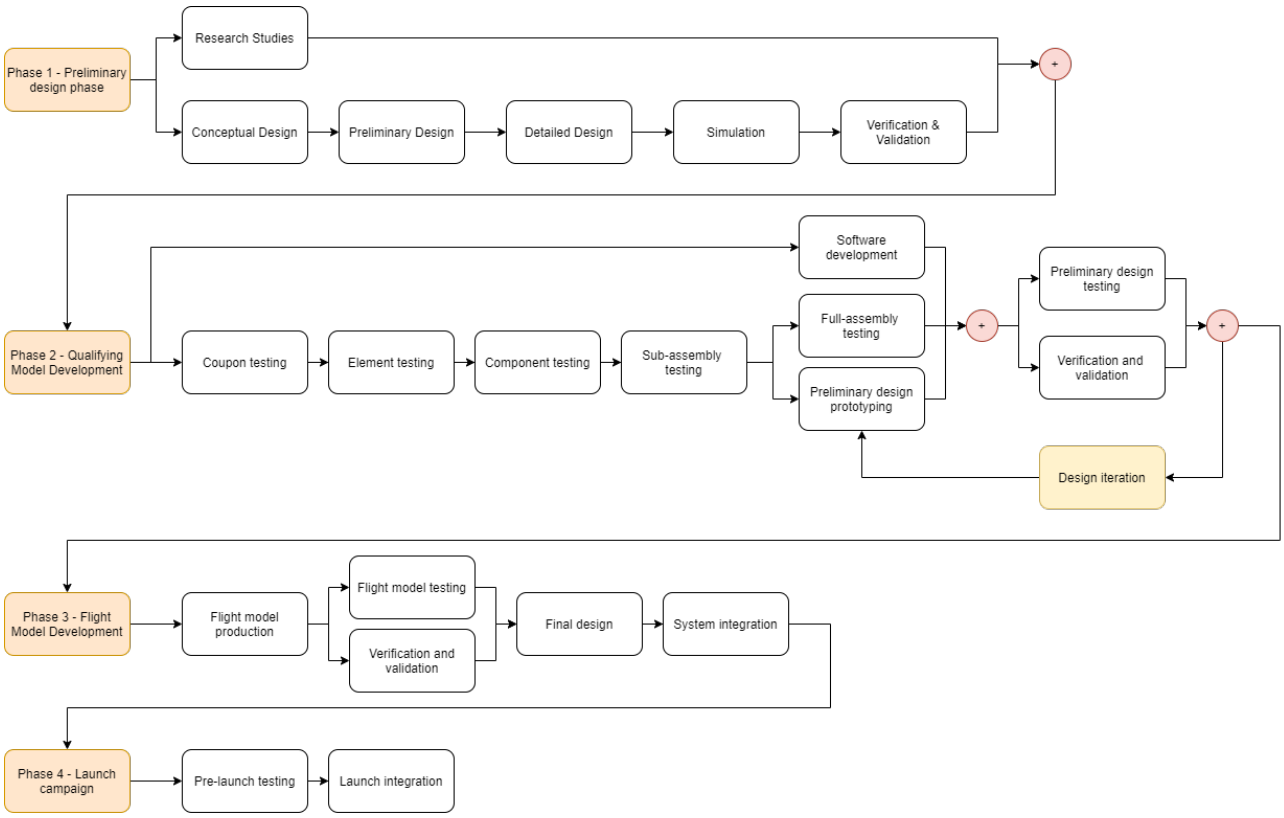

Figure 16.2: Project design and development logic diagram

17

Conclusion

This report outlined not only the design steps but also all the analyses carried out on the designed system and a series of future steps to be taken for improving the system. AWESOM is an automated airborne wind energy system which is tasked to provide enough power, namely 10 kW, to the Rhizome habitat on Mars. In the previous design phases, the design choices were generated and a trade-off has been carried out for each part of the system. The final configuration at the end of the trade-off was a ground-based power generation system with a swept wing, controlled from the ground by two tethers. The system is equipped with a short term buffer storage consisting of supercapacitors for energy required during a cycle, and a long term storage for yearly fluctuations of available wind resource.

The first step taken to start the conceptual design of the system, a detailed environmental analysis was performed, which resulted in a relocation of the habitat as the location chosen by the previous design team had an insufficient wind resource due to being inside a crater. After this, the wind resources were analysed and average wind speeds were found to be sufficient for the successful operation of AWESOM. It was also found that seasonal changes in the wind speed was significant, and the system's operation needs to be planned accordingly. After this analysis, the preliminary design of the system was evaluated as well. The chosen configuration of all the elements was put through a feasibility check since it was crucial to make sure the system was feasible before moving further into the design process. After the chosen configuration was found to be feasible, the configuration of the system and the functional analysis were presented. The functions of the system were broken down into six main phases: Earth-based production, transportation, Mars-based production, installation, operation, and end-of-life. System functions within each phase were presented in a Functional Breakdown Structure, and their ordering was shown with a Functional Flow Diagram.

Before the detailed design steps were initiated, two more analyses on the system were carried out since they had impact on the upcoming design choices. Firstly, the market analysis was performed, and the competitors were named as NASA, Tekniker and SpaceX. Following the identification of competitors, the SWOT analysis was carried out and the requirements coming from the market research were listed. These requirements were related to legal guidelines, sustainability goals, operation time and technical budgets of the system. Right after the market analysis, the resource allocation was performed in order to distribute the mass, volume and cost budgets among different parts of the system. Having a mass budget of 200 kg was proven to be the most difficult requirement to comply with, and this conclusion was taken as a warning sign during the design process.

At this point, all preliminary evaluations were done, and the process to size the system has begun. This sizing, or design, process was carried out by five different departments simultaneously: aerodynamics, control, structures, power and operation. During the sizing process, a Python-based power performance model was also developed simultaneously to be able to check the feasibility of design decisions and analyse the performance of the final design once all departments were done with their parts. The aerodynamics department started the design of the wing with a trade-off for the airfoil choice, which resulted with the choice of Wortmann FX 63137 airfoil. Then, a low aspect ratio and a high aspect ratio versions of the wing were compared, eventually coming to the conclusion that the low aspect ratio version was better. The wing design was completed by calculating a wing area of 60 m^2, wing span of 20 m and an aspect ratio of 6.67.

The second department is the control department which is responsible of the control system's design. First, the trajectory was chosen as a down-loop figure of eight to ensure efficiency and avoid entanglement of the tethers. Then, the control algorithm was designed, and turn radius was calculated which is an important input for the performance model. Then, the sensors and actuators were chosen and the architecture of the software was designed.

The next one is the structures and materials department. This department's focus was to size the wing which consists of wingbox, ribs and canopy. Firstly, the loads on the wing were defined. Then, the material selection was performed. At this point, a Python-based structural model of the wing was developed to determine the wingbox thickness, rib spacing, rib dimensions and total mass of the wing.

Another department is the power department which has significant importance in terms of the power production performance of the system. First, the configuration of the ground station was handled, and the main components

were named as: motor controller, internal control unit, generator, control motors, spool motor, slewing motor, brake actuator, buffer storage. In the rest of the section, the motors, drum and the buffer storage was sized. For the chosen motors, the rated power, rated torque and rotational speed was indicated. Then, the efficiencies were elaborated on as they are important to calculate the required power output to provide the 10 kW need of the habitat.

Finally, the operations and logistics department defined the system operation procedures, and designed a landing and launching system. After a trade-off study, the landing and launching method was chosen as the use of a mast with the help of decommissioned rovers of the habitat. In the end, plans for maintenance and end-of-life phases were outlined, and the system characteristics chapter was concluded with a summary of the mass and volume of each component of the preliminary design that is now complete.

After the sizing process was complete, the performance was analysed using the aforementioned simulation. This simulation output the total power produced, and compared it with how much power was required in total. The results showed that the system was capable of producing enough energy to cover the needs of the habitat. The system reduced 3.2& extra energy on top of the required amount.

Now that the system's design was justified, the interface design was presented. This interface design included a hardware & software block diagrams where the relationships of different parts of the system in terms of hardware and software were shown.One other interface design element was the communication flow diagram which outlined the flow of communication between these elements for successful operation.

After this step, the risk analysis was performed. This analysis showed that the most critical risks after the performed risk mitigation were damage on the wing or the tethers due to high aerodynamic loads or the failure of generator due to corrosion and insufficient lubrication.

Since several programming models were developed for the design of the system, verification and validation steps were taken. Unit and system tests were performed on the programs in order to verify them. The validation of the models were very challenging due to lack of real-life data from the operation environment. However, plans for validation which can be carried out in the future when data becomes available were outlined. Requirement verification was also completed by presenting a compliance matrix. By the end of this step, it was shown that most of the key requirements were complied with by AWESOM's preliminary design.

The sustainability aspect and the manufacturing plan of the system were also presented. Afterwards, RAMS analysis was carried out to determine the feasibility of the system in terms of reliability, availability, maintainability and sustainability. Then, the system was also analysed financially where a cost breakdown structure was presented, and a return on investment strategy was outlined. Finally, the report was concluded by explaining the plan for the future of the project including a logic diagram and Gantt chart.

Since the time the design team had for the project was very limited, not all the desirable steps could be taken during the design process. Therefore, every design section included a part about the recommendations for the future phases of AWESOM's design. These recommendations range from improving some assumptions in sizing to improving the accuracy of developed models. For future development of the project it is also crucial to renegotiate the mass budget that was given by the stakeholders as it became clear that this was far too low to match the other requirements at the same time. Another important improvement would be to consider the solar panels for the yearly power production since this would help quite significantly. The fact that the design team of AWESOM did not consider this contribution, the resulting system is over-designed. These two points make it very hard to determine what a realistic mass budget would be yet, so it would be wise to reconsider them first before committing to some requirements. Moreover, it would be a big improvement if a higher resolution climate model with more inputs is used as this would result in a more accurate design. Finally, in order to make a lighter system, the focus should be on improving the weight of the motor/generator as this is by far the heaviest component.

To summarise, this report focused on presenting the preliminary design of an automated Airborne Wind Energy System on Mars. The design process was explained in detail, and the final configuration was analysed in many different terms such as performance or sustainability. The report was concluded by sharing the vision of the design team for the future of the project, hoping to present a pathway to carry AWESOM from paper to Mars.

Bibliography

[1] J. Bluck. “Antarctic/Alaska-like Wind Turbines Could Be Used on Mars”. *NASA Ames Research Center* (Oct. 2001).

[2] Corte Vargas, F., et al. “Combined Airborne Wind and Photovoltaic Energy System for Martian Habitats” (2020).

[3] E. Millour, et al. *The Mars Climate Database (Version 5.3)*. Accessed on May 28th, 2021. 2018. URL: http://www-mars.lmd.jussieu.fr/mars/access.html.

[4] F. Forget, et al. “Improved general circulation models of the Martian atmosphere from the surface to above 80 km”. *Journal of Geophysical Research* 104 (E10 1999), pp. 24155–24176.

[5] Corte Vargas, F., et al. “Renewable energy for Mars habitat”. Design synthesis exercise midterm report, Faculty of Aerospace Engineering, Delft University of Technology. 2020.

[6] de Wachter, A. “Deformation and Aerodynamic Performance of a Ram-Air Wing”. MSc Thesis. Delft University of Technology, Sept. 2008.

[7] Horrocks, A., R. and Anand, S., C. *Handbook of Technical Textiles. Technical Textile Applications*. 2nd ed. Vol. 2. Woodhead, 2016. ISBN: 978-1-78242-465-9.

[8] Cordage Institute. *Fibers for Cable, Cordage, Rope and Twine. Comparative reference*. 2003.

[9] Caruso, M., Gül, D., Isidorova, V., van der Klugt, W., de Lange, M., Meyer Ranneft, T., Popescu Cabo, A.C., Tiagoo, K., Sambath, B. and Sanders, L. “Midterm Report Airborne Wind Energy on Mars”. Faculty of Aerospace Engineering, Delft University of Technology. 2021.

[10] Caruso, M., Gül, D., Isidorova, V., van der Klugt, W., de Lange, M., Meyer Ranneft, T., Popescu Cabo, A.C., Tiagoo, K., Sambath, B. and Sanders, L. “Baseline Report Airborne Wind Energy on Mars”. Faculty of Aerospace Engineering, Delft University of Technology. 2021.

[11] A.Cervone. *Aircraft aerodynamic analysis - Lift & Drag -ADSEE slides*. Nov. 2019-2020.

[12] Erhard, M., Strauch, H. *Flight control of tethered kites in autonomous pumping cycles for airborne wind energy*. Vol. 40. 2015, pp. 13–26.

[13] Jerez Venegas, M.S. “Path Optimization of a Pumping Kite System”. Master of Science thesis, Faculty of Aerospace Engineering, Delft University of Technology. 2017.

[14] Johannes Peschel. *A cost effective kite state estimator for reliable control of kites*. 2013.

[15] Uwe Ahrens, Moritz Diehl, Roland Schmehl. *Airborne Wind Energy*. Springer, 2013. ISBN: 978-3-642-39964-0.

[16] Verheul, R.F., Breukels, J. and Ockels, W.J. “Material selection and joining methods for the purpose of a high-altitude inflatable kite.” AIAA 2009-2338, 50th AIAA/ASME/ASCE/AHS/ASC Structures, Structural Dynamics, and Materials Conference, Palm Springs, CA, USA, 4-5 May 2009.

[17] Breukels, J. “An Engineering Methodology for Kite Design”. PhD thesis. Delft University of Technology, 2011.

[18] Weingarten, V.I., Seide, P. and Peterson J.P. “Buckling of Thin-Walled Circular Cylinders”. *NASA Space Vehicle Design Criteria (Structures)* (Sept. 1965).

[19] Hibbeler, R.C. *Mechanics of Materials*. tenth. Pearson Education, 2018.

[20] Ashby, M., Shercliff, H. and Cebon D. *Materials: Engineering, Science, Processing and Design*. Elsevier Ltd., 2014.

[21] Ahrens, U., Diehl, M. and Schmehl, R. *Airborne Wind Energy*. Vol. Green Energy and Technology. Springer, 2013.

[22] Vlasblom, M.P., Bosman, R.L.M. *Predicting the Creep Lifetime of HMPE Mooring Rope Applications*. Cordage institute. 2006.

[23] M. Yao, Y. Chen, Z. Wang, C. Shao, J. Dong, Q. Zhang, L. Zhang, X. Zhao. “Boosting gravimetric and volumetric energy density via engineering macroporous MXene films for supercapacitors”. *Chemical Engineering Journal* 395 (2020).

[24] L. Bruun, J.R. Millán Fernández, J. Hardeveld, S.R. Kethiri, H. Köster, S.L. Kramer, Y.C.A. de Raadt, B. van Regteren, M. van Ruremonde, B. Vlyminckx. “Midterm Report MARCO - POLO” (2021).

[25] Schmehl, R., Noom, M., van der Vlugt, R. “Traction Power Generation with Tethered Wings”. *Ahrens, U., M. Diehl, R. Schmehl (eds) Airborne Wind Energy, Green Energy and Technology.* (2013).

[26] Melin, T., Isikveren, A., Friswell, M. “Induced-Drag Compressibility Correction for Three-Dimensional Vortex-Lattice Methods”. *Journal of Aircraft* (2010).

[27] P. Williams, B. Lansdorp, and W. Ockels. “Modeling and Control of a Kite on a Variable Length Flexible Inelastic Tether.” In AIAA Modeling and Simulation Technologies Conference and Exhibit. 2007. DOI: 10.2514/6.2007-6705.

[28] U. Fechner. “A Methodology for the Design of Kite-Power Control Systems.” PhD thesis. 2016. DOI: https://doi.org/10.4233/uuid:85efaf4c-9dce-4111-bc91-7171b9da4b77.

[29] Bergsma, O.K., Sinke, J. and Vermeeren, C.A.J.R. *Materials and Manufacturing*. Faculty of Aerospace Engineering, Delft University of Technology. AE2600 Course Reader. Aug. 2006.

[30] Faludi, J. “Material Sustainability and Health - Characteristics of sustainable materials” (2020). Faculty of Industrial Design Engineering, Delft University of Technology.

[31] Olla, P. *Space Technologies for the Benefit of Human Society and Earth*. Springer, 2009.

[32] Alves Dias, P., Bobba, S., Carrara, S., Plazzotta, B. *The role of rare earth elements in wind energy and electric mobility*. Tech. rep. Publication Office of the European Union, Luxembourg, 2020. DOI: 10.2760/303258.

[33] G. Jiang and Stephen J. Pickering. “Recycling supercapacitors based on shredding and mild thermal treatment”. *Waste Management* 48 (2016), pp. 465–470. ISSN: 0956-053X. DOI: https://doi.org/10.1016/j.wasman.2015.10.027.

[34] M.P. Groover. *Fundamental of modern manufacturing Materials, Processes and systems*. 4th ed. Wiley, 2018. ISBN: 9781118231463.

[35] S. Bharti. “Advancement in Forging Process: A Review”. *International Journal of Science and Research* (2020).

[36] Isachenkov, M., Chugunov, S., Akahatov, I., Shishkovsky. “Regolith-based additive manufacturing for sustainable development of lunar infrastructure – An overview”. *Elsevier* (Jan. 2021).